NASA CR-72552
PWA FR-3169

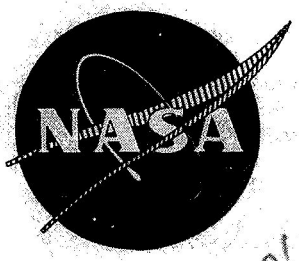



# SPACE STORABLE ENGINE CHARACTERIZATION

By
A. I. Masters, A. W. Brooke, And T. E. Bailey

PRATT & WHITNEY AIRCRAFT
FLORIDA RESEARCH AND DEVELOPMENT CENTER

Prepared for
NATIONAL AERONAUTICS AND SPACE ADMINISTRATION

NASA Lewis Research Center
Contract NAS3-12010
J. W. Gregory, Project Manager

NASA CR-72552
PWA FR-3169

# FINAL REPORT

# SPACE STORABLE ENGINE CHARACTERIZATION

By
A. I. Masters, A. W. Brooke, And T. E. Bailey

PRATT & WHITNEY AIRCRAFT
FLORIDA RESEARCH AND DEVELOPMENT CENTER
BOX 2691, WEST PALM BEACH, FLORIDA 33402

Prepared for
NATIONAL AERONAUTICS AND SPACE ADMINISTRATION

24 NOVEMBER 1969

Contract NAS3-12010

NASA Lewis Research Center
Cleveland, Ohio
J. W. Gregory, Project Manager
Liquid Rocket Technology Branch

# FOREWORD

This report was prepared by Pratt & Whitney Aircraft Division of United Aircraft Corporation under Contract NAS3-12010, "Space Storable Engine Characterization." The contract was administered by the Lewis Research Center of the National Aeronautics and Space Administration, Cleveland, Ohio. This document is the final report on the subject contract and summarizes the technical work accomplished during the period June 27, 1968 to March 21, 1969. The NASA Project Manager for the contract was John W. Gregory.

All work under the Contract was conducted at Pratt & Whitney Aircraft's Florida Research and Development Center. Many individuals within FRDC contributed to the contract technical effort. Those persons contributing the greatest time and effort included: D. J. Stout, J. A. McCabe, R. C. Mulligan, R. M. Hammond, G. L. Clark and J. Stettler (cycle analysis and turbopump performance); W. R. Kaminski and J. W. Neal (heat transfer); F. R. Landrum and E. D. Rush (weight and stress analysis); C. Peterson, R. M. Huls, G. J. Promozic, and B. J. Taylor (mechanical design); T. E. Bailey, A. I. Masters - Program Manager, and A. W. Brooke - Deputy Program Manager (program direction).

## ABSTRACT

Analyses were conducted for determination of an optimum cycle, turbomachinery arrangement, and design point for a 5000-lb (22.24-kN) thrust flox/methane pump-fed engine. The expander cycle with a geared drive turbopump was selected at nominally 500-psia (344.7-N/cm$^2$) chamber pressure, an expansion ratio of 70:1, and a mixture ratio of 5.25. A preliminary engine design including component layouts was completed for the selected configuration. Unique design features include a THERMAL SKIN® thrust chamber and a nozzle contour suitable for addition of a 100:1 nozzle extension. The design provides for uprating to 8000-lb (35.59-kN) thrust and throttling to 10% thrust.

CONTENTS

ILLUSTRATIONS

ILLUSTRATIONS (Continued)

ILLUSTRATIONS (Continued)

ILLUSTRATIONS (Continued)

ILLUSTRATIONS (Continued)

ILLUSTRATIONS (Continued)

ILLUSTRATIONS (Continued)

ILLUSTRATIONS (Continued)

ILLUSTRATIONS (Continued)

TABLES

TABLES (Continued)

# SECTION I
# SUMMARY

The objective of Contract NAS3-12010 was to define the most desirable operating conditions, cycle, and component configuration for a 5000-lb (22.24-kN) thrust flox/methane ($CH_4$) pump-fed engine. The program included extensive analysis based on data from previous flox/light hydrocarbon investigations and culminated in a complete engine preliminary design.

## A. CYCLE AND DESIGN POINT SELECTION

One unique feature of the study was the use of channel-type cooling passages in a thrust chamber using THERMAL SKIN®* rather than conventional tubular construction. Heat transfer analyses indicated that adequate cooling could be achieved, but that the cooling jacket pressure drop was greatly dependent upon fabrication methods and associated limitations that directly affect the coolant channel dimensions. Based on current photoengraving technology, dimensional limitations imposed for the study were: a maximum channel depth-to-width ratio of 2.0, a minimum land width of 0.025 in. (0.064 cm), and a minimum wall thickness of 0.020 in. (0.051 cm).

For comparison of applicable engine cycles and turbomachinery configurations, two design points were selected on the basis of thrust chamber cooling requirements and cycle considerations. They were:

1. F = 5000 lb, (22.24 kN), $P_c$ = 800 psia (551.6 N/cm$^2$), $\epsilon_e$ = 100, r - 5.25
2. F = 5000 lb, (22.24 kN), $P_c$ = 500 psia, (344.7 N/cm$^2$), $\epsilon_e$ = 60, r = 5.25

Cycle studies based on the first design point provided an evaluation of cycle performance and capabilities at near limiting conditions, but with somewhat restricted cycle flexibility. The second design point provided

---

*Thermal Skin is a registered trademark of United Aircraft Corporation that relates to laminated channel-type coolant passage construction. (See Section III.)

less difficult engine development requirements and increased operational flexibility within the same engine envelope.

The expander, gas generator, auxiliary heat exchanger, tapoff, and staged combustion cycles were compared at both design points. Turbopump configurations investigated were (1) a single turbine driving both pumps directly, (2) a single turbine with geared pumps, (3) series turbines, and (4) parallel turbines. The estimated delivered vacuum specific impulse, required fuel pump discharge pressure, and engine weight for the various cycle-turbopump combinations evaluated are shown in table I.

The different cycles and turbopump configurations were also compared qualitatively on the basis of complexity, development difficulty, design flexibility, ease of throttling, and production cost. The most significant differences in the qualitative ratings of the various cycles resulted from consideration of: (1) the presence of solid carbon and gaseous hydrogen fluoride in the turbine drive fluid of the gas generator, tapoff, and preburner cycles, which presents potential problems in turbine fouling and materials compatibility; (2) the problems of propellant distribution in the tapoff cycle to provide a satisfactory turbine working fluid without a substantial loss in performance; and, (3) the more severe turbomachinery requirements (higher fuel pump discharge pressure) of the expander and preburner cycles. On the basis of engine performance, engine weight, and the five qualitative factors, the expander and auxiliary heat exchanger cycles were selected for more detailed study.

Of the four turbopump configurations considered, the single turbine with geared pumps was judged superior for both the auxiliary heat exchanger and expander cycles. The direct drive configuration is limited in speed by the oxidizer pump seal requirements. Consequently, the fuel pump and turbine efficiencies are substantially lower than for the other arrangements, thereby increasing the auxiliary heat exchanger cycle losses and reducing the expander cycle power margin. Dual turbines, whether in series or parallel, were found to be heavier and resulted in increased control system complexity. In addition, admission areas became rather small for parallel turbines, particularly for the expander cycle.

# Table I. Cycle Performance Summary

| Cycle | $P_c$ psi ($N/cm^2$) | Single Direct Turbine Drive FPDP psi ($N/cm^2$) | Single Direct Turbine Drive $I_{vac}$ $lb_f$-sec/$lb_m$ (N-sec/kg) | Single Direct Turbine Drive Weight lb (kg) | Single Geared Turbine Drive FPDP psi ($N/cm^2$) | Single Geared Turbine Drive $I_{vac}$ $lb_f$-sec/$lb_m$ (N-sec/kg) | Single Geared Turbine Drive Weight lb (kg) | Parallel Turbines FPDP psi ($N/cm^2$) | Parallel Turbines $I_{vac}$ $lb_f$-sec/$lb_m$ (N-sec/kg) | Parallel Turbines Weight lb (kg) | Series Turbines FPDP psi ($N/cm^2$) | Series Turbines $I_{vac}$ $lb_f$-sec/$lb_m$ (N-sec/kg) | Series Turbines Weight lb (kg) |
|---|---|---|---|---|---|---|---|---|---|---|---|---|---|
| Gas Generator | 800 (551.6) | 1368 (943.2) | 399.7 (3920) | 144 (65.32) | 1368 (943.2) | 400.7 (3929) | 131 (59.42) | 1368 (943.2) | 400.4 (3927) | 143 (64.86) | 1368 (943.2) | 401.1 (3933) | 135 (61.24) |
| | 500 (344.7) | 751 (517.8) | 395.4 (3078) | 138 (62.60) | 751 (517.8) | 395.7 (3880) | 126 (57.15) | 751 (517.8) | 395.5 (3879) | 138 (62.60) | 751 (517.8) | 395.9 (3882) | 130 (58.97) |
| Chamber Tapoff | 800 (551.6) | 1368 (943.2) | 399.7 (3920) | 142 (64.41) | 1368 (943.2) | 400.7 (3929) | 129 (58.51) | 1368 (943.2) | 400.4 (3927) | 141 (63.96) | 1368 (943.2) | 401.1 (3933) | 133 (60.33) |
| | 500 (344.7) | 751 (517.8) | 395.4 (3878) | 136 (61.69) | 751 (517.8) | 395.7 (3880) | 124 (56.25) | 751 (517.8) | 395.5 (3879) | 136 (61.69) | 751 (917.8) | 395.9 (3882) | 138 (62.60) |
| Auxiliary Heat Exchanger | 800 (551.6) | 1368 (943.2) | 396.4 (3887) | 144 (65.32) | 1368 (943.2) | 398.4 (3907) | 131 (59.42) | 1368 (943.2) | 397.9 (3902) | 142 (64.41) | 1368 (943.2) | 399.4 (3917) | 137 (62.14) |
| | 500 (344.7) | 751 (517.8) | 393.6 (3860) | 138 (62.60) | 751 (517.8) | 394.9 (3873) | 126 (57.15) | 751 (517.8) | 393.9 (3863) | 137 (62.14) | 751 (517.8) | 394.7 (3871) | 132 (59.87) |
| Expander | 800 (551.6) | --- | --- | --- | 2025 (1396) | 404.4 (3966) | 122 (55.34) | | | | | | |
| | 500 (344.7) | 953 (657.1) | 397.8 (3901) | 119 (53.98) | 915 (657.1) | 397.8 (3901) | 115 (52.16) | | | | | | |
| Staged Combustion | 800 (551.6) | | | | 1550 (1068) | 404.4 (3966) | 127 (57.61) | | | | | | |

*Based on 94% $I_{vac}$ efficiency less turbopump leakage loss of 1.6 sec/$lb_m$ (15.69 N-sec/kg) and calculated cycle losses.

Because both the expander and auxiliary heat exchanger cycles looked completely feasible at both design points studied, final cycle selection for the preliminary design was based primarily on off-design operation. Throttling to 10% of design thrust and engine uprating were considered. Throttling was found to be feasible in three of the four cases; however, excessive bulk outlet temperature at minimum thrust at the higher pressure design point made it impractical for the expander cycle. Uprating to 8000-lb (35.59-kN) thrust was found to be feasible for the expander cycle at Design Point 2, but the closed cycle was power-limited at Design Point 1. Uprating of the auxiliary heat exchanger cycle was found to be feasible at both design points, but only with an appreciable loss in performance at both the design thrust and the uprated conditions. On the basis of engine specific impulse, weight, throttleability, and uprating potential, the expander cycle at Design Point 2 was believed to be the best all-around choice and was selected by NASA Lewis Research Center (LeRC) Project Manager for the preliminary engine design.

## B. ENGINE PRELIMINARY DESIGN

The engine preliminary design was based on the expander cycle with a gear driven turbopump. The nominal engine operating conditions were 5000-lb (22.24-kN) thrust, 500-psia (344.7-N/cm$^2$) chamber pressure, a nozzle expansion ratio of 70:1, and a thrust chamber mixture ratio of 5.25. The vacuum specific impulse was predicted to be 399.4 $lb_f$-sec/$lb_m$ (3917 N-sec/kg), based on 94% impulse efficiency and a seal leakage and gearbox coolant loss equivalent to 2.0 $lb_f$-sec/$lb_m$ (19.61 N-sec/kg) impulse. The exhaust nozzle is contoured to accept a nozzle extension that would increase the expansion ratio to 100:1 and add approximately 6.0-$lb_f$-sec/$lb_m$ (58.84 N-sec/kg) specific impulse. The basic engine design is capable of uprating to 8000-lb (35.59-kN) thrust and throttling to 10% thrust. The estimated engine weight is 98 lb (44.91 kg) without the nozzle extension.

Figure 1 shows the design point cycle schematic including engine control points for fixed thrust operation. Control requirements for throttling, tank head idle, and propellant utilization were also evaluated. The fuel turbopump speed is nominally 50,000 rpm

(5236 rad/s), and the oxidizer pump is geared to one-half the fuel pump speed, or 25,000 rpm (2618 rad/s). Thrust is controlled by varying the turbine bypass flow area, and mixture ratio is controlled by varying the oxidizer secondary flow to the coaxial dual-orifice injector.

The engine turbomachinery, controls, thrust chamber, and injector are predicted to operate satisfactorily over the required ranges of thrust, mixture ratio, heat flux levels, and pump inlet conditions.

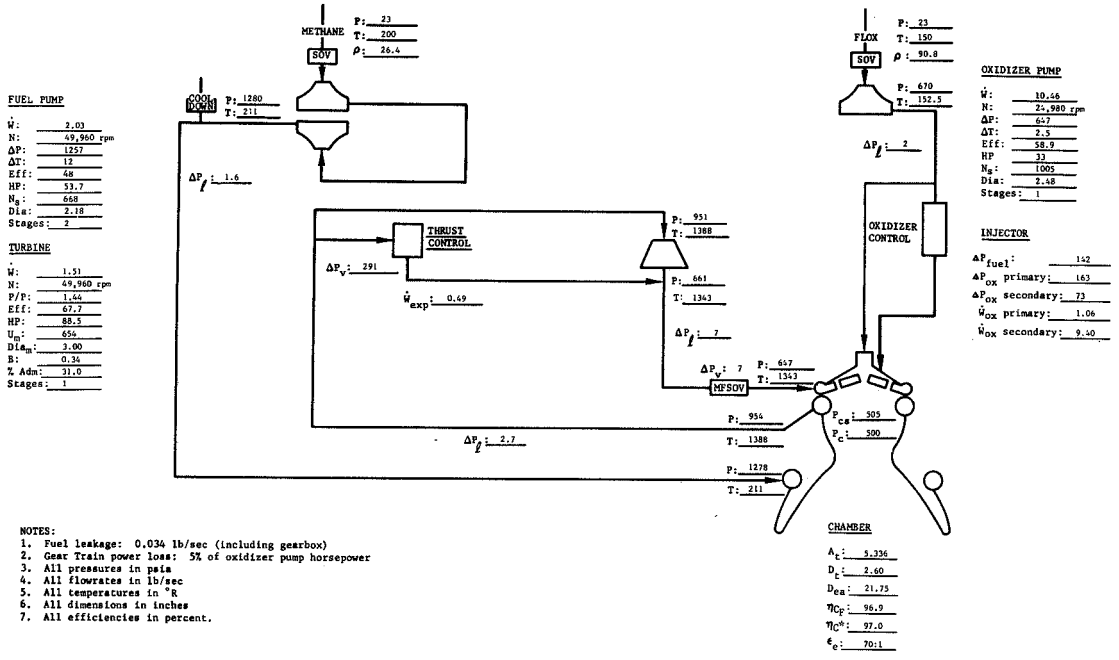


Figure 1. 5000-lb (22.24-kN) Flox/Methane Engine Cycle Schematic FD 27375.B

# SECTION II
# INTRODUCTION

## A. FLOX/METHANE ENGINE APPLICATIONS

Advanced upper-stage pump-fed rocket engines using high-energy space storable propellants can provide substantial payload increases or reduced launch vehicle weight, when compared with pressure-fed systems using earth storable propellants. These advanced stages include planetary orbiters, planetary probe landers, scientific solar probes, probes to the outer planets and astroids, planetary surface sample return vehicles, and a variety of manned and unmanned planetary or lunar return stages.

Flox/methane is an attractive space storable propellant combination for pump-fed engines because methane is (1) a good coolant and good turbine working fluid and (2) the propellants have a high enough boiling point and sufficiently compatible liquid temperature range for long term space storage. The desirable cooling characteristics of methane allow much higher combustion chamber pressures to be achieved than with other high energy space storable fuels. Higher chamber pressure means higher engine performance within a smaller envelope. This advantage is apparent when it is recognized that a flox/methane engine with an expansion ratio of 100:1 operating at 800-psia (551.6 $N/cm^2$) chamber pressure, could deliver a vacuum specific impulse 100 $lb_f$-sec/$lb_m$ (980.7 N-sec/kg) greater than that of a current $N_2O_4$/50% UDMH-50% $N_2H_4$ pressure-fed system operating at a chamber pressure of approximately 100 psia (68.9 $N/cm^2$) and delivering about 305 $lb_f$-sec/$lb_m$ (2991 N-sec/kg) specific impulse with an expansion ratio of 50. Additionally, the flox/methane engine would provide 50% reductions in exhaust nozzle length and diameter.

A large number of advanced high energy applications have thrust requirements in the range of 1000 to 10,000 lb (4.448 kN to 44.48 kN). Translating the increased specific impulse for flox/methane into payload for a typical mission, a 45 to 65% increase in landed Mars probe weight is possible when a pump-fed flox/$CH_4$ engine is used for orbital

capture propulsion rather than a pressure-fed $N_2O_4$/50-50 system. Greater payload gains are possible in more difficult missions such as planetary surface sample return.

In addition to providing performance gains, pump-fed engines using flox/methane provide a solution to one problem inherent in pressure-fed systems. Pressure-fed systems require long term storage of high pressure gas for pressurization of the propellant tanks. A leak in the gas system can cause mission failure; therefore, a complicated network of redundant valves, regulators, and plumbing is required for gas storage and control. It is possible with pump-fed engines that burn volatile propellants to provide all of the pressurizing gas directly from the engine turbopumps. This technique, known as "autogenous pressurization," eliminates the requirement for high pressure gas storage during long term space missions. In addition, the vapor pressure of the propellants, themselves, can sometimes be used to provide the tank head required for low-thrust engine firings or attitude control systems.

## B. FLOX/METHANE TECHNOLOGY

Analytical and experimental investigations of flox/methane and other flox/light hydrocarbon propellant combinations have been conducted by Pratt & Whitney Aircraft through independent studies that began in 1963 and under five NASA-LeRC contracts, the first of which started in June 1964. Three of these contracts (NAS3-4195, Reference 1; NAS3-6296, Reference 2; and NAS3-10294, Reference 3) were directed primarily toward application of flox/light hydrocarbon combinations to pressure-fed upper-stage engines. Nevertheless, accomplishments under these contracts provided valuable data pertaining to cooling requirements and injector performance that gave insight into higher chamber pressure requirements. The most significant conclusions related to flox/methane engine operation drawn from the three low pressure contracts were:

1. Flox/$CH_4$ provides high delivered vacuum specific impulse; however, nonequilibrium expansion losses and difficulties in achieving high combustion efficiency at high mixture ratios shift the mixture ratio for maximum performance to a lower value than the optimum theoretical mixture ratio.

2. Carbon deposition on the thrust chamber wall will reduce the chamber heat flux to lower values than those predicted by conventional boundary layer analysis.

3. Cooling under bulk boiling conditions is feasible, provided that circumferential variations in injector heat flux and coolant flow are not excessive.

4. Flox/$CH_4$ is hypergolic for the fluorine concentrations required to achieve high performance.

Contracts NAS3-7950 (Reference 4) and NAS3-11190 (References 5 and 6) dealt directly with flox/$CH_4$ pump-fed engine operation. Under Contract NAS3-7950, an RL10A-1 oxygen/hydrogen expander cycle engine was modified and tested with flox/$CH_4$. Nominal test conditions were 13,000-lb (57.83-kN) thrust, 250-psia (172.4-N/$cm^2$) chamber pressure, and 5.75 mixture ratio. Nine engine demonstration tests were conducted for a total engine operating time of 120 sec. The primary problem encountered was burnout of the tubular thrust chamber during the start transient. The cooling problems were attributed to the large coolant passages that were originally designed for hydrogen. It was recognized that reductions in coolant flow area would be required in critical heat transfer regions; accomplishment of these reductions was based on analysis. However, the large coolant passage volume also permitted an excessive mass of liquid methane to accumulate in the thrust chamber jacket during engine start, causing coolant flow reversals and thrust chamber burnout problems that were not initially anticipated, and which required solution during engine testing. The program demonstrated the feasibility of flox/$CH_4$ pump-fed engine operation and established the applicability of the expander cycle and an RL10 type control system to such an engine.

Contract NAS3-11190, Space Storable Regenerative Cooling Investigation, is directed toward improving thrust chamber cooling with hydrocarbon fuels using advanced thrust chamber fabrication techniques. Early analytical studies (Reference 4) provided predictions of cooling limits for various hydrocarbon fuels with flox and with oxygen-difluoride. On the basis of the study, flox/methane was selected for

the experimental phases of the program. Nominal test conditions were 5000-lb (22.24-kN) thrust and 500-psi (344.7-N/cm$^2$) chamber pressure. At the time this report was prepared, the experimental work was not complete. Water-cooled firings using Thermal Skin type thrust chambers had been conducted. The tests provided injector performance and chamber heat flux data that were used in the design of a regeneratively cooled Thermal Skin thrust chamber. The data obtained in the water-cooled tests and the experience in regenerative thrust chamber design and fabrication provided valuable background applicable to this study.

## C. OBJECTIVE AND PROGRAM ORGANIZATION

The objective of the work conducted under this program was to define the most desirable operating conditions, cycle, and component configuration for a 5000-lb (22.24-kN) thrust flox/$CH_4$ pump-fed engine. The eight month program included extensive heat transfer and cycle analysis using data from previous flox/light hydrocarbon investigations, and culminated in a complete preliminary engine design. The program consisted of two tasks: Task I, Engine Turbopump Drive Cycle Investigation, and Task II, Engine Preliminary Design Evaluation.

Task II, as indicated by its title, comprised the actual engine preliminary design effort. In Task I, the analyses necessary to select a design point within specified ranges of operating conditions, and an engine cycle were completed. The initial phase of Task I was a preliminary regenerative cooling analysis to evaluate the feasibility of regenerative cooling over the specified range so that two alternative design points could be selected, and to provide coolant temperature rise and pressure drop data for use in a Turbopump Drive Cycle Analysis, or screening of candidate cycles and turbopump arrangements. This analysis included cycle studies, performance estimation, weight estimation, and qualitative evaluation of factors, such as complexity, design difficulty, etc., at the selected design points. On the basis of the screening results, two-cycle-turbopump combinations were selected for more detailed evaluation at each of the two design points. Thrust chamber geometry and coolant passage designs were completed for each of the resulting four cases, which were then subjected to more detailed

analysis including evaluation of off-design operation and variations in several specified input parameters. The more detailed study is referred to as the Cycle Energy Balance study, to differentiate it from the initial screening. Upon completion of the evaluation, recommendations as to the relative merits of the four cases were made to NASA-LeRC Project Manager, who then selected a single cycle and design point for Task II.

## SECTION III
## ANALYTICAL EFFORT - TASK I

### A. GUIDELINES AND DESIGN PARAMETERS

Engine operating conditions for the Task I analysis were specified at the levels shown in Table II by contract.

Table II. Task I Design Parameters

| | |
|---|---|
| Vacuum Thrust | 5000 lb (22.24 kN) |
| Chamber Pressure | 300 - 1000 psia (206.8 - 689.5 $N/cm^2$) |
| Mixture Ratio | 4.75 - 5.75 |
| Nozzle Area Ratio | 40 - 100 |
| Delivered Vacuum Specific Impulse (Excluding Cycle Losses) | 94% of Theoretical Shifting Equilibrium |
| Propellant Inlet Conditions | |
| Liquid Methane | |
| Temperature | 170 - 260°R (94.44 - 144.4°K) |
| Pressure | 20 - 125 psia* (13.79 - 86.19 $N/cm^2$) |
| Liquid Flox | |
| Temperature | 150 - 200°R (83.33 - 111.1°K) |
| Pressure | 20 - 125 psia* (13.79 - 86.19 $N/cm^2$) |

*Based on pump requirements

Several design constraints were also imposed for the analysis, including the following:

1. Only regenerative cooling with liquid methane was to be considered.
2. The coolant jacket pressure drop was limited to a value less than chamber pressure, and preferably below 50% of chamber pressure.
3. The thrust chamber was to be nickel, with a maximum hot side wall temperature of 2160°R (1200°K).

4. Channel type coolant passage construction using advanced fabrication techniques such as electroforming, electrodischarge machining, chemical milling, or photoetching was to be given preference over conventional tubular construction.

In the first screening, six cycles and four turbopump arrangements were evaluated at two design points. The two design points, listed in Paragraph C, were selected after completion of a preliminary regenerative cooling analysis. The six cycles evaluated were the gas generator, chamber tapoff, auxiliary heat exchanger, expander, staged combustion, and composite expander. The turbopump arrangements were: (1) a single turbine with direct drive pumps, (2) a single turbine with gear driven pumps, (3) series turbines, and (4) parallel turbines. The cycles and turbopump configurations are described in paragraph C.

## B. PRELIMINARY REGENERATIVE COOLING ANALYSIS

The preliminary regenerative cooling analysis consisted of studies to verify that regenerative cooling was feasible over the range of operating conditions specified and to generate cooling jacket discharge temperature and pressure loss predictions for use in turbopump drive cycle analyses. The cooling studies were completed independently prior to the start of the Contract NAS3-12010 effort to expedite the program. Two sets of calculations were made, each reflecting particular assumptions of dimensional limitations for thrust chamber construction. Both sets included calculations based on heat flux levels corresponding to (1) no carbon deposition, Bartz short form method; (2) $Q_m/Q_p = 0.90$, where $Q_m/Q_p$ is the ratio of measured heat flux to the predicted heat flux neglecting carbon deposition; and (3) $Q_m/Q_p = 0.76$.

### 1. Chamber Fabrication Methods

The method of chamber fabrication imposes chamber coolant passage dimensional limitations. In turn, these dimensional limitations greatly influence the wall temperature - coolant pressure drop relationship. Two advanced methods of constructing thrust chambers with small coolant channels that were considered sufficiently developed to be feasible for the study were electrodeposition and use of photoetched plates (Thermal Skin).

Several methods are available for fabricating rocket thrust chambers by electrodeposition. The pioneer for this method has been Camin Laboratories, Inc. (Reference 7). In the technique they developed, the inner wall of the thrust chamber is formed by deposition of nickel on a mandrel which has been machined to the required internal dimensions. Next, the ribs or lands and outer wall are deposited. The size and shape of the lands and, therefore, of the cooling passages are established by applying a filler material over the entire inner shell and machining the filler to remove material in the areas where the lands are to be formed. The filler is removed after the lands are deposited, and wax is substituted so the outer shell can be deposited. The wax is then removed, thus opening the cooling passages.

The name Thermal Skin is applied to a sandwich wall construction in which coolant passages are etched by photoengraving into the mating faces of two flat plates. Figure 2 summarizes the steps for a small fluorine/hydrogen chamber that was constructed and test-fired independently by Pratt & Whitney Aircraft to demonstrate the feasibility of the concept. The flat plates are mated by brazing or diffusion bonding to provide a longitudinal thrust chamber segment or stave. A number of staves are then formed to the desired contour, trimmed, and welded together to form the thrust chamber.

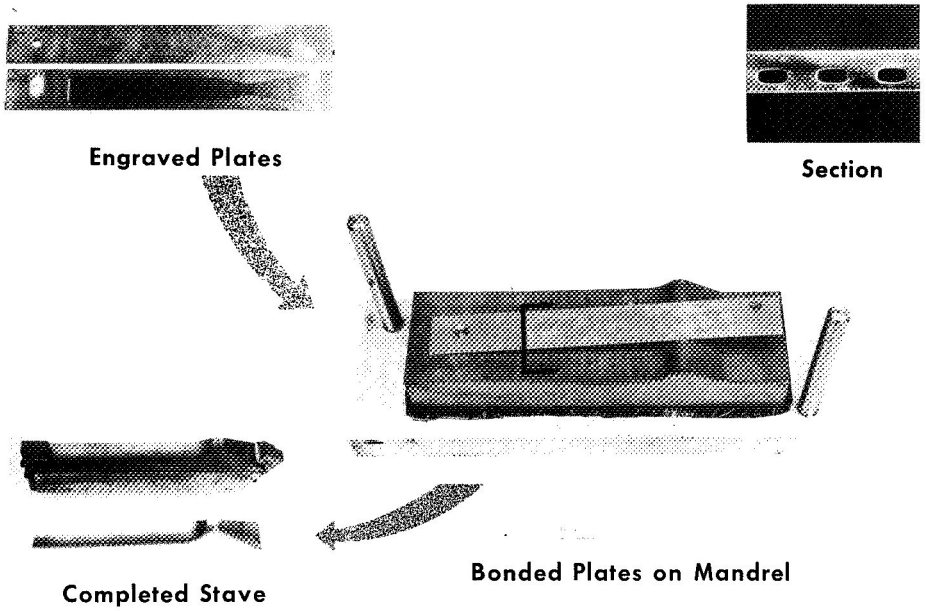


Figure 2. Thermal Skin Thrust Chamber Fabrication GS 6353B

Figure 3 illustrates the important passage dimensions for channel type construction. Thermal Skin and electrodeposited chambers each have dimensional limitations and materials requirements which are peculiar to the method of construction. The advantages and disadvantages of the two methods are greatly dependent upon the state-of-the-art of the various fabrication processes employed; however, based on current technology, the following conclusions may be made:

1. Electrodeposition is limited to pure metals, i.e., alloys cannot be deposited. With Thermal Skin, any metals that can be etched and brazed, or diffusion bonded may be utilized.

2. Photoetching provides greater flexibility for variations in passage width, land width, and passage branching. Variations in passage depth are more readily achieved with electrodeposition.

3. A high passage depth-to-width ratio is desirable for minimizing the coolant pressure drop. With Thermal Skin, a maximum depth-to-width ratio of 2.0 is possible with existing technology, while ratios of 3.0 or more are possible with moderate development. Depth-to-width ratios up to 3.0 to 5.0, depending on passage width, are currently feasible with electrodeposition.

4. Minimum land width and wall thickness are approximately the same for the two fabrication methods.

5. The fabrication cost would be approximately the same for individual thrust chambers fabricated by the two methods; however, quantity production would favor Thermal Skin.

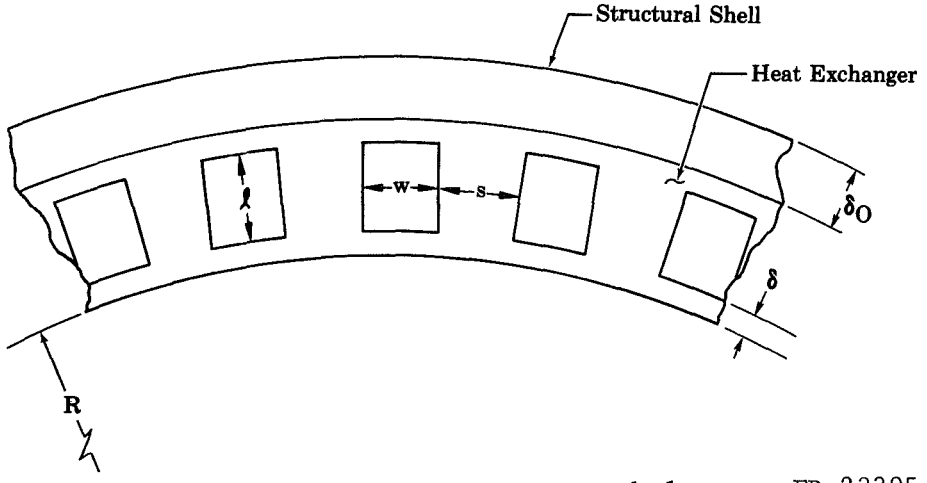


Figure 3. Cross Section of Typical Nontubular Wall Structure FD 23395

In summary, a higher depth-to-width ratio was found to be the only significant advantage of electrodeposition for this application. On the other hand, Thermal Skin offered several important advantages. Initial analyses indicated that the depth-to-width ratios achievable with Thermal Skin provided acceptable thrust chamber coolant pressure drops; consequently, the preliminary regenerative cooling analysis was based upon the use of Thermal Skin construction. This choice was continually reviewed during the Task I studies, and the possibility of an electrodeposited thrust chamber was also considered in the Task II preliminary design. In most cases, the jacket pressure drop encountered would not be greatly affected by the choice of fabrication method; consequently the conclusions from the heat transfer and cycle analyses are valid for electroformed as well as Thermal Skin thrust chambers.

2. Dimensional Requirements

The assumed coolant passage dimension limits for thrust chamber fabrication are summarized in table III. Case I is considered to be achievable with moderate development of engraving techniques while Case II is more consistent with current manufacturing technology.

For all of the preliminary regenerative cooling analyses, the chamber contraction ratio, $\epsilon_e$, was fixed at 4.0 and the characteristic length, L*, was set at 30 in. (76.20 cm). These values were selected on the basis of studies conducted under the Contract NAS3-11190 Space Storable Regenerative Cooling Investigation (References 5 and 6) and without the benefit of experimental data that later became available. As discussed in Paragraph D, the values selected for the later and more detailed study under Task I and for the Task II, Engine Preliminary Design Evaluation, were equal to or higher than the values used for the preliminary analysis.

Table III. Thermal Skin Fabrication Limits

| | Case I | Case II |
|---|---|---|
| Hot Side Wall Thickness | 0.010 in. (0.025 cm) | 0.020 in. (0.051 cm) |
| Maximum Passage Depth/Width Ratio, d/w | 3.0 | 2.0 |
| Minimum Land Width, S | 0.015 in. (0.038 cm) | 0.025 in. (0.064 cm) |
| Technology Required | Moderate Development | Current |

3. Calculated Results

For both sets of assumed dimensional limits (Case I and II), calculations were made for two inlet-pressure-to-chamber-pressure ratios, $P_{in}/P_c$. A value of $P_{in}/P_c$ of 1.5 was selected as typical of open cycles, such as a gas generator engine, while a $P_{in}/P_c$ of 3.0 was used to represent closed cycles, such as the expander cycle. Assuming single pass, counterflow cooling, coolant temperature rise and pressure drop were calculated for the extremes of mixture ratio (4.75 and 5.75) at each of the three heat flux levels ($Q_m/Q_p$ = 0.765, 0.90, and 1.0, or no carbon deposition). Thus, curves of jacket $\Delta P$ and $\Delta T$ vs chamber pressure were generated for 24 cases, and expansion ratios of 40, 60, and 100 were considered for each case. A sample curve (for Case II, $P_{in}/P_c$ = 3.0, $Q_m/Q_p$ = 0.9, r = 5.75, and $\epsilon_e$ = 100) is presented in figure 4. A complete set of 24 plots with curves for each of the three expansion ratios is included in Appendix A.

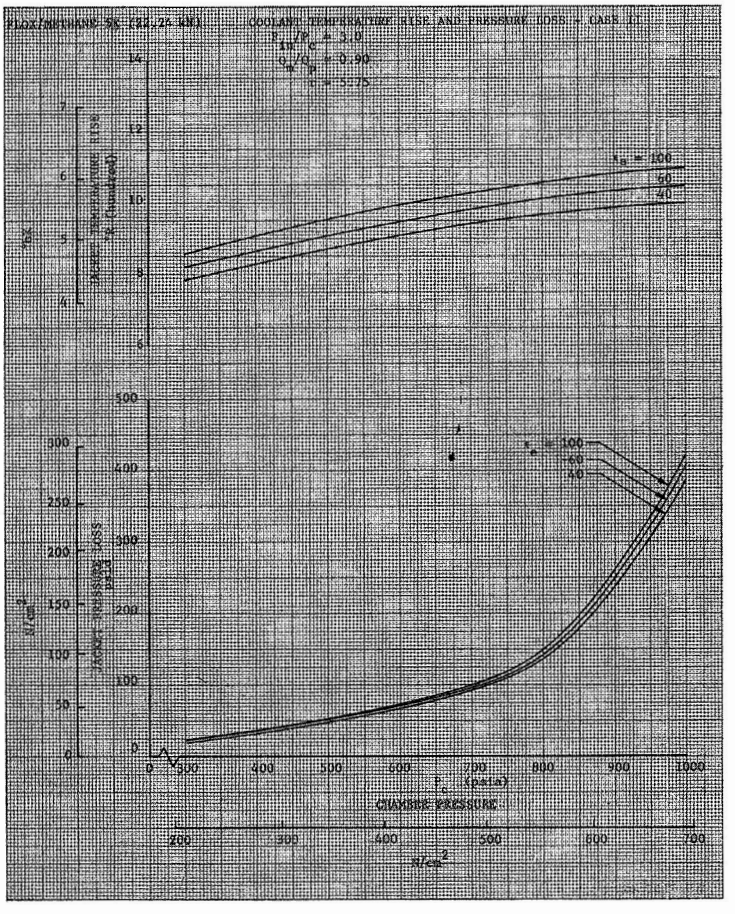


Figure 4. Flox/Methane 5000-lb (22.24 kN) Coolant Temperature Rise and Pressure Loss - Case II DF 70822

To determine the heat transfer requirements for any combination of intermediate design conditions, a method was formulated to interpolate the coolant temperature rise and pressure drop using the parametric data of curves in figures A-1 through A-24 of Appendix A. Thus, a detailed calculation was not required for each cycle-design point combination of interest. The fact that the general shape of the $\Delta P$ and $\Delta T$ versus $P_c$ curves is retained for all combinations of operating variables indicates that the influence of one variable on $\Delta P$ or $\Delta T$ is relatively independent of the other variables. Therefore, the entire range of interest for the five operating variables considered could be evaluated parametrically using one correction curve for each variable, or five sets of curves. Figure 4 was used as a reference plot of $\Delta P$ and $\Delta T$ versus $P_c$, and influence curves were constructed to provide correction factors, b, over the range of interest for $Q_m/Q_p$, $P_{in}/P_c$, r, and $\epsilon_e$. The influence curves are presented in figures 5 through 9. The reference $\Delta P$ and $\Delta T$ vs $P_c$ plot, figure 5, is for the base point reference values:

$$\begin{aligned} Q_m/Q_p &= 0.90 \\ P_{in}/P_c &= 3.0 \\ r &= 5.75 \\ \epsilon_e &= 100 \end{aligned}$$

To facilitate the study, the correction factors of figures 6 through 9 necessary to find the coolant $\Delta P$ and $\Delta T$ for other values of $Q_m/Q_p$ $P_{in}/P_c$, r, and $\epsilon_e$ were programed as continuous functions for a digital computer. With the programs, rapid calculation of a large number of data points was readily accomplished.

4. Evaluation of Preliminary Cooling Analysis

Results for the Case I assumptions of dimensional limitations indicated that regenerative cooling was feasible for the entire range of all of the operating variables considered. Furthermore, only if $Q_m/Q_p$ exceeded 0.90 did the chamber pressure drop become high enough to have a significant influence on engine cycle considerations. Even for high $Q_m/Q_p$ values, high pressure drop became a problem only at the most severe cooling conditions, i.e., maximum chamber pressure and low $P_{in}/P_c$.

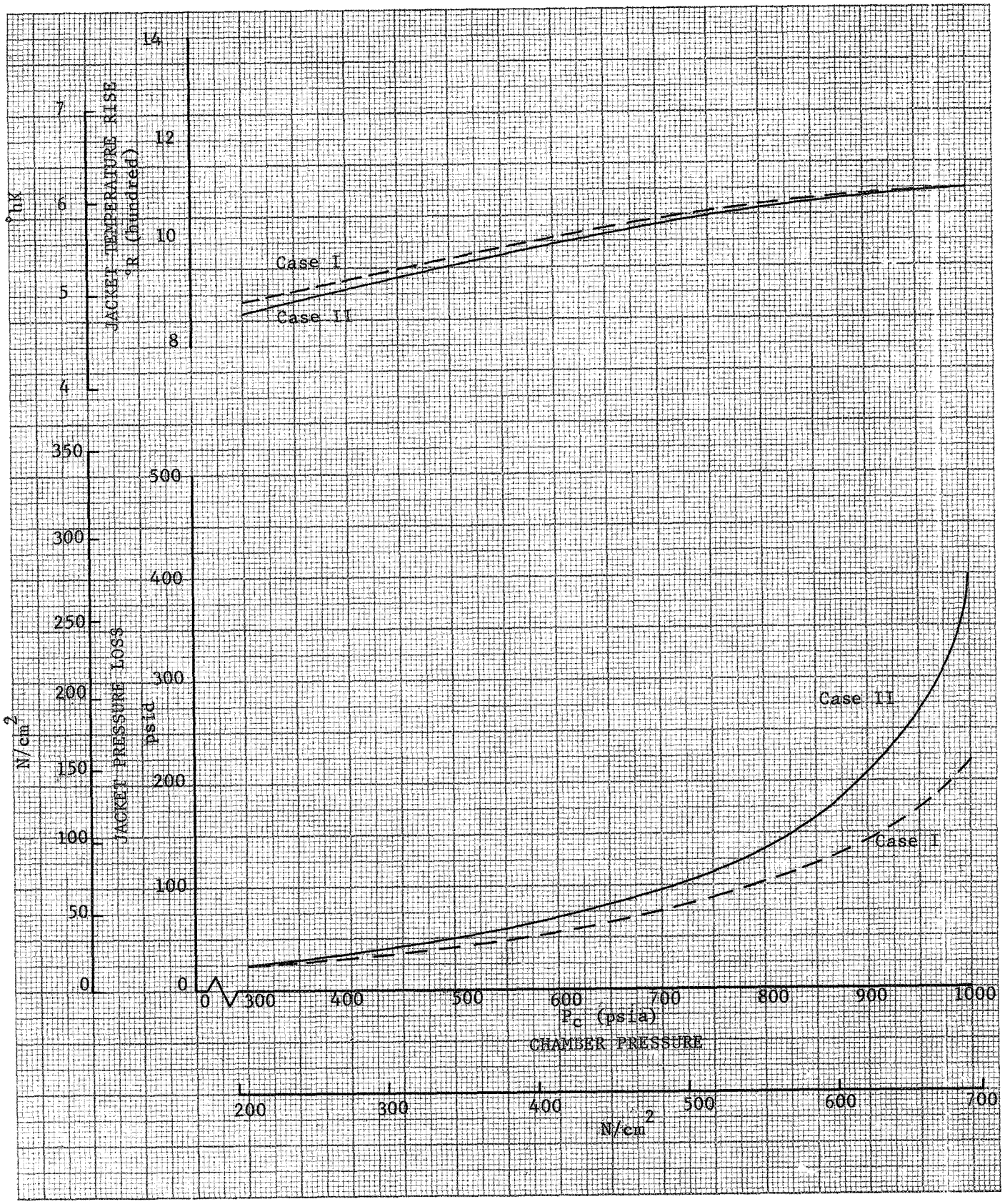


Figure 5. Chamber Pressure Influence DF 70825

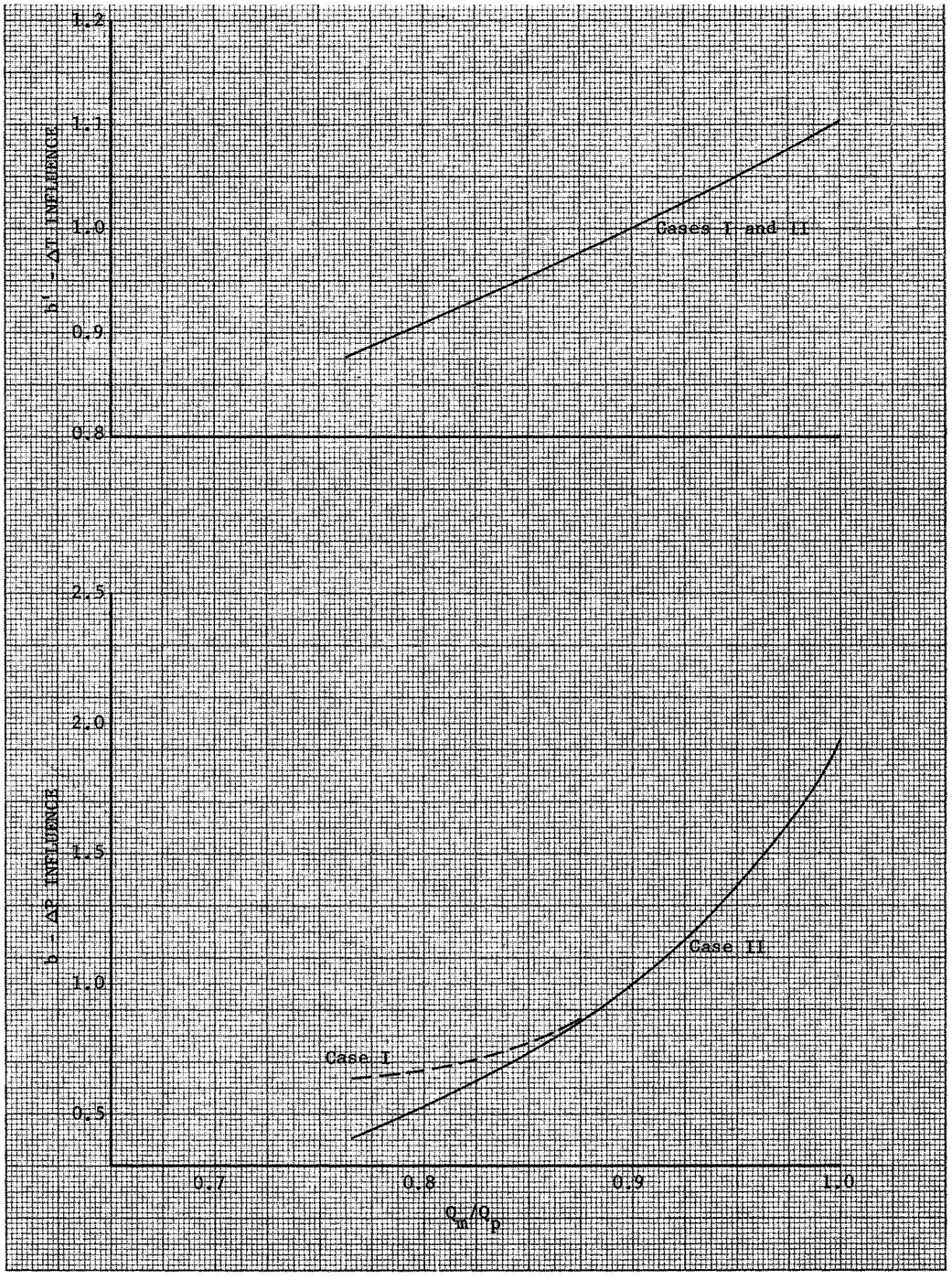


Figure 6. Heat Flux Ratio Influence DF 70826

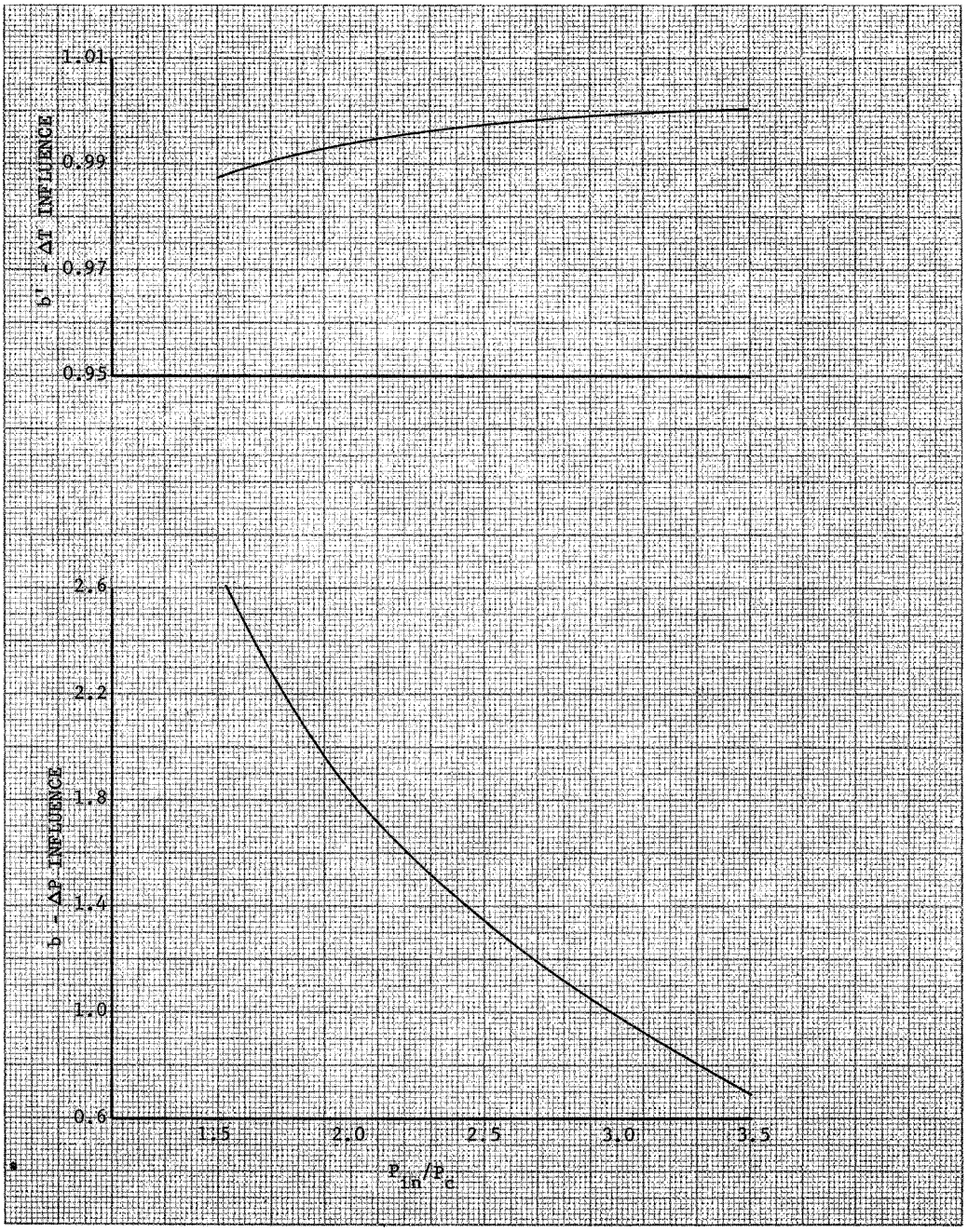


Figure 7. Inlet Pressure/Chamber Pressure Influence DF 70827

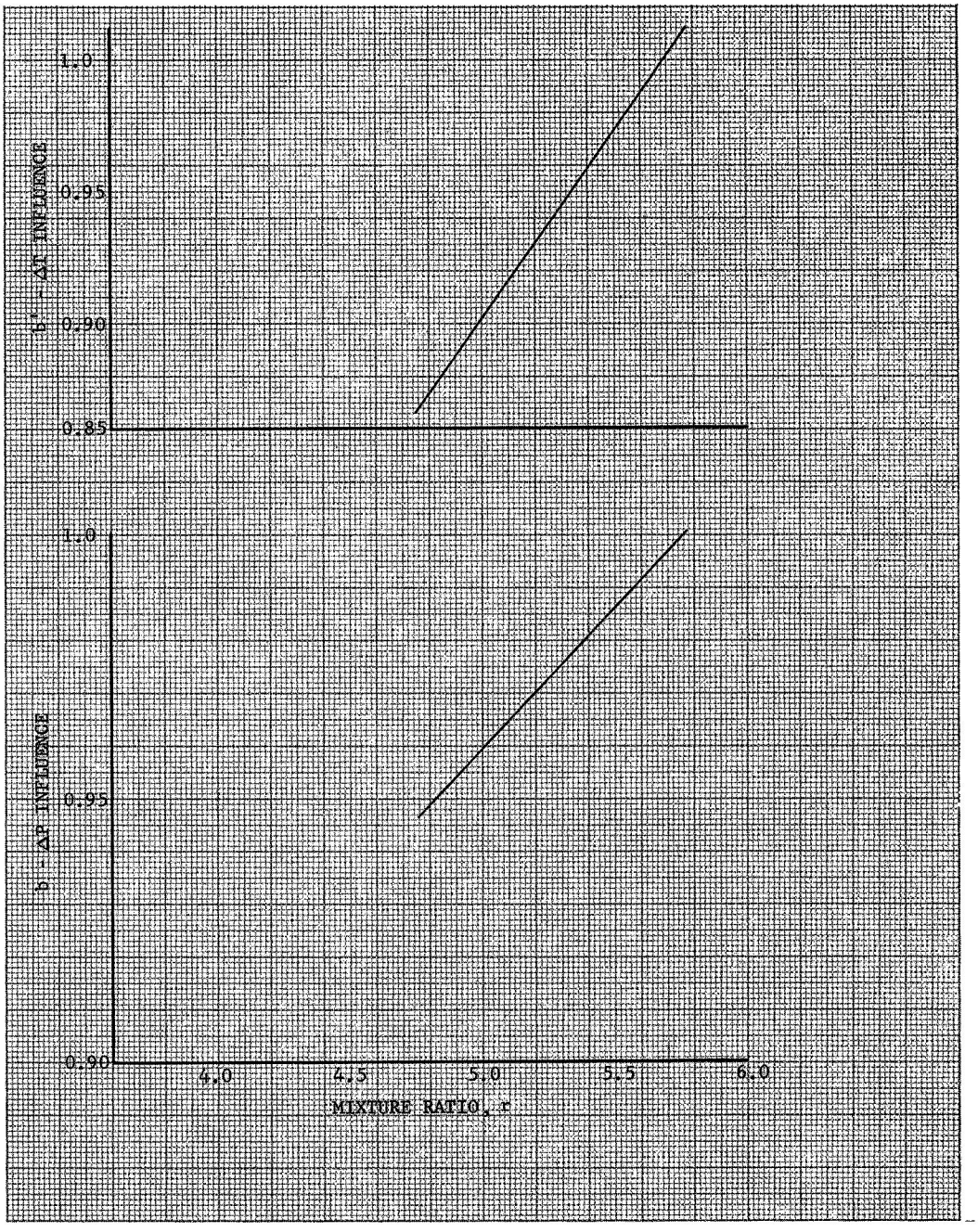


Figure 8. Mixture Ratio Influence DF 70790

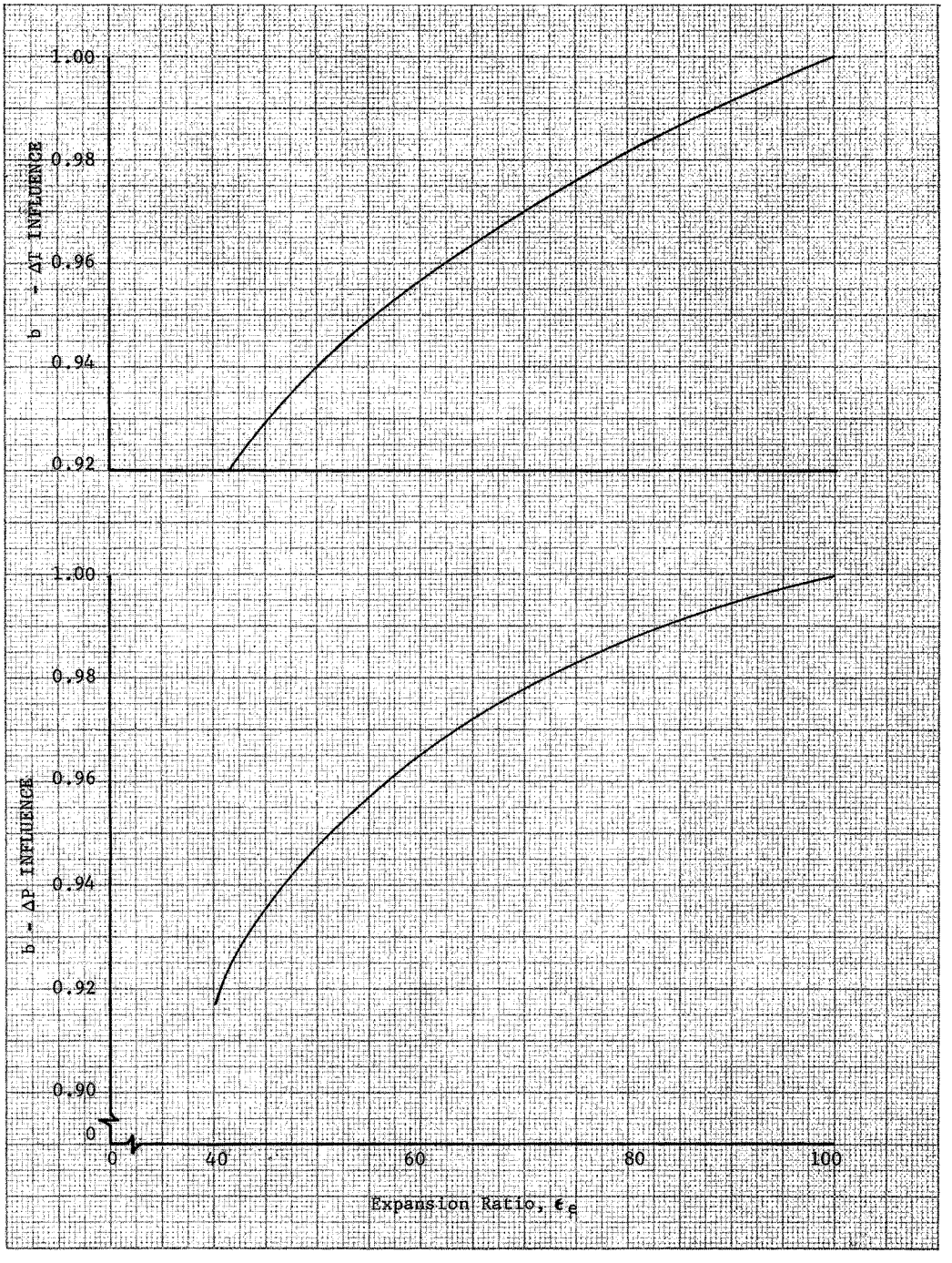


Figure 9. Expansion Ratio Influence DF 70792

For the more conservative Thermal Skin channel design limitations of Case II, the cooling requirements were more significant. As shown in figure 4, the jacket pressure drop for Case II is approximately double that for Case I at 1000-psia (689.5-N/cm$^2$) chamber pressure. This increased pressure drop restricts high pressure cycle operation; in expander cycles it makes a power balance more difficult to achieve, and it appreciably increases performance losses in open cycles. As a result, chamber pressures above 800 to 900 psia (551.6 to 620.5 N/cm$^2$) appear impractical with current chamber fabrication limitations.

The aforementioned considerations formed the basis for selection of two design points, discussed early in paragraph C. However, the information generated permits several other significant conclusions to be drawn:

1. While the differences in channel geometry between Case I and Case II have a significant effect on jacket $\Delta P$, they have little effect on $\Delta T$.
2. $Q_m/Q_p$ and $P_{in}/P_c$ have sizable effects on coolant jacket pressure drop, while $\epsilon_e$ and r have much less influence (figures 6 through 9).
3. The differences in the channel geometries for Case I and Case II produce no significant difference in the influence of $Q_m/Q_p$, $P_{in}/P_c$, r, and $\epsilon_e$ on jacket $\Delta P$ (figures 5 through 8).
4. $Q_m/Q_p$ and r have the most significant effects on jacket $\Delta T$ while variations in $P_{in}/P_c$ have practically no effect.

## C. TURBOPUMP DRIVE CYCLE ANALYSIS

### 1. Design Point Selection

The primary objective of the Turbopump Drive Cycle Analysis was the selection of two-cycle-turbopump configuration combinations at each of two selected design points. The two design points were selected largely on the basis of cooling limitations established in the Preliminary Regenerative Cooling Analysis described above. It was felt that the most realistic approach would be to rely on the results for the more conser-

vative fabrication limit assumptions (Case II). In addition, there were several basic cycle considerations which also contributed, including:

1. Use of the Case II Thermal Skin fabrication limitations made it difficult to balance the expander cycle above 800 to 900 psia (551.6 to 620.5 $N/cm^2$).
2. As chamber pressure is increased, the gas generator cycle and other open cycles show no performance improvements above approximately 800 psia (551.6 $N/cm^2$) based on a fixed nozzle exit diameter. (Based on a fixed nozzle expansion ratio, gas generator cycle performance peaks at approximately 300 psia or 206.8 $N/cm^2$.)
3. Experimental data from previous programs indicated that the mixture ratio for maximum delivered performance would be somewhat lower than the theoretical peak performance mixture ratio. Lower mixture ratios also simplify cooling requirements.
4. For the most direct comparison of the two design points, it was desirable that both design points fit within the same engine envelope.

On the basis of all considerations, the two design points listed in table IV were recommended to and approved by the NASA-LeRC Project Manager. The design points provided a nearly identical envelope so that results would allow direct evaluation of the tradeoffs between performance and development difficulty and flexibility.

Table IV. Design Points for Task 1

| Design Point | Vacuum Thrust | Chamber Pressure | Nozzle Expansion Ratio | Oxidizer to Fuel Ratio |
|---|---|---|---|---|
| 1 | 5000 lb (22.24 kN) | 800 psia (551.6 $N/cm^2$) | 100 | 5.25 |
| 2 | 5000 lb (22.24 kN) | 500 psia (344.7 $N/cm^2$) | 60 | 5.25 |

2. Cycle Description

a. Classification of Cycles

Rocket engine cycles may be categorized according to the source of the turbine working fluid (e.g., gas generator, regenerative cooling jacket, etc.), or by the manner in which the working fluid is utilized after it passes through the turbine. In the latter instance, there are two possibilities: (1) the turbine working fluid is returned to the combustion chamber after flowing through the turbine and is expanded through the main thrust chamber and exhaust nozzle to make efficient use of its energy; or, (2) the working fluid leaving the turbine is discharged overboard or expanded at a pressure ratio lower than that of the primary combustion products, thus at lower performance levels. Cycles of the first type are identified as closed cycles, while those of the second type are referred to as open cycles. In general, closed cycles produce higher specific impulse but require higher pump discharge pressures for the working fluid than do open cycles at the same pressure level. Early rocket engines utilized open cycles almost exclusively. As turbomachinery technology has advanced and engine performance requirements have become more stringent, closed cycles have received increased consideration and greater use. Application of closed cycles should be further stimulated by a long-term trend toward increased engine chamber pressure, because open cycle performance losses increase with increases in required pump power.

Table V classifies the rocket engine cycles of interest to the proposed program by the categories discussed:

Table V. Categorization of Rocket Engine Cycles

| Working Fluid Source | Cycle | |
|---|---|---|
| | Open | Closed |
| Thrust Chamber Cooling Jacket | Auxiliary Heat Exchanger or Fuel Tapoff | Expander |
| Gas Generator | Gas Generator | Staged Combustion |
| Main Combustion Chamber | Tapoff | |

In addition to the five cycles listed in table V, a composite expander cycle, which is neither completely open or closed, was found to have certain potential advantages and was, therefore, given consideration in the study. Brief descriptions and illustrative schematics for the six cycles are included in the paragraphs b through g.

b. Gas Generator Cycle

A typical gas generator cycle, shown schematically in figure 10,* depicts the most usual arrangement wherein the fuel and oxidizer for the gas generator are extracted from the main propellant flow at the pump discharge. In upper-stage engines operating at very low ambient pressures it might be possible to supply the gas generator with propellants at nominal tank pressure. Such an approach would simplify starting by eliminating the need for a separate starting propellant supply, but it generally results in a requirement for excessively large turbines.

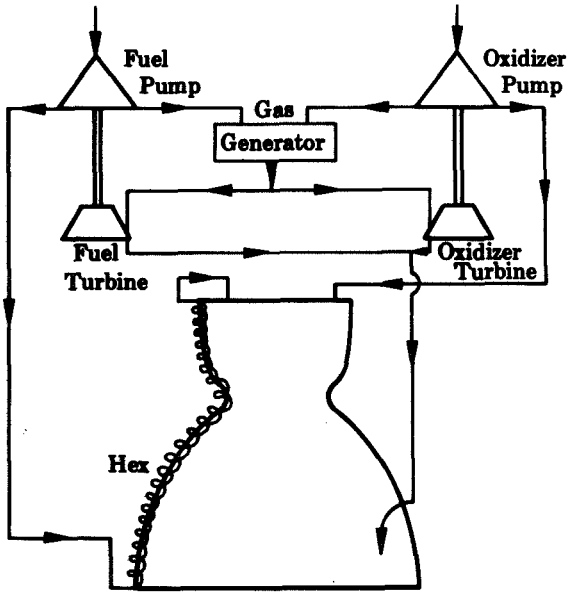


Figure 10. Propellant Flow Schematic for Gas Generator Cycle FD 24234

* Separate parallel turbines are shown in figure 10, and the illustrative schematics for other cycles in the interest of consistency of presentation; however, there are other options for the turbopump arrangement which are discussed later in paragraph h.

Solid propellant charges and decomposed monopropellants have been employed to drive the turbopumps in gas generator type systems. However, the use of a third propellant in deep space mission propulsion systems is objectionable because of the complexity of the added system, and the solid propellant approach is not adaptable to unlimited restart capability. Therefore, operation with a bipropellant gas generator using propellants from the main propellant supply system was considered exclusively. Gas generator operation is simplified for the flox/methane combination by the hypergolicity of the propellants.

The gas generator cycle is capable of providing very high chamber pressure. System pressure drop between the pump discharge and the thrust chamber is lower than in closed cycles, and high pressure ratio turbines that allow near maximum energy extraction from the turbine working fluid are typical. However, any chamber pressure advantage must be analyzed relative to delivered performance because the gas generator flowrate degrades specific impulse. (The specific impulse loss is slightly offset by the energy input to the propellants by the turbopump, but this effect is small). Losses can be reduced through the use of an expansion nozzle downstream of the turbine, or by ducting the turbine discharge into the main chamber nozzle.

c. Tapoff Cycle

The primary difference between the tapoff cycle (figure 11) and the gas generator cycle is the elimination of the gas generator. Instead of a separate combustor to supply the turbine working fluid, hot gases are bled from the main combustion chamber, typically near the injector face, in an area where the injector-induced mixture ratio profile provides a supply of gases at a temperature consistent with turbine material limitations. The primary advantage of the tapoff cycle is the elimination of the weight and complexity of a separate combustor. This advantage may be partially, if not completely, offset by the difficulty of establishing an acceptable injector mixture ratio profile over the entire range of operating conditions.

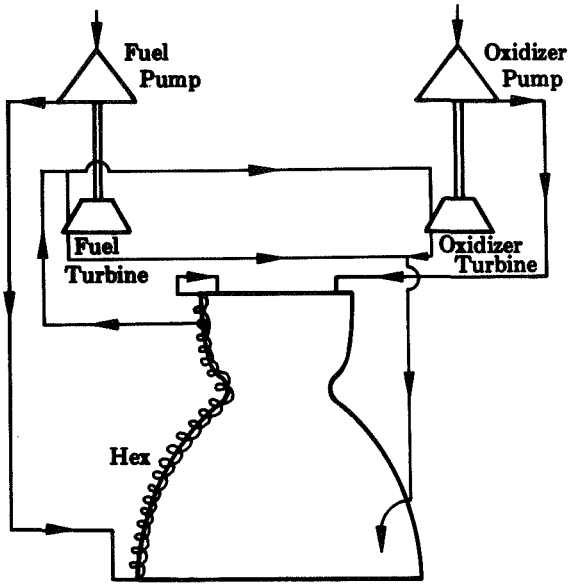


Figure 11. Propellant Flow Schematic for Chamber Tapoff Cycle FD 24235

d. Auxiliary Heat Exchanger Cycle

The auxiliary heat exchanger cycle shown in figure 12 is similar to the gas generator system but uses one of the propellants, rather than combustion products, to drive the turbine. It has essentially the same advantages as the gas generator system, while providing a cleaner, less corrosive turbine working fluid. For the flox/methane propellant combination the working fluid would be methane. The energy level of the fuel is increased in a heat exchanger that might consist of part or all of the regeneratively cooled thrust chamber jacket or might be a separate heat exchanger within the combustion chamber, or a combination of both. When the entire thrust chamber is used as the heat exchanger, the cycle is usually referred to as the fuel tapoff cycle. When a separate heat exchanger is used, it is sized to provide a discharge temperature which must be a compromise between material requirements and cycle performance loss.

e. Expander Cycle

The expander cycle, shown schematically in figure 13, is basically a modified Brayton cycle. The working fluid, usually the fuel, is pressurized by the fuel pump, passed through the thrust chamber jacket

where it picks up energy in providing cooling, and is then expanded through a turbine to drive the propellant pumps. All of the fuel is then injected into the thrust chamber.

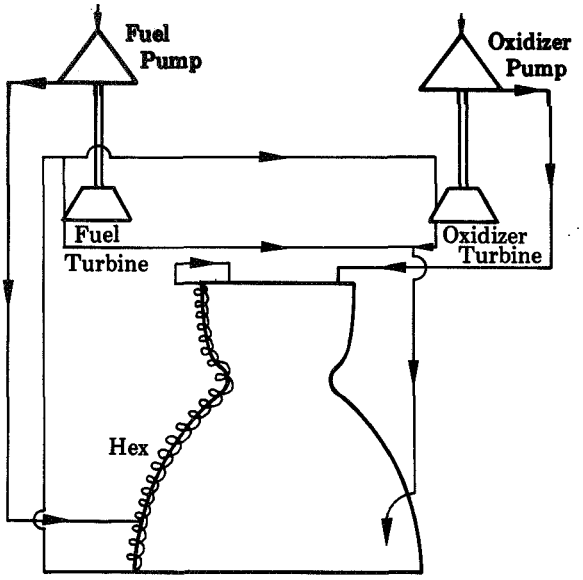


Figure 12. Open Auxiliary Heat Exchanger Cycle FD 24233A

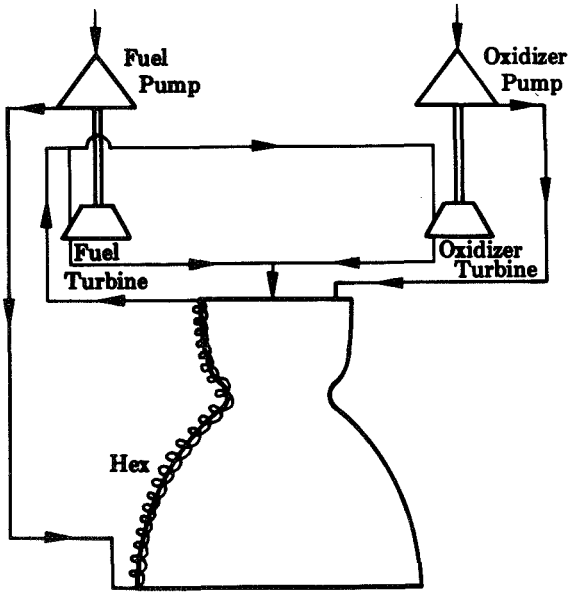


Figure 13. Propellant Flow Schematic for Expander Cycle FD 24230

The RL10 oxygen/hydrogen engine is an expander cycle engine. Its fuel enters the cooling jacket at cryogenic temperatures and supercritical pressure, and the temperature is increased above critical during passage through the jacket. Hydrogen is an excellent fluid for this application, but the physical and thermodynamic properties of methane also make it ideally suited for an expander cycle. The critical pressure is low enough to be readily maintained (673 psia; 464.7 $N/cm^2$) thereby preventing boiling in the jacket, and the critical temperature (343°R; 190.6°K) is low enough to assure 100% quality throughout the turbine even if turbine exit conditions are below the critical pressure.

Generally, 90 to 95% of the fuel is ducted through the turbine in an expander cycle to provide the required turbopump power. A bypass flow of 5 to 10% of the total is considered necessary to provide control margin and assure adequate cycle power. The bypass flow is mixed with the turbine discharge flow upstream of the injector. In this type of system, controlling the turbine bypass flow is a convenient and relatively simple method to maintain a constant thrust level while compensating for propellant inlet conditions and engine-to-engine variations.

The primary advantage of the expander cycle is that all of the propellants are burned in the main thrust chamber and expanded with high efficiency to achieve maximum engine performance. Chamber pressure and mixture ratio are as easily controlled as in the open cycle, and because the expander cycle rocket engine does not require a separate combustion chamber or control to maintain the proper mixture ratio or gas temperature entering the turbine, it is less complex than the gas generator cycle in many respects.

The performance and simplicity advantages of the expander cycle must be weighed against its fuel turbomachinery requirements, which are more stringent than those of open cycles because of the added turbine pressure loss in the fuel circuits. In addition, the expander cycle is subject to maximum chamber pressure limits. As chamber pressure increases, the turbopump power requirements and the available turbine power increase at different rates. Ultimately, the required power increases more rapidly until a chamber pressure limit is reached.

f. Staged-Combustion Cycle

The staged-combustion cycle fuel flowpath, shown schematically in figure 14, is similar to that of the expander cycle up to the heat exchanger exit. At this point, part or all of the fuel is injected into the preburner and ignites with a small percentage of the oxidizer flow to provide a high-temperature, low mixture ratio working fluid to the turbine. Turbine discharge flow is then injected directly into the main combustion chamber, where it reacts with the remaining oxidizer (and fuel). For a given chamber pressure, the oxidizer pump discharge pressure must be considerably higher than for other cycles because a portion of the oxidizer flow must pass through the preburner and turbine before injection into the main chamber. Because most of the oxidizer flow bypasses the preburner, it might be possible with a two-stage oxidizer pump to withdraw the main chamber flow after the first stage to reduce pump power requirements, but this must be evaluated for specific cases.

The staged-combustion cycle offers the same high performance as the expander cycle, but is not as power limited because the turbine inlet temperature is not limited to jacket coolant discharge temperature. Thus, higher chamber pressures are attainable, providing performance exceeding that of any open cycle while offering a competitive package size.

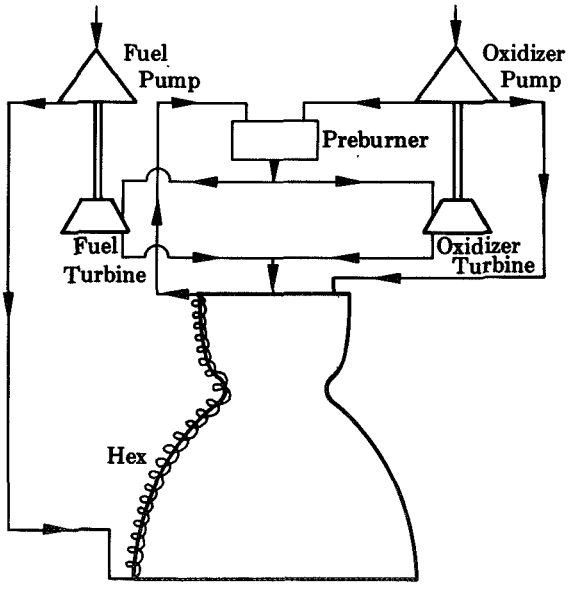


Figure 14. Propellant Flow Schematic for Staged Combustion Cycle FD 24231

The high specific impulse and chamber pressure of the staged-combustion cycle are obtained at the cost of increased pump discharge pressure and high line and heat exchanger internal pressures, as well as the necessity for using high temperature combustion products as the working fluid. As a result, the preburner cycle is generally heavier than other cycles for a given chamber pressure.

g. Composite Expander Cycle

The specific impulse losses of the auxiliary heat exchanger system can be minimized and the pressure limits of the expander cycle can be extended through use of a cycle utilizing a two-stage turbine in the manner shown in figure 15. The total fuel flow is routed from the cooling jacket and expanded through a subsonic turbine stage, as with the expander cycle. The major portion of the fuel is then routed to the injector, and the remainder is expanded through a supersonic turbine stage and discharged overboard through a secondary nozzle. The advantages of the "composite" cycle are (1) the energy derived from chamber cooling is utilized to provide much of the power required to drive the pumps (as in an expander cycle), therefore, performance losses associated with propellant use for turbine drive are minimized; and, (2) the pressure limits and versatility for off-design operation are extended beyond conventional expander cycle limits. Thus, this cycle is particularly well suited where closed cycle power requirements are marginal, and its performance can approach that of the expander cycle.

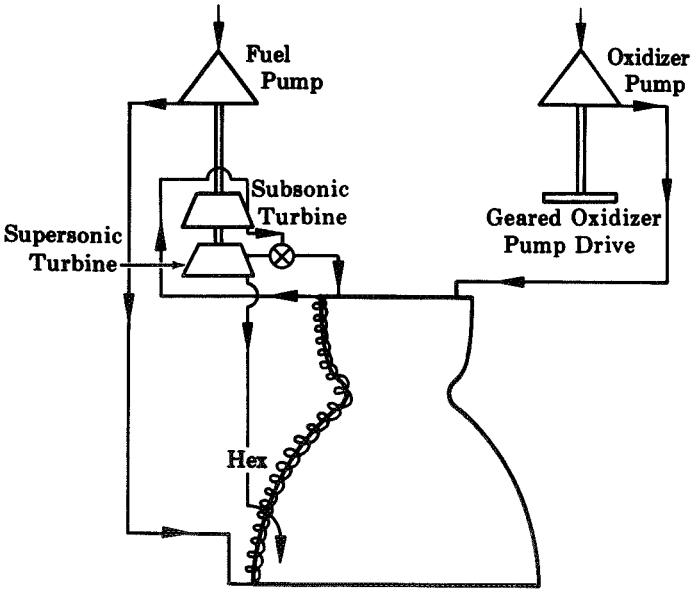


Figure 15. Expander/Gas Generator Composite Cycle FD 24521

h. Turbopump Arrangements

The cycle schematics presented in figures 10 through 15 show a turbopump arrangement with two parallel turbines; however, there are other turbopump configurations to be considered in optimizing the various cycles. The parallel arrangement is compared with three other conventional turbopump arrangements in figure 16; these are separate series turbines driving the fuel and oxidizer pumps, a single turbine driving both pumps directly and a single turbine driving both pumps, but with one driven through a gearbox. Parallel independent drive turbines permit both fuel and oxidizer flowpaths and turbopump speeds to be optimized independently, and in applications where turbine pressure ratios should be minimized, this scheme is advantageous. However, in low thrust applications where the required turbine flowrate is low (as in this study), small turbine admission areas can limit component efficiency.

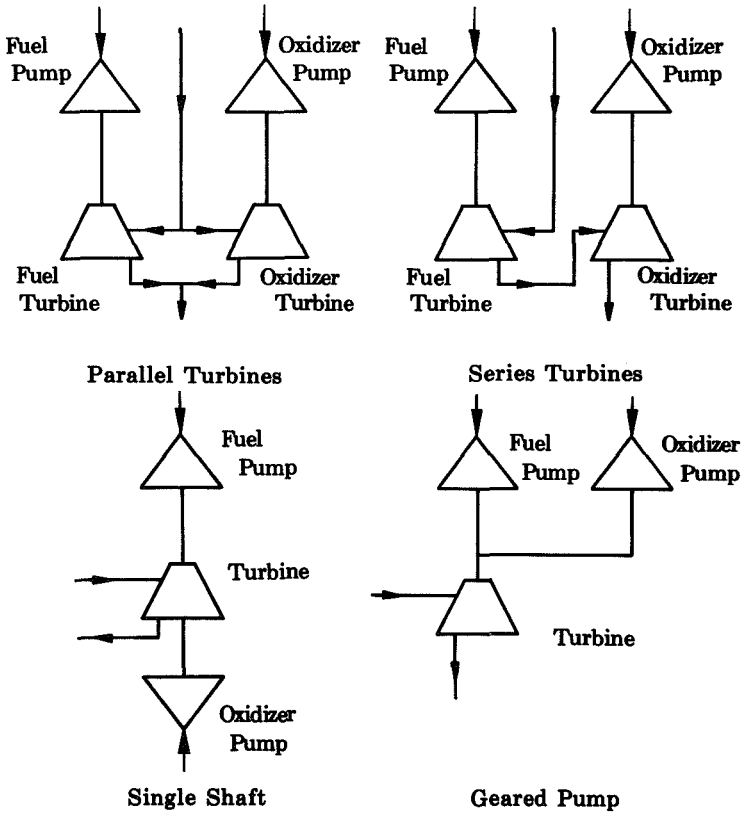


Figure 16. Turbopump Arrangements FD 24237A

Independent fuel and oxidizer turbopump matching is possible with dual series as well as dual parallel turbines. Because of system interactions the series arrangement presents more complicated control require-

ments, but the flow through each turbine is maximized, hence admission problems are less severe than for parallel turbines. The series arrangement is primarily applicable to open cycles, where turbine back pressure is low and the available total turbine pressure ratio is high.

A single turbine driving both pumps directly is perhaps the simplest arrangement and permits weight savings. However, due to the reduction of flexibility through the fixing of all components on a common shaft, turbopump performance cannot fully be optimized to meet system demands.

Use of gearing permits a single turbine to drive both pumps at different rotational speeds, but at a fixed speed ratio. The complexity of the engine system is greatly reduced through the use of a single turbine, but some operating flexibility is lost because of the fixed pump speed ratio. Under certain circumstances in high power transmission applications, gear design considerations may impose a speed limit affecting component efficiency or weight. Generally, in addition to the reduced complexity, the total engine weight (including the gearbox) can be less than that for a two-turbine arrangement.

3. Component Analysis

Before a valid comparison of the various cycle and turbopump arrangements could be made, it was necessary to conduct a preliminary study to optimize operating variables such as pump and turbine speed, turbine inlet pressure, etc. Critical variables were evaluated to establish their effect on cycle performance and turbopump efficiency, and operating limits were defined. In addition, the influence of speed on critical turbopump dimensions and on the oxidizer pump seal rubbing velocity was investigated to assure feasibility for mechanical design. Based on the results of this component analysis, near optimum cycle operating conditions were established to insure that each cycle was compared on a favorable basis.

In evaluating pump performance, the familiar "Worthington" curve, which uses the similarity parameter, specific speed ($N_s$), to relate efficiencies measured in pump tests was used. The flowrates and specific speeds in this study were beyond the range of available curves, so the extrapolated version shown in figure 17 was employed. The extrapolations were made mathematically using a digital computer program based

on curve fits for the available information. The fact that there is little, if any, data for pumps of the sizes considered leads to some question as to the accuracy of the predictions. As discussed later, factors such as mechanical losses represent a greater proportion of the total power, and clearances become more critical in the small units. However, the approach taken was felt to provide reasonable relative values between cases. The absolute level, which is difficult to confirm, is of particular interest in the case of closed cycles. The expander cycle is somewhat limited in available turbopump power, and low turbomachinery efficiencies might prevent achievement of acceptable power balances. However, in Task II existing design systems were used to generate estimates of the various elements of pump efficiency for the configurations established, and the overall efficiencies determined from these values indicated that the values obtained from figure 17 were not overly optimistic.

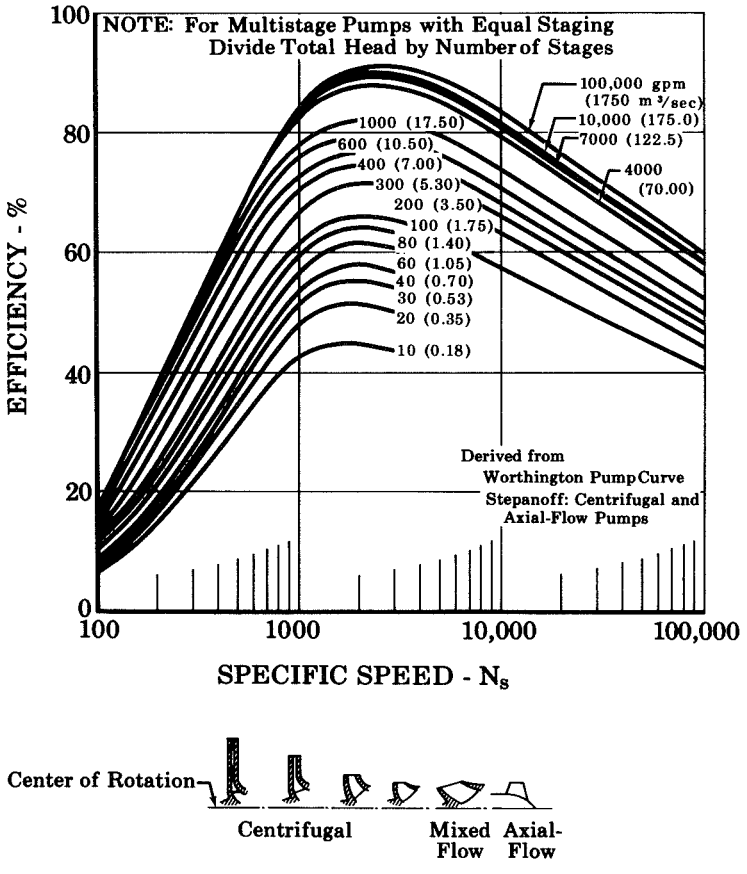


Figure 17. Efficiency of a Centrifugal Pump Stage at Design Point FD 23986A

a. Oxidizer Pump

With the exception of the preburner cycle, the oxidizer pump requirements are similar for all cycles considered in this study. The pump discharge pressure is established by the chamber pressure and the injector and control valve pressure losses. The oxidizer pump flowrate for the gas generator and tapoff cycles is approximately 1.0% higher than for the other cycles by the amount of flow required to drive the turbine, but the effects of this difference on the physical characteristics of the pump are small and were neglected. Therefore, for the purposes of analysis, the same pump requirements were used at each design point for all but the preburner cycle. The injector pressure loss was set at 25% of chamber pressure and the design point control valve pressure loss was assumed to be 50 psia (34.47 $N/cm^2$), yielding the following:

| | Design Point 1 (800 psia; 551.6 $N/cm^2$) | Design Point 2 (500 psia; 344.7 $N/cm^2$) |
|---|---|---|
| Flowrate | 53.0 gpm (12.02 $m^3/sec$) | 53.6 gpm (12.17 $m^3/sec$) |
| Discharge Pressure | 1050 psia (723.9 $N/cm^2$) | 675 psia (465.4 $N/cm^2$) |

The oxidizer pump characteristics for each of the design points were evaluated over a speed range from 5000 to 50,000 rpm (523.6 to 5236 rad/s). Figure 18 presents calculated oxidizer pump efficiencies vs speed for both design points. Corresponding impeller diameters and blade heights are shown in figures 19 and 20 for blade tip angles of 22.5 and 90 deg (0.40 and 1.80 rad), which are the usually accepted extremes for centrifugal pumps. Maximum suction specific speed was assumed at 25,000. Suction specific speeds of 30,000 to 40,000 have been demonstrated in cryogenic pumps, and values of 27,000 have been demonstrated in $LF_2$ tests of a modified RL10A3-3 oxidizer pump. However, in view of the small physical size of the pump, and the fact that contract specified requirements could be met using it, the 25,000 level was selected. Required pump inlet pressures are shown in figure 21; the maximum is 36.8 psia (25.37 $N/cm^2$) at 50,000 rpm (5236 rad/s).

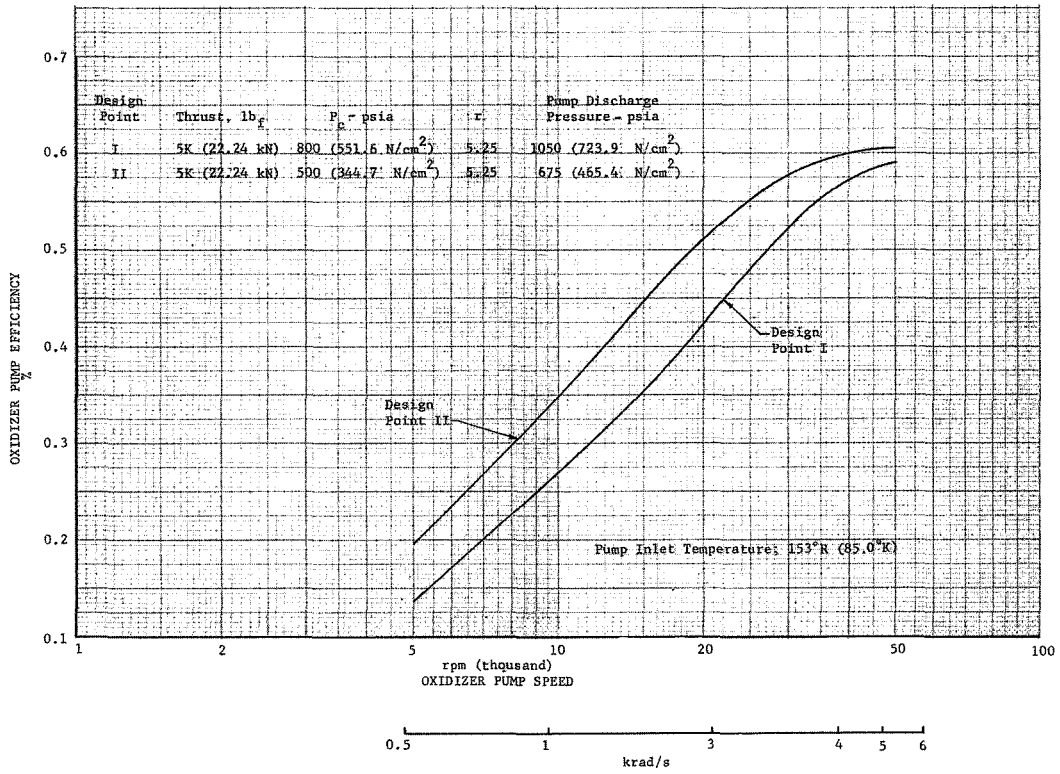


Figure 18. Variation in Oxidizer Pump Efficiency With Speed DF 70829

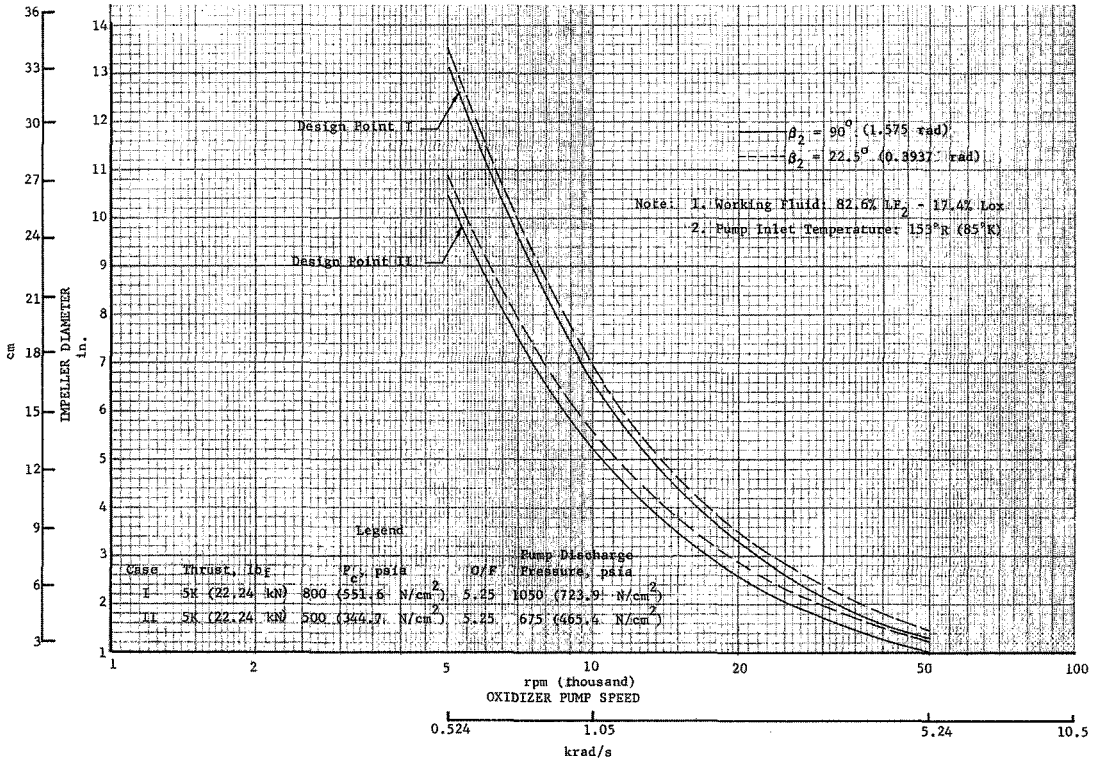


Figure 19. Variation in Required Oxidizer Pump Impeller Diameter With Speed DF 70830

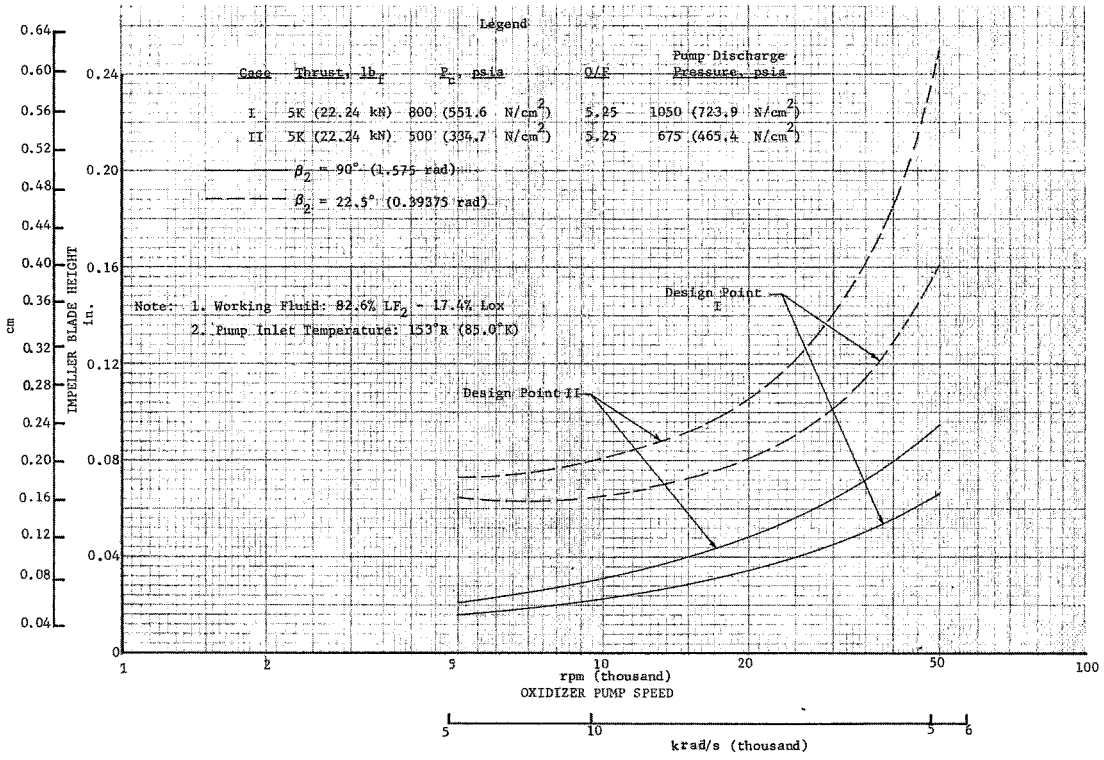


Figure 20. Variation in Required Oxidizer Pump Impeller Blade Height With Speed

DF 70831

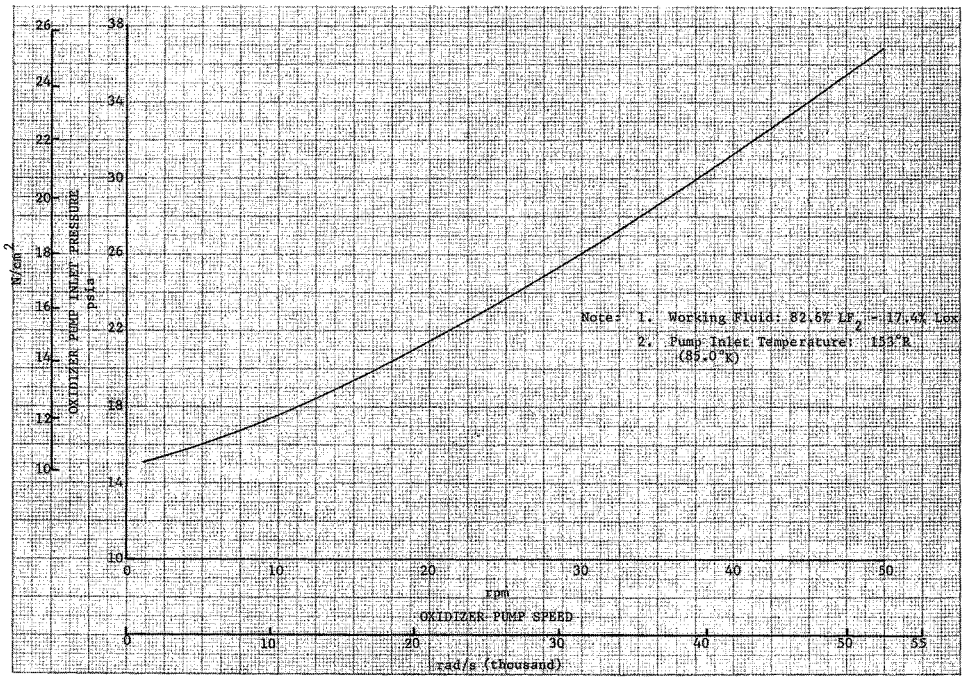


Figure 21. Oxidizer Pump Inlet Pressure Requirement for 25,000 Suction Specific Speed

DF 70832

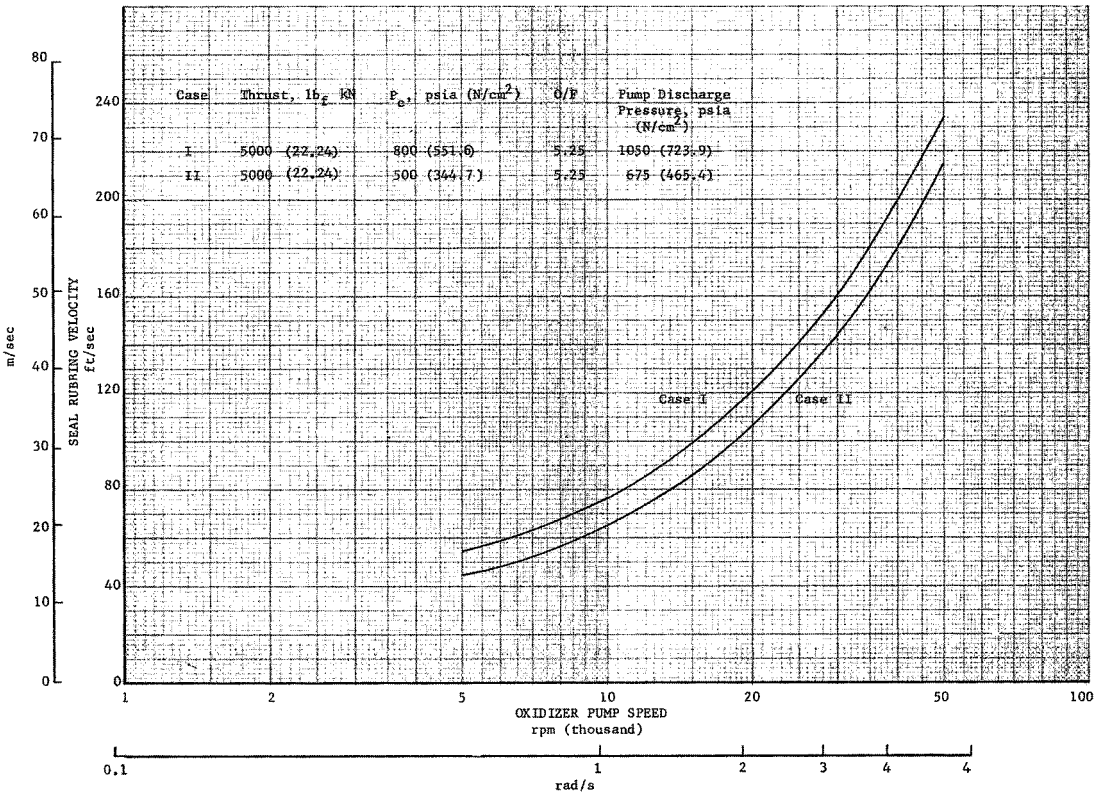


Figure 22. Variation in Required Oxidizer Pump Seal Rubbing Velocity With Speed

DF 71768

Shaft seal rubbing velocity calculations, figure 22, were based on dimensions associated with a solid shaft designed to transmit the required torque. Rubbing velocities up to 145 ft/sec (44.20 m/sec.) have been demonstrated for fluorine compatible seal materials in tests at Pratt & Whitney Aircraft (Reference 8). However, this was accomplished with seal assemblies and loadings consistent with the RL10 engine oxidizer pump. By using reduced loadings consistent with the pump configuration, as was done in the Task II preliminary design, increases in velocity should be obtainable with existing materials technology. At this point in the program, the loading could not be established, but a limit of 180 to 190 ft/sec (54.86 to 57.91 m/sec) was established as a reasonable target.

The base speed of 37,500 rpm (3927 rad/s) was chosen for cycle comparison purposes at both design points, since the knee points in the efficiency vs speed curves occurred at approximately this speed and the assumed seal rubbing velocity limit was being approached. The base

speed was held constant, but trade factors were established to define the effect of oxidizer pump speed variations on cycles.

The rotational speeds considered resulted in bearing DN's that are relatively low (less than $10^6$) which was considered desirable to permit application of a rolling element bearing operating in liquid flox. Flox-cooled bearings can be mounted forward of any shaft seals so that shaft overhang can be minimized, thereby reducing the possibility or severity of critical speed problems. Minimal shaft overhang also reduces radial deflections and permits tight clearances to be maintained. This is particularly desirable in view of the small impeller blade heights and diameters for which clearances must be optimized (as must other pump features) to assure satisfactory performance.

b. Fuel Pump

(1) Open Cycles

Fuel pump requirements for open cycles are predictable with reasonable accuracy without extensive cycle analysis. The pump discharge pressure is established by the chamber pressure and the pressure losses in the cooling jacket and the injector. For this study, the fuel injector pressure loss was set to provide a fuel-to-oxidizer injection momentum ratio of 2, and cooling jacket pressure loss results were taken from the preliminary regenerative cooling analysis. As in the instance of the oxidizer pump, flowrates vary slightly with the different cycles, but the effects on the physical characteristics of the pump are small enough to be negligible. The open cycle pump discharge pressures used for this initial evaluation were:

| | Design Point 1 (800 psia: 551.6 $N/cm^2$) | Design Point 2 (500 psia: 344.7 $N/cm^2$) |
|---|---|---|
| Flowrate | 53.5 gpm (12.14 $m^3/sec$) | 53.9 gpm (12.23 $m^3/sec$) |
| Discharge Pressure | 1220 psia (84.12 $N/cm^2$) | 754 psia (519.9 $N/cm^2$) |

The characteristics of two-stage centrifugal pumps* for the two design points were evaluated over a speed range from 10,000 rpm to 100,000 rpm (1047 to 10470 rad/s). Figure 23 shows the calculated fuel pump efficiencies vs speed. The impeller diameters and blade heights, again for 22.5 and 90-deg (0.3927 and 1.571 rad) blade angles, are shown in figures 24 and 25. Required pump inlet pressures calculated at a suction specific speed of 25,000 are shown in figure 26; the maximum was 27.2 psia (12.34 N/cm$^2$) at 100,000 rpm (10470 rad/s).

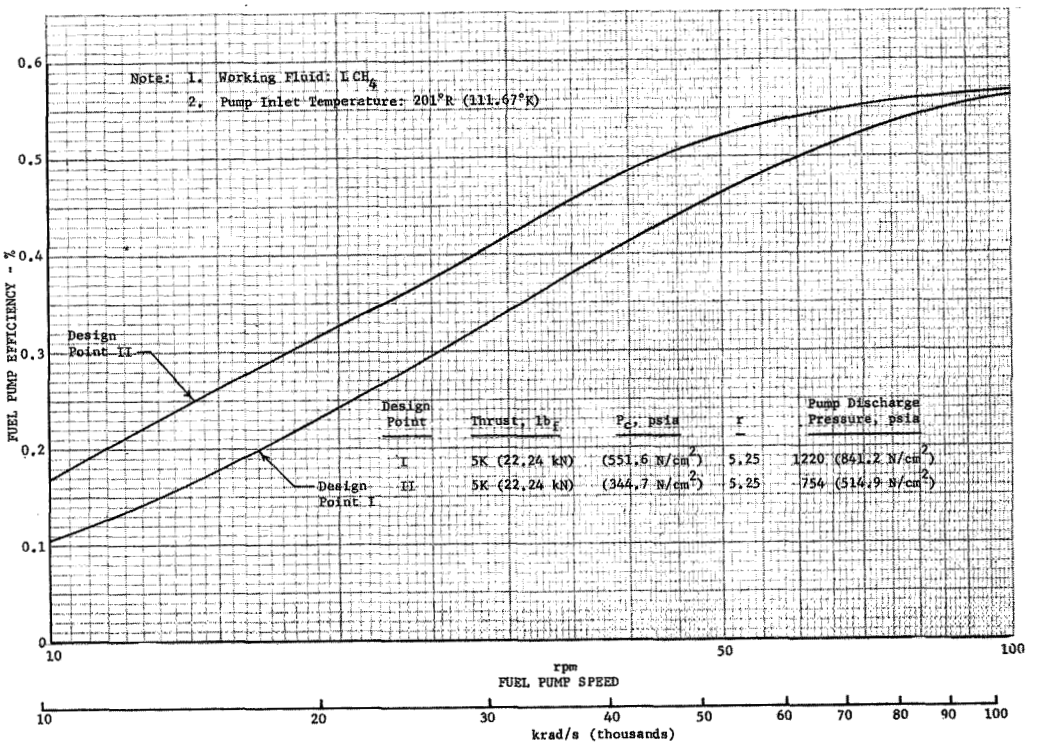


Figure 23. Variation in Fuel Pump Efficiency With Speed DF 70834

* One-stage pumps were not considered because of the reduced efficiency resulting from the halved specific speed of one, as compared to two stages. For the fuel pump speeds of interest, this was predicted to amount to approximately 12 percentage points in efficiency.

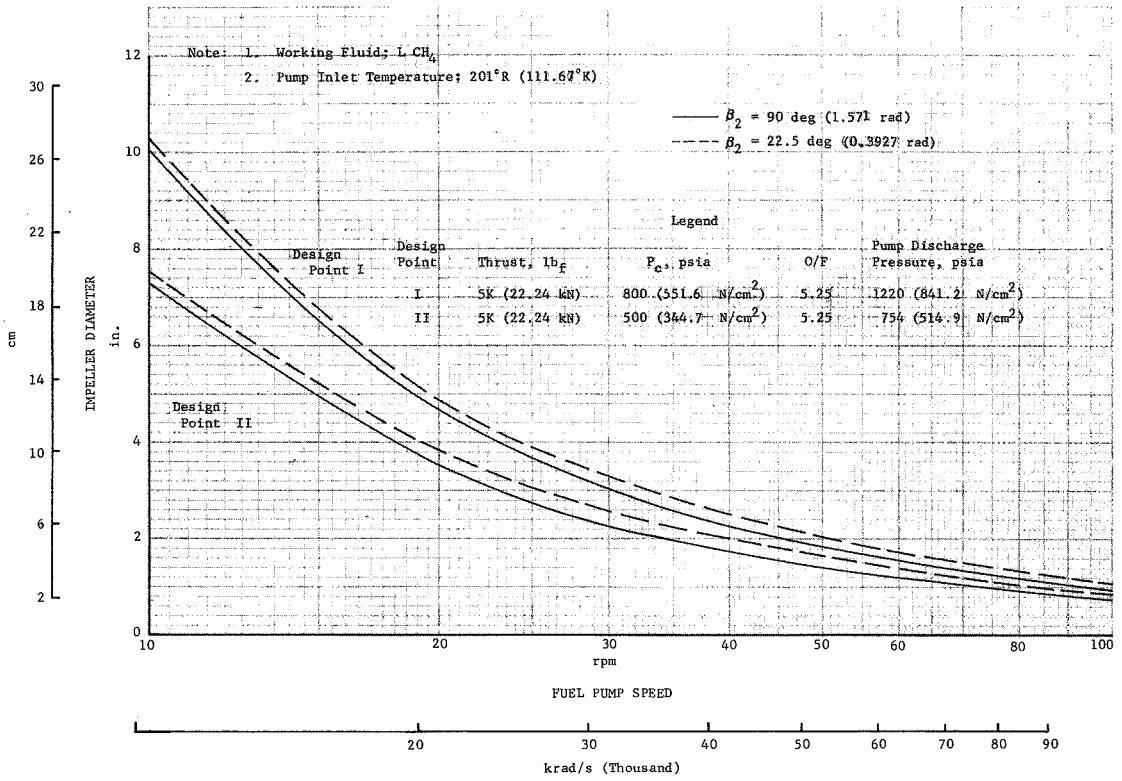


Figure 24. Variation in Required Fuel Pump Impeller Diameter With Speed DF 70835

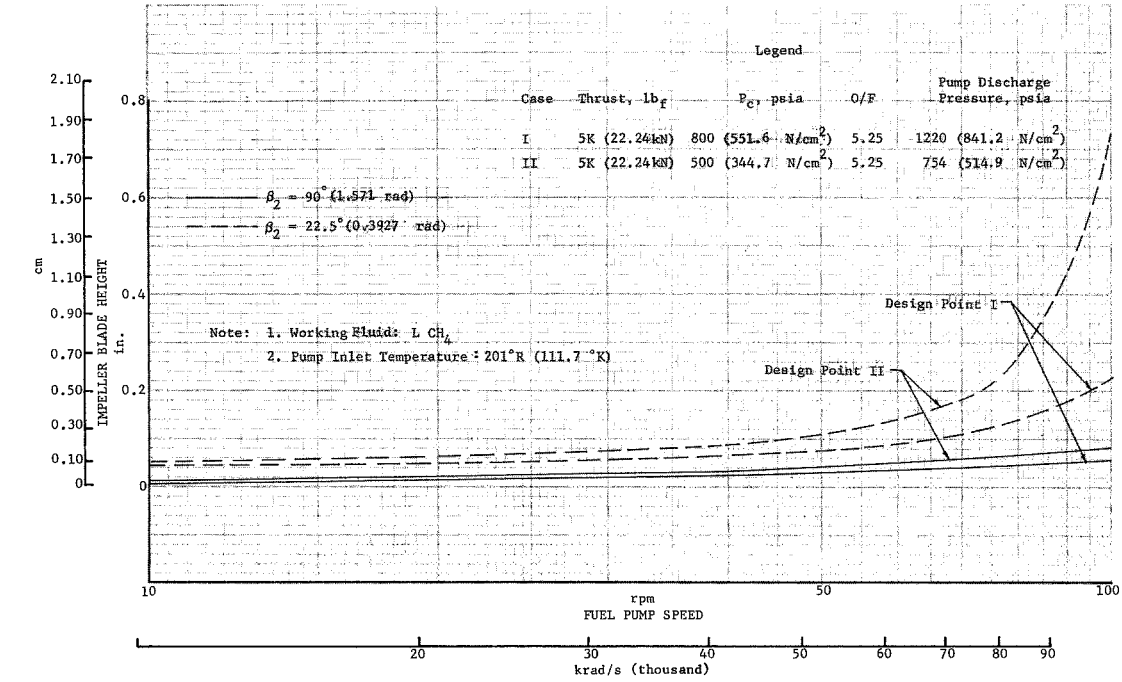


Figure 25. Variation in Required Fuel Pump Impeller Blade Height With Speed DF 70836

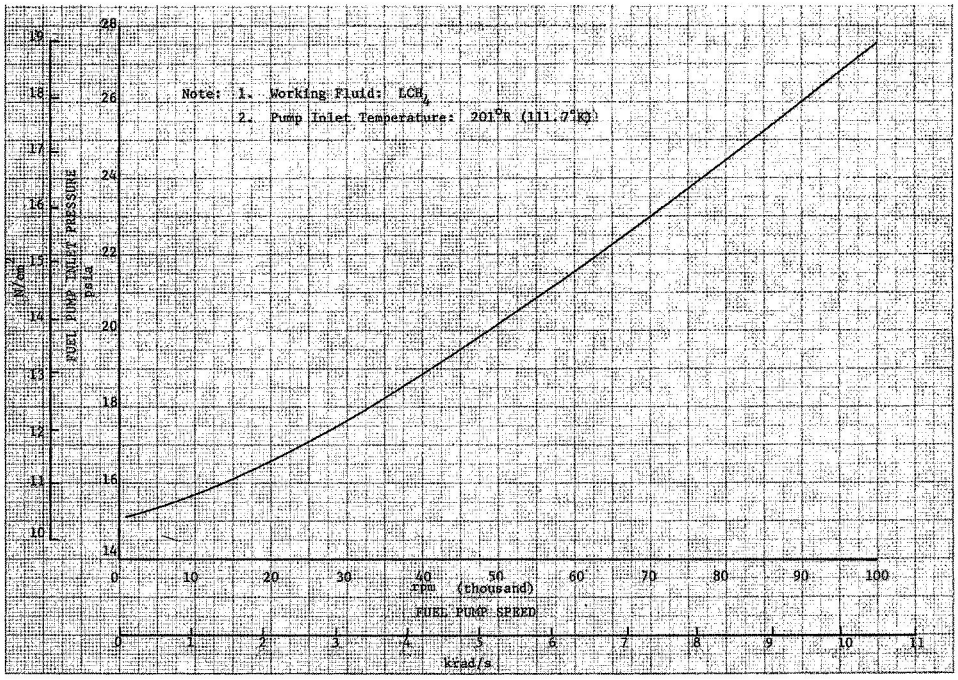


Figure 26. Fuel Pump Inlet Pressure Requirement for 25,000 Suction Specific Speed

DF 70837

(2) Closed Cycles

For closed cycles, fuel pump discharge pressure requirements are increased over those of open cycles so that the pressure ratio across the turbine necessary to provide pump power can be attained. Because of system interactions, it was necessary to accomplish preliminary cycle calculations to establish the necessary levels. For the calculations, an oxidizer pump speed of 37,500 rpm (3927 rad/s), turbine speed equal to fuel pump speed, and 10% excess horsepower were assumed. These assumptions are based on a single turbine driving both pumps through a gearbox. The oxidizer speed was based on the maximum value established previously, and the 10% excess power was based on typical margins allowed with expander cycle engines. Expander cycle fuel pump efficiencies vs fuel pump speed at the 800-psia (551.6 $N/cm^2$) design point are shown in figure 27. It will be noted that the efficiency is 8% to 15% lower than for the open cycle pumps at the same speed. This is because of the increased headrise and consequently lower specific speed. Reasonable variations in the turbine and oxidizer pump speeds were found to have only small effects on fuel pump requirements. The pump diameters and

blade heights are also shown in figure 27. Diameters are larger than those of open cycle fuel pumps because of the additional pressure rise requirements, and blade heights are correspondingly smaller.

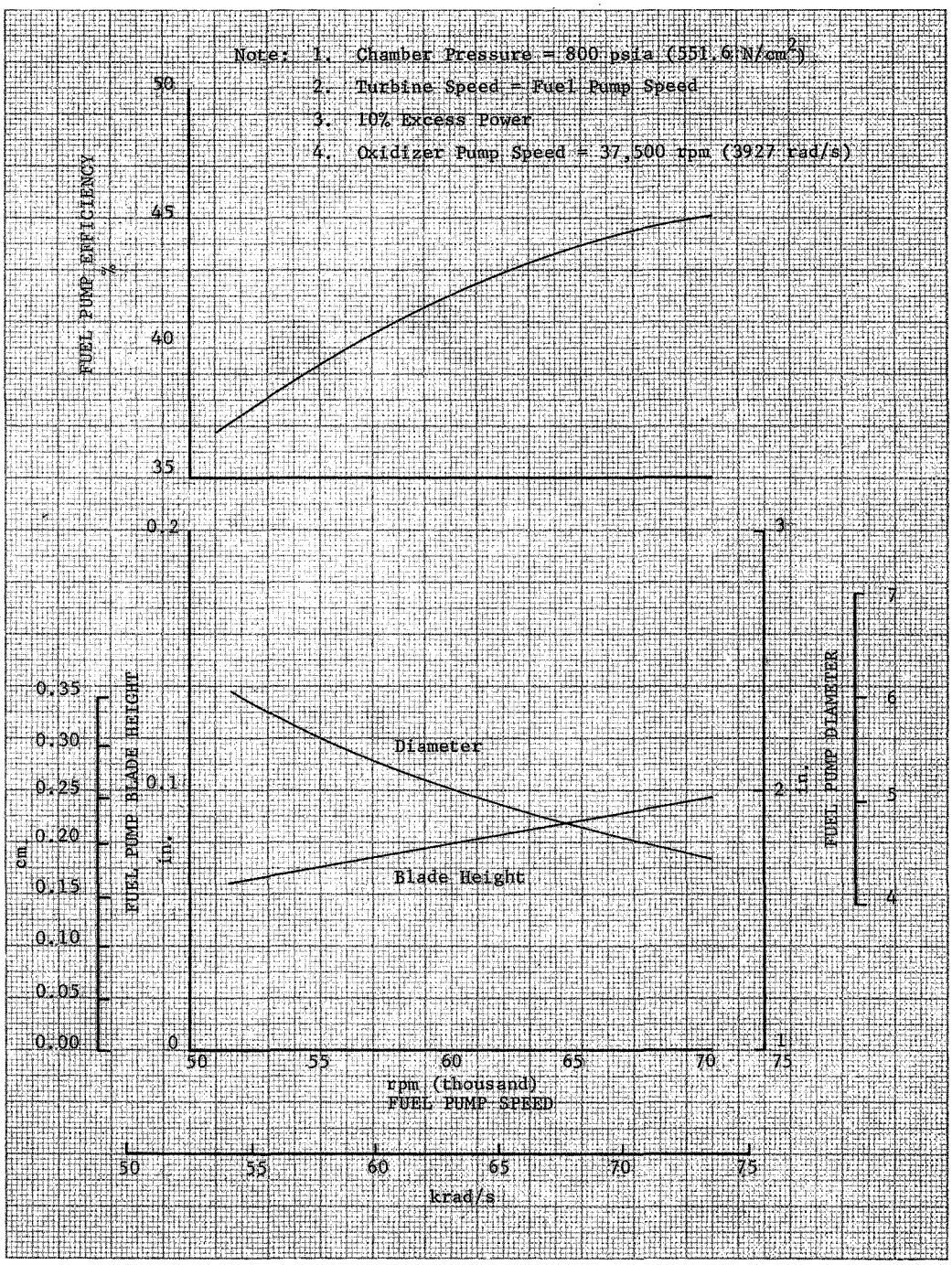


Figure 27. Expander Cycle Fuel Pump Characteristics DF 70838

c. Turbine

(1) Open Cycles

Open cycle turbine efficiencies were investigated parametrically using the method outlined by Balje in Reference 9. Single stage turbines with pressure ratios of 3 to 30 and two-stage turbines with pressure ratios of 20 to 30 were considered. Tip speed was limited to 1700 ft/sec (518.2 m/sec), a level considered to be a reasonable maximum from the stress standpoint, in all cases.

Two-stage turbines and turbines with pressure ratios greater than 20 produced little performance improvement relative to increased design complexity; consequently, a single stage turbine with a pressure ratio of 20 was tentatively selected for the cycle comparison. Turbine efficiencies for a single turbine operating at a pressure ratio of 20 and driving both pumps through a gearbox at a constant turbine rotational speed of 75,000 rpm (78540 rad/s) are shown as a function of turbine inlet pressure in figure 28 for the auxiliary heat exchanger cycle at the design points. Turbine requirements for the other open cycles are nearly identical to those of the auxiliary heat exchanger cycle, and therefore the effects are similar. As shown in figure 28, an increase in efficiency occurs as the turbine inlet pressure is reduced. This increase results from the lower turbine exit density and consequently improved specific speed characteristics. The turbine diameter was limited by the tip speed to 5.2 in. (13.21 cm) for 75,000 rpm (78540 rad/s). Resulting blade heights and arcs of admission are shown in figures 29 and 30. The values shown are not significantly different than those of some presently operational turbines; therefore design problems should be minimal.

Turbine efficiency vs speed characteristics were investigated for the auxiliary heat exchanger cycle with the results shown in figure 31. This plot was prepared for a constant turbine inlet pressure of 300 psia or 206.8 $N/cm^2$ (based upon cycle considerations, overall losses are relatively insensitive to inlet pressure); note that the turbine speed could be reduced to as low as 55,000 rpm (57600 rad/s) without incurring a severe efficiency penalty.

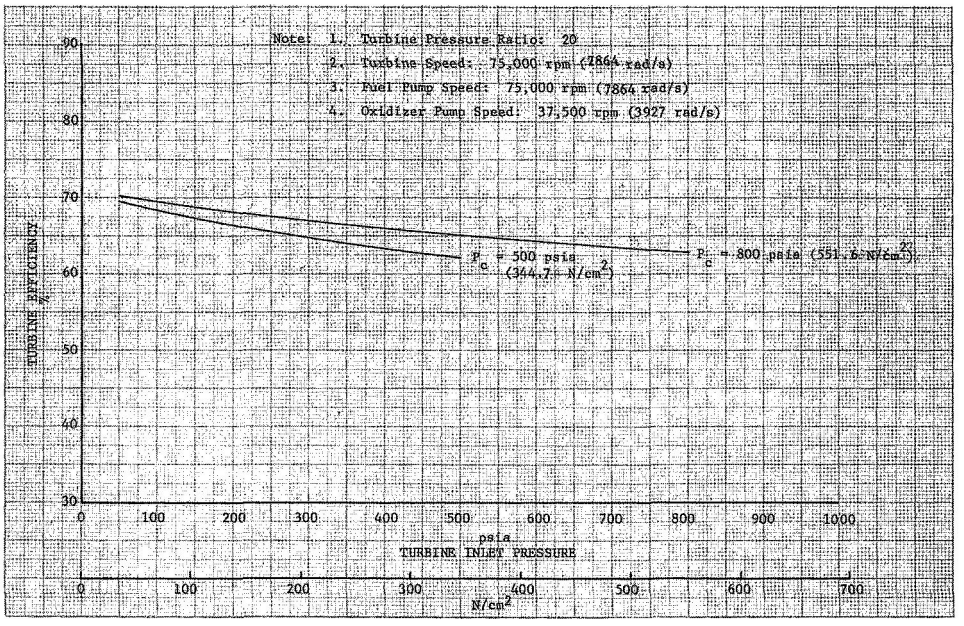


Figure 28. Auxiliary Heat Exchanger Turbine Efficiency vs Inlet Pressure (Single Stage Partial Admission Turbine) DF 70839

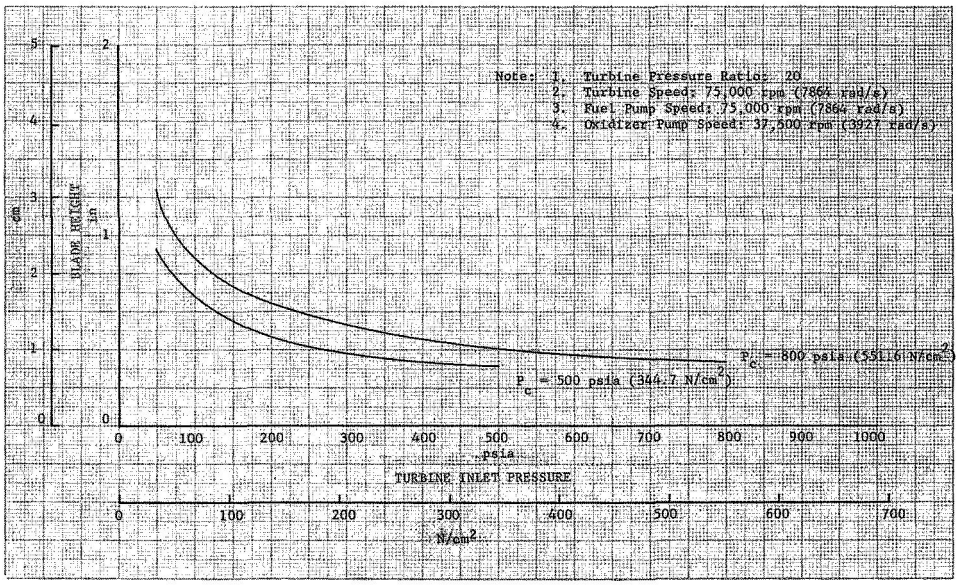


Figure 29. Auxiliary Heat Exchanger Turbine Blade Height vs Inlet Pressure (Single Stage Partial Admission Turbine) DF 70840

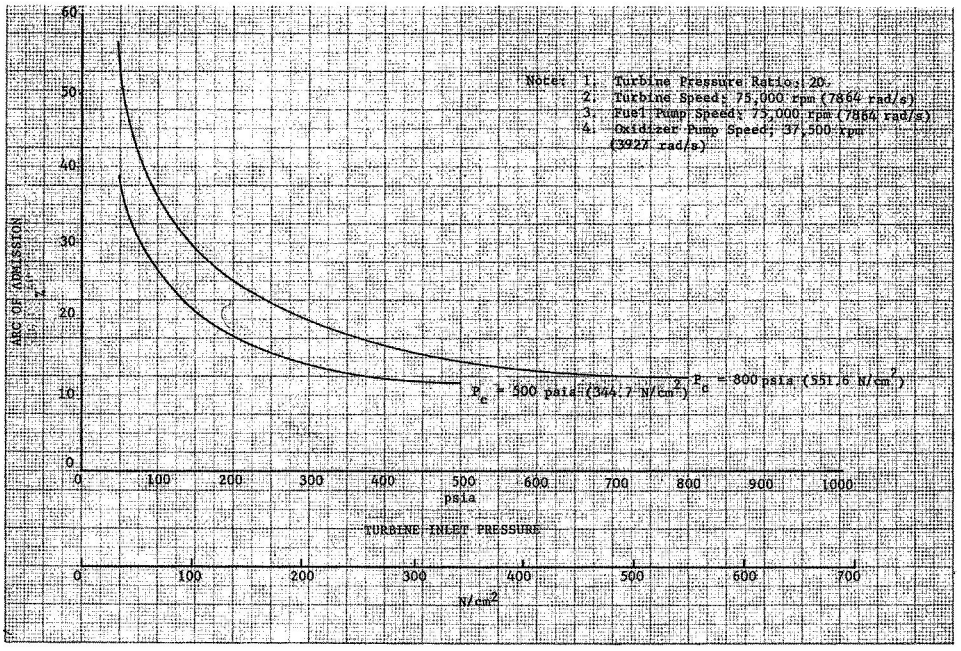


Figure 30. Auxiliary Heat Exchanger Turbine Arc of Admission vs Inlet Pressure (Single Stage Partial Admission Turbine) DF 70841

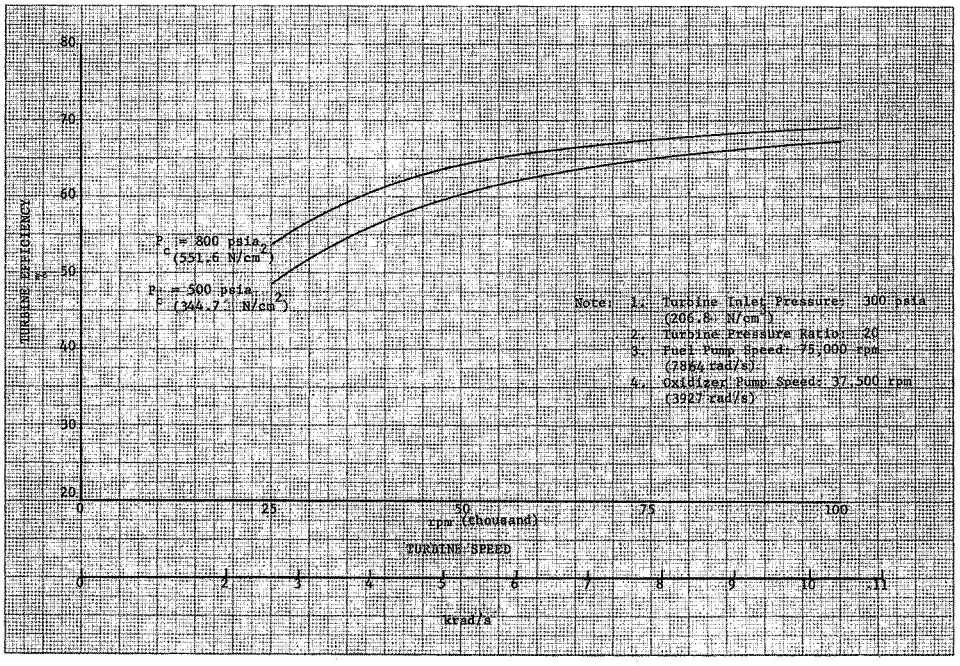


Figure 31. Auxiliary Heat Exchanger Turbine Efficiency vs Speed (Single Stage Partial Admission Turbine) DF 70842

Design point performance of the auxiliary heat exchanger cycle was also estimated for series and parallel turbine configurations, again using an oxidizer-side turbomachinery speed of 37,500 rpm (3927 rad/s) and a fuel-side turbomachinery speed of 75,000 rpm (7854 rad/s). The following efficiencies were predicted:

Turbine Efficiency Comparison
Auxiliary Heat Exchanger Cycle

| | Fuel Pump Drive Turbine Efficiency, % | Flox Pump Turbine Drive Efficiency, % | Overall Turbine Efficiency,% |
|---|---|---|---|
| Parallel Turbine | | | |
| 800 psia (551.6 $N/cm^2$) Design | 64.5 | 54.0 | 59.4* |
| 500 psia (344.7 $N/cm^2$) Design | 60.3 | 50.1 | 53.7* |
| Series Turbines | | | |
| 800 psia (551.6 $N/cm^2$) Design | 67.1 | 68.3 | 67.7* |
| 500 psia (344.7 $N/cm^2$) Design | 63.2 | 62.0 | 62.5* |
| Single Turbine Geared Drive | | | |
| 800 psia (551.6 $N/cm^2$) Design | -- | -- | 65.3 |
| 500 psia (344.7 $N/cm^2$) Design | -- | -- | 64.9 |

*Equivalent Efficiency

Because of the reduced admission arcs for parallel turbines, compared to a single-geared turbine, the equivalent overall efficiency is reduced by 5.9% for an 800-psia (551.6 $N/cm^2$) system, and by 11.2% for the lower chamber pressure. For series turbines, each of which passes the total flow, a minor advantage (2.4%) is shown at the higher pressure design point, but this disappears at the lower chamber pressure level.

(2) Closed Cycles

Based upon preliminary cycle calculations made to permit investigation of turbomachinery requirements, the turbine power necessary for the expander cycle was 70 hp (52200 W) for the 500-psia (344.7-$N/cm^2$) design point, and 147 hp (109600 W) for the 800-psia (551.6-$N/cm^2$) design point. Respective pressure ratios of 1.32 and 1.79 were required to

balance the cycles. The turbine efficiencies for this cycle showed minimal variation over a speed range from 37,500 to 50,000 rpm (3927 to 5236 rad/s) for the 500-psia (344.7-N/cm$^2$) design point, and from 60,000 to 75,000 rpm (6283 to 8273 rad/s) for the 800-psia (551.6 N/cm$^2$) design point. The turbine characteristics in these speed ranges were:

| | Expander Cycle | |
|---|---|---|
| | Design Point 1 (800 psia; 551.6 N/cm$^2$) | Design Point 2 (500 psia; 344.7 N/cm$^2$) |
| Efficiency | 68 to 70 % | 70 to 73 % |
| Diameter | 3.0 in. (7.62 cm) | 3.0 to 3.3 in. (7.62 to 8.38 cm) |
| Blade Height | 0.260 to 0.265 in. (0.661 to 0.678 cm) | 0.36 to 0.37 in. (0.915 to 0.940 cm) |
| Arc of Admission | 14.4 to 14.5 % | 19 to 20 % |

The dimensions for the closed cycle turbines are smaller than those shown in figures 29 and 30 for open cycle machines. There is a general lack of experimental data for turbines of these sizes, and therefore the design of turbines for closed cycles may be somewhat more difficult than for open cycles.

d. Controls

No effort was made to define control characteristics for the preliminary cycle analysis; however cycle requirements were reviewed to assure that required control pressure losses were provided for. The only instance where a specific allowance was required was for an oxidizer flow control valve, and for this component a pressure loss of 50 psid (34.47 N/cm$^2$) was assumed for all cycles.

With respect to turbine power controls, a turbine bypass control was assumed for the expander cycle. Thus, the only requirement was an area parallel to the turbine which imposed no restriction.

Throttling controls were assumed for open cycles. The large pressure differential between the pump discharges and the turbine inlet in open cycles is available for control purposes and for component losses. Therefore, with a turbine inlet pressure of 300 psia (206.8 N/cm$^2$, adequate

differential pressures are available for control without additional power penalties. For the gas generator cycle, controls were considered to be located in the liquid feed lines upstream of the gas generator. At the turbine inlet temperatures being considered, only minimum mixture-ratio perturbations can be tolerated so mixture ratio as well as total flow would have to be controlled. The control valve effective areas will be small; the effective areas calculated for cavitating venturi type controls for Design Point 1 were 0.0011 and 0.0035 $in.^2$ (0.00710 and 0.0026 $cm^2$) for the fuel and oxidizer controls, respectively. These represent diameters of 0.021 and 0.037 in. (0.0534 and 0.0940 cm) which might present problems in development, but do not affect cycle power requirements.

e. Gas Generator

Difficulty has been commonly encountered in achieving high combustion efficiencies with gas generators burning hydrocarbon fuels at low oxidizer-to-fuel ratios. For lox/RP combinations, combustion temperature has been found to drop off more rapidly than the calculated equilibrium flame temperature as mixture ratio is reduced. (See figure 32.) This dropoff is caused by the practical problems of achieving efficient combustion near the flammability limits and by difficulty in achieving equilibrium fuel decomposition at low temperatures (1500 to 2200°R; 833.3 to 1222°K); however, the phenomenon also reflects errors in the calculated equilibrium temperature that result because thermodynamic data for the decomposition products are incomplete. Similar problems can be expected with flox/light hydrocarbon combinations; however, while experimental data for lox/RP are readily available, no such data are available for flox/light hydrocarbon combinations. In view of the lack of experimental data, a gas generator combustion efficiency ( $\eta c^*$) of 95% was arbitrarily selected for the flox/methane combination. Based on oxygen/RP data, this appears to be a somewhat optimistic number, but it was felt that a lower value which would penalize performance was not justified since, in practice, somewhat lower efficiencies would not seriously affect the cycle.

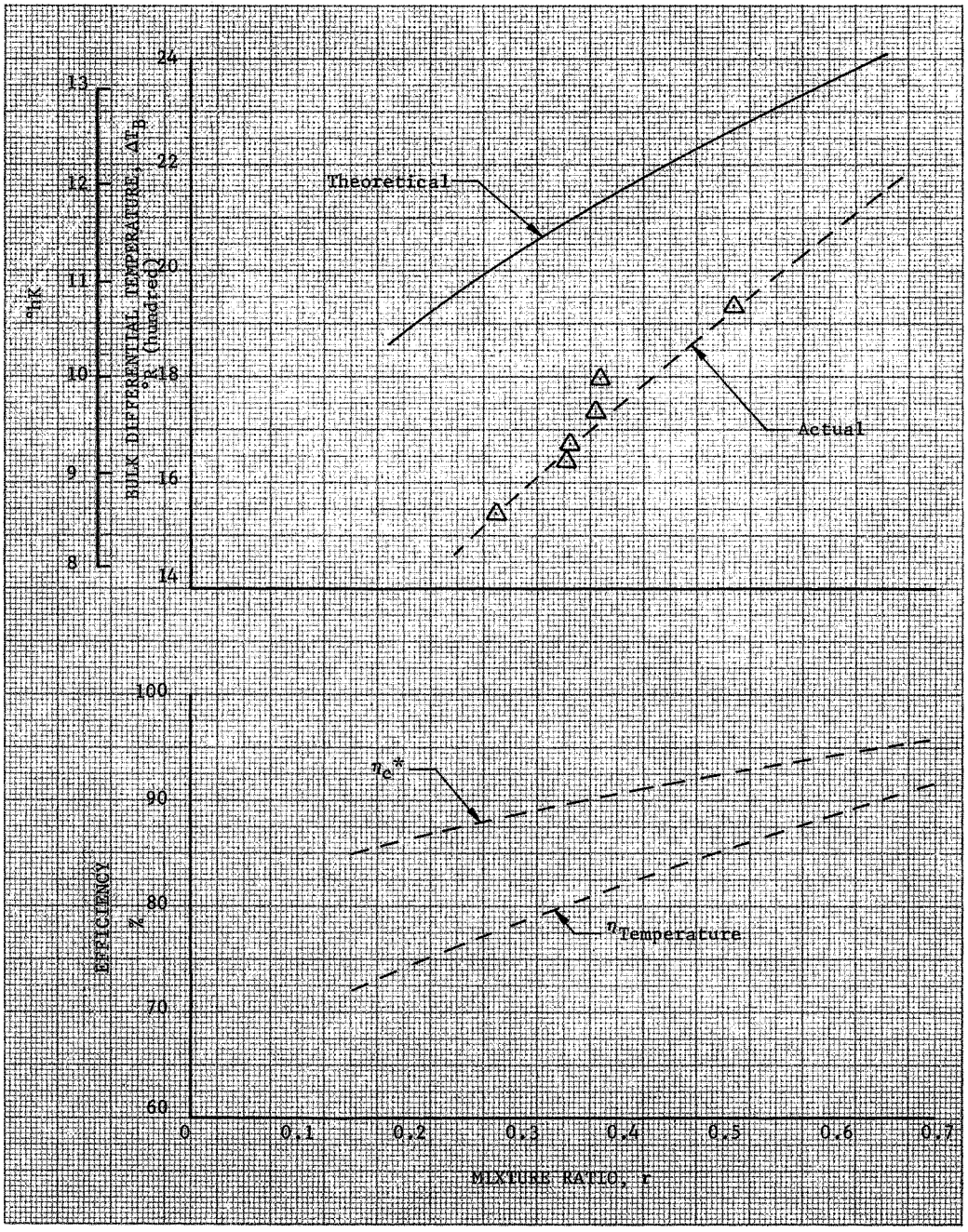


Figure 32. Comparison of Theoretical With Actual Gas Generator Performance (LOX/RP-1)

DF 70843

4. Matrix Reduction

The six cycles, four turbopump arrangements, and two design points specified by the contract plan created a matrix of 48 combinations to be considered in the preliminary cycle analysis. However, not all turbopump arrangements are practical with each of the cycles or design points and detailed consideration of such combinations was not warranted. For this reason, a preliminary screening was made to eliminate those cycle-turbopump-design point combinations that showed obvious disadvantages. The results of this screening are summarized in table VI. Circled numbers, indicating the design point, are shown where cycle performance calculations were completed. Where one or both design points are not listed, the cycle-turbopump combination was eliminated from further consideration on the basis of the reason given.

Cycle calculations were completed for the gas generator, chamber tapoff, and auxiliary heat exchanger cycles for both design points and for all four turbopump configurations. The results for these open cycles indicated little or no advantage for dual series or parallel turbines. Therefore for the closed cycles where turbine admission area is more critical because of the increased working fluid density and the inherent problem of control system complexity is compounded by thrust chamber-turbopump interactions, dual turbines were not considered. The geared drive single turbine and the single-turbine, direct drive configurations were evaluated for the expander cycle but the cycle could not be balanced (i.e., power was not adequate) at Design Point 1 unless rotational speeds of over 37,500 rpm (3926 rad/s) were considered. From the standpoint of oxidizer seal rubbing velocities, 37,500 rpm (3926 rad/s) was considered to be a maximum; therefore, the direct drive configuration was not considered acceptable.

The primary advantage of the staged combustion cycle is its capability for higher pressure operation than the expander cycle, which is less complex, so it was evaluated only at the higher pressure design point (Design Point 1). The composite cycle provides advantages over the expander cycle only in cases where the expander cycle is power-limited, and since neither of the expander configurations investigated

were found to be power-limited at their design point, the composite cycle was not investigated in detail.

5. Cycle Performance

As indicated in table VI, cycle performance was computed for the gas generator, auxiliary heat exchanger, expander, and preburner cycles. The thrust chamber, injector, and control system pressure drops used were defined above. For the open cycles, the turbine exhaust gases were expanded to the main thrust chamber exit pressure using a nozzle thrust coefficient efficiency of 97%. Fuel leakage for bearing and gear cooling was estimated at 0.05 lb/sec (0.0227 kg/sec) for all cases. Where applicable, gearing losses were assumed to be 5% of the total geared pump horsepower.

a. Auxiliary Heat Exchanger Cycle

Single-stage turbines with pressure ratios of 3, 10, 20, and 30 and two-stage turbines with pressure ratios of 20 and 30 were evaluated for the auxiliary heat exchanger cycle at turbine inlet pressures ranging from the main thrust chamber pressure down to 50 psia (34.47 $N/cm^2$). The engine impulse losses associated with fuel usage for turbine drive are shown as a function of turbine inlet pressure in figure 33 for Design Point 1 and in figure 34 for Design Point 2. Operating conditions assumed in generating these plots were:

1. Turbine inlet temperature = 1700°R (944.4°K)
2. Turbine speed = 75,000 rpm (7854 rad/s)
3. Fuel pump speed = 75,000 rpm (7854 rad/s)
4. Oxidizer pump speed = 37,500 rpm (3926 rad/s).

The curves in figures 33 and 34 show that reductions in cycle losses are achieved as turbine pressure ratio is increased and that, for any given pressure ratio, the effect of turbine inlet pressure is small. A turbine inlet pressure at which minimum cycle losses are incurred can be detected, even though it is not always sharply defined. The minimum loss point results from interactions between the isentropic cycle performance and obtainable turbine efficiencies. Maximum cycle performance is obtained at the maximum inlet pressure and pressure ratio. Turbine efficiency, however, is a maximum at low turbine inlet pressures (because of the increased volumetric flow) and at low pressure ratios (because of low turbine Mach numbers).

Table VI. Matrix Reduction Summary

| Cycle | Turbopump Configuration | | | |
|---|---|---|---|---|
| | A. Single Turbine Direct Drive | B. Single Turbine Geared Drive | C. Parallel Turbines | D. Series Turbines |
| 1. Gas Generator | (1) (2*) | (1) (2) | (1) (2) | (1) (2) |
| 2. Chamber Tapoff | (1) (2) | (1) (2) | (1) (2) | (1) (2) |
| 3. Auxiliary Heat Exchanger | (1) (2) | (1) (2) | (1) (2) | (1) (2) |
| 4. Expander | Excessive Oxidizer Pump Speed Required for Design Point 1.<br>(2) | (1) (2) | Turbine Admission Area and Specific Speed Requirements Are Critical | Control System Complexity |
| 5. Staged Combustion | Advantages Limited to High Pressure; Excessive Oxidizer Pump Speed Required for Design Point 1 | Advantages Limited to High Pressure<br>(1) | Turbine Admission Area and Specific Speed Requirements Are Critical | Advantages Limited to High Pressure Control System Complexity |
| 6. Composite Expander | No Advantage Unless Expander Cycle Cannot Be Balanced | No Advantage Unless Expander Cycle Cannot Be Balanced | Turbine Admission Area and Specific Speed Requirements Are Critical | Excessive Turbine Pressure Drop |

* Number in circles indicate design points to be evaluated under Task IC.

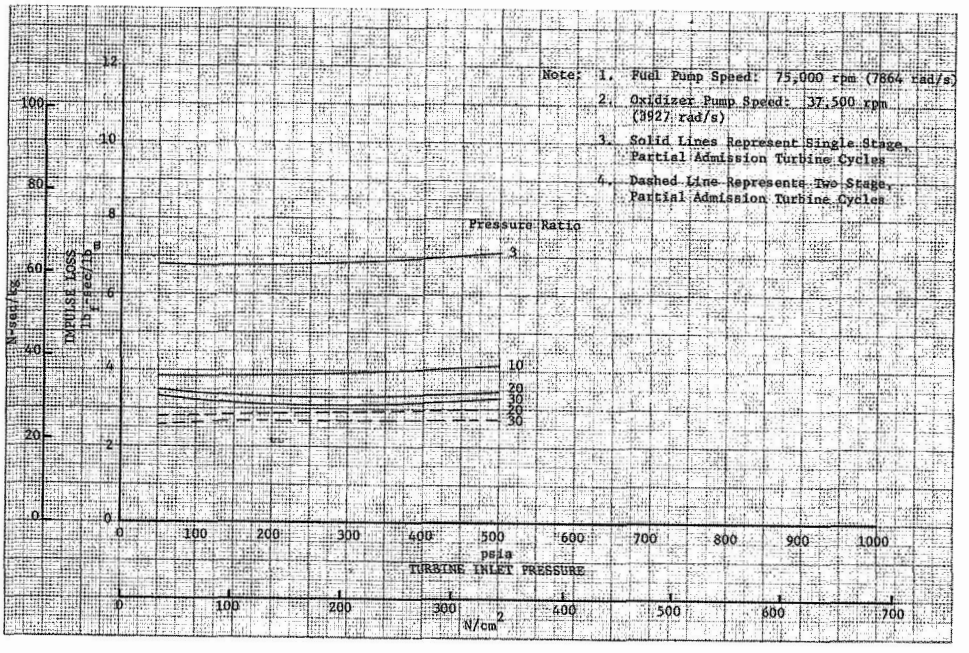


Figure 33. Auxiliary Heat Exchanger Impulse Loss vs Turbine Inlet Pressure - Geared Drive: $P_c$ = 500 psia (344.7 N/cm$^2$)

DF 70845

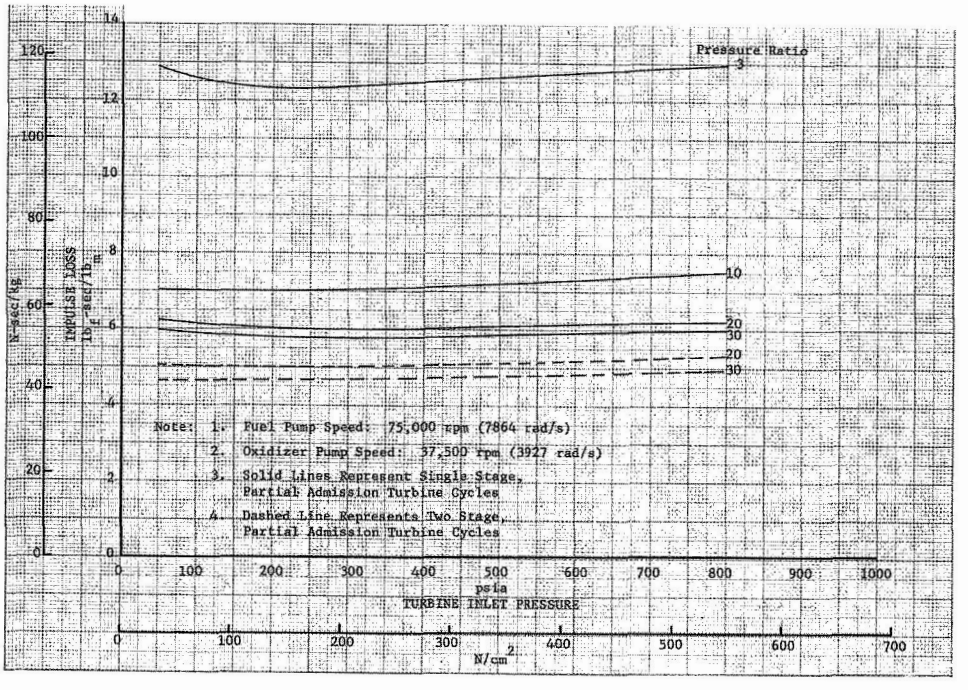


Figure 34. Auxiliary Heat Exchanger Impulse Loss vs Turbine Inlet Pressure - Geared Drive: $P_c$ = 800 psia (551.6 N/cm$^2$)

DF 70844

For all but the lower pressure ratio condition, an inlet pressure of 300 psia (206.8 $N/cm^2$) appears to provide close to minimum losses. Impulse improvements for two-stage turbines over single-stage units are indicated; these were approximately 1.0 $lb_f$-sec/$lb_m$ (9.81 N-sec/kg) for Design Point 1 and 0.4 $lb_f$-sec/$lb_m$ (3.92N-sec/kg) for Design Point 2. However, the advantage must be considered with regard to the added weight and complexity of the two-stage machine.

Figures 35 and 36 are engine cycle schematics for the auxiliary heat exchanger cycle with geared single turbines driving the pumps for Design Points 1 and 2 at the reference cycle conditions, i.e., fuel pump and turbine speed equal 75,000 rpm (7854 rad/s), oxidizer pump speed 37,500 rpm (3927 rad/s) and turbine inlet temperature 1700°R (944.44°K). Computations were made to investigate the penalties for reducing turbomachinery speed and turbine inlet temperature; the speeds of the various elements of the turbopump were varied independently for the analysis (i.e., gearing and coupling arrangements were neglected). Impulse losses for a single-stage turbine configuration are shown in figure 37 for Design Point 1 and figure 38 for Design Point 2. Note that the turbomachinery speeds can all be reduced significantly without imparing cycle performance; however, if possible, turbine inlet temperature should not be reduced below 1700°R (944.4°K).

Figures 39 and 40 show the impulse loss vs turbine inlet pressure for the direct drive turbomachinery configurations. For the same pressure ratio (20), the losses are increased over those of geared configurations by approximately 1.2 $lb_f$-sec/$lb_m$ (11.77 N-sec/kg) at Design Point 1 and 0.7 $lb_f$-sec/$lb_m$ (6.87 N-sec/kg) at Design Point 2. The effect of varying turbomachinery speed for a single stage direct-drive configuration is shown in figure 41 for both design points; note that speed has a much more significant effect in this instance and that somewhat greater advantage is shown for a two-stage unit than in the case of a geared pump.

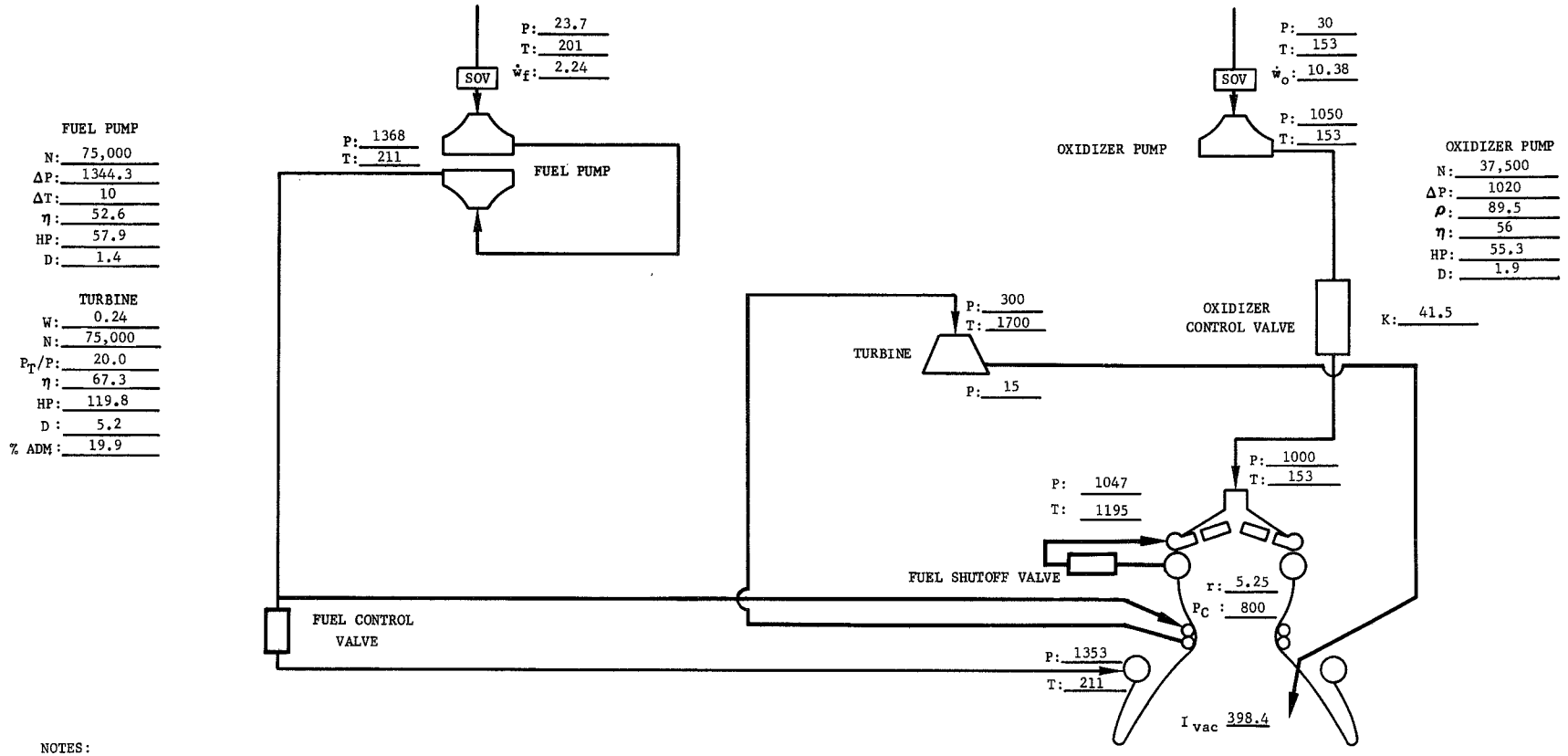


NOTES:
1. Fuel leakage; 0.05 lb/sec (includes SV-10, SV-6, SV-8 leakage and gearbox coolant).
2. Gear train horsepower loss; 5% of oxidizer pump required horsepower.
3. All pressures in psia.
4. All temperatures in °R.
5. All flowrates in lb/sec.
6. All dimensions in inches.
7. All efficiencies in percent.

Figure 35. Auxiliary Heat Exchanger (5K Thrust; Flox/$CH_4$ Engine; Chamber Pressure = 800; Chamber Mixture Ratio = 5.25) FD 25026B

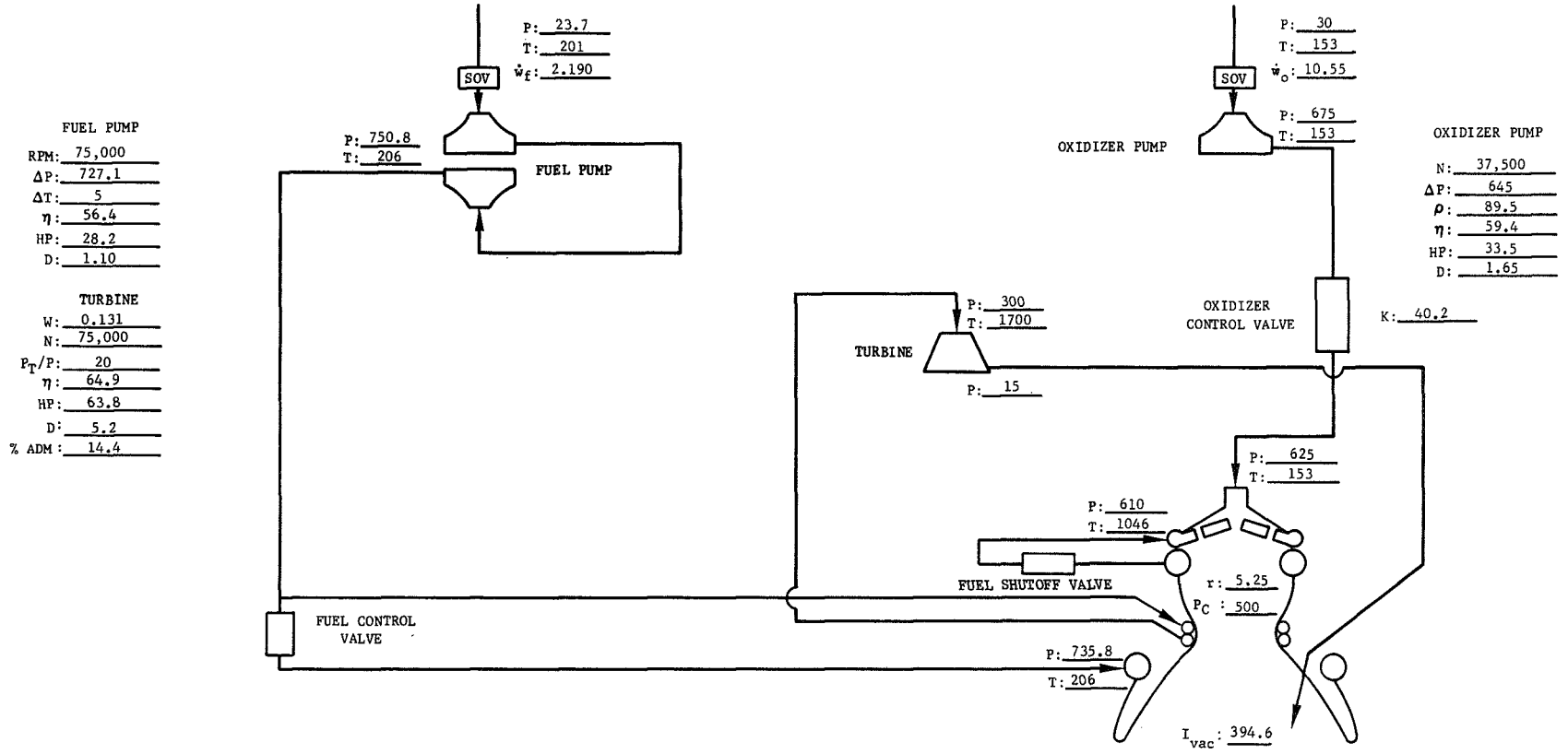


NOTES:
1. Fuel leakage; 0.05 lb/sec (includes SV-10, SV-6, SV-8 leakage and gearbox coolant).
2. Gear train horsepower loss; 5% of oxidizer pump required horsepower.
3. All pressures in psia.
4. All temperatures in °R.
5. All flowrates in lb/sec.
6. All dimensions in inches.
7. All efficiencies in percent.

Figure 36. Auxiliary Heat Exchanger (5K Thrust; Flox/$CH_4$ Engine; Chamber Pressure = 500; Chamber Mixture Ratio = 5.25) FD 25025C

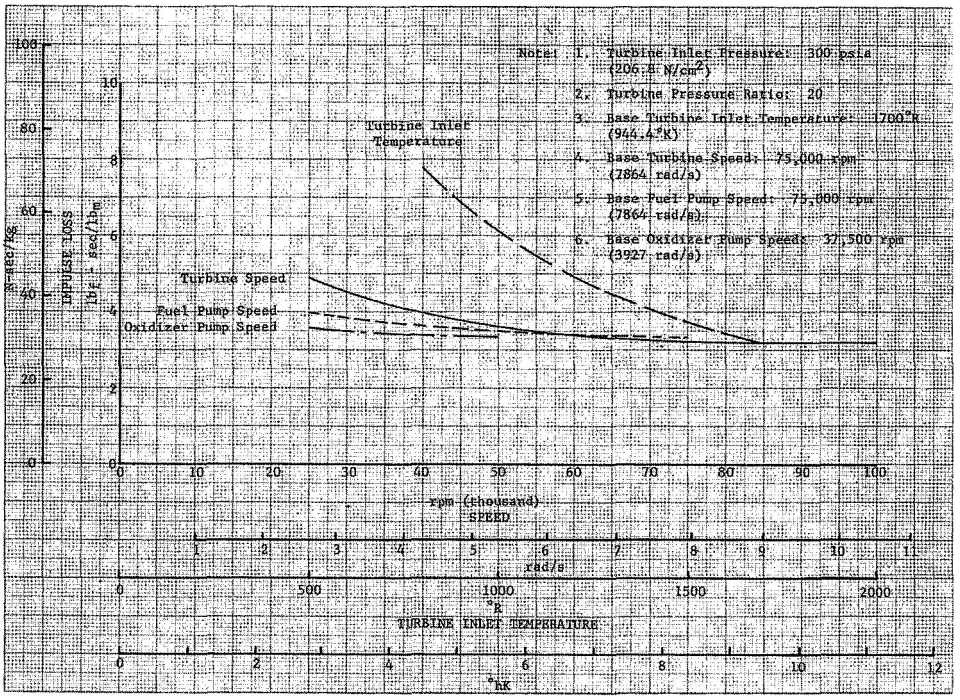


Figure 37. Auxiliary Heat Exchanger Impulse Loss vs Turbine and Pump Speeds and Turbine Inlet Temperature - Single Stage Partial Admission Turbines; $P_c$ = 500 psia (344.7 N/cm$^2$) DF 70796

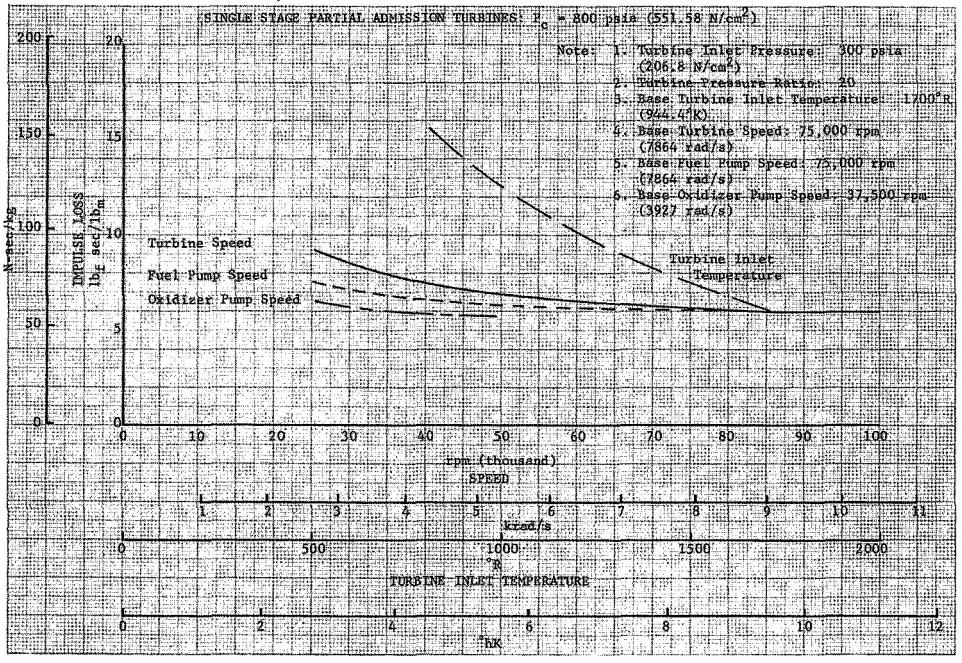


Figure 38. Auxiliary Heat Exchanger Impulse Loss vs Turbine and Pump Speeds and Turbine Inlet Temperature - Single Stage Partial Admission Turbines; $P_c$ = 800 psia (551.6 N/cm$^2$) DF 70794

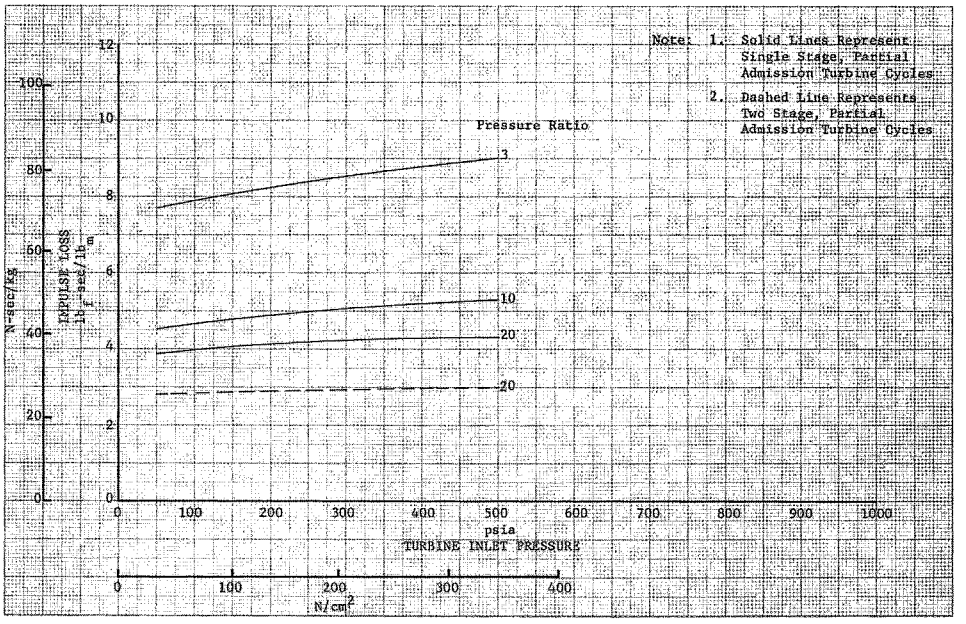


Figure 39. Auxiliary Heat Exchanger Impulse Loss vs Turbine Inlet Pressure - Direct Drive: Speed = 37,500 rpm (3927 rad/s); $P_c$ = 500 psia (344.7 $N/cm^2$) DF 70847

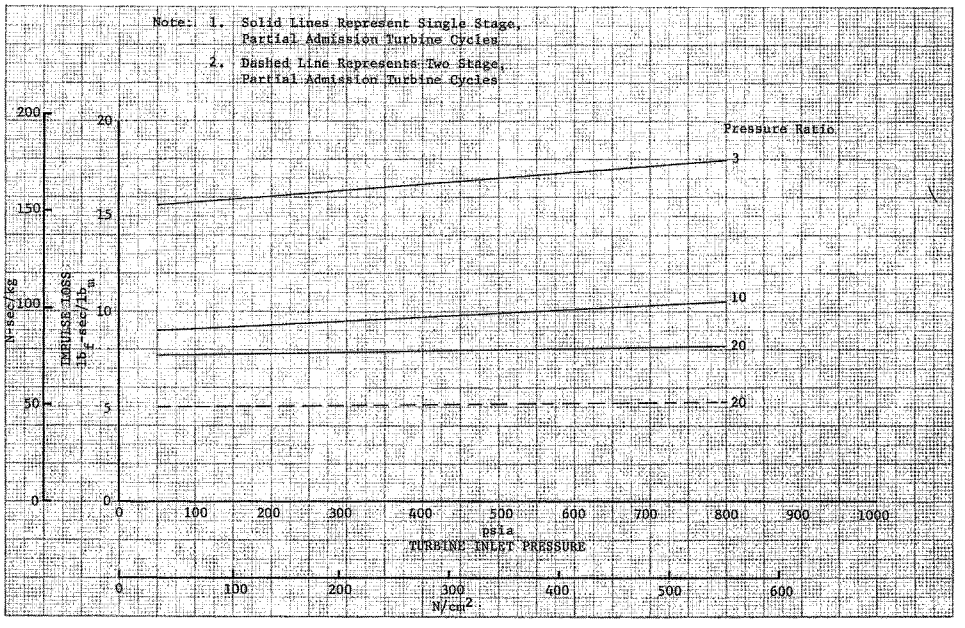


Figure 40. Auxiliary Heat Exchanger Impulse Loss vs Turbine Inlet Pressure - Direct Drive: Speed = 37,500 rpm (3927 rad/s); $P_c$ = 800 psia (551.6 $N/cm^2$) DF 70846

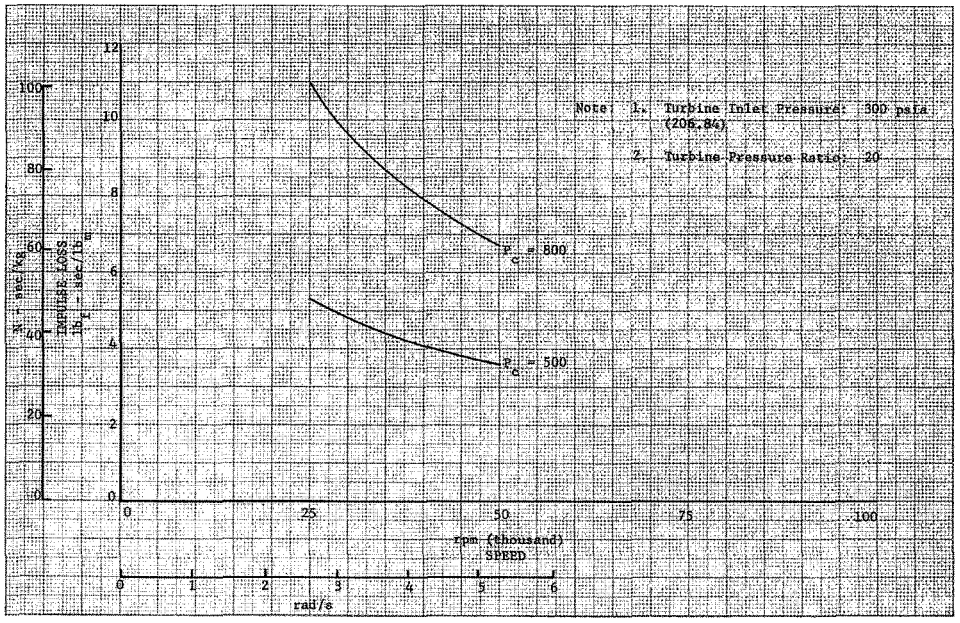


Figure 41. Auxiliary Heat Exchanger Impulse Loss vs Speed (Direct Drive: Single Stage Partial Admission) DF 70798

The cycle performance for parallel and series turbines at the two design points was calculated at a turbine inlet pressure of 300 psia (206.8 $N/cm^2$), with a fuel side turbomachinery speed of 75,000 rpm (7854 rad/s) and an oxidizer-side turbomachinery speed of 37,500 rpm (3927 rad/s). The pressure ratio was 20, and, in the case of the series turbines, this was the overall pressure ratio for both turbines. The impulse losses for the parallel turbines were 6.5 and 3.9 $lb_f$-sec/$lb_m$ (63.74 and 38.25 N-sec/kg) for Design Points 1 and 2, respectively. Corresponding losses for the series turbines were 5.0 and 2.9 $lb_f$-sec/$lb_m$ (49.03 and 28.44 N-sec/kg), so again, the increased loss associated with the reduced admission areas of parallel turbines was shown, and an improvement was indicated for the series arrangement.

b. Gas Generator Cycle

The impulse losses calculated for a geared turbine-drive gas generator cycle are shown vs turbine inlet pressure at a pressure ratio of 20 in figure 42. Both the fuel pump and turbine speeds were 75,000 rpm (7854 rad/s), and the oxidizer pump speed was 37,500 rpm (3929 rad/s). The turbine inlet temperature was 1850°R (1027°K).

It will be noted that the trends of figure 42 are similar to those of figures 33 and 34 for the auxiliary heat exchanger cycles. The effects of reduced turbomachinery speeds and turbine temperature on the gas generator cycle are similar to those shown in figures 37 and 38 for the auxiliary heat exchanger. Balanced cycles are shown in figures 43 and 44 for the single turbine-geared pump configuration at the two design points. The cycle impulse loss was 3.7 $lb_f$-sec/$lb_m$ (36.29 N-sec/kg) at Design Point 1 and 2.1 $lb_f$-sec/$lb_m$ (20.59 N-sec/kg) at Design Point 2. Impulse losses were also calculated for the direct drive, parallel turbine, and series turbine configurations; these are compared with those for the geared arrangement below.

| Turbopump Arrangement | Impulse Loss | | | |
|---|---|---|---|---|
| | Design Point 1 | | Design Point 2 | |
| | $lb_f$-sec/$lb_m$ | (N-sec/kg) | $lb_f$-sec/$lb_m$ | (N-sec/kg) |
| Single Turbine, Geared | 3.7 | (36.28) | 2.1 | (20.59) |
| Single Turbine, Direct Drive | 7.0 | (68.65) | 3.4 | (33.34) |
| Parallel Turbines | 4.0 | (39.23) | 2.3 | (22.56) |
| Series Turbines | 3.3 | (32.36) | 1.9 | (18.63) |

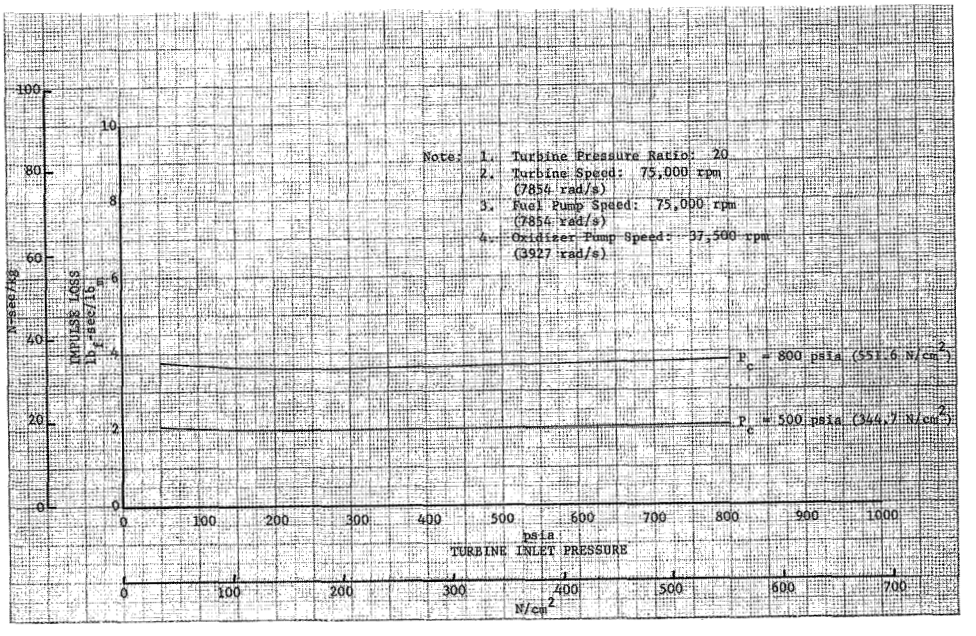


Figure 42. Gas Generator Impulse Loss vs Turbine Inlet Pressure (Single Stage Partial Admission Turbine) DF 70800

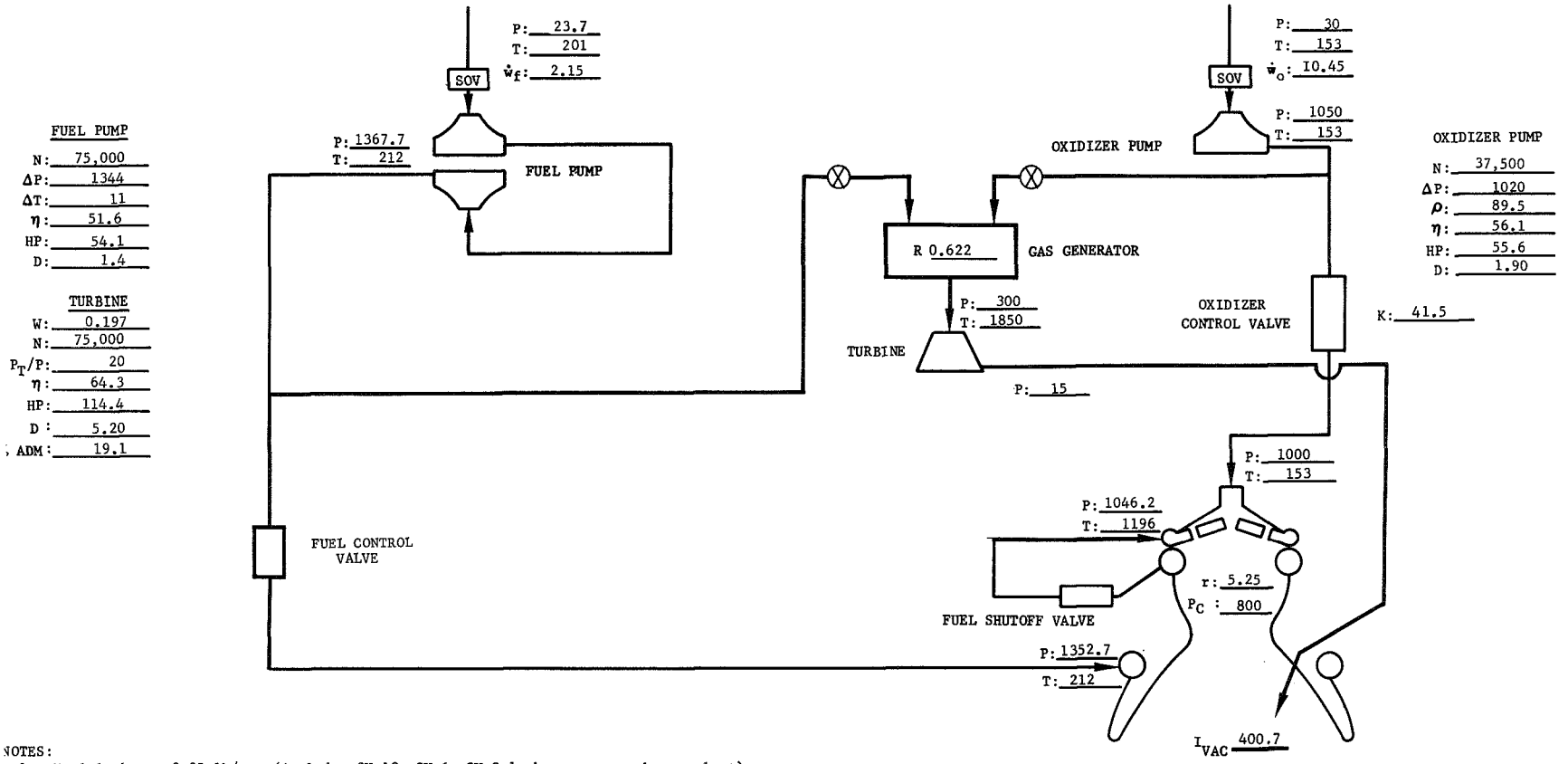


NOTES:
1. Fuel leakage; 0.05 lb/sec (includes SV-10, SV-6, SV-8 leakage and gearbox coolant).
2. Gear train horsepower loss; 5% of oxidizer pump required horsepower.
3. All pressures in psia.
4. All temperatures in °R.
5. All flowrates in lb/sec.
6. All dimensions in inches.
7. All efficiencies in percent.

Figure 43. Gas Generator Cycle Schematic (5K Thrust; Flox/$CH_4$ Engine; Chamber Pressure = 800; Chamber Mixture Ratio = 5.25) FD 25017A

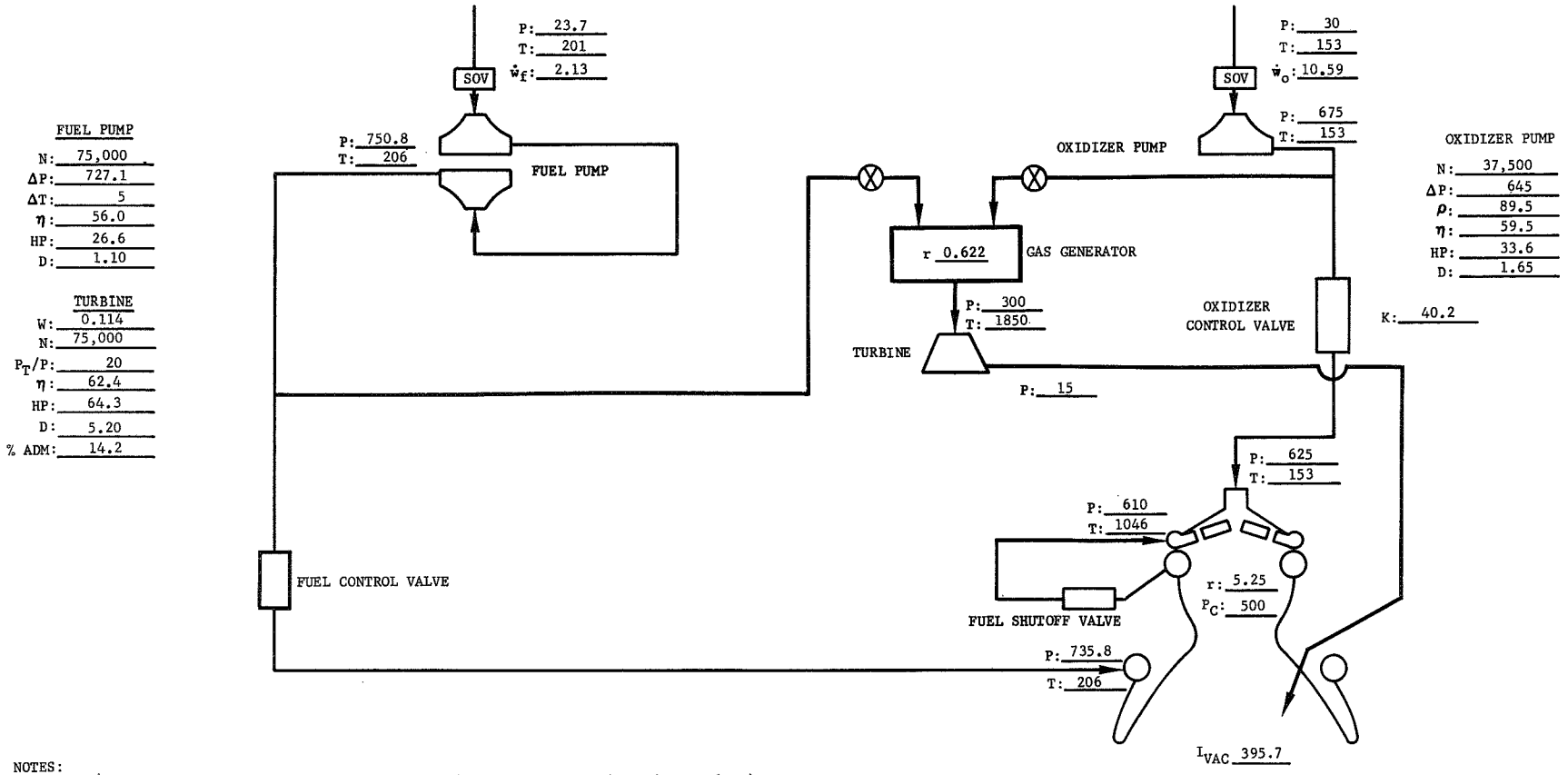


NOTES:
1. Fuel leakage; 0.05 lb/sec (includes SV-10, SV-6, SV-8 leakage and gearbox coolant).
2. Gear train horsepower loss; 5% of oxidizer pump required horsepower.
3. All pressures in psia.
4. All temperatures in °R.
5. All flowrates in lb/sec.
6. All dimensions in inches.
7. All efficiencies in percent.

Figure 44. Gas Generator Cycle Schematic (5K Thrust; Flox $CH_4$ Engine; Chamber Pressure = 500; Chamber Mixture Ratio = 5.25) FD 25027A

c. Chamber Tapoff Cycle

The energy balance for the chamber tapoff cycle is identical with the gas generator; therefore, analytical results for the gas generator cycle are directly applicable to the tapoff cycle, and the cycles shown in figures 43 and 44 would be representative except for the source of the turbine working fluid.

d. Expander Cycle

The fuel pump discharge pressure required for the expander cycle must be sufficient to provide the necessary turbine pressure ratio to balance the cycle. For a given design point (chamber pressure and thrust), as the fuel pump discharge pressure is increased both the available turbine power and required pump power are increased. Initially, the turbine power increases at a faster rate than does the pump power and the excess power margin is increased. Ultimately, the relationship between available and required power is reversed, and a maximum pump discharge pressure, with zero excess power, is reached. Normally, 5% to 10% of excess power in the form of turbine bypass flow is considered necessary to provide sufficient control margin and cycle power. Figures 45 and 46 are balanced cycle sheets for the expander cycle with geared single turbine at the two design points, using turbopump performance selected to give 10% bypass flow. Fuel pump and turbine speed were 75,000 rpm (7854 rad/s and the oxidizer pump speed was 37,500 rpm (3927 rad/s for both points

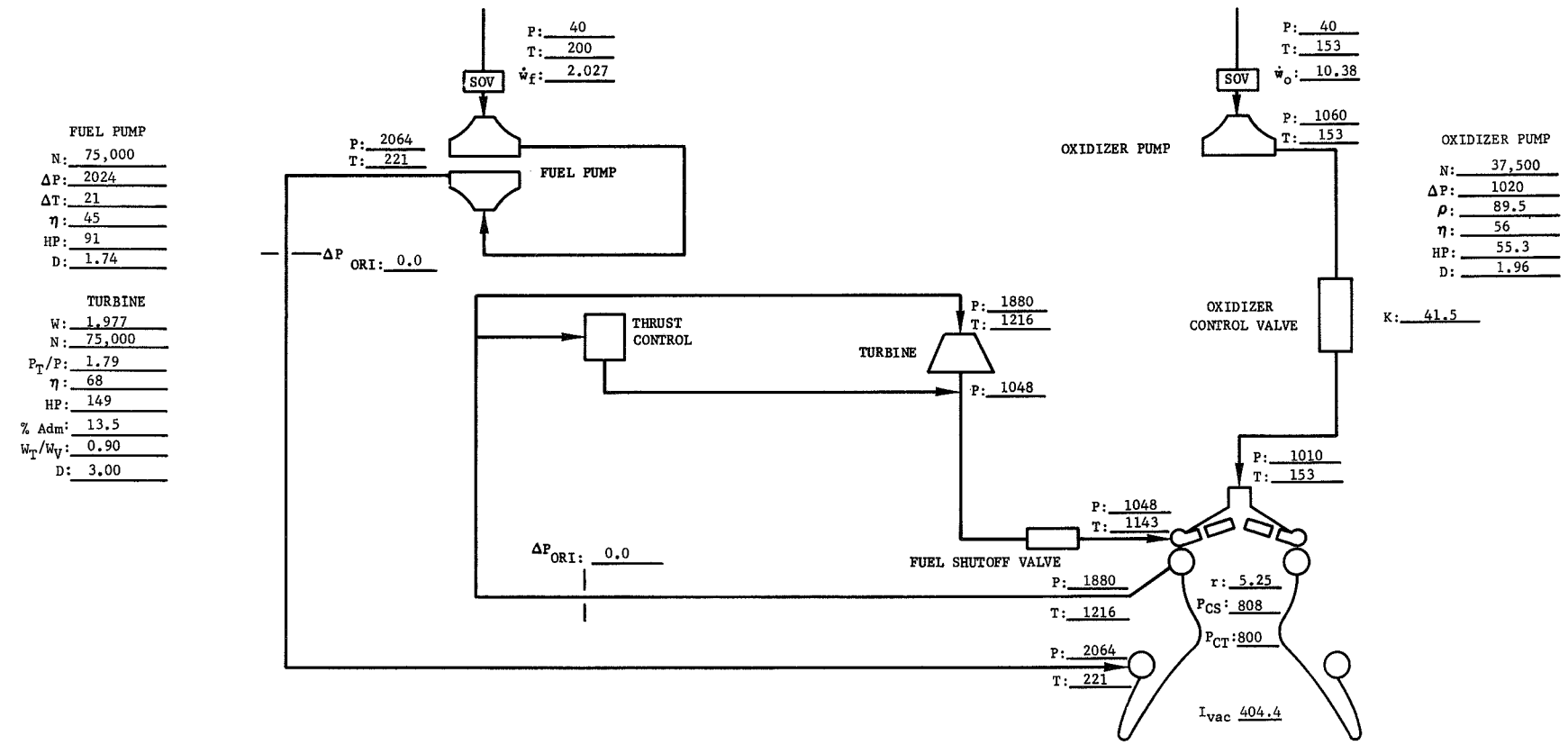


NOTES:
1. Fuel leakage; 0.05 lb/sec (includes SV-10, SV-6, SV-8 leakage and gearbox coolant).
2. Gear train horsepower loss; 5% of oxidizer pump required horsepower.
3. All pressures in psia.
4. All temperatures in °R.
5. All flowrates in lb/sec.
6. All dimensions in inches.
7. All efficiencies in percent.

Figure 45. Expander Cycle Schematic (5K Thrust; Flox/$CH_4$ Engine; Chamber Pressure = 800; Chamber Mixture Ratio = 5.25)

FD 25024A

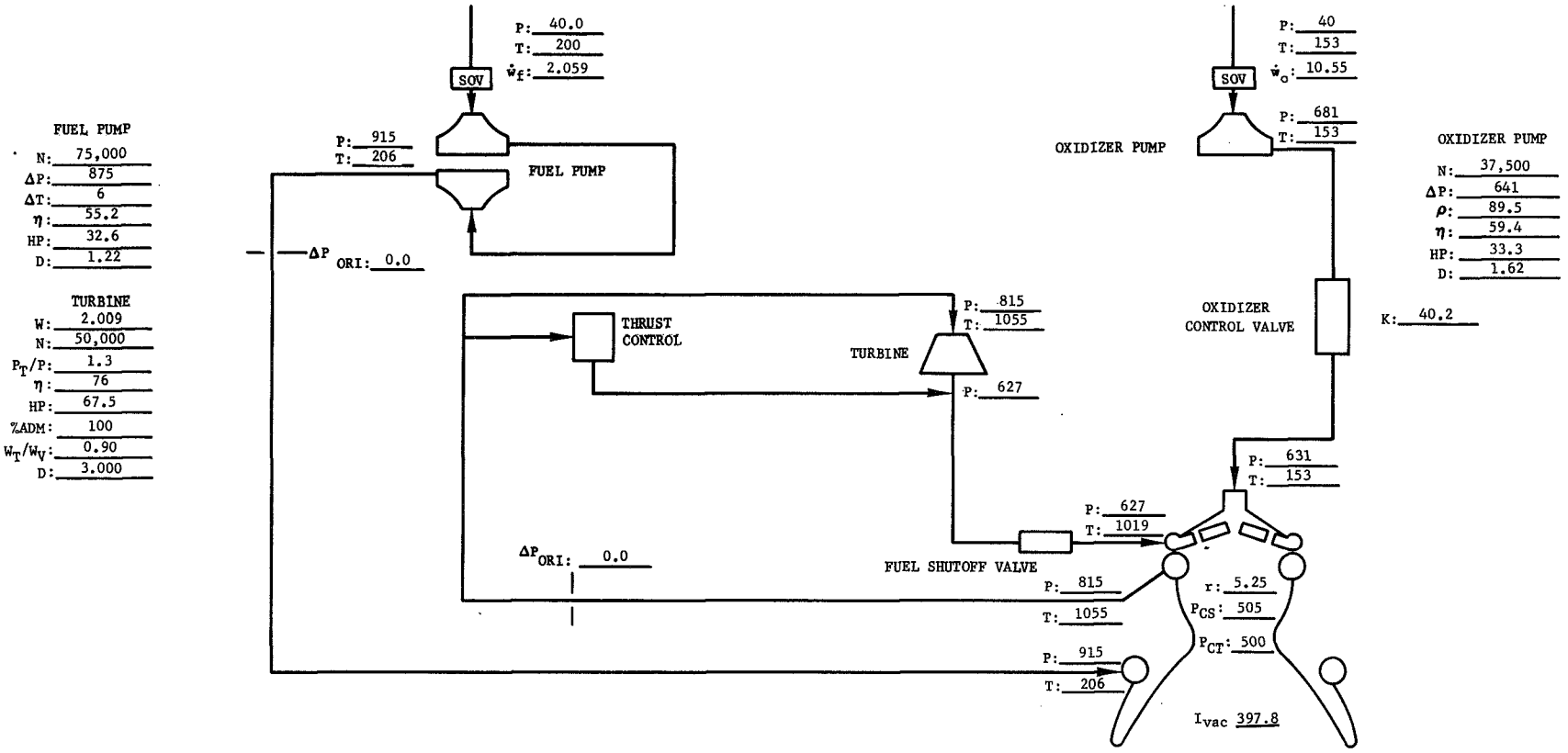


NOTES:
1. Fuel leakage; 0.05 lb/sec (includes SV-10, SV-6, SV-8 leakage and gearbox coolant).
2. Gear train horsepower loss; 5% of oxidizer pump required horsepower.
3. All pressures in psia.
4. All temperatures in °R.
5. All flowrates in lb/sec.
6. All dimensions in inches.
7. All efficiencies in percent.

Figure 46. Expander Cycle Schematic (5K Thrust; Flox/$CH_4$ Engine; Chamber Pressure = 500; Chamber Mixture Ratio = 5.25) FD 25024A

Figure 47 shows how the excess power available in the expander cycle varies as a function of fuel pump discharge pressure (the configuration is Design Point 2 using a single geared turbine drive configuration). Note that by increasing fuel pump discharge from 2064 psia (1408 $N/cm^2$) to approximately 2800 psia (1931 $N/cm^2$), the excess power increases to approximately 25% which, as can be seen from the shape of the curve, is approaching a maximum. With 25% excess power, approximately 15% to 20% would be available for uprating the engine or for providing for design uncertainties after allowing for the normal 5% to 10% bypass flow. Figure 48 illustrates the fuel pump discharge pressure required to balance the expander cycle with 10% excess power as turbomachinery speeds are changed. Varying oxidizer pump speed between 25,000 and 37,500 rpm (2618 and 3927 rad/s has approximately the same effect as varying turbine speed between 60,000 and 75,000 rpm (6283 and 7854 rad/s), the limit lines of the oxidizer pump speed envelope. Fuel pump speeds can be reduced to 50,000 to 60,000 rpm (5236 to 6283 rad/s), depending on turbine and oxidizer pump condition, without significant effect, which indicates that the turbomachinery speeds can be reduced significantly for the expander cycle without a severe penalty in fuel pump discharge pressure.

As noted above, dual turbine turbopump arrangements were not evaluated in detail for the expander cycle because of restricted turbine inlet area. However, preliminary calculations for the parallel turbine arrangement indicated that excess horsepower was reduced by approximately 10% because of the reduction in turbine efficiency.

The problems of predicting pump and turbine efficiencies for the small size rotating machinery considered were mentioned in the discussion of component analysis. The values used in the study were believed to be realistic. Although a reduction in turbopump efficiency may be readily compensated by an increase in the turbine working fluid flowrate in an open cycle engine, the expander cycle is limited in the maximum power available to the turbine and therefore may be more seriously affected by deviations in efficiency. The available power in the expander cycle is also affected by the heat transfer level. These factors could affect development difficulty and for this reason a special study of expander cycle sensitivity to such changes was included in the comparative evaluation.

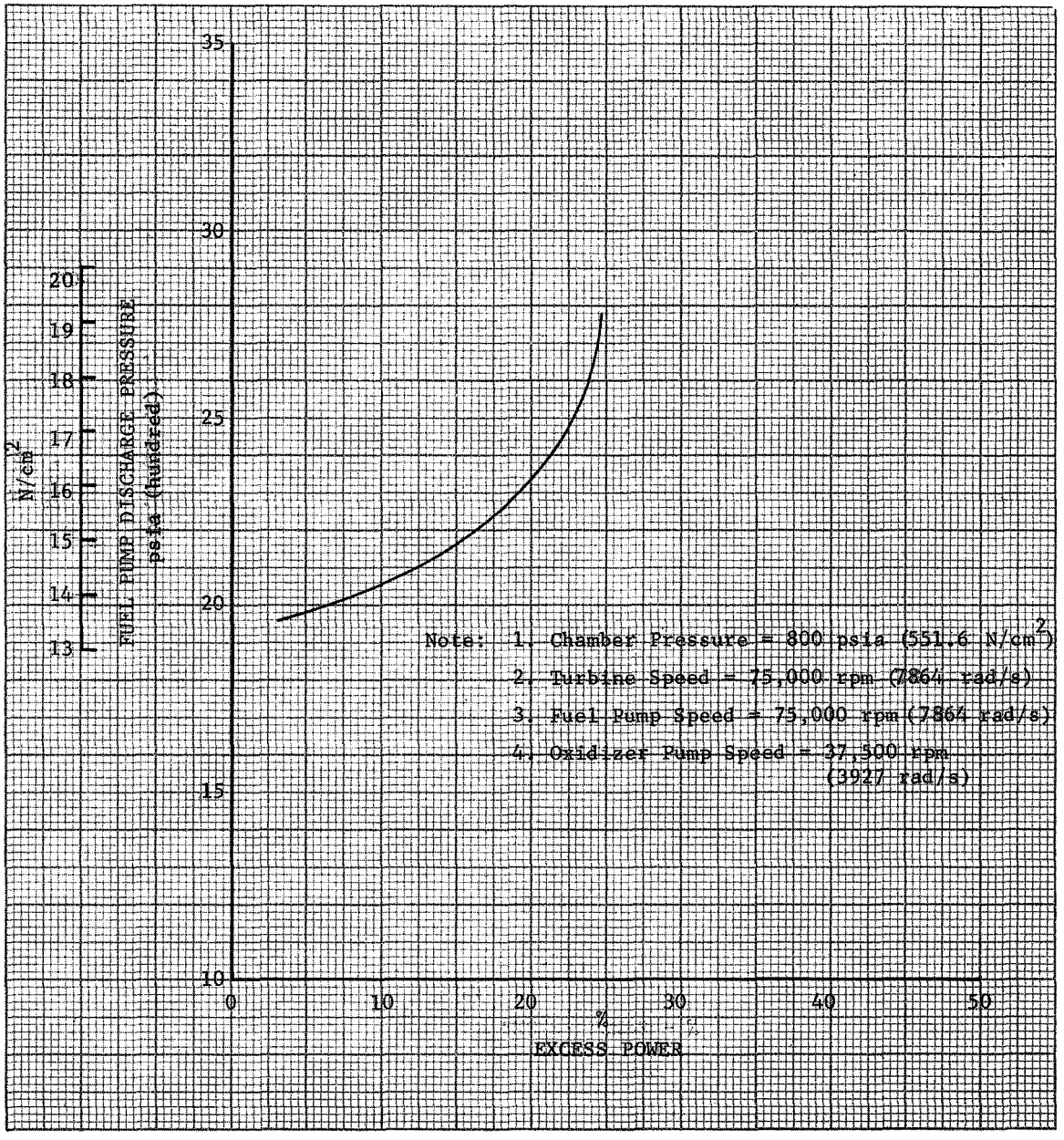


Figure 47. Expander Cycle Fuel Discharge Pressure vs Excess Power for a 5000 lb (22.24 kN) Flox/Methane Engine

DF 70848

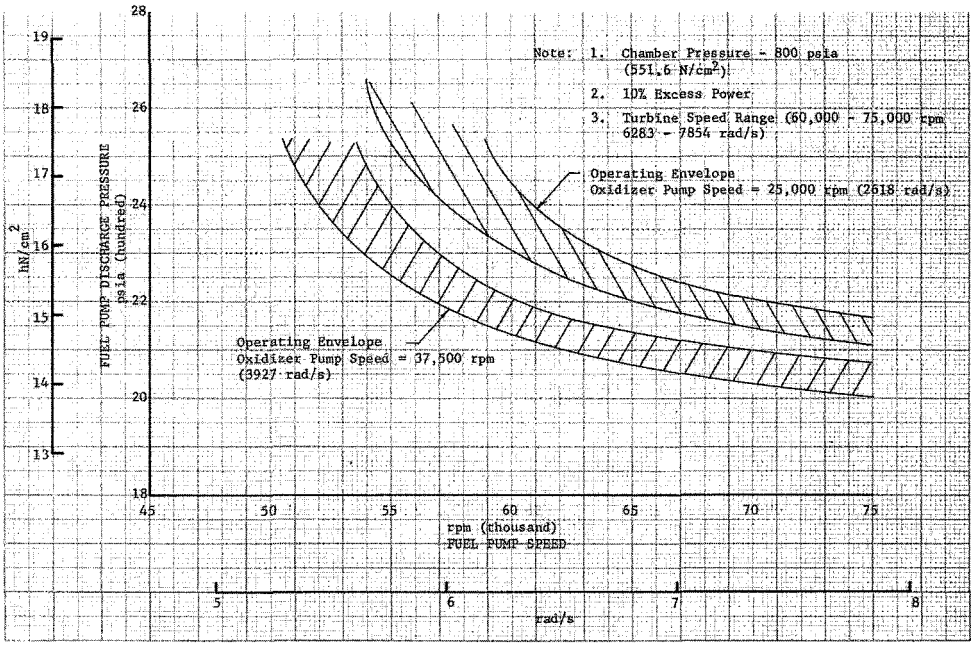


Figure 48. Expander Cycle Fuel Pump Discharge Pressure Requirements for a 5000 lb (22.24 kN) Flox/Methane Engine

DF 70849

To assess the effect of lower than predicted turbopump efficiency on the thermodynamic feasibility of the expander cycle, a series of cycles were balanced at the more stringent high chamber pressure design point with reduced efficiency rotating machinery. Figure 49 shows the effect of arbitrary reductions in fuel pump efficiency on the fuel pump discharge pressure. The right ends of the curves correspond to the fuel pump efficiencies used in the basic analysis (i.e., 45% for a 10% bypass flow, or turbine weight flow fraction of 0.90). As fuel pump efficiency is reduced, the required fuel pump discharge pressure increases. However, an arbitrary reduction of 10% in fuel pump efficiency produced only a 10% to 20% increase in required fuel pump discharge pressure, and, as shown, adequate cycle power margins can be maintained.

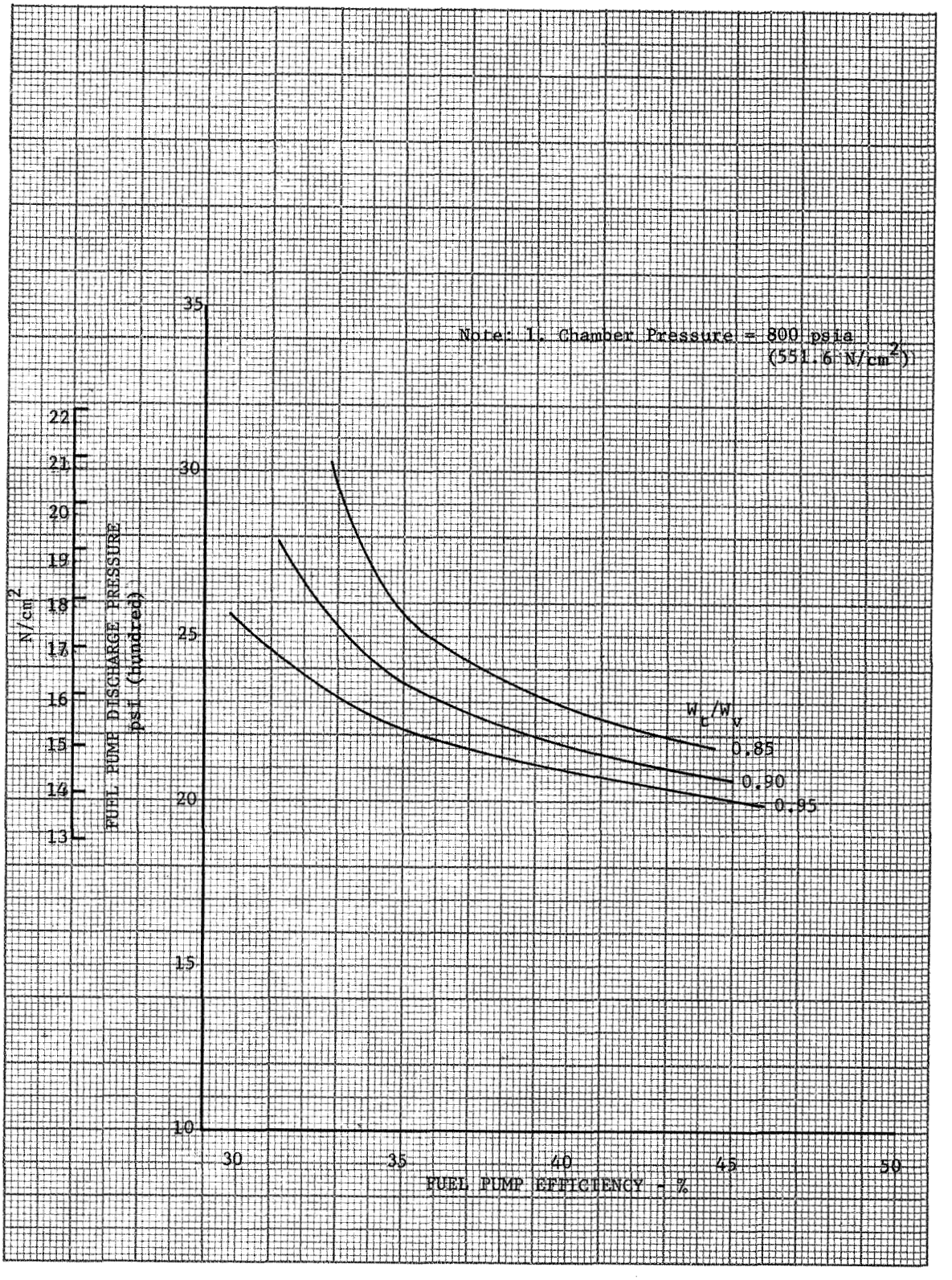


Figure 49. Expander Cycle Fuel Pump Discharge Pressure Requirements for Varying Pump Efficiencies 5000 lb (22.24 kN) Flox/Methane Engine

DF 70850

Figure 50 shows the effect of simultaneously decreasing the efficiency of the fuel pump, oxidizer pump, and turbine. As shown, for 10% bypass flow, an arbitrary decrease of 5% in the efficiences of all three components produces an increase of 500 psia (344.7 $N/cm^2$) in the fuel pump discharge pressure required to balance the cycle which, as can be seen, is attainable. Figure 50 also shows that the use of a turbine flow ratio of 0.90 rather than 0.95 (the minimum requirement) is equivalent to a 2.0% efficiency margin on all major turbopump components.

To simplify the analysis of variations in thrust chamber heat transfer on expander cycle margin, increases in jacket pressure loss only were assumed. This provides a degree of conservatism, since concurrent increases in $\Delta T$ would also be expected. Results are shown in figure 51 which presents the fuel pump discharge pressure requirement as a function of jacket $\Delta P$. The left ends of the curves correspond to the values used in the basic studies. Note that, for a turbine flow fraction of 0.90, doubling the coolant jacket pressure drop increases the required fuel pump discharge pressure by only 200 psi (137.9 $N/cm^2$). Thus, large increases in jacket pressure drop can be tolerated with very little affect on cycle feasibility.

Because positive displacement pumps might offer higher efficiencies in small sizes, the use of this type of fuel pump in conjunction with the expander cycle was also investigated briefly. Figure 52 shows that the excess power (turbine bypass flow) may be increased by over 20% and the turbine speed reduced to 50,000 rpm (5236 rad/s) because of the increased efficiency provided by a positive displacement fuel pump. Using a positive displacement pump and reducing the oxidizer pump and turbine speed to 30,000 rpm (3142 rad/s) provides a 5% to 8% increase in turbine power over the reference configuration.

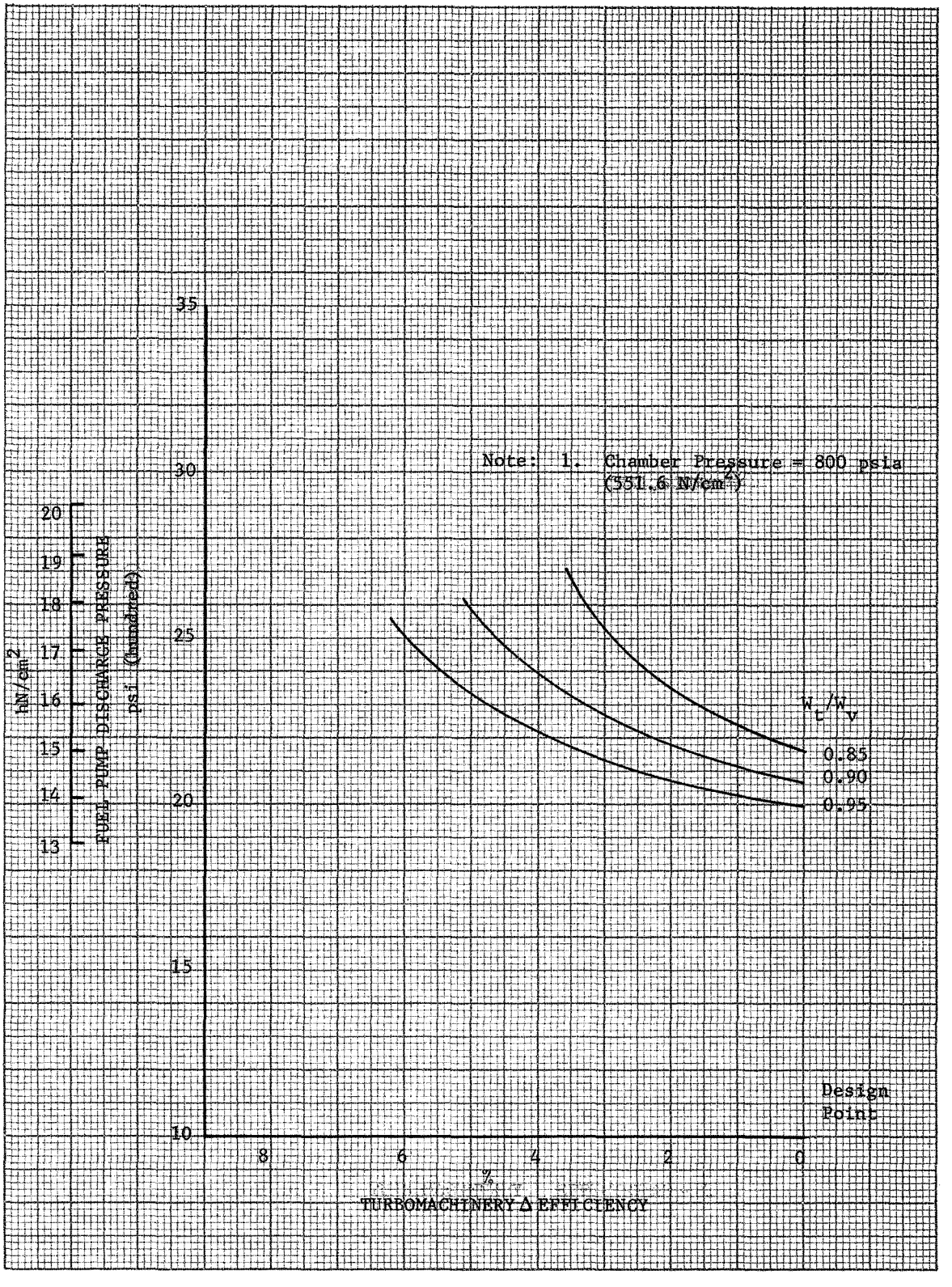


Figure 50. Expander Cycle Fuel Pump Discharge Requirements for Degradation In Turbomachinery Efficiency 5000 lb (22.24 kN) Flox/Methane Engine

DF 70851

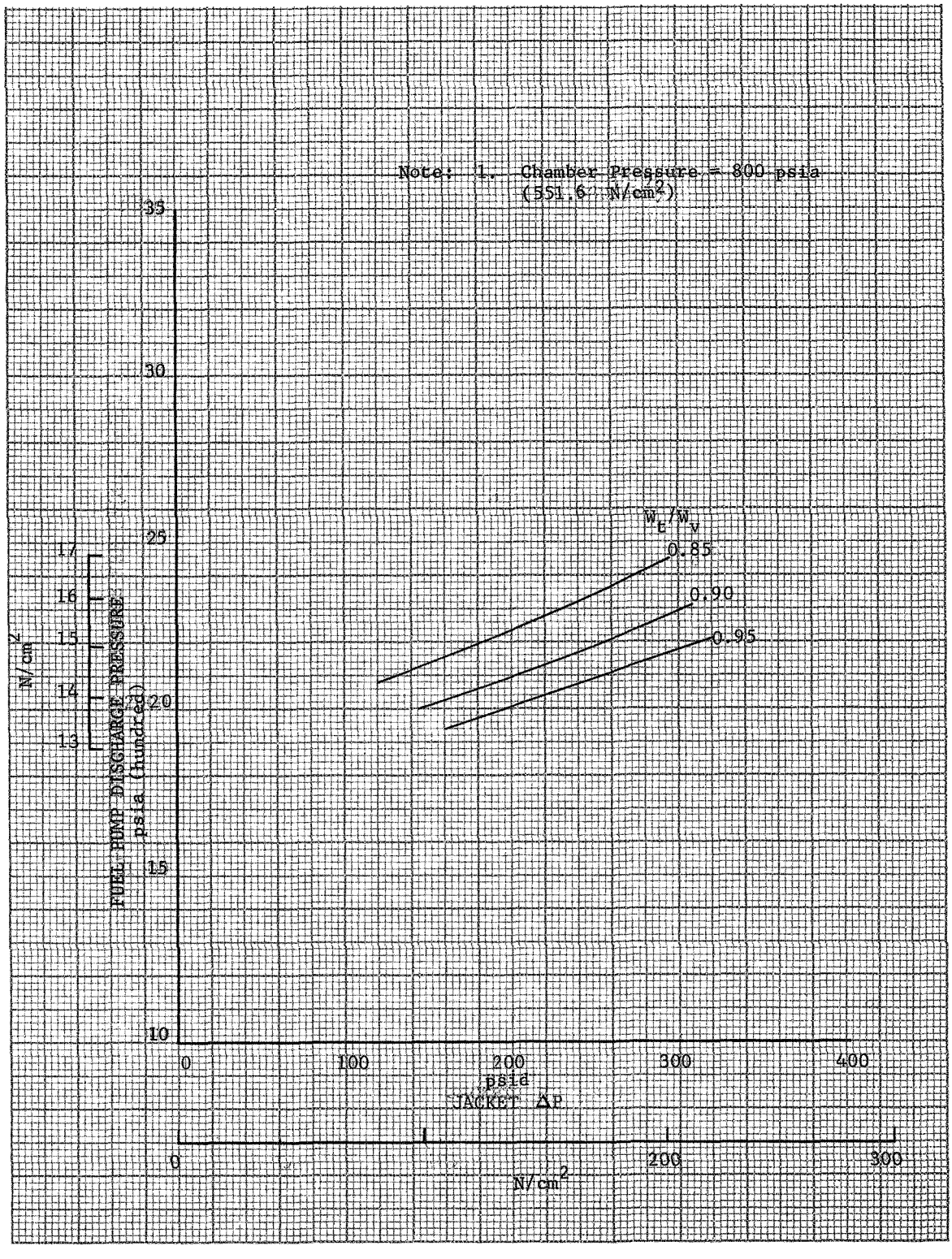


Figure 51. Expander Cycle Fuel Pump Discharge Requirements for Varying Jacket Pressure Loss 5000 lb (22.24 kN) Flox/Methane Engine

DF 70852

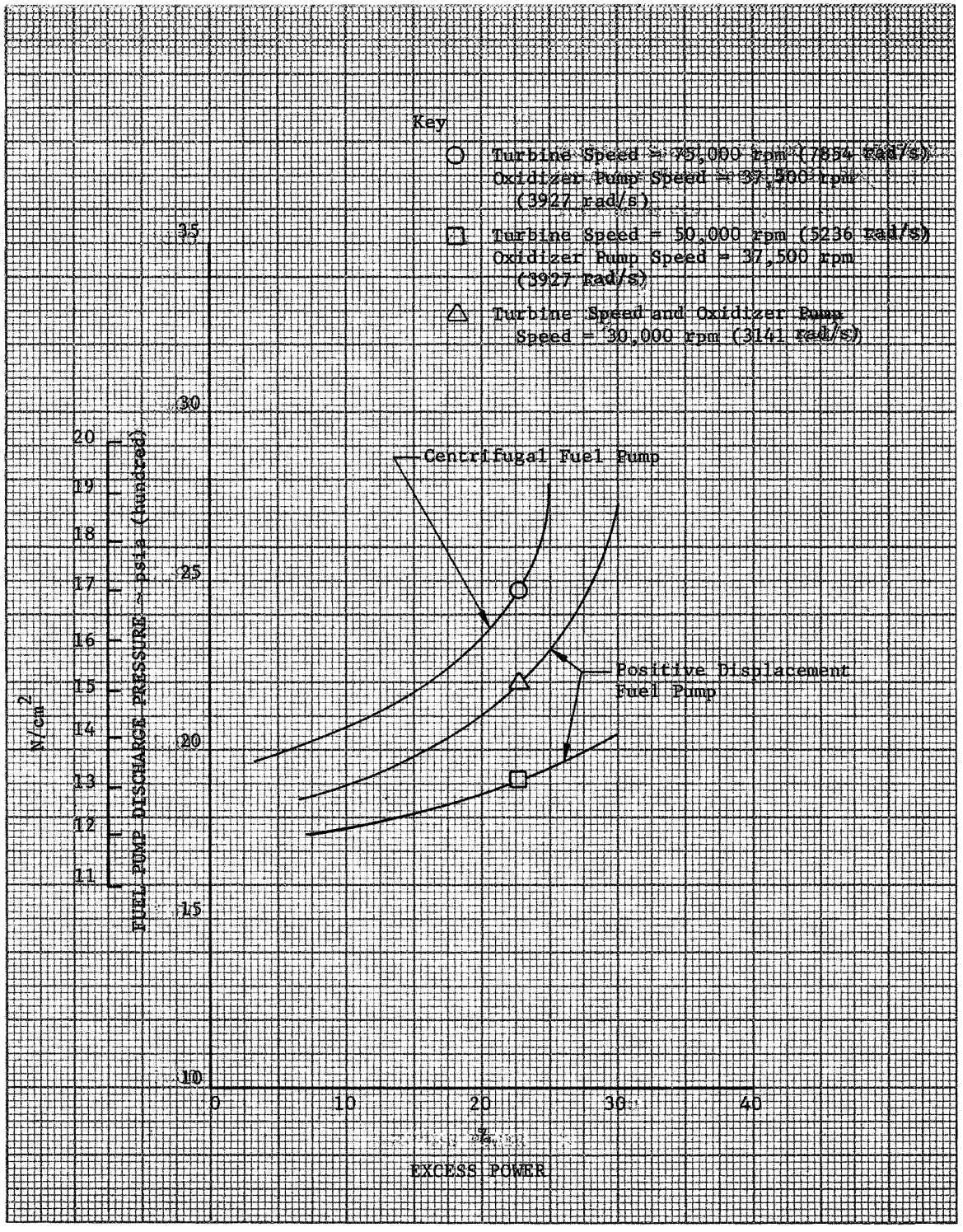


Figure 52. Expander Cycle Fuel Pump Discharge Pressure vs Excess Power for a 5000 lb (22.24 kN) Methane Engine $P_c$ = 800 psia (551.6 N/cm$^2$)

DF 70853

e. Preburner Cycle

The only major advantage of the closed preburner cycle over the closed expander cycle is the capability it provides for extending the upper chamber pressure limit on operation. Analysis showed that the expander cycle had the capability for operation at the higher chamber pressure design point, 800 psia (551.6 $N/cm^2$); therefore there was no necessity for detailed consideration of the more complex cycle. However, to permit a comparison, a preburner cycle was balanced at Design Point 1.

The cycle schematic for the 800 psia (551.6 $N/cm^2$) chamber pressure preburner engine is shown in figure 53. Both the fuel pump and turbine speeds are 75,000 rpm (7854 rad/s), and the oxidizer pump speed is 37,500 rpm (3927 rad/s). The preburner combustion temperature was set at 1850°R (1028°K). All of the fuel and sufficient oxidizer to maintain the 1850°F (1028°K) combustion temperature pass through the preburner and turbine and the remainder of oxidizer is injected into the main chamber.

6. Estimated Engine Weights

Preliminary estimates of weight were made for the cycles and turbomachinery configurations analyzed. These weights are shown with the respective engine impulses and fuel pump discharge pressures in table VII. Design layouts were not prepared at this stage of the study; therefore a base engine weight for one configuration was established and the weights of the remaining cycles and pump arrangements were scaled from it. The resulting estimates are primarily a guide to the relative merits of each configuration. The base configuration was the Design Point 2 expander cycle engine. Its weight was estimated to be 115 lb (52.16 kg); this value was established based on stress calculations made for the thrust chamber and for the turbomachinery gears, shafts, and housings. The pump impeller and turbine rotor weights were based on typical scaling factors relating flow, rotor speed, and diameter. The plumbing, manifold, and valve weights were

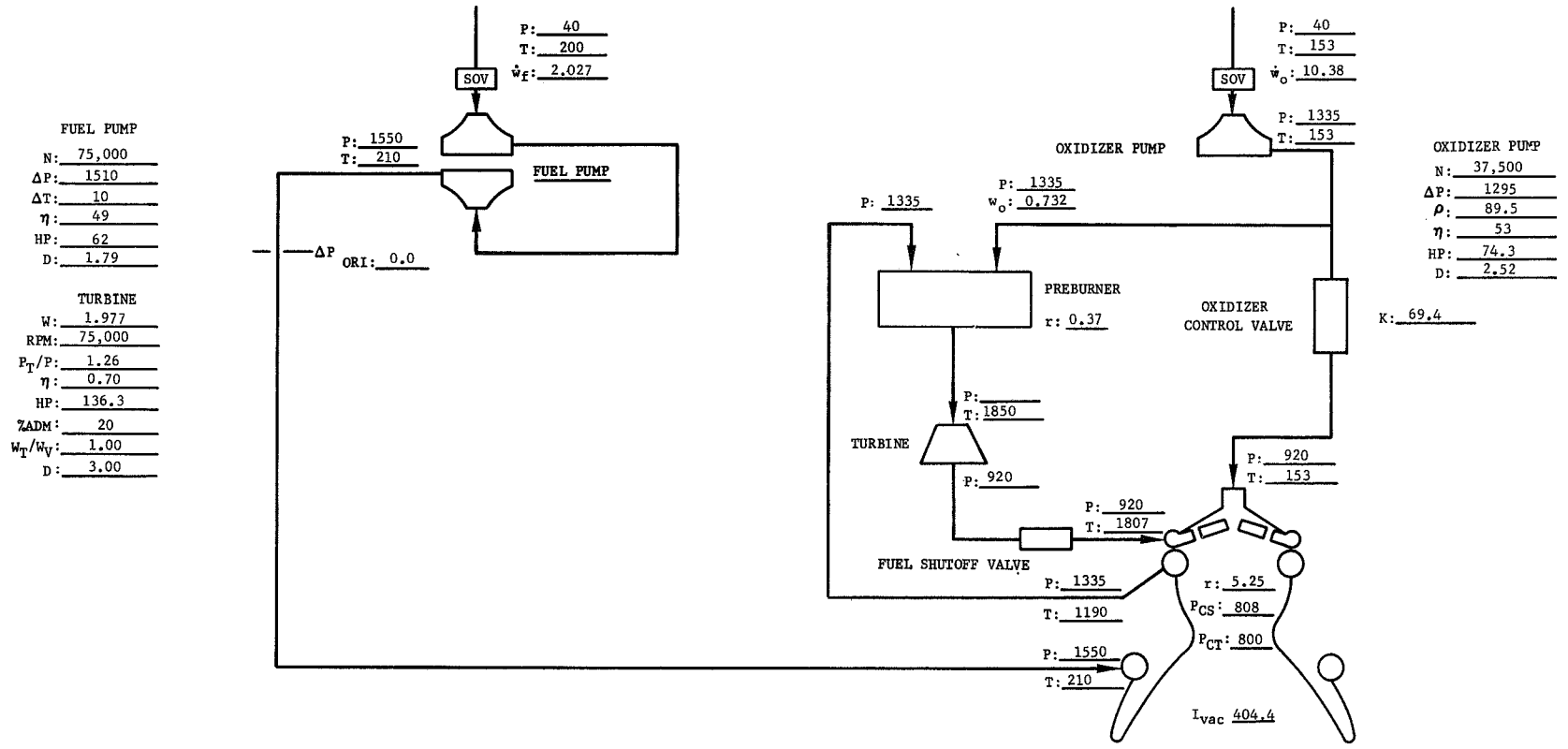


NOTES:
1. Fuel leakage; 0.05 lb/sec (includes SV-10, SV-6, SV-8 leakage and gearbox coolant).
2. Gear train horsepower loss; 5% of oxidizer pump required horsepower.
3. All pressures in psia.
4. All temperatures in °R.
5. All flowrates in lb/sec.
6. All dimensions in inches.
7. All efficiencies in percent.

Figure 53. Preburner Cycle Schematic (5K Thrust; Flox/$CH_4$ Engine; Chamber Pressure = 800; Chamber Mixture Ratio = 5.25) FD 25022B

scaled from the RL10 engine. A breakdown of the Design Point 2 expander cycle weight estimate was:

| Component | Percentage of Total Engine Weight |
|---|---|
| Thrust Chamber | 32 |
| Turbopumps | 23 |
| Lines and Valves | 37 |
| Mounts and Brackets | 8 |

D. PRELIMINARY CYCLE SELECTION

In addition to specific impulse and engine weight, it was necessary to consider other factors such as complexity, difficulty of development, production cost, etc., in the selection of the most desirable engine cycle. Performance in terms of engine specific impulse and weight can be evaluated numerically with reasonable accuracy; however, quantitive evaluation of complexity, difficulty of development, etc., is difficult under any circumstance and virtually impossible unless detailed design drawings are available and a complete development plan is generated. Therefore, consistent with available information and the scope of the turbopump drive cycle analyses, the method selected for evaluating the various cycles with respect to such nonnumerical factors was to rank them on a relative qualitative basis. Paragraphs 1 through 5, below, describe the ranking of the various cycles and turbopump combinations on the basis of five factors considered: complexity, development difficulty, design flexibility, ease of throttling, and production cost. Paragraph 6 presents combined rankings of the factors.

1. Complexity

The relative complexity of the various cycles and turbopump configurations may be considered in terms of the number of components, differences in steady state and transient control requirements, special manufacturing process requirements and manufacturing tolerances, and differences in the internal fluid dynamics and manifolding. Based on these considerations, the problem areas that appeared to affect engine complexity most directly include those described below.

## Table VII. Cycle Performance Summary

| Cycle | $P_c$ | Single Turbine - Direct Drive | | | Single Turbine - Geared Drive | | | Parallel Turbines | | | Series Turbines | | |
|---|---|---|---|---|---|---|---|---|---|---|---|---|---|
| | psi ($N/cm^2$) | FPDP psi ($N/cm^2$) | $I_{vac}$ $lb_f$-sec/$lb_m$ (N Sec/kg) | Wt - lb (kg) | FPDP psi ($N/cm^2$) | $I_{vac}$ $lb_f$-sec/lb (N Sec/kg) | Wt - lb (kg) | FPDP psi ($N/cm^2$) | $I_{vac}$ $lb_f$-sec/$lb_m$ (N Sec/kg) | Wt - lb (kg) | FPDP psi ($N/cm^2$) | $I_{vac}$ $lb_f$-sec/lb (N Sec/kg) | Wt - lb (kg) |
| Gas Generator | 800 | 1368 | 399.7 | 144 | 1368 | 400.1 | 131 | 1368 | 400.4 | 143 | 1368 | 401.1 | 135 |
| | (551.6) | (942.8) | (3920) | (65.3) | (942.8) | (3910) | (59.4) | (942.8) | (3910) | (64.9) | (942.8) | (3930) | (61.2) |
| | 500 | 751 | 395.4 | 138 | 751 | 395.7 | 126 | 751 | 395.5 | 138 | 751 | 395.9 | 130 |
| | (344.7) | (517.8) | (3880) | (62.6) | (517.8) | (3920) | (57.1) | (517.8) | (3920) | (62.6) | (517.8) | (3880) | (58.9) |
| Chamber Tapoff | 800 | 1368 | 399.7 | 142 | 1368 | 400.7 | 129 | 1368 | 400.4 | 141 | 1368 | 401.1 | 133 |
| | (551.6) | (942.8) | (3920) | (64.4) | (942.8) | (3930) | (58.5) | (942.8) | (3930) | (63.9) | (942.8) | (3930) | (60.3) |
| | 500 | 751 | 395.4 | 136 | 751 | 395.7 | 124 | 751 | 395.5 | 136 | 751 | 395.9 | 138 |
| | (344.7) | (517.8) | (3880) | (61.7) | (517.8) | (3880) | (56.2) | (517.8) | (3920) | (61.7) | (517.8) | (3880) | (62.6) |
| Auxiliary Heat | 800 | 1368 | 396.4 | 144 | 1368 | 398.4 | 131 | 1368 | 397.9 | 142 | 1368 | 399.4 | 137 |
| | (551.6) | (942.8) | (3890) | (65.3) | (942.8) | (3910) | (59.4) | (942.8) | (3900) | (64.4) | (942.8) | (3920) | (62.1) |
| Exchanger | 500 | 751 | 393.6 | 138 | 751 | 394.6 | 126 | 751 | 393.9 | 137 | 751 | 394.9 | 132 |
| | (344.7) | (517.8) | (3860) | (62.6) | (517.8) | (3870) | (57.1) | (517.8) | (3860) | (62.1) | (517.8) | (387) | (59.7) |
| Expander | 800 | --- | --- | --- | 2025 | 404.4 | 122 | | | | | | |
| | (551.6) | | | | (1396) | (3970) | (55.3) | | | | | | |
| | 500 | 953 | 397.8 | 119 | 915 | 397.8 | 115 | | | | | | |
| | (344.7) | (657.0) | (3920) | (54.0) | (630.9) | (3900) | (52.1) | | | | | | |
| Staged Combustion | 800 | | | | 1550 | 404.4 | 127 | | | | | | |
| | (551.6) | | | | (1068) | (3960) | (57.6) | | | | | | |

1.6 $lb_f$-sec/$lb_m$ (15.69 N-sec/kg) = Leakage flow of 0.05 lb/sec (0.0227 kg/sec)

a. Solid Carbon in the Turbine and Gas Generator

The presence of solid carbon could cause fouling of the turbine and of a gas generator injector with a resulting loss in turbine power. With lox/RP-1 gas generators having approximately the same weight fractions of solid carbon in the exhaust as flox/methane, turbine fouling has been found to be sensitive to the gas generator combustion temperature. With flox/methane no experimental gas generator data are available, but the very small blade dimensions and clearances required for a 5,000 lb (22.24 kN) engine cause possible fouling to be of major concern, and protection for the turbine would add complexity. Solid carbon is considered a potential problem with all cycles using combustion products for turbine drive, i.e., the gas generator, tapoff, and preburner cycles.

b. Control of Low Flowrates

For a gas generator, oxidizer flowrate at full thrust would be only 0.075 lb/sec (0.0340 kg/sec). A cavitating venturi to control this flow would have a throat area of only 0.021 in. (0.0529 cm). An annular variable area cavitating venturi for throttling would have an annulus width of under 0.010 in. (0.0252 cm) at full thrust and this would be reduced at throttled conditions. Orifices would have larger diameters than cavitating venturis, but would provide less positive control. The control of flowrates at this low level to provide both mixture ratio and total flow within acceptable limits therefore may not be possible with conventional approaches; it presents no insurmountable problems, but it does create the possibility of added complexity, such as use of throttle or bypass valves in the hot gas system, in the gas generator cycle.

c. Start Transient Requirements

If a bootstrap start can be used, system complexity is considerably reduced. Without detailed transient studies, the feasibility of a bootstrap start cannot be fully assessed. It does appear, however, that a bootstrap start would be more difficult with gas generator and preburner cycles because of mixture ratio and flow control requirements during transient operation.

d. Coolant Flow Control and Channel Dimensional Tolerances

Coolant passage dimensions are generally smaller for the closed cycles. Channel tolerance requirements are not, however, more severe for the closed cycle engines because the lower jacket pressure drops and reduced coolant density changes through the jacket cause the coolant distribution to be inherently more uniform than for the open cycles. It was therefore concluded that there are no significant manufacturing differences between thrust chambers for the various cycles.

e. Turbopump Requirements

Fuel pump and turbine dimensional requirements for the closed cycles are more severe than for the open cycles. With regard to the various turbopump configurations, the relative complexity is primarily a function of the number of components and the control system requirements.

f. Ranking

On the basis of the considerations above, the relative complexity of the various cycles and turbopump arrangements was judged to be as given in table VIII.

Table VIII. Relative Complexity of Cycles and Turbopump Arrangements*

| Cycles | Turbopump Arrangements |
|---|---|
| 1. Auxiliary Heat Exchanger | 1. Single Turbine, Direct Drive |
| 2. Tapoff | 2. Single Turbine, Geared Drive |
| 3. Gas Generator | 3. Parallel Turbines |
| 4. Expander | 4. Series Turbines |
| 5. Composite | |
| 6. Preburner | |

* Least complex ranked first.

2. Development Difficulty

Primary factors affecting the difficulty of development are considered to be bearing and seal limitations, materials limitations, ease and extent of component testing possible, and accuracy of design analysis. The most significant problem areas associated with these considerations were believed to be as described below.

a. Gas Generator Exhaust Products

It is likely that solid carbon in the gas generator exhaust would seriously hinder turbopump development as described in paragraph 1.a. HF in the exhaust could prove highly corrosive, require the use of more advanced materials, and possibly necessitate use of unusual shutdown procedures. The gas generator, tapoff, and preburner cycles would all be affected by these problems.

b. Pump Geometry

The small pump impeller and turbine vane and blade geometries associated with low flowrates and relatively high pressures make predictions of fluid dynamic efficiencies less accurate than for turbopumps of more usual sizes. Bearing, seal, and gearing losses are also relatively higher and accurate prediction is more important than for more conventional applications. These problems are slightly more severe with closed cycles than with open cycles because of the higher fuel pump pressure rise, higher turbine power requirements, and higher turbine working fluid density.

c. Lack of Gas Generator Property Data

Experience with lox/RP-1 engines has shown that the combustion temperature and gas thermodynamic properties are significantly different than the theoretically predicted values. Empirical data are available for lox/RP-1 gas generators; however, no such data exist for flox/methane. The data could readily be obtained as a part of a development program, but additional time would be required before accurate evaluations of delivered performance could be made.

d. Interrelationship of Thrust Chamber and Turbomachinery

The energy of the turbine working fluid in the expander cycle is dependent on heat exchange within the cooling jacket; consequently, any deviation in the chamber heat flux from the values assumed for design will influence the available turbine power. This necessitates either that turbopump development be delayed until experimental chamber data are available, or that adequate margins be established in the initial design.

In the tapoff cycle, turbine power is even more critically tied to thrust chamber operation. The propellants must be distributed so that gases may be withdrawn at a temperature compatible with turbine materials and power requirements. At the same time, any major maldistribution of propellants will seriously affect engine performance. It is anticipated that an optimum compromise between these two conflicting requirements would place significant restrictions on the thrust chamber and injector development effort.

e. Ranking

The relative ranking of the various cycles and turbopump configurations with respect to development difficulty is given in table IX.

Table IX. Relative Development Difficulty of Cycles and Turbopump Arrangements

| Cycles | Turbopump Arrangements |
|---|---|
| 1. Auxiliary Heat Exhanger | 1. Single Turbine, Geared Drive |
| 2. Expander | 2. Single Turbine, Direct Drive |
| 3. Gas Generator | 3. Parallel Turbines |
| 4. Composite | 4. Series Turbines |
| 5. Tapoff | |
| 6. Preburner | |

3. Design Flexibility

Design flexibility features in this application were considered to be ease of uprating, the ability to handle variations in mixture ratio and $Q_m/Q_p$, and the ease with which the engine could be converted to other propellant combinations. Major restrictions on flexibility are described below.

a. Cycle Power Limits

Limits on cycle power may restrict the ability of the closed cycles, particularly the expander cycle, to be uprated or operated at off-design conditions.

b. Injector Effects on Cycle

Because almost any variation in the cycle would affect injector operation, the flexibility of the tapoff cycle is limited, i.e., any variation in thrust, mixture ratio, etc., is likely to cause changes in

the composition of the gases tapped off the chamber or injector at any fixed location. This would affect turbine inlet temperature or might cause compromises that would produce an excessive drop in thrust chamber performance.

c. Heat Transfer Limits

Off-design operation causes variations in jacket wall temperatures and pressure drops which can, in some instances, limit flexibility. Most seriously affected from this standpoint would be the expander and auxiliary heat exchanger cycles.

d. Ranking

Table X summarizes the relative ranking of the cycles and turbopumps for flexibility.

Table X. Relative Design Flexibility of Cycles and Turbopump Configurations

| Cycles | Turbopump Arrangements |
|---|---|
| 1. Gas Generator | 1. Series Turbines |
| 2. Preburner | 2. Parallel Turbines |
| 3. Composite | 3. Single Turbine, Geared Drive |
| 4. Auxiliary Heat Exchanger | 4. Single Turbine, Direct Drive |
| 5. Expander | |
| 6. Tapoff | |

4. Ease of Throttling

Throttling may be limited by jacket cooling limits, injector operation at low thrust, or prohibitive control requirements. The most significant potential limits on a low thrust flox/methane engine are described below.

a. Cooling Limits

Excessive wall temperatures or coolant bulk temperatures can be encountered as the engine is throttled. However, it is not possible to identify potential problems without analyses so for the purposes of qualitative rating, all cycles were considered equal in this regard.

The required analyses were completed for two cycles selected for further study at each of the two design points, and results are thoroughly discussed in Section III, paragraph F.

b. Injector Effects

The same factors that limit the design flexibility of the tapoff cycle (paragraph 3) would also be expected to provide difficulty with throttling.

c. Bulk Boiling Cooling

Cooling with bulk boiling was shown to be feasible under Contract NAS3-10294 (Reference 3); however, it presents special problems in control of flow, stability, and jacket coolant distribution. The higher jacket pressure associated with closed cycles reduces the thrust range over which bulk boiling would normally be encountered and some what reduces the extent of the problem. It would be possible to throttle coolant flow downstream of the cooling jacket to eliminate bulk boiling; however, this would result in an increased turbopump power requirement that would increase open cycle losses and provide additional limitations on closed cycle operation.

d. Solid Carbon in the Turbine and Gas Generator

If it is assumed that carbon fouling can be eliminated at full thrust this would not ensure that the problem would not recur at throttled conditions. Throttled versions of the tapoff, gas generator, and preburner cycles might, therefore, require additional development to overcome carbon fouling.

e. Ranking

In view of the above, throttling appeared to be feasible with all of the cycles considered and with all of the turbopump configurations except the single turbine with direct drive (which is subject to large efficiency degradation because of the low speed at full thrust). However, this conclusion was reached without the benefit of cycle analysis for throttled operation (which was accomplished later for selected cycles), so a completely accurate ranking was not possible. Table XI, therefore, simply represents the best attempt to rate the various cycles and turbopump arrangements on the basis of the qualitative considerations.

Table XI. Relative Ease of Throttling of Cycles and Turbopump Configurations

| Cycles | Turbopump Arrangements |
|---|---|
| 1. Auxiliary Heat Exchanger | 1. Parallel Turbines |
| 2. Composite | 2. Single Turbine, Geared Drive |
| 3. Preburner | 3. Series Turbines |
| 4. Gas Generator | 4. Single Turbine, Direct Drive |
| 5. Expander | |
| 6. Tapoff | |

5. Production Cost

Development cost would be expected to reflect complexity and difficulty of development. Factors considered most influential with regard to engine production cost were the complexity of the turbopump configuration and the intricacy of the internal passages and their dimensional requirements, the thrust chamber coolant passage geometry, the number of valves and accessory components, and special material requirements. Specific factors that influenced the rankings are presented in the following paragraphs.

a. Pump Design Tolerances

The smaller internal dimensions and consequent tighter tolerances on internal dimensions indicate the turbopump costs would be somewhat higher for the closed cycles.

b. HF in Turbine Working Fluid

The presence of HF and higher turbine inlet temperatures would require use of more advanced turbine materials for the gas generator, tapoff, and preburner cycles.

c. Ranking

The relative cost ranking of the various cycles and turbopump configurations is shown in table XII.

Table XII. Relative Production Cost of Cycles and Turbopump Configurations

| Cycles | Turbopump Arrangements |
|---|---|
| 1. Auxiliary Heat Exchanger | 1. Single Turbine, Direct Drive |
| 2. Gas Generator | 2. Single Turbine, Geared Drive |
| 3. Expander | 3. Parallel Turbines |
| 4. Tapoff | 4. Series Turbines |
| 5. Composite | |
| 6. Preburner | |

6. Combined Ranking

Based upon equal weighting of the five factors considered in paragraphs 1 through 5, a combined ranking of the cycles and the turbopump arrangements was made. The results of this ranking are given in table XIII.

Table XIII. Overall Relative Ranking Based on Factors Considered

| Cycles | Turbopump Arrangements |
|---|---|
| 1. Auxiliary Heat Exchanger | 1. Single Turbine, Geared Drive |
| 2. Gas Generator | 2. Single Turbine, Direct Drive |
| 3. Expander | 3. Parallel Turbines |
| 4. Composite | 4. Series Turbines |
| 5. Preburner | |
| 6. Tapoff | |

The cycle-turbopump arrangement combinations were compared at both design points using performance and weight data and the combined qualitative rankings. The individual cycle ranking and turbopump ranking lists of table XIII were used to establish a combined ranking for the various cycle-turbopump combinations. The relative importance of differences between cycle and turbopump arrangement consideration is primarily a matter of judgment. As a guide, the qualitative difference between the first and last turbopump arrangement was judged to be about half as great as the qualitative difference between the first and last cycle.

To permit simultaneous consideration of the qualitative rankings and performance parameters, a rating plot technique was used. The qualitative rankings established position on the vertical scale of the plots, and a performance rating factor based on vacuum specific impulse and engine weight determined the locations on the horizontal scale. Earlier analyses of typical missions applicable to low thrust space storable engines had indicated that 20 lb (9.07 kg) of engine weight affected stage $\Delta V$ to the same extent as 1 $lb_f$-sec/$lb_m$ (9.81 N-sec/kg) of specific impulse. Using this as a trade factor, the cycle performance rating was calculated as:

$$PR = \Delta I_{vac} - \Delta Wt/20$$

where the $\Delta$ values represent differences from the average of all of the cycle data given in table VII.

Rating plots are presented in figure 54 for Design Point 1 and figure 55 for Design Point 2. Note that the auxiliary heat exchanger cycle appeared superior on the basis of the qualitative ranking, the expander cycle offered the highest performance rating, and the gas generator cycle provided a compromise between the qualitative rating and performance maxima of the auxiliary heat exchanger and expander cycles, respectively. The single turbine with geared pumps was indicated to be the most desirable for all of the cycles.

Figure 56 presents a combined rating plot for both design points. The relative performance parameters were readily adjusted to a new average for the comparison, but there was no straightforward way to handle qualitative factors. Therefore, in view of the higher chamber pressure, an arbitrary reduction in the qualitative ratings for Design Point 1 were made, the extent being essentially a matter of judgment. The reduction is believed to be realistic; for example, a comparison of the expander cycle at Design Point 2 ($P_c$ = 500 psia; 344.7 N/$cm^2$) with the auxiliary heat exchanger cycle at Design Point 1 ($P_c$ = 800 psia; 551.6 N/$cm^2$) with a single turbine, geared pumps in both cycles, provides a useful insight into the relative qualitative characteristics of the two design points. Both cycles have similar materials and component requirements except that the auxiliary heat exchanger cycle must have additional thrust chamber manifolding for the heat exchanger. Both

cycles utilize turbines driven by heated methane rather than combustion products, and the expander cycle has a somewhat lower pump discharge pressure than the auxiliary heat exchanger cycle at the higher chamber pressure. A cursory comparison would, therefore, suggest that the expander cycle at Design Point 2 would have a slightly higher qualitative rating than the auxiliary heat exchanger at Design Point 1. This comparison is in agreement with the results shown in figure 56. Figure 56 also shows that when the design point is included as an additional factor in the rating, the auxiliary heat exchanger at Design Point 2 rates highest qualitatively, the expander cycle at Design Point 1 rates highest on a performance basis, and the auxiliary heat exchanger cycle at Design Point 1 and the expander cycle at Design Point 2 provide median compromises between the two rating variables.

The ranking plots showed no clear superiority for any cycle-turbopump arrangement on the combined basis of performance and qualitative rating at either design point, but rather showed the auxiliary heat exchanger to be superior from the standpoint of development considerations while the expander provided highest performance. The gas generator provided a compromise, but an overriding concern over turbine fouling led to its rejection. Thus, on the basis of the cycle rating, the auxiliary heat exchanger and expander cycles with a single turbine, geared pump configuration at both design points were judged as superior choices to any other for further analysis. This recommendation was made to and approved by the NASA-LeRC Project Manager and the study proceeded to the next phase.

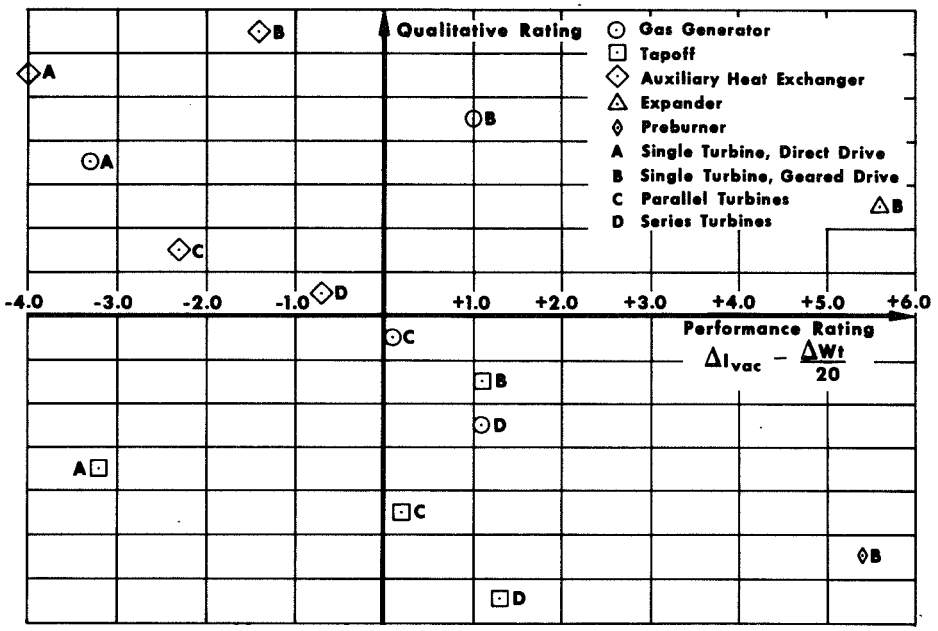


Figure 54. Qualitative Rating/Performance Comparison Design Point 1 (800 psia; 551.6 N/cm$^2$)

GS 8869A

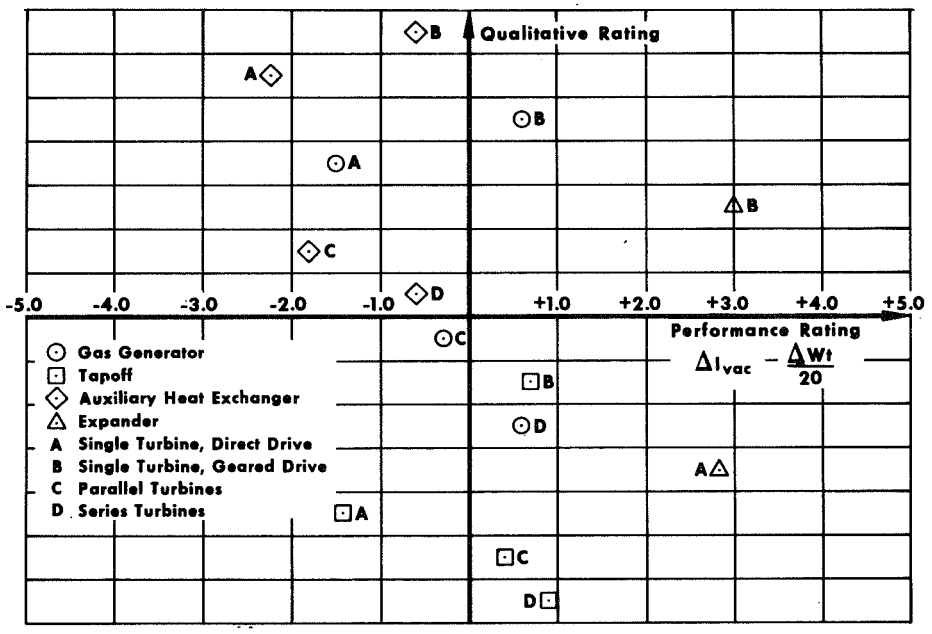


Figure 55. Qualitative Rating/Performance Comparison Design Point 2 (500 psia; 544.7 N/cm$^2$)

GS 8870A

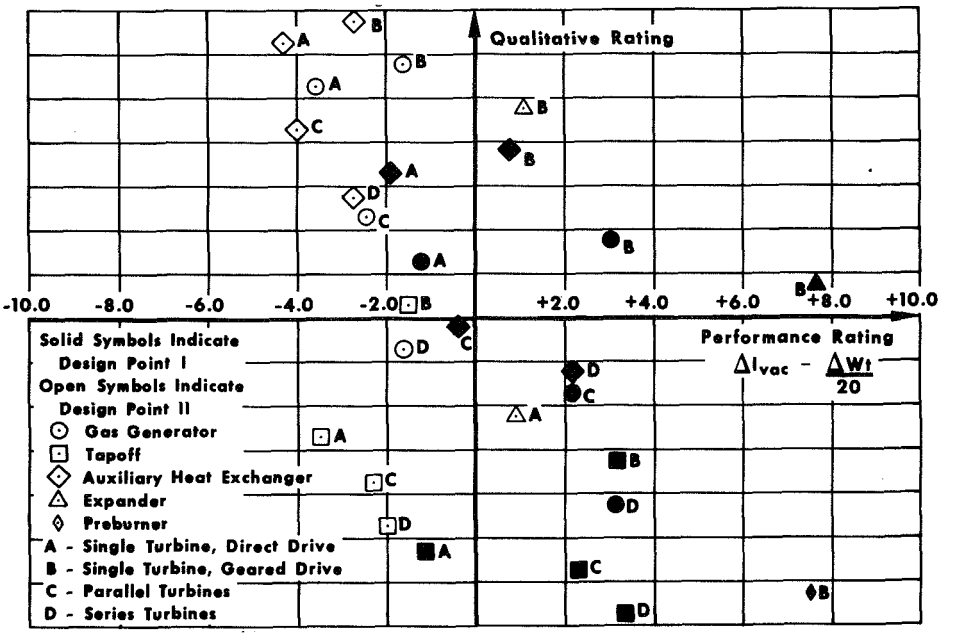


Figure 56. Qualitative Rating/Performance Comparison Design Points 1 and 2' GS 8868A

## E. THRUST CHAMBER GEOMETRY AND COOLING REQUIREMENTS

Before proceeding with the "Cycle Energy Balance," or final screening, important thrust chamber and coolant passage dimensions tentatively set in the preliminary regenerative cooling analysis were finalized for each of the cycles selected at both design points. The fixed geometries were then evaluated at off-design conditions to determine the effects of variations in $Q_m/Q_p$, r, and $P_c$ on coolant bulk temperature rise, coolant pressure drop, and thrust chamber wall temperature.

### 1. Chamber Performance

In accordance with contract requirements, delivered engine performance for all phases of the study was based on 94% of the theoretical specific impulse less cycle losses. Table XIV shows nominal performance exclusive of cycle losses for the two design points. For closed cycles, the cycle losses are limited to bearing coolant and seal leakage losses and are nominally less than 0.5%. For open cycles, the vacuum impulse will be lower by an additional 1 to 2%.

For purposes of thrust chamber design, the 94% vacuum impulse efficiency was considered to result from a characteristic exhaust velocity efficiency ( $\eta_{c^*}$) of 97%, which establishes thrust coefficient effi-

ciency as 96.91%. Theoretical performance data required were generated using a computer program based on analytical procedures developed by Stuart Brinkley (Reference 10). JANAF thermochemical data were used for the calculations. Results were compared with calculations made using the NASA Lewis Research Center combustion deck (Reference 11) and found to agree to within 0.2%.

Table XIV. Predicted Performance Exclusive of Cycle Losses

| | Design Point 1 | Design Point 2 |
|---|---|---|
| Thrust | 5000 lb (2268 kg) | 5000 lb (2268 kg) |
| Chamber Pressure, $P_c$ | 800 psia (551.6 N/cm$^2$) | 500 psia (344.7 N/cm$^2$) |
| Mixture Ratio, r | 5.25 | 5.25 |
| Nozzle Expansion Ratio | 100 | 60 |
| Theoretical Vacuum Specific Impulse, $I_{vac}$ | 431.9 $lb_f$-sec/$lb_m$ (4235 N-sec/kg) | 424.9 $lb_f$-sec/$lb_m$ (4167 N-sec/kg) |
| Vacuum Impulse Efficiency, $I_{vac}$ (%) | 94.0 | 94.0 |
| Delivered Vacuum Impulse, $I_{vac}$ | 406.0 $lb_f$-sec/$lb_m$ (3981 N-sec/kg) | 399.4 $lb_f$-sec/$lb_m$ (3917 N-sec/kg) |
| Theoretical Characteristic Velocity, c* | 7145 ft/sec (2178 m/sec) | 7104 ft/sec (2165 m/sec) |
| Characteristic Velocity Efficiency, c*, (%) | 97.0 | 97.0 |
| Delivered Characteristic Exhaust Velocity, c* | 6931 ft/sec (2113 m/sec) | 6800 ft/sec (2072 m/sec) |
| Theoretical Vacuum Thrust Coefficient, $C_{Fvac}$ | 1.945 | 1.865 |
| Vacuum Thrust Coefficient Efficiency, $C_F$ | 96.91 | 96.91 |
| Delivered Vacuum Thrust Coefficient, $C_{Fvac}$ | 1.885 | 1.865 |
| Propellant Flowrate, $\dot{w}$ | 12.2 lb/sec (5.53 kg/sec) | 12.2 lb/sec (5.53 kg/sec) |

2. Chamber Geometry

a. Combustion Chamber

The combustion chamber contraction ratio and length were based on consideration of injection and combustion requirements, engine weight, and heat transfer.

Analysis under Contract NAS3-11190 showed that a contraction ratio of 4.0 provided acceptable injection thrust-per-element (77.0) and element densities for a 5000-lb (22.24 kN) thrust, 500-psia (344.7-N/cm$^2$) chamber pressure flox/methane thrust chamber, or the equivalent of Design Point 2 (Reference 6). For contraction ratios much below 4.0 the required element densities surpass what is regarded as current technology, i.e., approximately 3 per inch, if the thrust-per-element is maintained. To achieve the same thrust-per-element at 800 psia (551.6 N/cm$^2$) a contraction ratio of 6.4 would be required. For a fixed chamber length, which was ultimately selected, such a high contraction ratio would significantly increase L* requirements resulting in a substantially higher chamber weight and a coolant temperature rise. A contraction ratio of 5.0 and thrust-per-element of 100 appear to be a desirable compromise between engine size and injection requirements.

The subsonic portion of the thrust chamber used in Contract NAS3-11190 consisted of a throat section and two cylindrical spool pieces. The chamber length could be varied by removing one of the spool pieces, and in this manner the effect of chamber length on combustion efficiency and heat transfer was evaluated. The thrust chamber contours used in the preliminary regenerative cooling analysis were based on similar geometries, i.e., cylindrical combustion chambers, but with theoretical rather than experimental heat flux profiles. The flexibility of removable spool pieces is not required for a flightweight design, and the cylindrical chamber configuration has been found to cause several design problems. First, the rapid change in flow area and velocity in the throat entrance of the Contract NAS3-11190 cylindrical design was found to produce a higher than predicted heat flux upstream of the nozzle throat. Similar results have been found with other chambers having sharp convergence angles, and boundary layer theory predicts that the problem is reduced with more gradual convergence. Second, rapid

convergence at the throat increases the L* for a given chamber length. In experimental testing of a 65 element coaxial injector in the cylindrical $\epsilon_c$ = 4.0 thrust chamber, an $\eta_{c*}$ of 97% was demonstrated with an L* of 52, but only 95.5% was obtained with an L* of 30 (Reference 6). However, it is believed that the injector was not fully optimized, and furthermore, most experimental data indicate combustion efficiency is related more to actual chamber length than to L*. For a given chamber length the engine weight and total heat transfer increase with increasing L*. Therefore a gradual convergence chamber contour of a length approaching that of the Contract NAS3-11190 L* = 52 in. (134.1 cm) chamber, but with a resulting lower L* was assumed; the finalized combustion chamber contour is shown in figure 57.

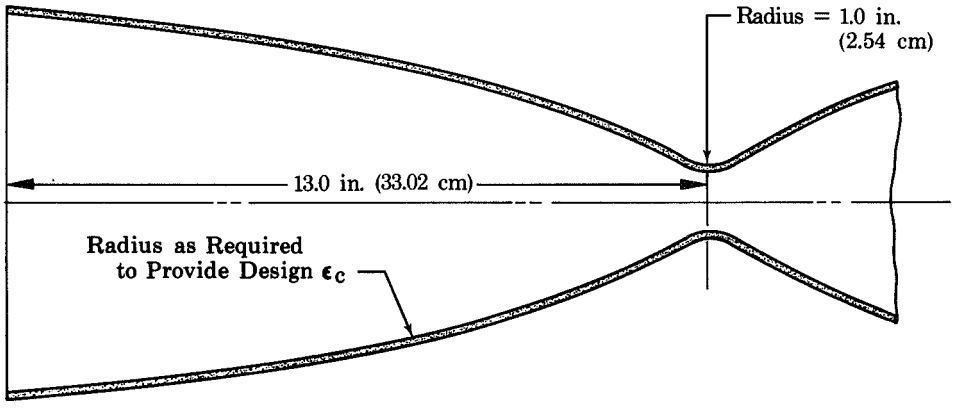


Figure 57. Combustion Chamber Contour FD 25589A

The distance from the injector plane to the nozzle throat was set at 13.0 in. (33.02 cm). Thirteen inches (33.02 cm) have been found to be an optimum combustion chamber length in many experimental investigations. Experimental flox/methane tests conducted under Contract NAS3-6296 (Reference 2) indicated that increasing the chamber length from 13 to 23 in. (33.02 to 58.42 cm) provided no measurable increase in performance. Under Contract NAS3-11190, an increase in length from 9.5 to 14.2 in. (24.13 to 36.07 cm) provided a 1.6% increase in characteristic velocity efficiency at a mixture ratio of 5.25 (Reference 6). Thus, the limited data for flox/methane appear to substantiate the extensive data from other propellant combinations that 13.0 in. (33.02 cm) is a reasonable choice for thrust chamber length. Using the selected contour and contraction ratio, 13.0 in. (33.02 cm)

thrust chamber designs provide an L* of 42.5 in. (108.0 cm) at Design Point 1 and an L* of 36.0 in. (91.44 cm) at Design Point 2.

b. Expansion Nozzle

The exhaust nozzle contours for the two design points were established using P&WA's design method for truncated perfect nozzles (Reference 12). Figure 58 shows graphically the effect of length and untruncated design area ratio ($A_D$) on performance as a function of the exhaust nozzle diameter ratio ( $D/D_T$). The $C_{Fvac}$ data shown are theoretical isentropic thrust coefficients corrected for friction and divergence losses. The dotted lines define three methods of nozzle truncation which are commonly employed. The maximum $C_F$ on the vertical line determines the maximum performance which can be achieved for a given nozzle length. The maximum $C_F$ value on the horizontal line determines the maximum performance which can be achieved with a given nozzle expansion ratio. And the maximum $C_F$ value on the constant $A_S/A_T$ line defines the maximum performance obtainable with a given nozzle surface area (or nozzle weight). The three truncations are termed minimum length, maximum performance, and minimum surface nozzles, respectively. Another term commonly used by P&WA is "maximum payload nozzle." This truncation is based on an optimized trade-off between nozzle weight and performance as determined from numerous mission studies. Maximum payload nozzle performance (as determined by the $C_F$ for a given area ratio) is approximately midway between that of the maximum performance and minimum surface nozzles.

The nozzle truncation for the two design points was selected after consideration of the slope of a performance versus weight curve. Figure 59 shows predicted performance as a function of nozzle length for the two design points; the predicted variation in performance is based entirely on changes in the calculated friction and divergence losses. Figure 60 presents the calculated nozzle weight vs performance curve for the two design points based on a nozzle weight per unit area of 0.020 $lb/in^2$ (1.406 $gm/cm^2$), approximated from channel dimensional requirements established in preliminary studies. As in the case of engine weight treatment in the cycle selection described above, a trade-off factor of 20 lb (9.07 kg) of engine weight for 1 $lb_f$-sec/$lb_m$ (9.81 N-sec/

kg) of specific impulse was used. The slope of this trade-off factor is seen in figure 60 to correspond to the nozzle weight vs engine performance curve at the maximum performance truncation. In an actual application, there would probably be a vehicle interstage weight increase associated with increased nozzle length that could be significantly greater than the increase in engine weight, but this cannot be established without detailed definition of the vehicle design. However, it can be seen from figure 60 that there is a "knee" in the performance vs weight curve at the "maximum payload" point. This knee is common to virtually all engine designs; thus, most engines will optimize very near this knee, or maximum payload point, for a wide range of performance-weight tradeoff factors and effective weights per unit surface area (including interstage weight), and for this reason, a maximum payload truncation was selected for both design points.

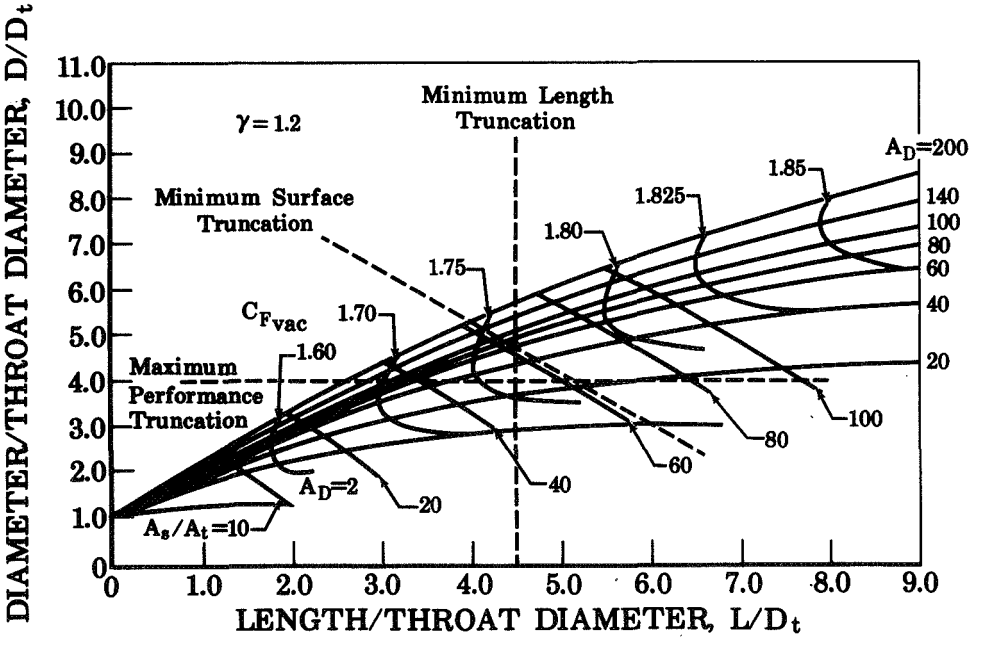


Figure 58. Perfect Nozzle Contours FD 6268B

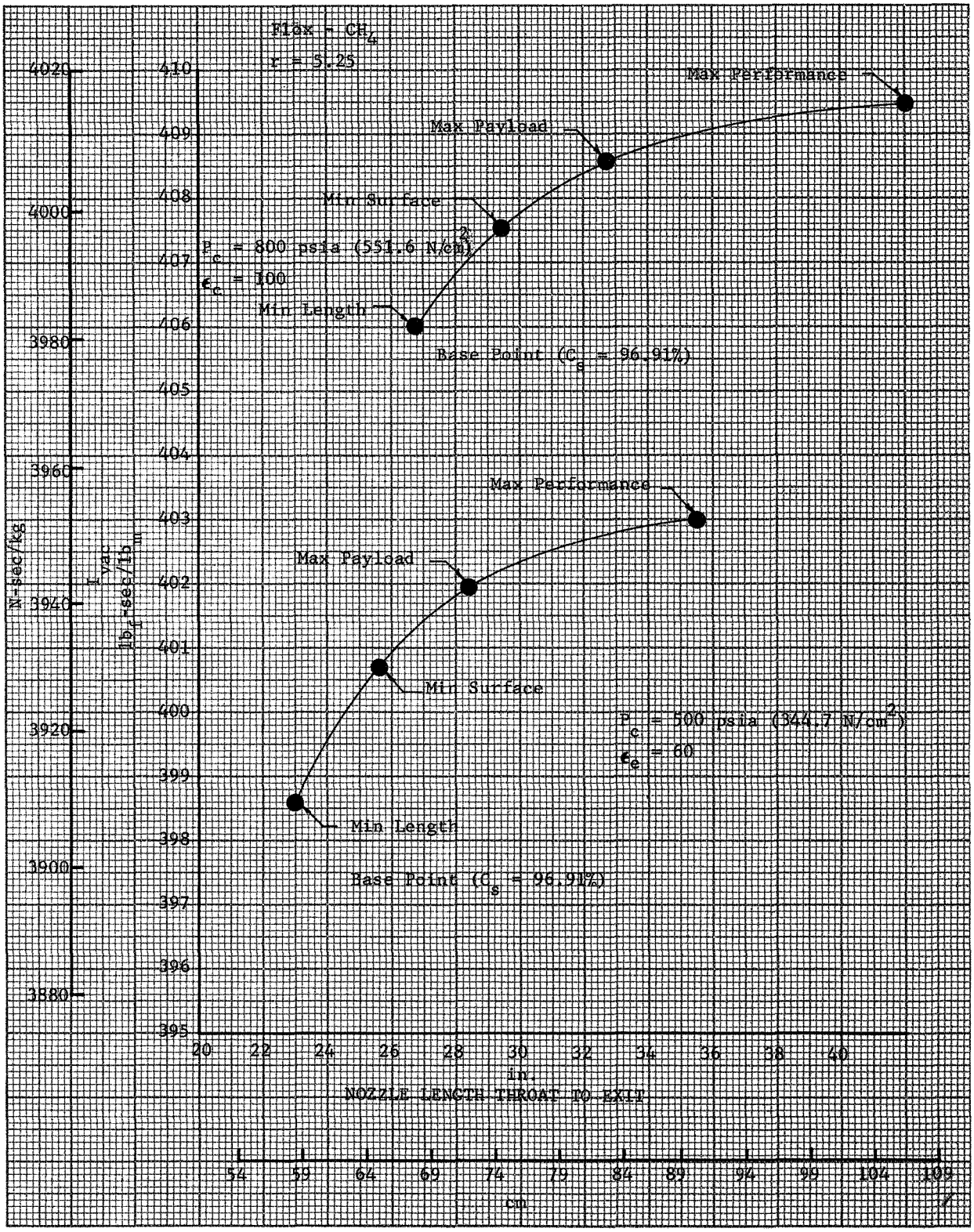


Figure 59. Nozzle Length Optimization DF 70854

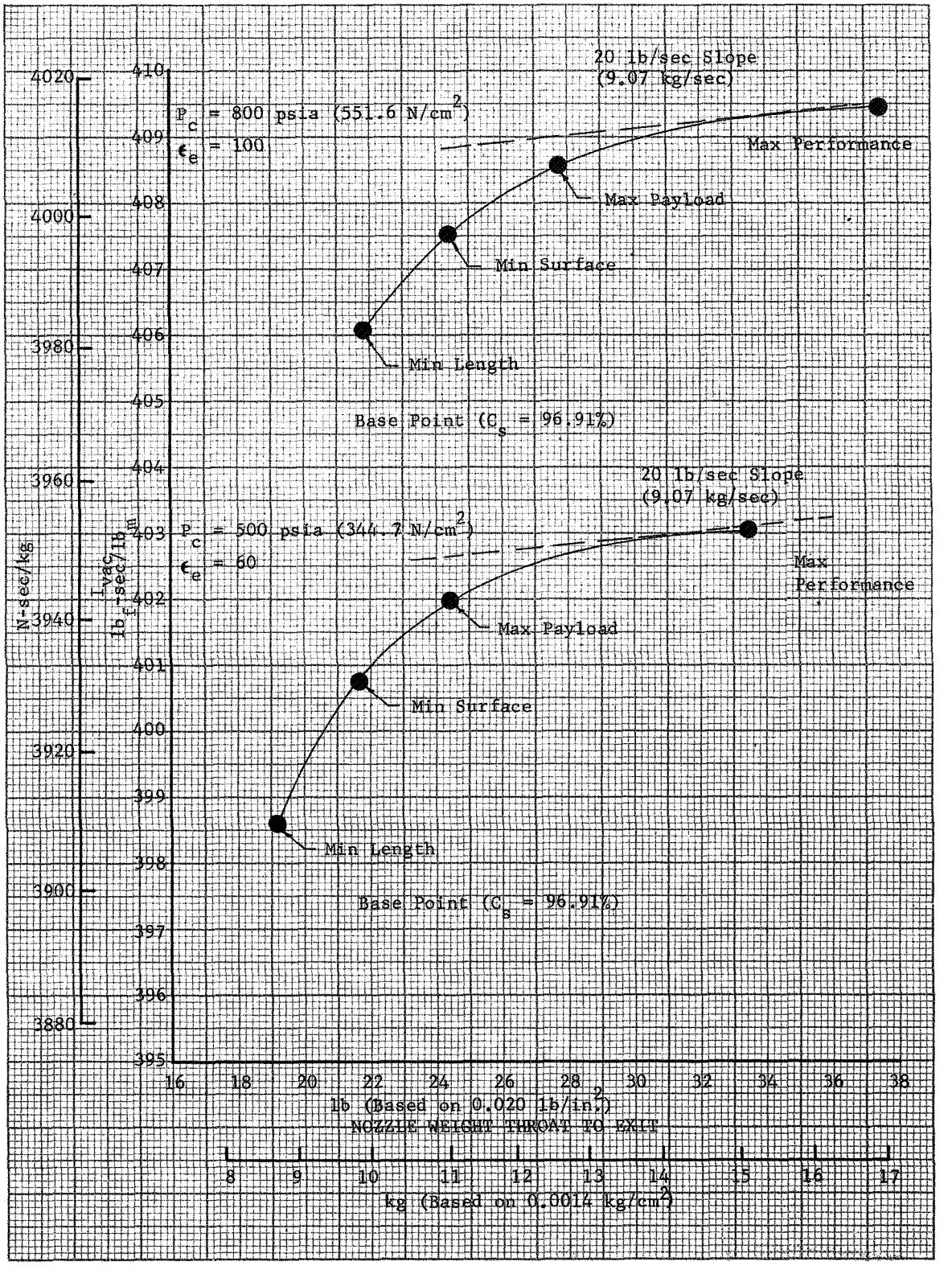


Figure 60. Nozzle Weight Optimization DF 70855

Design values for the nozzles at the two design points are summarized in table XV. In accordance with the Pratt & Whitney design method, nozzle contours are typically described in terms of a perfect nozzle contour truncated to the design area ratio. Therefore, for a given expansion ratio, design area ratios close to the actual area ratio produce longer nozzles. Other investigators frequently describe bell nozzle length in terms of a percentage of a 15 deg (0.262 rad) half-angle conical nozzle; values of this parameter are also included in table XV for comparison. It should be noted that the $C_s$ values used here are greater than those used for the performance predictions of table XIV, which are based upon achievement of 94% vacuum specific impulse efficiency. The differences provide margins for Kinetic losses, nozzle - $\eta c^*$ interactions, etc., or can simply be considered as conservatism in the calculations.

Table XV. Nozzle Description

| Design Point | Chamber Pressure psia ($N/cm^2$) | Truncated Expansion Ratio | Untruncated Expansion Ratio | % of Conical Nozzle | Length in. (cm) | $C_s$ (%) |
|---|---|---|---|---|---|---|
| 1 | 800 (551.6) | 100 | 162 | 89.4 | 30.75 (78.11) | 97.84 |
| 2 | 500 (344.7) | 60 | 95 | 84.1 | 27.56 (70.00) | 97.82 |

3. Coolant Passage Geometry

The thrust chamber internal cooling passage geometry for the expander and auxiliary heat exchanger cycles at Design Points 1 and 2 is shown in figures 61 through 64. In all instances, the passages were designed for a $Q_m/Q_p$ of 1.0 and a maximum hot wall temperature of 2160°R (1200°K). The geometry was established at the design points for both auxiliary heat exchanger cycles and for the expander cycle at the 800 psia (551.6-$N/cm^2$) chamber pressure level. The chamber coolant passages for the 500-psia (344.7-$N/cm^2$) expander cycle (Design Point 2) were designed to permit uprating to 8,000-lb (35.59 kN) thrust. The coolant flow path for the auxiliary heat exchanger is shown in figure 65. This configuration allows the heat exchanger for turbine flow to

be an integral part of the thrust chamber and to be located in a low heat flux region with minimum manifolding. The thrust chamber flow traverses the jacket in a single pass counter to the combustion gas flow.

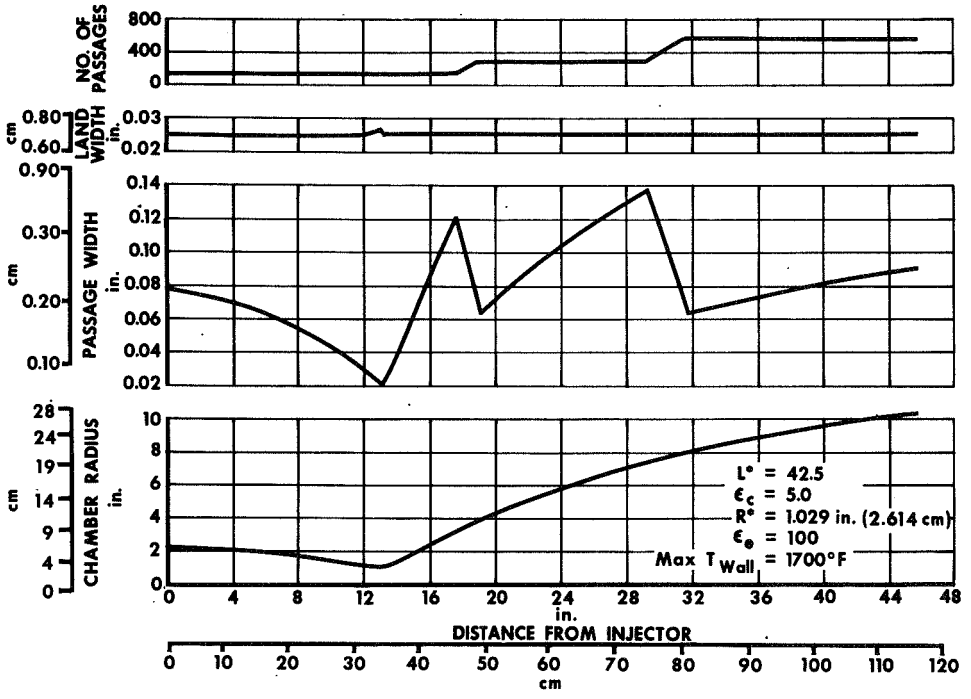


Figure 61. Thrust Chamber Cooling Passage Geometry Expander Cycle Design Point 1 GS 9575A

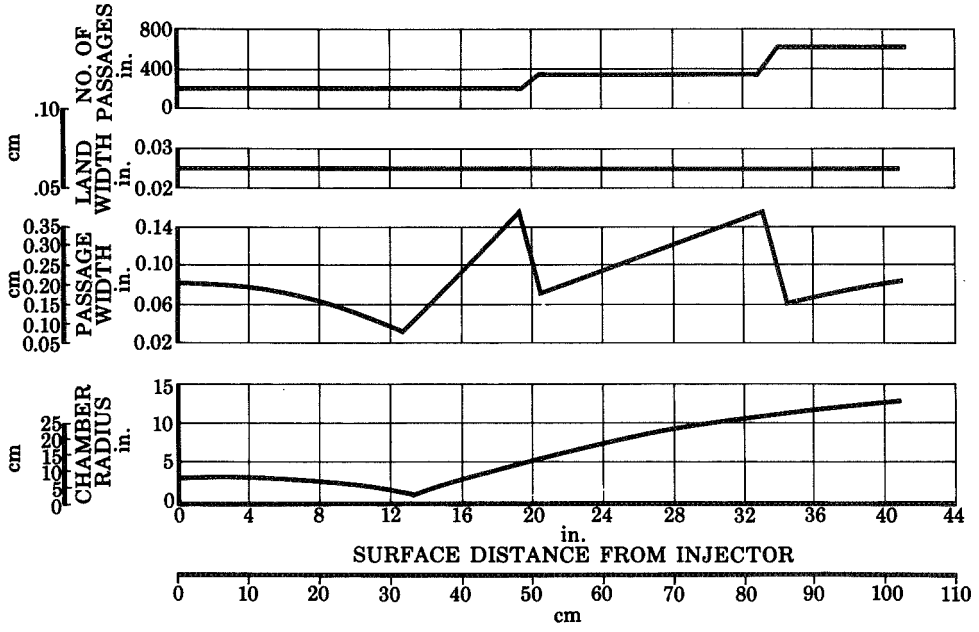


Figure 62. Thrust Chamber Cooling Passage Geometry Expander Cycle Design 2 FD 29219

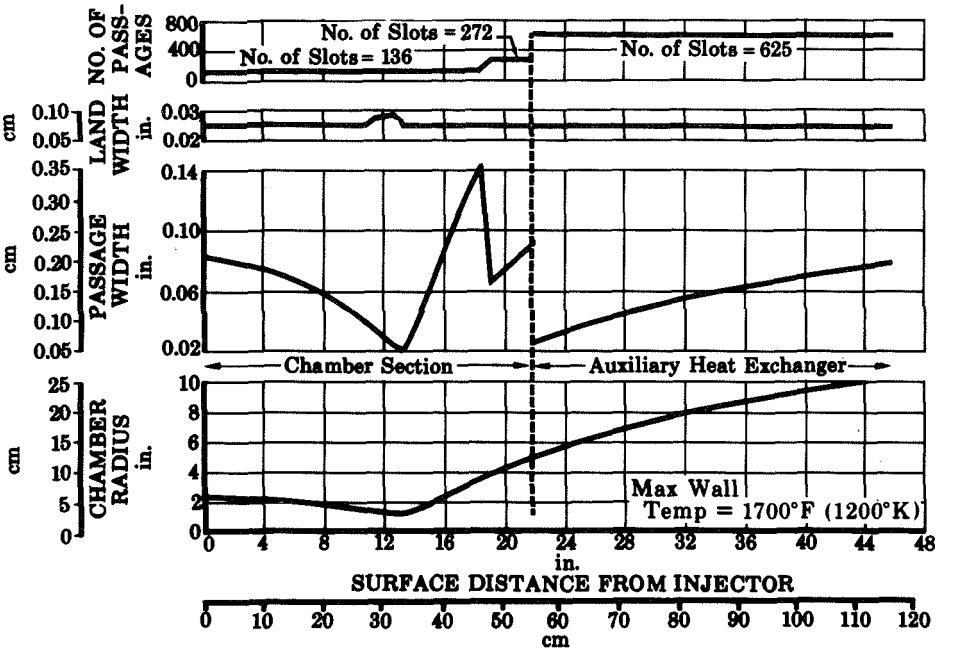


Figure 63. Thrust Chamber Cooling Passage Geometry Auxiliary Hex Cycle Design 1

FD 27935

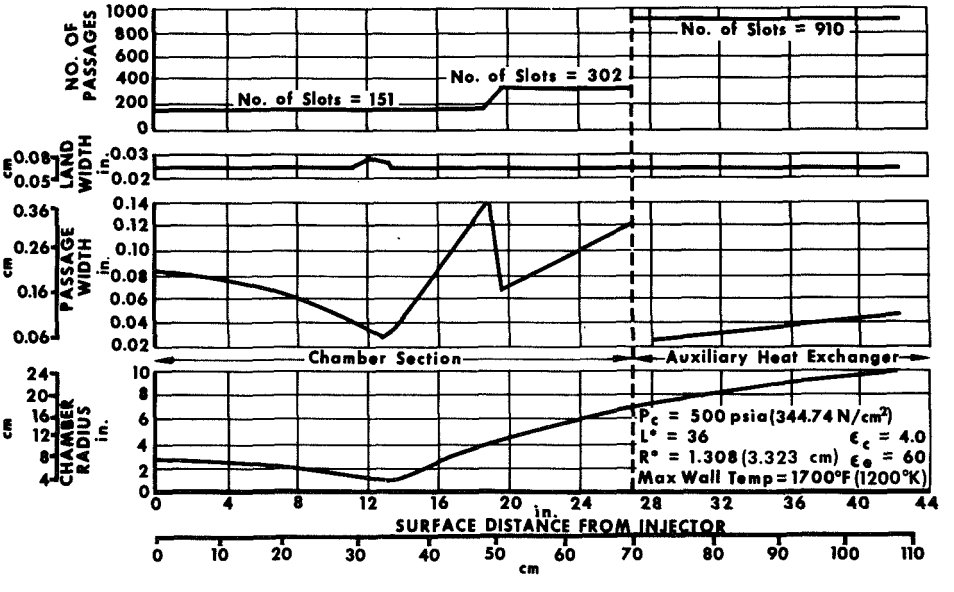


Figure 64. Thrust Chamber Cooling Passage Geometry Auxiliary Hex Cycle Design Point 2

GS 9577A

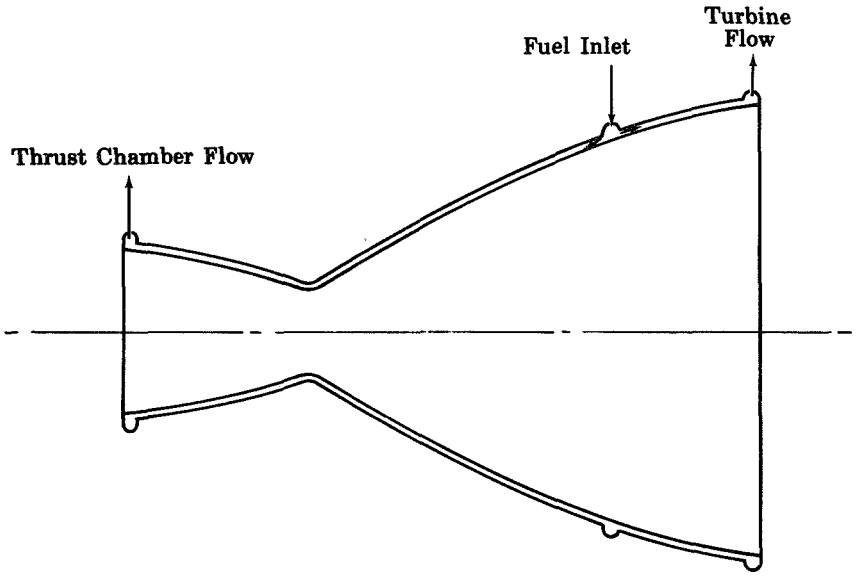


Figure 65. Auxiliary Heat Exchanger Configuration FD 25588

Major coolant channel dimensions and nominal design point cooling conditions are summarized in table XVI for the auxiliary heat exchanger and expander cycles at both design points. For the auxiliary heat exchanger cycle, both the main thrust chamber and auxiliary heat exchanger cooling conditions are listed. Also included in table XVI are the cooling conditions for the Design Point 2 expander cycle uprated to 8000-lb (35.59 kN) thrust (Design Point 2A). The jacket pressure drops shown in table XVI are substantially higher than those originally predicted in the preliminary regenerative cooling analysis. This is because of the increased chamber length selected for the final analysis and the more conservative limitation of design $Q_m/Q_p = 1.00$ for a maximum chamber wall temperature of 2160°R (1200°K) ($Q_m/Q_p = 0.90$ was used in the preliminary work). The maximum wall temperatures given in table XVI reflect temperatures for a $Q_m/Q_p$ of 0.90, the value predicted in actual usage, rather than the design value of 1.0. Because the coolant passage geometry for the Design Point 2 expander cycle was based on an 8000-lb (35.59 kN) thrust operating level to allow the uprating capability, (design at the higher reference point provided a further reduction in the 5000-lb (22.24 kN) thrust wall temperature.

Table XVI. Cooling Channel Dimensions and Cycle Design Point* Cooling Conditions

| | Expander Cycle | | | Auxiliary Heat Exchanger Cycle | |
|---|---|---|---|---|---|
| | Design Point 1 | Design Point 2 | Design Point 2A | Design Point 1 | Design Point 2 |
| Thrust | 5000 lb<br>22240 N | 5000 lb<br>22240 N | 8000 lb<br>35590 N | 5000 lb<br>22240 N | 5000 lb<br>22240 N |
| Chamber Pressure | 800 psia<br>551.6 N/cm$^2$ | 500 psia<br>344.7 N/cm$^2$ | 800 psia<br>551.6 N/cm$^2$ | 800 psia<br>551.6 N/cm$^2$ | 500 psia<br>344.7 N/cm$^2$ |
| Jacket Inlet Pressure | 2210 psia<br>1448 N/cm$^2$ | 1231 psia<br>848.8 N/cm$^2$ | 2053 psia<br>1415 N/cm$^2$ | 1472 psia<br>1015 N/cm$^2$ | 856 psia<br>590.2 N/cm$^2$ |
| Jacket $\Delta P$ | 498 psi<br>343.4 N/cm$^2$ | 335 psi<br>231.0 N/cm$^2$ | 457 psi<br>315.1 N/cm$^2$ | 444 psi<br>306.1 N/cm$^2$ | 267 psi<br>184.1 N/cm$^2$ |
| Jacket Outlet Temperature | 1560°R<br>866.7°K | 1415°R<br>786.1°K | 1340°R<br>744.4°K | 1332°R<br>739.4°K | 1331°R<br>722.8°K |
| Maximum Wall Temperature | 2030°R<br>1128°K | 1911°R<br>1061°K | 2006°R<br>1114°K | 1966°R<br>1092°K | 1989°R<br>1105°K |
| Passage Depth | 0.043 in.<br>0.1092 cm | 0.051 in.<br>0.1296 cm | 0.051 in.<br>0.1296 cm | 0.047 in.<br>0.1193 cm | 0.060 in.<br>0.1523 cm |
| No. of Passages at throat | 141 | 163 | 163 | 136 | 151 |
| Minimum Passage Width | 0.021 in.<br>0.0544 cm | 0.026 in.<br>0.0661 cm | 0.026 in.<br>0.0661 cm | 0.023 in.<br>0.0584 cm | 0.030 in.<br>0.0762 cm |
| Auxiliary Heat Exchanger | | | | | |
| Area Ratio Inlet Manifold | | | | 23.4 | 33.3 |
| Number of Passages | | | | 625 | 910 |
| Passage Depth | | | | 0.015 in.<br>0.0381 cm | 0.015 in.<br>0.0381 cm |
| Minimum Passage Width | | | | 0.025 in.<br>0.661 cm | 0.025 in.<br>0.661 cm |
| Outlet Temperature | | | | 1700°R<br>944.4°K | 1700°R<br>944.4°K |
| Pressure Drop | | | | 10 psi<br>6.90 N/cm$^2$ | 5 psi<br>3.45 N/cm$^2$ |
| Maximum Wall Temperature | | | | 1725°R<br>958.3°K | 1725°R<br>958.3°K |

* $Q_m/Q_p = 0.90$, r= 5.25

4. Off-Design Cooling Characteristics

a. Requirements

The off-design cooling characteristics of the thrust chambers were evaluated over the following ranges of operating variables:

| | Design Point 1 | Design Point 2 |
|---|---|---|
| $P_c$ | 80 to 800 psia (55.16 to 5516 N/cm$^2$) | 50 to 500 psia (34.47 to 344.7 N/cm$^2$); 50-800 psia (34.47 to 5516 N/cm$^2$) for the expander cycle |
| $Q_m/Q_p$ | 0.76 - 1.2 | 0.76 - 1.2 |
| $P_{in}/P_c$ | 2.4 - 4.0 | 2.4 - 4.0 |
| r | 4.0 - 5.75 | 4.0 - 5.75 |

The entire ranges of coolant pressure drop, coolant bulk temperature rise, and maximum thrust chamber wall temperatures of interest for the four operating variables can be evaluated parametrically with seven sets of curves for each cycle and design point. Representative curves for the expander cycle at Design Point 1 are given in figures 66 through 68. A complete set of curves for all cycles and design points is included in Appendix A (figures A-25 through A-36).

Jacket pressure loss can be represented by three sets of curves as shown in figure 66. Base $\Delta P/P_c$ data were calculated at a mixture ratio of 5.25 and a $Q_m/Q_p$ of 1.0. These data are shown in the top set of curves as a function of chamber pressure with lines of constant $P_{in}/P_c$. The other influence curves in the illustration provide corrections to the base data for changes in mixture ratio or $Q_m/Q_p$. It was established that the influence factors were independent of the other operating variables. Similar curves for determination of jacket temperature rise and for determination of the maximum wall temperatures are shown in figures 67 and 68, respectively. The effect of inlet pressure on the jacket temperature rise and on wall temperature is negligible; therefore no influence curves are shown for these variables.

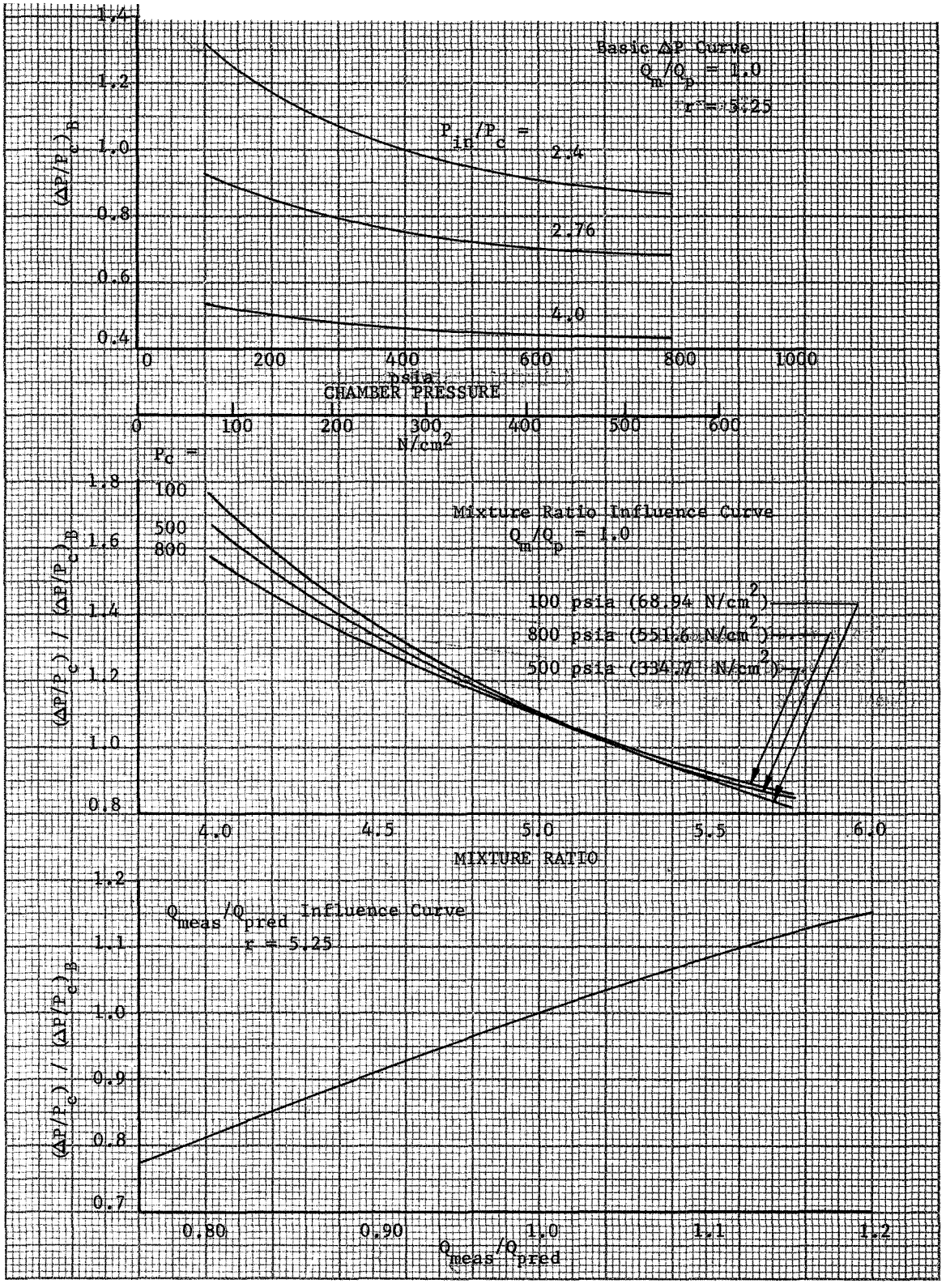


Figure 66. Thrust Chamber Cooling Characteristics Design I - Expander Cycle Jacket Pressure Drop

DF 70858

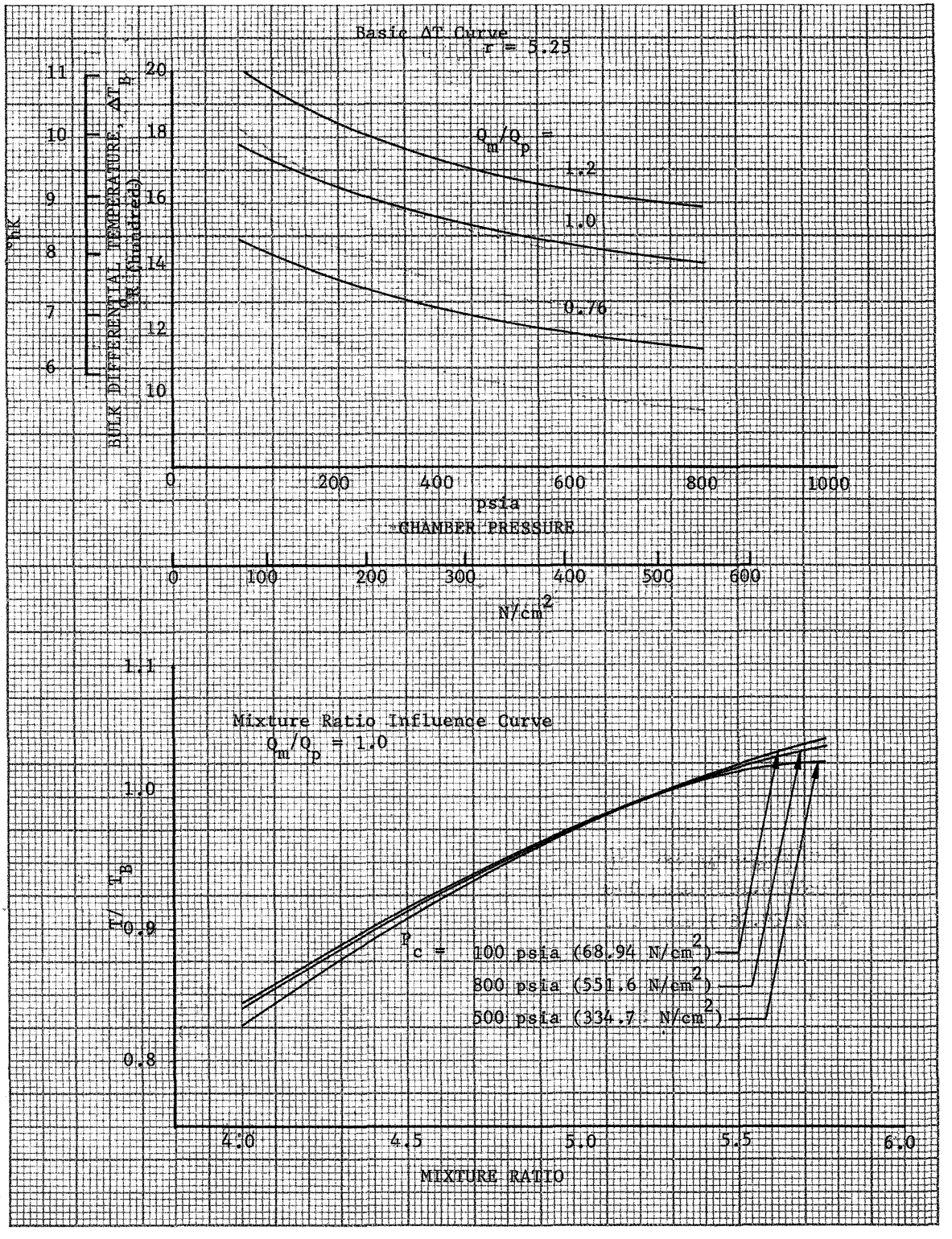


Figure 67. Thrust Chamber Cooling Characteristics Design I - Expander Cycle Bulk Temperature Ratio

DF 70859

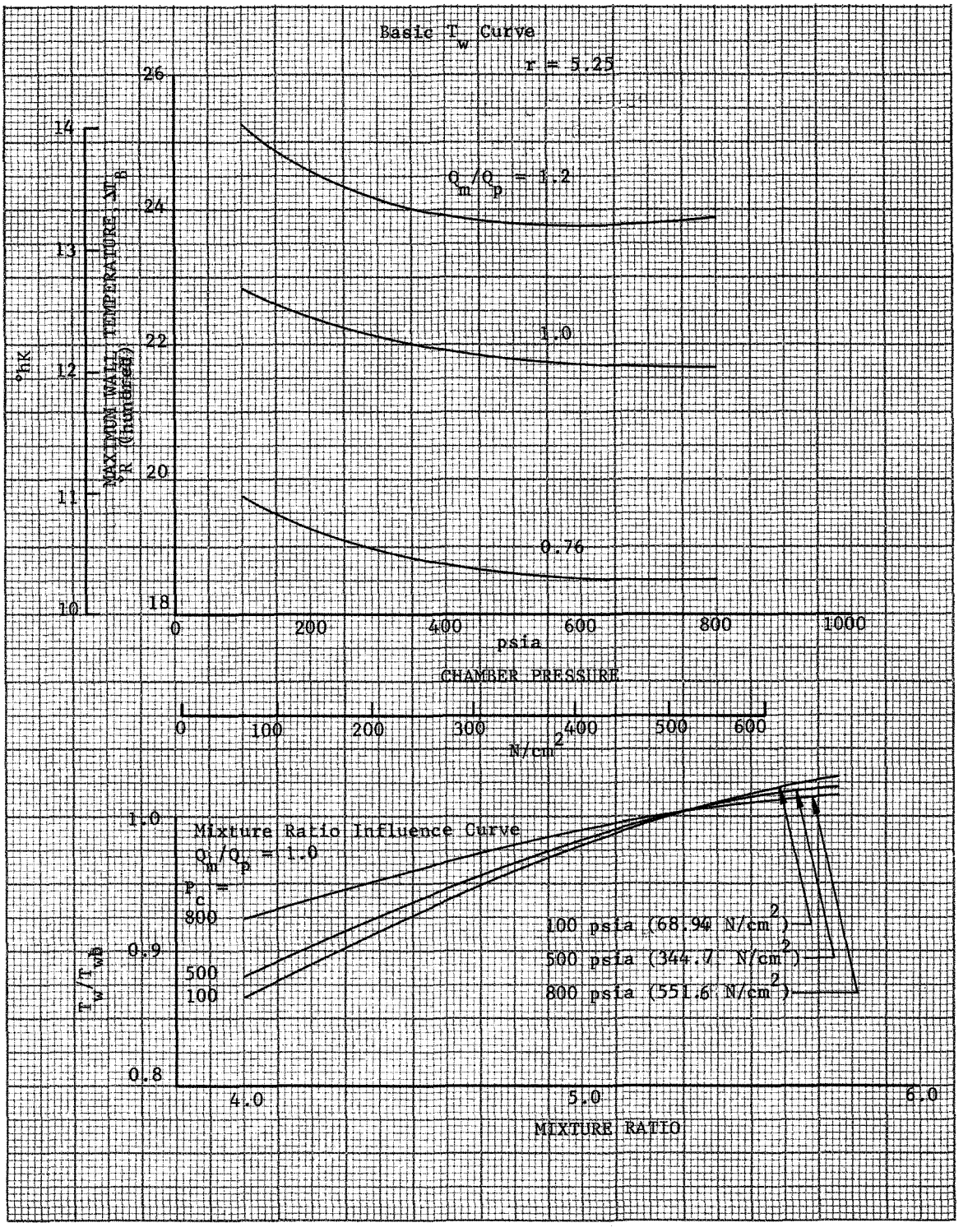


Figure 68. Thrust Chamber Cooling Characteristics Design I Expander Cycle Maximum Wall Temperature

DF 70860

b. Maximum Wall Temperature

Figures 69 and 70 present maximum wall temperature as a function of thrust for the expander cycle at Design Points 1 and 2. Wall temperature vs thrust was also calculated for the auxiliary heat exchanger cycle, and both design points were found to have values nearly identical to those shown for the expander cycle at Design Point 2. The small increase in wall temperature at reduced thrust over that at design point encountered with the expander cycle at Design Point 1 is not a problem because the internal pressures are so greatly reduced at throttled conditions that stress is not a problem. However, the high wall temperatures predicted at all thrust levels for $Q_m/Q_p$ values over 1.0 indicate that a severe problem may be encountered if local heat fluxes cannot be controlled.

c. Coolant Temperature

Figure 71 shows the calculated coolant bulk outlet temperature as a function of mixture ratio and $Q_m/Q_p$ for the expander cycle at Design Point 1. A curve showing the influence of mixture ratio on coolant outlet temperature is also included. The curves show significant increases in outlet temperature as thrust is decreased. It is desirable to keep the fuel temperature in the thrust chamber coolant passages below the incipient thermal decomposition temperature ($T_{ID}$) to prevent carbon formation and possible fouling or plugging of the coolant passages. In Reference 5, the point of incipient thermal decomposition of methane was taken as 1865°R (1036°K) based on an arbitrary decomposition limit of 1.0% per hour. The limiting decomposition temperature was evaluated at the film temperature (the mean value of the coolant side wall temperature and the coolant bulk temperature), which is on the order of 50° to 200°R (27.78 to 111.1°K) above the coolant bulk temperature. Thus, the coolant outlet temperatures indicated in figure 71 would limit throttling unless $Q_m/Q_p$ was maintained at a low value or the mixture ratio at low thrust was reduced.

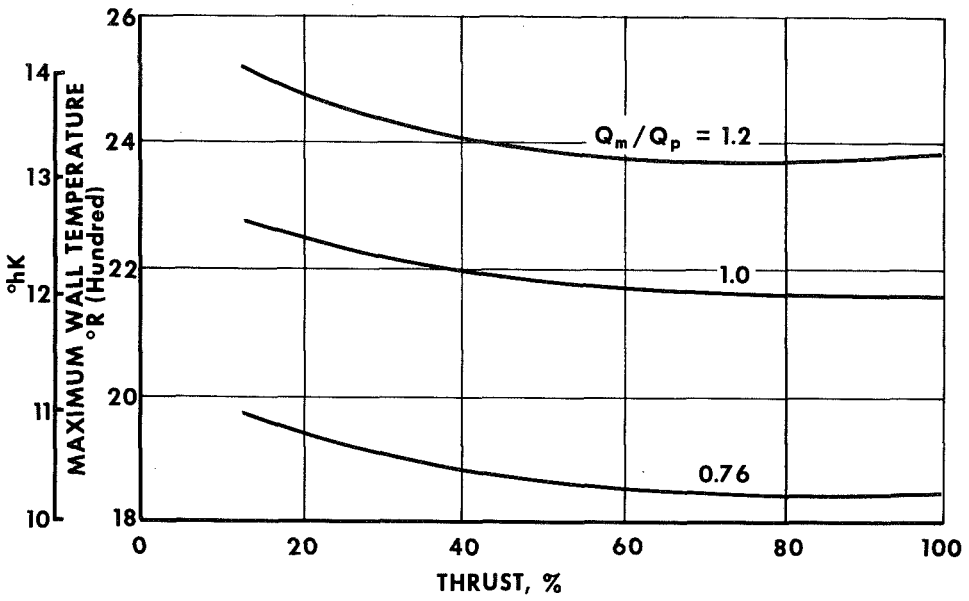


Figure 69. Thrust Chamber Cooling Characteristics Design Point 1 - Expander Cycle Maximum Wall Temperature GS 9579A

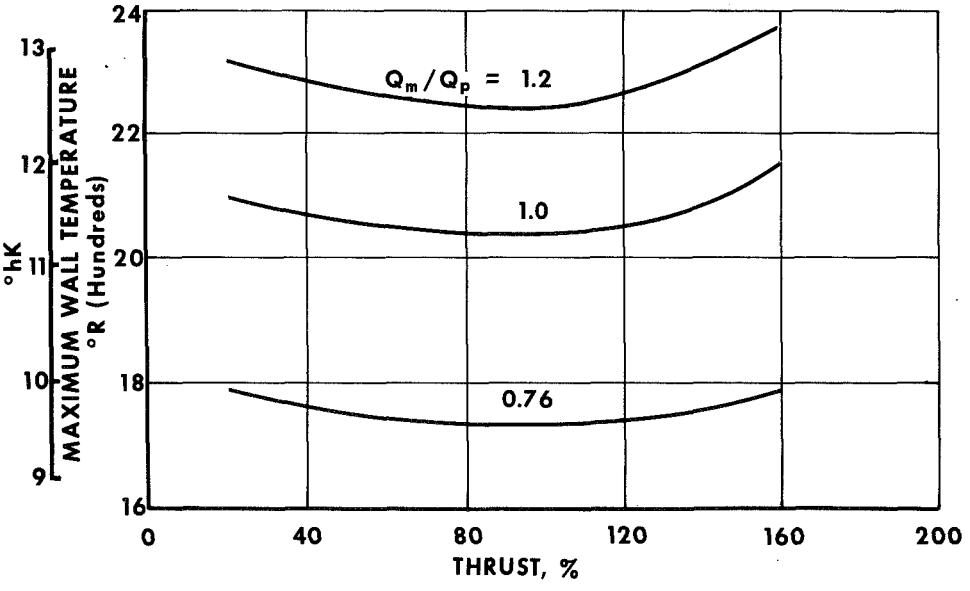


Figure 70. Thrust Chamber Cooling Characteristics Design Point 2 - Expander Cycle Maximum Wall Temperature GS 9580A

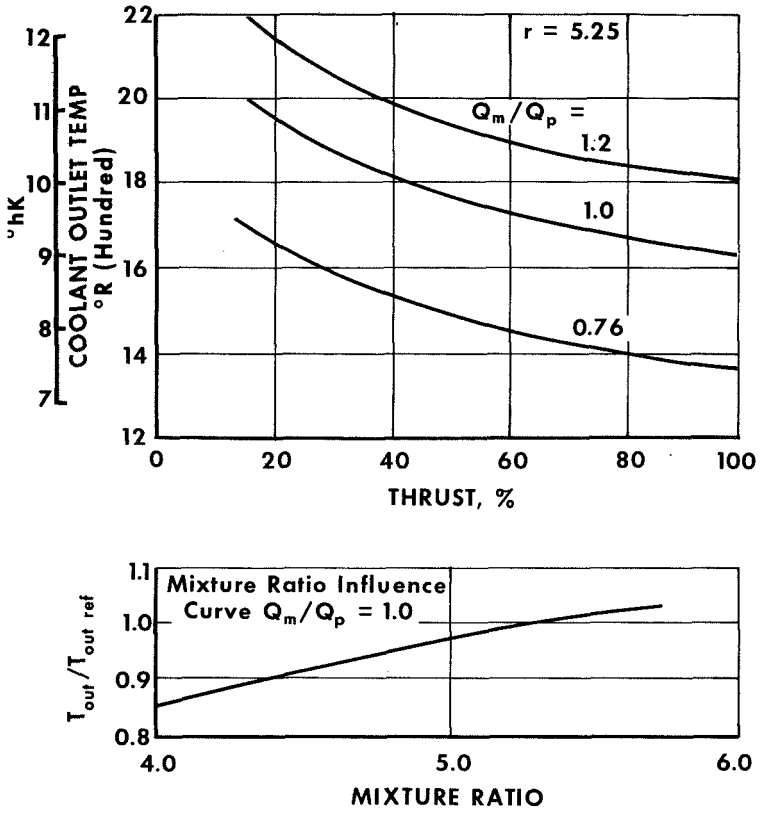


Figure 71. Thrust Chamber Cooling Characteristics Design Point 1 - Expander Cycle Bulk Temperature GS 9581A

Figure 72 shows the minimum chamber pressure obtainable with the expander cycle at Design Point 1 as a function of $Q_m/Q_p$ and mixture ratio when the 1865°R (1036°K) film temperature limit is observed. For constant mixture ratio throttling to 10% thrust, $Q_m/Q_p$ would be limited to approximately 0.77. On the other hand, for a $Q_m/Q_p$ of 0.9, mixture ratio would have to be reduced to below 4.3 to maintain a satisfactory film temperature.

The film temperature limitation on throttling indicated in figure 72 was found to be restrictive only for the expander cycle at Design Point 1. Figure 73 compares the film temperature limits at 10% thrust for all four cases studied. The curves show the maximum $Q_m/Q_p$ value that can be tolerated for a given value of mixture ratio. It can be seen that for constant mixture ratio throttling at the design mixture ratio of 5.25, while the expander cycle at Design Point 1 is limited to a $Q_m/Q_p$ value of 0.77, the other three cases have nearly equal $Q_m/Q_p$

limits of 0.90 to 0.95. Testing under Contract NAS3-11190 has indicated that for characteristic velocity efficiencies of 97% and higher $Q_m/Q_p$ values of approximately 0.90 will be achieved (Reference 6). Thus, constant mixture ratio throttling would be feasible in three of the four cases.

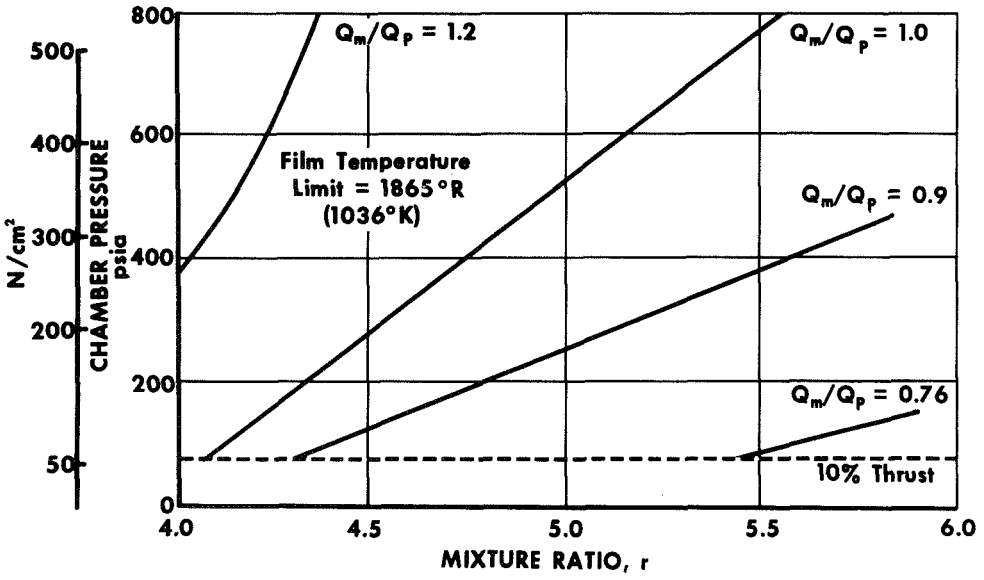


Figure 72. Expander Cycle Fuel Decomposition Limits Design Point 1 GS 9582A

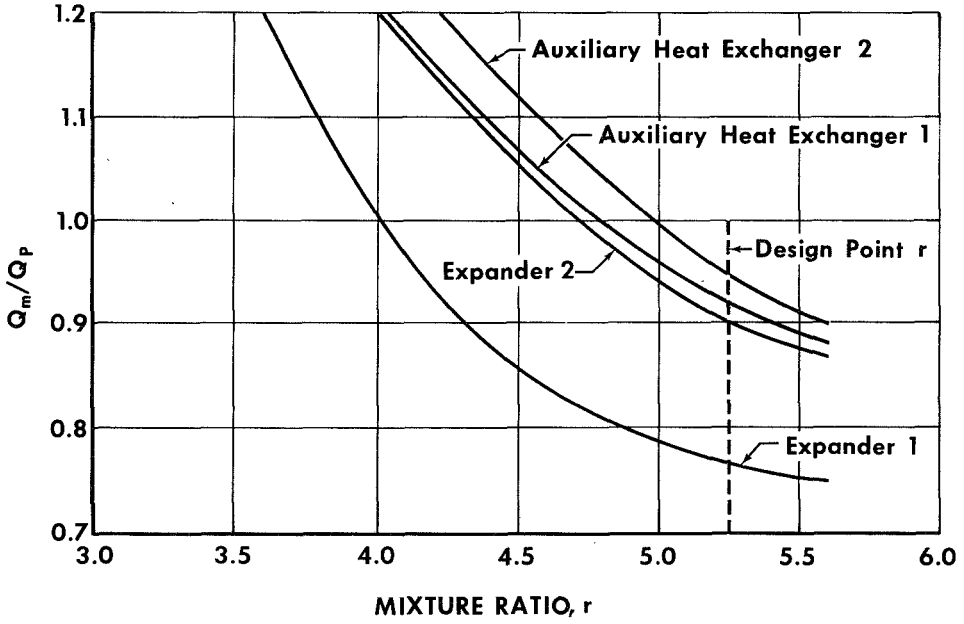


Figure 73. Thrust Chamber Fuel Decomposition Limits at 10% Thrust GS 9621

d. Bulk Boiling

At full thrust, supercritical conditions are maintained throughout the cooling jacket for all four cases; however, bulk boiling occurs at throttled conditions. As discussed in detail in Reference 5, film boiling is almost always encountered with bulk boiling, and the initiation of film boiling may result in excessive local wall temperatures. Therefore, detailed analysis of the cooling in the bulk-boiling region was deemed necessary. The most severe bulk boiling condition was found to occur at the maximum $Q_m/Q_p$ and minimum thrust. Table XVII lists the maximum wall temperature encountered in the bulk-boiling region at 10% thrust and a $Q_m/Q_p$ of 1.0, and identifies the point in the nozzle where bulk boiling is complete. The study indicated that the configuration of the coolant flow path results in a substantially higher boiling region wall temperature with the auxiliary heat exchanger cycle than with the expander cycle. However, none of the peak temperatures encountered were excessive. At intermediate thrusts the calculated wall temperatures in the boiling region were less than those shown in table XVII. However, with the auxiliary heat exchanger cycle, near-critical cooling is encountered in the high heat flux regions (near the dome on a T-H diagram) at intermediate thrust levels, and the validity of the boiling relationships is more questionable in this regime than in any other area.

Table XVII. Bulk Boiling Results

| Cycle | Design Point | Max Wall Temp in Boiling Region | Area Ratio Where Boiling is Complete |
|---|---|---|---|
| Expander | 1 | 611°R (339.4°K) | 26.0 |
| Expander | 2 | 657°R (365.0°K) | 17.0 |
| Aux Hex | 1 | 1503°R (835.0°K) | 3.6 |
| Aux Hex | 2 | 1146°R (636.7°K) | 5.8 |

F. CYCLE ENERGY BALANCE

1. Design Point Cycle Balances

The criteria for the design point cycle balances in the final evaluation were identical to the criteria established for the initial screening with the exception of the cooling jacket pressure drop and

temperature rise data, which were revised after selection of cycles for detailed analysis. Figure 74 shows the cycle schematic for the expander cycle engine at Design Point 1. The cycle was balanced with a turbine bypass flow of 10%. The fuel pump-turbine rotational speed is 60,000 rpm (6283 rad/s) and the oxidizer pump speed is 30,000 rpm (3141 rad/s). These speeds were chosen at the approximate knee of the fuel pump discharge pressure vs speed curve prepared earlier. The fuel pump discharge pressure required to balance the cycle was 2210 psia (1524 $N/cm^2$).

The cycle schematic for the expander cycle at Design Point 2 is shown in figure 75. As noted above, a design goal for this engine was the capability of uprating to a thrust level of 8000-lb (35.59 kN). The cooling jacket passages and injector flow areas were sized for the uprated thrust level, and the turbomachinery speeds were selected so that they would be within acceptable levels over the entire range of operation. At the design point (5000-lb or 22.24-kN thrust), the turbine bypass flow was 25%, the oxidizer injector pressure drop was 15.8% of chamber pressure, the fuel-to-oxidizer injection momentum ratio was 3.42, the fuel pump-turbine speed was 50,500 rpm (5288 rad/s)and the oxidizer pump speed was 25,250 rpm (2644 rad/s). The fuel pump discharge pressure required to balance the cycle was 1231 psia (848.8 $N/cm^2$).

The cycle schematics for the auxiliary heat cycle engines are shown in figures 76 and 77. The turbine inlet pressure for both designs was set at 300 psia (206.8 $N/cm^2$), which was established as a near-optimum value in earlier analyses. The rotational speeds were set at 60,000 rpm (6283 rad/s) for the fuel pump and turbine, and 30,000 rpm (3141 rad/s) for the oxidizer pump. These values were selected at the knee of the cycle impulse loss vs speed curves prepared earlier. The delivered impulse levels are 399.0 $lb_f$-sec/$lb_m$ (3913 N-sec/kg) at Design Point 1 and 394.9 $lb_f$-sec/$lb_m$ (3873 N-sec/kg) at Design Point 2. These values are less than the expander cycle by 5.4 and 2.9 $lb_f$-sec/$lb_m$ (52.96 and 28.40 N-sec/kg) for Design Points 1 and 2, respectively.

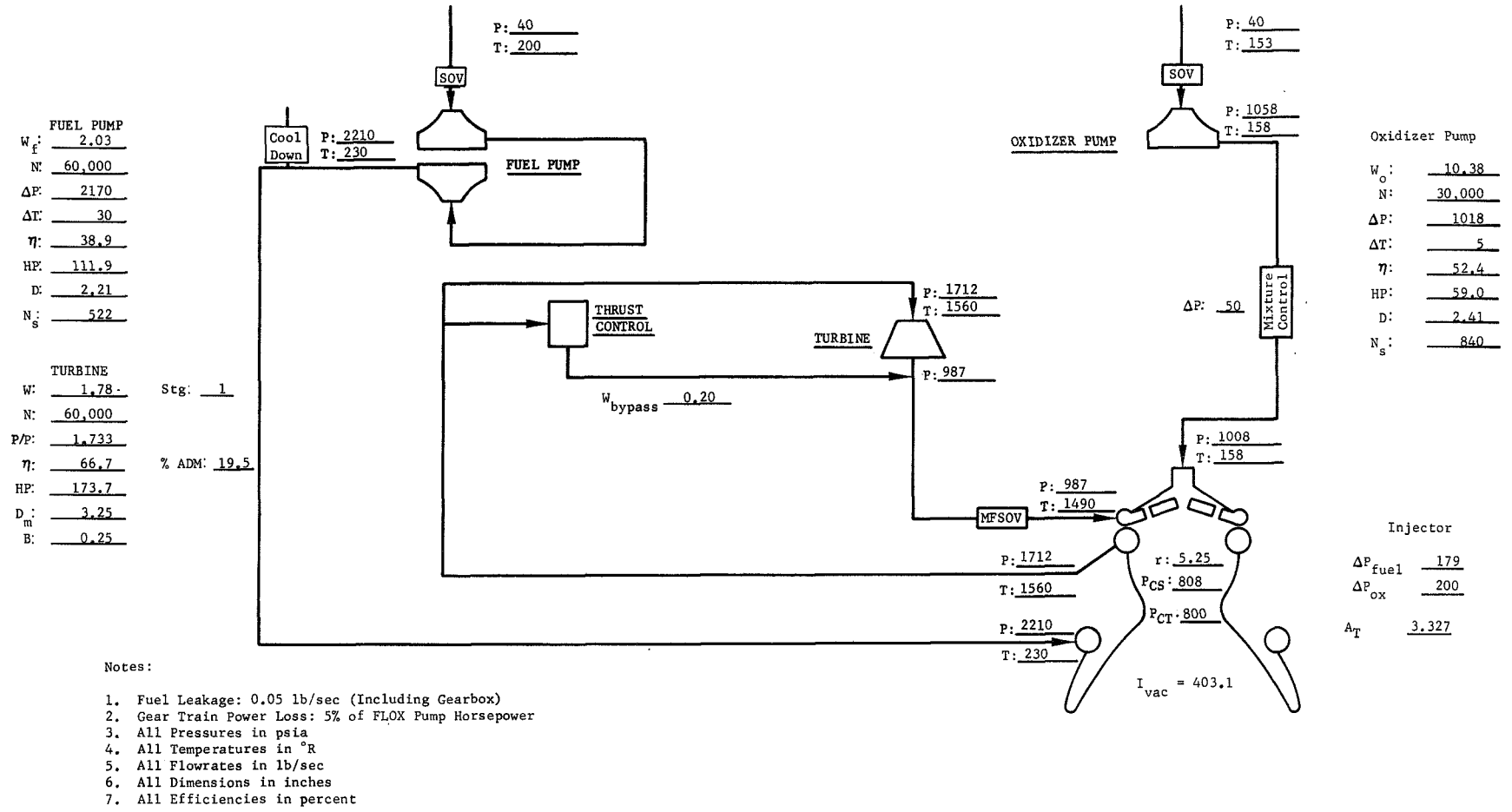


Notes:

1. Fuel Leakage: 0.05 lb/sec (Including Gearbox)
2. Gear Train Power Loss: 5% of FLOX Pump Horsepower
3. All Pressures in psia
4. All Temperatures in °R
5. All Flowrates in lb/sec
6. All Dimensions in inches
7. All Efficiencies in percent

Figure 74. Expander Cycle - Design Point 1

GS 9622

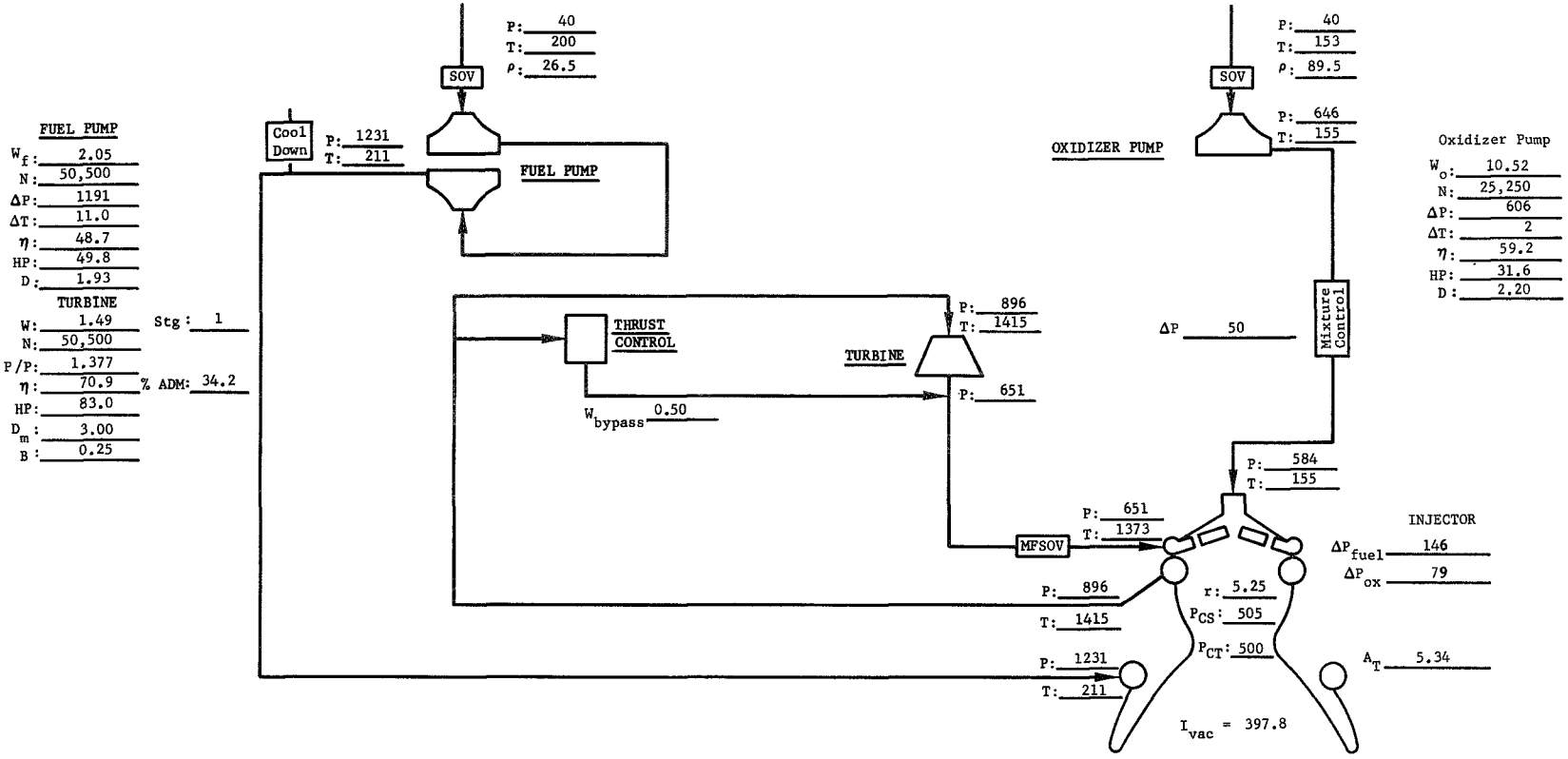


Notes:

1. Fuel Leakage: 0.05 lb/sec (Including Gearbox)
2. Gear Train Power Loss: 5% of FLOX Pump Horsepower
3. All Pressures in psia
4. All Temperatures in °R
5. All Flowrates in lb/sec
6. All Dimensions in inches
7. All Efficiencies in percent

Figure 75. Expander Cycle - Design Point 2

GS 9623A

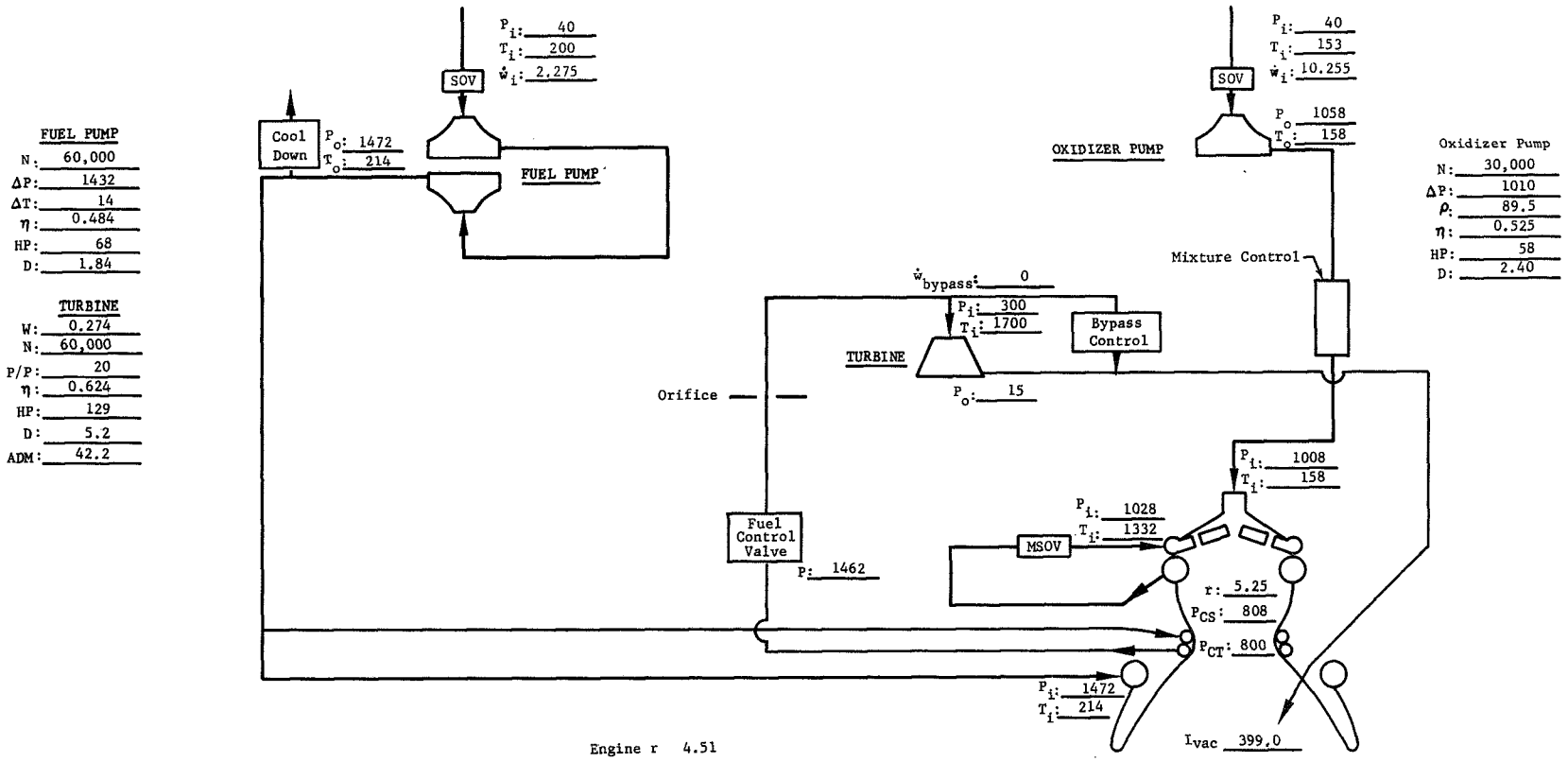


Notes:

1. Fuel Leakage: 0.05 lb/sec (Including Gearbox)
2. Gear Train Power Loss: 5% of FLOX Pump Horsepower
3. All Pressures in psia
4. All Temperatures in $^{o}R$
5. All Flowrates in lb/sec
6. All Dimensions in inches
7. All Efficiencies in percent

Figure 76. Auxiliary Heat Exchanger Cycle - Design Point 1

GS 9629A

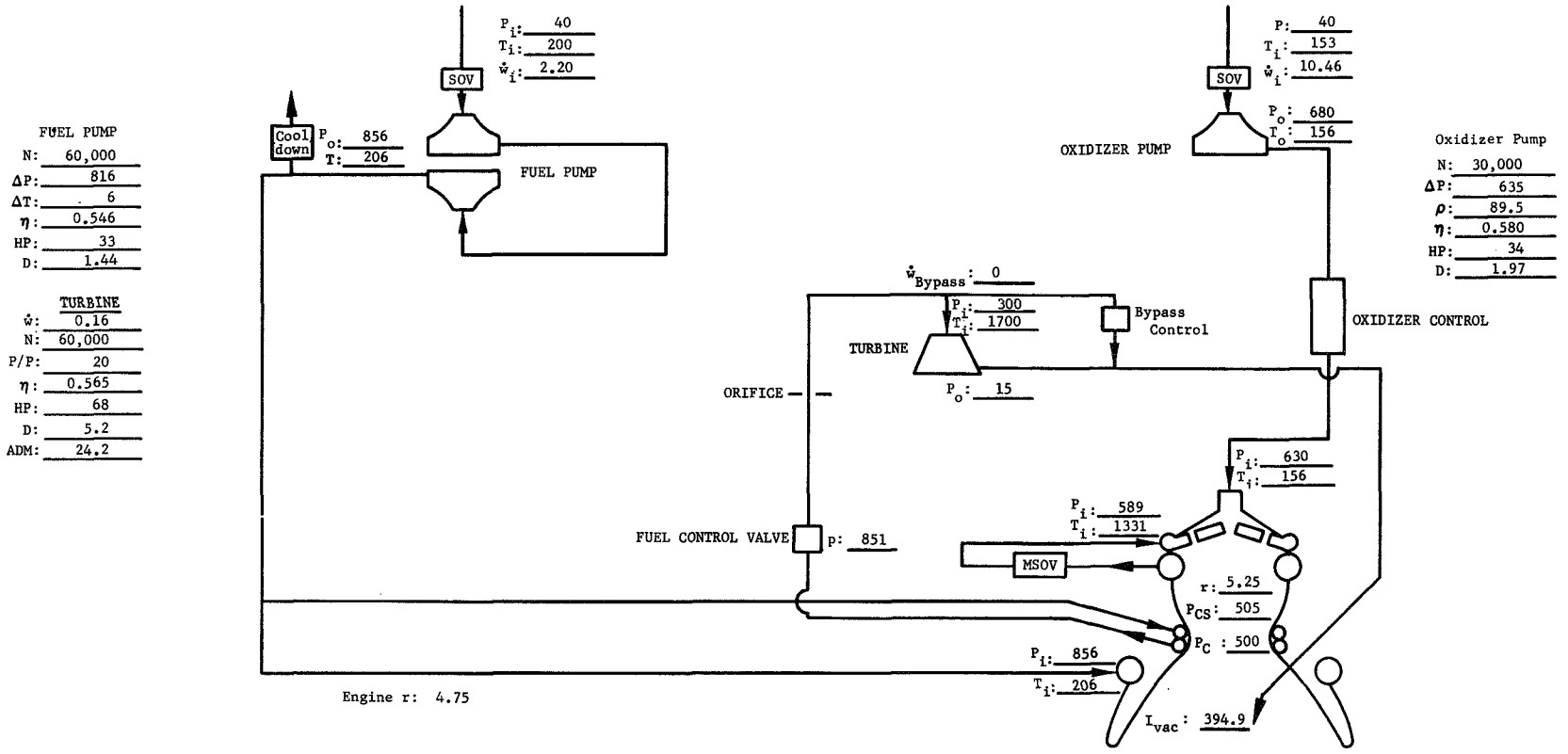


Notes:

1. Fuel Leakage: 0.05 lb/sec (Including Gearbox)
2. Gear Train Power Loss: 5% of FLOX Pump Horsepower
3. All Pressures in psia
4. All Temperatures in $^{o}R$
5. All Flowrates in lb/sec
6. All Dimensions in inches
7. All Efficiencies in percent

Figure 77. Auxiliary Heat Exchanger Cycle - Design Point 2

GS 9630A

The cooling jacket discharge temperature for the auxiliary heat exchanger at Design Point 1 was 1332°R (740.0°K) as compared to the 1143°R (635°K) calculated in the initial screening. Because of the increased jacket discharge temperature, a fuel tapoff cycle was considered. This cycle is identical to the auxiliary heat exchanger cycle except that the separate heat exchanger for the turbine flow is not required. The total fuel flow is routed through the cooling jacket, and the required turbine flow is extracted at the jacket discharge. With this cycle, the turbine inlet temperature is lower than that obtainable with a separate heat exchanger. Therefore, higher cycle impulse losses are incurred, but the complexity of the additional heat exchanger is eliminated. Table XVIII compares the fuel tapoff cycle with the auxiliary heat exchanger cycle. The fuel pump discharge pressure required for the fuel tapoff cycle is 278 psi (191.7 $N/cm^2$) greater than that required for the auxiliary heat exchanger cycle. Also, an additional impulse loss of 2.4 $lb_f$-sec/$lb_m$ (23.54 N-sec/kg) is incurred with the fuel tapoff cycle. The increased fuel pump discharge pressure is caused primarily by an increase in the coolant pressure drop in the region of the throat. The increased impulse loss is caused by the combination of the reduced turbine inlet temperature, the difference in the region in which heat lost to the turbine is extracted, and the increased horsepower requirements of the fuel pump. Based on these considerations, no further attention was given to the tapoff arrangement, and the auxiliary heat exchanger cycle was retained for the off-design analysis.

Table XVIII. Fuel Tapoff Cycle Comparison, Design Point 1

| | Fuel Tapoff Cycle | Auxiliary Heat Exchanger Cycle |
|---|---|---|
| Chamber Pressure | 800 psia (551.6 $N/cm^2$) | 800 psia (551.6 $N/cm^2$) |
| Chamber Mixture Ratio | 5.25 | 5.25 |
| $Q_m/Q_p$ | 0.9 | 0.9 |
| Turbine Speed | 60,000 rpm (6283 rad/s) | 60,000 rpm (6283 rad/s) |

Table XVIII. Fuel Tapoff Cycle Comparison, Design Point 1 (Cont'd)

| Turbine Inlet Temp | 1425°R (806.7°K) | 1700°R (944.4°K) |
|---|---|---|
| Fuel Pump Discharge Press. | 1750 psia (1207 N/cm$^2$) | 1472 psia (1015 N/cm$^2$) |
| Vacuum Impulse | 395.7 $lb_f$-sec/$lb_m$ (3890 N-sec/kg) | 399.0 $lb_f$-sec/$lb_m$ (3913 N-sec/kg) |

2. Off-Design Cycle Balances

Variations in thrust, $Q_m/Q_p$, and mixture ratio were evaluated in the off-design studies. The engine configuration for these studies was identical to the configuration established at the design point. The results of the off-design calculations for the expander cycle at Design Point 1 are summarized in table XIX. The first three columns show the effect of variations in $Q_m/Q_p$. The effects are minimal; the turbine bypass flow increases from 5.3% at a $Q_m/Q_p$ of 0.76 to 12.4% at a $Q_m/Q_p$ of 1.0. The fourth column shows the effect of reducing mixture ratio. At a mixture ratio of 4.75 the turbine speed is increased by 3170 rpm (332.0 rad/s), and the turbine bypass flow is reduced by 1%. A mixture ratio point of 5.75 was also attempted but the calculation failed because the engine, as configured, did not have sufficient control capability in the oxidizer control valve. This condition could be corrected easily by providing an increased oxidizer control valve pressure drop at the design point. The last two columns of table XIX show the effect of throttling to 10% thrust. The engine was throttled by opening the turbine bypass flow area so that it passed 50.7% of the total fuel flow at minimum thrust. Because of the methane coking limit, it was necessary to reduce mixture ratio to 4.3 at the 10% thrust level. At the 10% thrust level, the oxidizer injector pressure drop was 2.1 psi (1.448 N/cm$^2$) or 2.6% of chamber pressure. This is obviously undesirable for good combustion stability so, if the limitation on oxidizer injector pressure drop at design point is accepted, a throttling injector will be required to throttle to 10% thrust.

Table XIX. Off Design Table Expander Cycle, Design Point 1

| | | | | | | |
|---|---|---|---|---|---|---|
| Chamber Pressure, psia ($N/cm^2$) | 800 (551.6) | 800 (551.6) | 800 (551.6) | 800 (551.6) | 400 (275.8) | 80 (55.15) |
| Mixture Ratio | 5.25 | 5.25 | 5.25 | 4.75 | 5.25 | 4.30 |
| $Q_m/Q_p$ | 0.76 | 0.9 | 1.0 | 0.9 | 0.9 | 0.9 |
| Turbine Bypass Flow, % | 5.3 | 10.0 | 12.4 | 9.0 | 29.3 | 50.7 |
| Turbine Speed, rpm (rad/s) | 59,360 (6216) | 60,000 (6283) | 60,490 (6334) | 63,170 (6615) | 39,190 (4104) | 17,010 (1781) |
| Turbine Inlet Temperature, °R (°K) | 1411 (783.9) | 1568 (871.1) | 1668 (926.6) | 1495 (830.5) | 1670 (927.8) | 1704 (946.7) |
| Fuel Pump Discharge Pressure, psia ($N/cm^2$) | 2150 (1482) | 2210 (1524) | 2252 (1553) | 2387 (1646) | 1038 (715.7) | 236 (162.7) |
| Oxidizer Pump Discharge Pressure, psia ($N/cm^2$) | 1030 (710.1) | 1058 (729.4) | 1079 (743.9) | 1200 (827.4) | 520 (358.5) | 136 (90.04) |
| Oxidizer Injector $\Delta P$, psi ($N/cm^2$) | 200 (137.9) | 200 (137.9) | 200 (137.9) | 198 (136.5) | 51 (35.16) | 2.1 (1.44) |
| Fuel Injector $\Delta P$, psi ($N/cm^2$) | 159 (109.6) | 179 (123.4) | 192 (132.4) | 207 (142.7) | 100 (68.95) | 32.6 (22.48) |
| Injector Momentum Ratio | 1.8 | 2.0 | 2.13 | 2.31 | 4.33 | 32.9 |

The results of off-design calculations for the expander cycle at Design Point 2 are summarized in table XX. The first three columns show the effect of variations in the $Q_m/Q_p$ level at 5000-lb (22.24 kN) thrust. Again, the effects were minimal; the turbine bypass flow increased from 22% at $Q_m/Q_p$ of 0.76 to 28% at a $Q_m/Q_p$ of 1.0 Columns 4 and 5 show the effect of variations in mixture ratio to 4.75 and 5.75. Columns 6 through 9 show the effect of variations in $Q_m/Q_p$ at the uprated thrust level. Again the effects are minimal; turbine bypass flow increased from 6% at a $Q_m/Q_p$ of 0.76 to 13% at a $Q_m/Q_p$ of 1.0. Columns 9 and 10 show the effect of throttling to 10% thrust. As in the case of Design Point 1, the oxidizer injector pressure drop was too low for good combustion and control system stability at the 10% thrust level, indicating a necessity for a throttling injector. A dual orifice throttling injector was evaluated for this engine and is discussed later in paragraph C.3.

The results of the off-design calculations for the auxiliary heat exchanger cycle engines are summarized in tables XXI and XXII. Initially, it was felt that the turbine flow for this cycle could be controlled with a single throttle valve located upstream of the turbine. However, with this type of control the film temperature in the auxiliary heat exchanger coolant passages exceeded the methane coking limit during off-design operation, because the turbine flow necessary to provide the required pump power was less than the flow required to maintain acceptable film temperatures. Therefore, a turbine bypass control was added in addition to the throttle valve. With the two-valve system, total auxiliary heat exchanger flow can be controlled at a level that maintains the discharge temperature below 1700°R (944.4°K) over the entire operating range.

Table XX. Off Design Table Expander Cycle, Design Point 2

| | 1 | 2 | 3 | 4 | 5 | 6 | 7 | 8 | 9 | 10 |
|---|---|---|---|---|---|---|---|---|---|---|
| Chamber Pressure, psia ($N/cm^2$) | 500 (344.7) | 500 (344.7) | 500 (344.7) | 500 (344.7) | 500 (344.7) | 800 (551.6) | 800 (551.6) | 800 (551.6) | 200 (137.9) | 50 (34.47) |
| Mixture Ratio | 5.25 | 5.25 | 5.25 | 4.75 | 5.75 | 5.25 | 5.25 | 5.25 | 5.25 | 5.25 |
| $Q_m/Q_p$ | 0.76 | 0.9 | 1.0 | 0.9 | 0.9 | 0.76 | 0.9 | 1.0 | 0.9 | 0.9 |
| Turbine Bypass Flow, % | 22 | 25 | 28 | 25 | 25 | 6 | 10 | 13 | 43 | 58 |
| Turbine Speed, rpm (rad/s) | 49,950 (5278) | 50,500 (5288) | 50,850 (5372) | 52,470 (5560) | 49,210 (5163) | 67,225 (7063) | 68,000 (7121) | 68,520 (7194) | 30,150 (3204) | 12,960 (1414) |
| Turbine Inlet Temperature, °R (°K) | 1273 (707.2) | 1415 (786.1) | 1511 (839.4) | 1338 (743.3) | 1487 (826.1) | 1213 (673.9) | 1340 (744.4) | 1442 (801.1) | 1572 (873.3) | 1729 (960.6) |
| Fuel Pump Discharge Pressure, psia ($N/cm^2$) | 1201 (828.0) | 1231 (848.7) | 1250 (861.8) | 1300 (896.3) | 1186 (817.7) | 1991 (1372.7) | 2053 (1415) | 2091 (1442) | 493 (339.9) | 124 (85.49) |
| Oxidizer Pump Discharge Pressure, psia ($N/cm^2$) | 630 (434.4) | 646 (445.4) | 656 (452.3) | 704 (485.4) | 607 (418.5) | 1025 (706.7) | 1058 (729.4) | 1077 (742.6) | 276 (190.3) | 85 (58.60) |
| Oxidizer Injector $\Delta P$, psi ($N/cm^2$) | 79 (54.46) | 79 (54.46) | 79 (54.46) | 78 (53.77) | 81 (55.84) | 200 (137.9) | 200 (137.9) | 200 (137.9) | 13.0 (8.96) | 0.8 (0.55) |
| Oxidizer Injector $\Delta P$, % | 15.8 | 15.8 | 15.8 | 15.6 | 16.2 | 25.0 | 25.0 | 25.0 | 6.5 | 1.6 |
| Fuel Injector $\Delta P$, psi ($N/cm^2$) | 129 (88.94) | 146 (100.7) | 157 (108.2) | 167 (115.1) | 130 (89.63) | 191 (131.7) | 214 (147.5) | 234 (161.3) | 68.6 (47.29) | 19.9 (13.72) |
| Injection Momentum Ratio | 3.07 | 3.42 | 3.65 | 3.91 | 3.02 | 1.81 | 2.0 | 2.16 | 9.61 | 42.6 |

Table XXI. Off Design Table For Auxiliary Heat Exchanger Cycle, Design Point 1

| | | | | | |
|---|---|---|---|---|---|
| Chamber Pressure - psia ($N/cm^2$) | 800 (551.6) | 800 (551.6) | 800 (551.6) | 500 (344.7) | 80 (55.15) |
| Mixture Ratio | 5.25 | 5.25 | 5.25 | 5.25 | 5.25 |
| $Q_m/Q_p$ | 0.76 | 0.90 | 1.0 | 0.9 | 0.9 |
| Impulse Loss - $lb_f$-sec/$lb_m$ N-sec/kg | 6.7 (65.71) | 5.4 (52.96) | 5.5 (53.94) | 6.4 (62.76) | 7.3 (71.59) |
| Turbine Flow - lb/sec (kg/sec) | 0.32 (0.142) | 0.274 (0.122) | 0.28 (0.124) | 0.16 (0.0711) | 0.03 (0.0133) |
| Turbine Bypass Flow - lb/sec (kg/sec) | 0 | 0 | 0.08 (0.0356) | 0.03 (0.0133) | 0.005 (0.00222) |
| Turbine Speed - rpm (rad/s) | 58,012 (6074) | 60,000 (6283) | 60,136 (6300) | 46,680 (4922) | 18,000 (1885) |
| Turbine Inlet Temp, $^oR$ ($^oK$) | 1422 (788.9) | 1700 (944.4) | 1700 (944.4) | 1700 (944.4) | 1700 (944.4) |
| Fuel Pump Discharge Press. - psia ($N/cm^2$) | 1375 (948.0) | 1472 (1015) | 1490 (1027) | 964 (664.6) | 170 (117.2) |
| Oxidizer Pump Discharge Press-psia ($N/cm^2$) | 964 (664.6) | 1050 (723.9) | 1056 (724.6) | 697 (480.6) | 130 (89.63) |
| Oxidizer Injector $\Delta P$ - psi ($N/cm^2$) | 196 (135.1) | 200 (137.9) | 195 (134.4) | 81 (55.84) | 2 (1.37) |
| Fuel Injector $\Delta P$ - psi ($N/cm^2$) | 182 (125.5) | 192 (132.3) | 224 (154.4) | 142 (97.90) | 27 (18.61) |
| Injection Momentum Ratio | 1.78 | 2 | 2.14 | 3.3 | 25.5 |

Table XXII. Off Design Table For Auxiliary Heat Exchanger Cycle, Design Point 2

| | | | | | | |
|---|---|---|---|---|---|---|
| Chamber Pressure - psia ($N/cm^2$) | 500 (344.7) | 500 (344.7) | 500 (344.7) | 250 (172.4) | 100 (68.94) | 50 (34.47) |
| Mixture Ratio | 5.25 | 5.25 | 5.25 | 5.25 | 5.25 | 5.25 |
| $Q_m/Q_p$ | 0.76 | 0.9 | 1.0 | 0.9 | 0.9 | 0.9 |
| Impulse Loss - $lb_f$-sec/$lb_m$ (N-sec/kg) | 5.4 (52.96) | 2.9 (28.44) | 3.0 (29.42) | 3.1 (30.40) | 3.6 (35.30) | 2.7 (26.48) |
| Turbine Flow - lb/sec (kg/sec) | 0.25 (0.111) | 0.157 (0.0698) | 0.162 (0.0720) | 0.068 (0.0302) | 0.029 (0.0129) | 0.012 (0.00535) |
| Turbine Bypass Flow - lb/sec (kg/sec) | 0 | 0 | 0.005 (0.002) | 0.017 (0.00755) | 0.008 (0.00355) | 0.005 (0.00222) |
| Turbine Speed - rpm (rad/s) | 59,192 (6178) | 60,000 (6283) | 60,714 (6388) | 40,752 (4294) | 24,246 (2513) | 15,000 (1571) |
| Turbine Inlet Temp, $^oR$ ($^oK$) | 1161 (6667) | 1700 (9444) | 1700 (9444) | 1700 (9444) | 1700 (9444) | 1700 (9444) |
| Fuel Pump Discharge Press. - psia ($N/cm^2$) | 817 (563.3) | 856 (590.2) | 873 (60.19) | 439 (302.7) | 187 (128.9) | 95 (65.50) |
| Oxidizer Pump Discharge Press.- psia ($N/cm^2$) | 655 (451.6) | 675 (465.4) | 702 (484.0) | 362 (299.6) | 160 (110.3) | 80 (55.15) |
| Oxidizer Injector P - psi ($N/cm^2$) | 124 (85.49) | 120 (82.73) | 124 (85.49) | 42 (28.95) | 5 (3.44) | 1 (0.680) |
| Fuel Injector P - psi ( $N/cm^2$) | 69 (47.57) | 78 (53.77) | 86 (59.29) | 52 (35.85) | 17 (11.72) | 8 (5.51) |
| Injection Momentum Ratio | 1.2 | 2.0 | 2.2 | 4.2 | 11.8 | 28 |

The first three columns in the off-design data summary tables show the effect of variations in $Q_m/Q_p$, and the remainder of the columns show the effect of throttling to 10% thrust. It will be noted that increased cycle losses are incurred when $Q_m/Q_p$ either increases or decreases from the design point value. The auxiliary heat exchanger is sized at the design point to provide a discharge temperature of 1700°R (944.4°K) at a $Q_m/Q_p$ of 0.9. At $Q_m/Q_p$ values less than 0.9, the turbine inlet temperature is reduced, and the cycle losses are increased. At $Q_m/Q_p$ values greater than 0.9, the heat exchanger flow must be increased over that required by the turbine to maintain a heat exchanger outlet temperature of 1700°R (944.4°K). The excess flow is bypassed around the turbine and again the cycle impulse losses are increased. As with the expander cycle, oxidizer injector pressure drops at 10% thrust were found to be inadequate, indicating a probable requirement for a throttling injector.

3. Dual Orifice Throttling Injector

A dual orifice throttling injector was evaluated for the expander cycle as Design Point 2. The control schematic for this injector is shown in figure 78. Under three Air Force contracts, it has been demonstrated that excellent performance can be obtained over a wide throttling range with this injector concept.

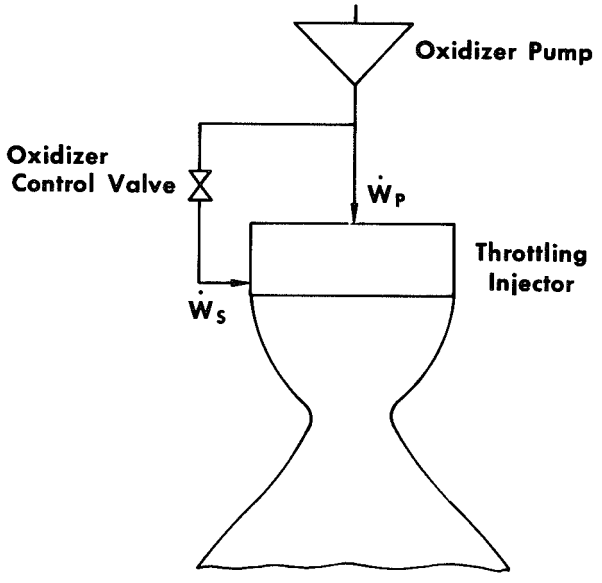


Figure 78. Throttling Injector Control Schematic GS 9584

With the dual orifice injector, a parameter than can be varied to optimize performance is the oxidizer flow split, $W_p/(W_p + W_s)$. In tests of a dual orifice injector with fluorine/hydrogen, the flow split for optimum performance was determined to be approximately 8% to 10% at full thrust and 50% at the 10% thrust level. The characteristics of the expander cycle at Design Point 2 are quite compatible with these levels. The overall available oxidizer injector pressure drop is the difference between the oxidizer pump discharge pressure and chamber pressure; these values in the cycle can be obtained from table XX. To obtain the optimum flow split at the 10% thrust level, the primary injector area was sized to pass one-half the oxidizer flow (0.535 lb/sec; 0.243 kg/sec) at the available pressure drop of 35 psi (24.13 $N/cm^2$). At the 8000-lb (35.59 kN) thrust level, the pressure drop available was 254 psi (175.1 $N/cm^2$), and the flowrate through the primary flow area (sized at the 10% thrust level) was 1.44 lb/sec (0.655 kg/sec), corresponding to a flow split of 8.65%. Pertinent injector characteristics are summarized in table XXIII. The injector flow split schedule vs thrust is very close to the optimum values that were experimentally determined for the fluorine/hydrogen injector.

Table XXIII. Dual Orifice Throttling Expander Cycle, Design Point 2

| | | | | |
|---|---|---|---|---|
| Chamber Pressure - psia ($N/cm^2$) | 800 (551.5) | 500 (344.7) | 200 (137.8) | 50 (34.47) |
| Primary Flow - lb/sec (kg/sec) | 1.44 (0.655) | 1.10 (0.050) | 0.79 (0.0359) | 0.535 (0.243) |
| Secondary Flow - lb/sec (kg/sec) | 15.22 (6.90) | 9.38 (4.25) | 3.47 (1.57) | 0.535 (0.243) |
| Flow Split, % | 8.65 | 10.5 | 18.6 | 50 |
| Secondary $\Delta P$ - psi ($N/cm^2$) | 200 (137.8) | 76 (52.4) | 10 (6.89) | 0.25 (0.172) |
| Primary $\Delta P$ - psi ($N/cm^2$) | 254 (175.1) | 146 (100.6) | 76 (52.4) | 35 (24.1) |
| Control Valve $\Delta P$ -psia ($N/cm^2$) | 54 (37.2) | 70 (48.2) | 66 (45.5) | 34.75 (24.1) |
| Control Valve $A_{Cd}$ - $in^2$ ($cm^2$) | 0.327 (2.110) | 0.177 (1.142) | 0.068 (0.439) | 0.014 (0.0904) |

4. Pump Inlet Condition Variations

Variations in pump inlet conditions were evaluated at the 8000-lb (35.59 kN) thrust level for the Design Point 2 expander cycle engine. The Design Point 2 expander cycle at the uprated thrust level was chosen because it was considered to be the most severe condition, but the trends would be similar for any cycle. A closed loop turbine bypass control that maintained constant chamber pressure was assumed. Figure 79 shows the manner in which mixture ratio would change as the oxidizer pump inlet temperature is varied. The calculations were made with the fuel pump inlet conditions set at the design point level and the oxidizer pump inlet pressure regulated to the level dictated by the pump suction requirements. It will be noted that mixture ratio is reduced as the oxidizer pump inlet temperature is increased. This is because of the reduced oxidizer density and hence lower pump pressure rise. Two lines are shown; one assumes a fixed area oxidizer control valve; the other uses the built-in $\Delta P$ of the oxidizer control valve (50 psi; 34.47 $N/cm^2$) for propellant utilization. At an oxidizer inlet temperature of 162°R (90.00°K) the pressure drop across the oxidizer control valve was reduced to zero. Therefore, no controlling capability was available at temperatures higher than this value, and mixture ratio changes were indicated.

The total results of the inlet condition evaluation are summarized in table XXIV. The first four columns correspond to the data that was plotted in figure 79. It will be noted that the maximum oxidizer pump inlet pressure allowable under the contract (125 psia; 86.18 $N/cm^2$), was required at an inlet temperature of 198°R (110.0°K). At the maximum pump inlet temperature (200°R; 111.1°K), the required inlet pressure was 134 or 9 psi (92.39 or 6.21 $N/cm^2$) greater than specified in the ground rules. At the 5000-lb (22.24 kN) thrust level, the required oxidizer pump inlet pressure was found to be within the contract limitations over the entire range of conditions considered.

# Table XXIV. Effect of Propellant Inlet Conditions on Mixture Ratio Expander Cycle, Design Point 2

| | 1 | 2 | 3 | 4 | 5 | 6 | 7 | 8 | 9 | 10 |
|---|---|---|---|---|---|---|---|---|---|---|
| Oxidizer Pump Inlet Temp, °R | 150 | 162 | 198 | 200 | 153 | 153 | 153 | 150 | 171 | 200 |
| (°K) | (83.3) | (90.0) | (110.0) | (111.1) | (85.0) | (85.0) | (85.0) | (83.3) | (95.0) | (111.1) |
| Oxidizer Pump Inlet Press., psia | 29 | 40 | 125 | 134 | 40 | 40 | 40 | 29 | 53 | 134 |
| ($N/cm^2$) | (19.3) | (27.6) | (86.2) | (92.4) | (27.6) | (27.6) | (27.6) | (20) | (36.5) | (92.4) |
| Fuel Pump Inlet Temp, °R | 200 | 200 | 200 | 200 | 170 | 183 | 260 | 170 | 209 | 260 |
| (°K) | (111.1) | (111.1) | (111.1) | (111.1) | (94.4) | (101.7) | (144.4) | (94.4) | (116.1) | (144.4) |
| Fuel Pump Inlet Press., °R | 40 | 40 | 40 | 40 | 20 | 20 | 125 | 20 | 30 | 125 |
| (°K) | (22.2) | (22.2) | (22.2) | (22.2) | (22.2) | (22.2) | (69.4) | (22.2) | (16.6) | (69.4) |
| Mixture Ratio - Fixed Oxidizer Control | 5.25 | 5.08 | 4.73 | 4.72 | 4.96 | 5.04 | 6.17 | 4.96 | 5.08 | 5.25 |
| Mixture Ratio - Variable Oxidizer Control | 5.25 | 5.25 | 4.91 | 4.90 | 5.08 | 5.25 | 5.25 | 5.12 | 5.25 | 5.25 |
| Fuel Pump Discharge Press. - Fixed Oxidizer Control, psia | 2,047 | 2,095 | 2,267 | 2,275 | 2,122 | 2,105 | 2,023 | 2,170 | 2,108 | 2,083 |
| ($N/cm^2$) | (1,787) | (1,821) | (1,939) | (1,945) | (1,839) | (1,827) | (1,771) | (1,872) | (1,829) | (1,812) |
| - Variable Oxidizer Control, psia | 2,047 | 2,045 | 2,180 | 2,188 | 2,082 | 2,046 | 2,100 | 2,069 | 2,050 | 2,083 |
| ($N/cm^2$) | (1,787) | (1,786) | (1,879) | (1,885) | (1,812) | (1,787) | (1,825) | (1,803) | (1,789) | (1,812) |
| Oxidizer Control Pressure Drop - Fixed Oxidizer Control, psia | 49 | 46 | 83 | 84 | 45 | 58 | 114 | 51 | 47 | 92 |
| ($N/cm^2$) | (33.8) | (31.7) | (57.2) | (57.9) | (31.0) | (40.0) | (78.6) | (35.2) | (32.5) | (63.5) |
| - Variable Oxidizer Control, psia | 49 | 0 | 0 | 0 | 0 | 0 | 262 | 0 | 0 | 92 |
| ($N/cm^2$) | (34) | | | | | | (181) | | | (63) |
| Turbine Speed - Fixed Oxidizer Control, rpm | 67,930 | 68,980 | 72,240 | 72,320 | 67,850 | 68,160 | 70,350 | 67,870 | 69,810 | 73,170 |
| (rad/s) | (7114) | (7224) | (7565) | (7573) | (7105) | (7138) | (7367) | (7107) | (7310) | (7662) |
| - Variable Oxidizer Control, rpm | 67,930 | 67,910 | 70,220 | 70,270 | 66,090 | 66,700 | 73,400 | 66,770 | 68,560 | 73,170 |
| (rad/s) | (7114) | (7112) | (7353) | (7359) | (6921) | (6985) | (7686) | (6992) | (7180) | (7662) |
| Turbine Bypass Flow - Fixed Oxidizer Control, lb/sec | 10.5 | 10.3 | 9.8 | 9.8 | 10.3 | 10.2 | 4.3 | 10.1 | 9.9 | 9.7 |
| (kg/sec) | (4.76) | (4.67) | (4.45) | (4.45) | (4.67) | (4.63) | (1.95) | (4.58) | (4.49) | (4.40) |
| - Variable Oxidizer Control, lb/sec | 10.5 | 10.8 | 10.6 | 10.6 | 10.7 | 10.8 | 8.3 | 10.9 | 10.6 | 9.7 |
| (kg/sec) | (4.76) | (4.99) | (4.81) | (4.81) | (4.83) | (4.99) | (3.77) | (4.94) | (4.81) | (4.40) |

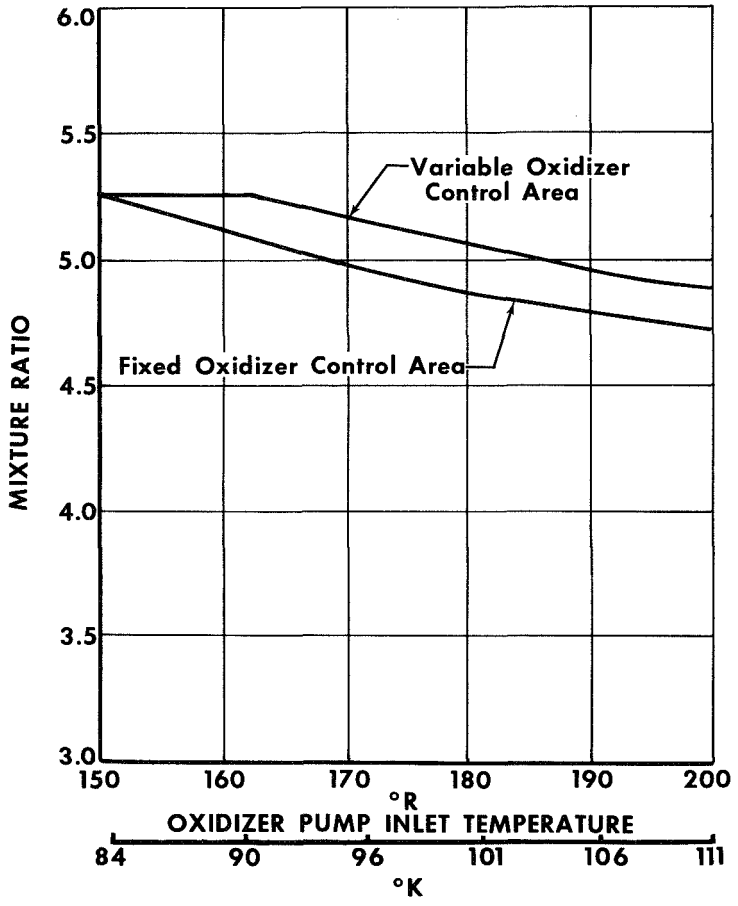


Figure 79. Effect of Oxidizer Pump Inlet Temperature on Engine Mixture Ratio GS 9644B

Columns 5 through 7 of table XXIV show the effect of variations in fuel pump inlet temperature. The oxidizer inlet conditions were set at the design point levels for these calculations. With the control valve assumed, mixture ratio variation for propellant utilization is not possible at fuel inlet temperatures less than 183°R (101.7°K). The mixture ratio variation with a fixed oxidizer control is from 4.96 to 6.17, and if the available oxidizer valve $\Delta P$ (which was assumed at only 50 psi; 34.47 $N/cm^2$) is employed for propellant utilization, the maximum variation can be reduced to the range between 5.08 and 5.25. The required fuel pump inlet pressures were within the contract limits over the entire range of conditions studied.

The conditions considered in the first seven columns of table XXIV are probably much too severe. In an actual mission, both the oxidizer

and fuel temperatures would probably increase proportionately. The last three columns represent this condition. Column 8 represents the condition where both the fuel and oxidizer temperatures are at the minimum values. Column 9 represents the temperatures at which a propellant utilization valve becomes operable, and column 10 represents the maximum temperatures for both propellants. The mixture ratio variation with a fixed oxidizer control was from 4.96 to 5.25. If the available oxidizer $\Delta P$ is employed for propellant utilization, the range of variation can be reduced to 5.12 to 5.25. Although the evaluation of a propellant utilization system is beyond the scope of this contract, the engine flexibility is sufficient to ensure that propellant utilization control is feasible. For complete propellant utilization, an oxidizer valve $\Delta P$ of approximately 150 psi (103.4 $N/cm^2$) would be required, and this would require an increase in fuel pump discharge pressure of only approximately 50 psi (34.47 $N/cm^2$).

5. Cycle Recommendations for Task II

The design point and off-design cycle studies completed in the Cycle Energy Balance phase substantiated the performance advantage of the expander cycle over the auxiliary heat exchanger cycle, and also indicated some other advantages for uprating capability of the expander cycle at Design Point 2 which were not apparent in the earlier screening. Table XXV compares the performance and weight of the four cycle-design point cases investigated. The Design Point 1 expander cycle was shown to be fully feasible at full thrust and provided over 5.0 $lb_f$-sec/$lb_m$ (49.03 N-sec/kg) higher specific impulse than the other three cases. Furthermore, the expander cycle at Design Point 1 was found to be appreciably lighter than the auxiliary heat exchanger cycle at either design point. On the other hand, heat transfer limitations would make throttling more difficult for the Design Point 1 expander cycle, and power requirements would make uprating of the engine to any significantly higher thrust and chamber pressure impossible.

Contrary to the qualitative ratings compiled under Task IC, the Design Point 2 expander cycle was found to be equal to or better than the two auxiliary heat exchanger cycles from the standpoint of complexity, flexibility, and ease of throttling. This resulted from lowering the design point turbomachinery speed for the lower chamber

pressure expander cycle. A speed reduction was possible because of the substantial power margin of the expander cycle at Design Point 2, which, because the expander cycle is a closed cycle, results in no performance loss. Similar improvements in the qualitative characteristics of the auxiliary heat exchanger cycle could also be achieved by a reduction in turbomachinery speed, but only at the expense of performance.

In summary, then, although there were small differences, it appeared that both the expander cycle and auxiliary heat exchanger cycles provided acceptable performance, and that the weight differences were not significant enough to a mission to be given great importance. The small performance improvement provided by the expander cycle was therefore selected and the expander cycle at Design Point 2 was recommended if engine throttling or uprating were required. If the engine was to be restricted to fixed thrust, the expander cycle at Design Point 1 was recommended to provide maximum performance. The expander cycle at Design Point 2 was selected by the NASA-LeRC Project Manager for the Task II preliminary design.

Table XXV. Weight and Performance Summary

| | Design Point 1 | Design Point 2 |
|---|---|---|
| Expander | | |
| $I_{vac}$ @ 100% thrust | 404.4 $lb_f$-sec/$lb_m$ (3966 N-sec/kg) | 397.8 $lb_f$-sec/$lb_m$ (3901 N-sec/kg) |
| $I_{vac}$ @ 10% thrust | 382.9 $lb_f$-sec/$lb_m$ (3756 N-sec/kg) | 372.8 $lb_f$-sec/$lb_m$ (3656 N-sec/kg) |
| Weight | 122 lb (55.34 kg) | 115 lb (52.16 kg) |
| Auxiliary Hex | | |
| $I_{vac}$ @ 100% thrust | 399.0 $lb_f$-sec/$lb_m$ (3923 N-sec/kg) | 394.9 $lb_f$-sec/$lb_m$ (3874 N-sec/kg) |
| $I_{vac}$ @ 10% thrust | 375.6 $lb_f$-sec/$lb_m$ (3683 N-sec/kg). | 370.1 $lb_f$-sec/$lb_m$ (3629 N-sec/kg) |
| Weight | 131 lb (59.42 kg) | 126 lb (57.15 kg) |

# SECTION IV
# DESIGN EFFORT - TASK II

## A. DESIGN REQUIREMENTS AND APPROACH

### 1. Requirements

The design conditions specified by the NASA-LeRC Project Manager for the expander cycle with a single turbine and geared pumps selected for the Task II engine preliminary design were as shown in table XXVI. In addition, it was stated that the engine should have the capability of being uprated in thrust to 8000 lb (35.59 kN) and throttled 10:1, although these were not firm design requirements.

Table XXVI. Design Requirements for Expander Cycle with a Single Turbine and Geared Pumps - Task II

| | |
|---|---|
| Propellants | Liquid Methane<br>Liquid flox (82.6% fluorine) |
| Thrust (vacuum) | 5000 lbs (22.24 kN) |
| Mixture Ratio | 5.25 |
| Nozzle Expansion Ratio | 70:1 |
| Chamber Contraction Ratio | 4:1 |
| Chamber Pressure | 500 psia (344.7 $N/cm^2$) |
| Propellant Inlet Temperature | |
| Methane | 200°R (111.1°K) |
| Flox | 150°R (83.33°K) |
| Required Oxidizer Pump NPSP | 12 psi (8.27 $N/cm^2$) |
| Required Fuel Pump NPSP | 8 psi (5.52 $N/cm^2$) |

The values shown in table XXVI are essentially the same as those used for Design Point 2 in the Task I analysis except that propellant inlet requirements were stated differently (i.e., as required NPSP) and the nozzle expansion ratio was increased from 60:1 to 70:1.

The two design points in Task I were selected to provide a constant engine envelope so that comparison would be facilitated, and the area ratios were established based on a reasonable value of 100:1 for the 800 psia (551.58 $N/cm^2$) chamber pressure case. Considered independently, an upper stage 5000-lb (22.24 kN) thrust flox/methane engine operating at 500-psia (344.7 $N/cm^2$) chamber pressure would have an

optimum nozzle expansion ratio above 60:1 for most missions. On the other hand, the jacket coolant temperature rise would be increased with higher expansion ratios if a regeneratively cooled nozzle extension were used, and this is undesirable from the standpoint of the fuel decomposition limits at the 10% thrust level. Based on these considerations, the regeneratively cooled expansion ratio of 70:1 was selected, and additionally, the capability of adding a radiation cooled skirt to further increase expansion ratio was taken into account. This produced a nozzle contour based on a maximum payload truncation with an area ratio of 100:1. When cut off at 70:1, the maximum payload 100:1 nozzle becomes roughly equivalent to a 70:1 minimum surface truncation. This minimum surface contour is more compatible with a nozzle extension than other truncations because of its higher exit divergence angle. Furthermore, since the minimum surface truncation is considerably shorter than a maximum payload truncation, the 70:1 minimum surface nozzle provides approximately the same nozzle surface and coolant temperature rise as the 60:1 maximum payload nozzle considered in Task I. This is shown in table XXVII.

The 2.0 -$lb_f$-sec/$lb_m$ (19.61-N-sec/kg) performance increases for the $\epsilon_e$ = 70 nozzle over $\epsilon_e$ = 60 shown in the table is based on a constant $\eta I_{vac}$ of 94% for both cases and does not account for the variation in the predicted nozzle thrust coefficient efficiencies, or stream thrust coefficients, $C_s$, for the two nozzle configurations. If calculated $C_s$ values are used with an $\eta_{c*}$ of 97% and a performance loss due to cycle leakage of 2.0 $lb_f$-sec/$lb_m$ (19.61 N-sec/kg) the calculated full thrust specific impulse would be:

| $\epsilon_e$ | Nozzle Contour | $C_s$ | $I_{vac}$ $lb_f$-sec/$lb_m$ | N-sec/kg |
|---|---|---|---|---|
| 60 | Max. Payload | 0.9782 | 401.3 | 3935 |
| 70 | Min. Surface | 0.9754 | 401.1 | 3933 |
| 100 | Max. Payload | 0.9784 | 407.0 | 3991 |

Table XXVII. Comparison of Cooling Conditions and Performance for Task I and II Nozzle Geometries (Design Point 2 - Expander Cycle)

| | Task IB Chamber | Task II Chamber | |
|---|---|---|---|
| | | (Without Radiation Cooled Skirt) | (With Radiation Cooled Skirt) |
| Expansion Ratio | 60 | 70 | 100 |
| Perfect Nozzle Design Area Ratio | 95 | 162 | 162 |
| Contour | Max Payload | Min Surface | Max Payload |
| Jacket, $\Delta P$ | 335 psi* (230.9 $N/cm^2$) | 309 psi* (213.0 $N/cm^2$) | 309 psi* (213.0 $N/cm^2$) |
| Jacket, $\Delta T$ | 1204°R*(668.9°K) | 1176 °R*(653.3°K) | 1176 °R*(653.3°K) |
| $I_{vac}$ | 397.8 $lb_f$-sec/$lb_m$ (3901 N-sec/kg) | 399.8 $lb_f$-sec/$lb_m$** (3921 N-sec/kg) | 403.9 $lb_f$-sec/$lb_m$** (3961 N-sec/kg) |
| Nozzle Length | 27.8 in. (70.61 cm) | 26.2 in. (66.55 cm) | 38.9 in. (98.81 cm) |
| Nozzle Diameter | 20.2 in. (51.31 cm) | 21.8 in. (55.37 cm) | 26.0 in. (66.04 cm) |

* $Q_m/Q_p = 0.90$

** Based on same leakage loss as assumed in Task I

As discussed in paragraph E, the difference between the performance values shown above and those given in table XXVII may be considered to be a margin for kinetic losses, nozzle-$\eta_c$* interactions or simply conservatism in the calculations. Based on predicted nozzle performance, however, it is apparent that there is no actual specific impulse advantage for the 70:1 minimum surface configuration. Rather, the real benefit is in reduced length and compatibility for attachment of a nozzle extension.

2. Approach

The fact that engine throttling and uprating were not requirements for the engine preliminary design meant that these capabilities were to be evaluated as special cases. It was apparent from the Task I analysis that if throttling or uprating were to receive serious consideration, it would be necessary to incorporate requirements for these capabilities in the injector, thrust chamber, and turbomachinery, and this was done in the preliminary design. However, control system requirements are inherently difficult to finalize until component testing is well underway, particularly when vehicle and mission requirements are not fully defined. Therefore, it was decided to limit the actual design of the control system to fixed thrust operation and consider uprating and throttling only on an analytical basis.

Cycle performance calculations for the preliminary design configuration were completed based upon the 70:1 nozzle and including refinements over the Task I analyses such as inclusion of calculated valve pressure drops, line losses, and leakage losses, in place of estimates. The resulting design point cycle schematic for the Task II preliminary design study is shown in figure 80. The vacuum specific impulse of 399.4 $lb_f$-sec/$lb_m$ (3916.77 N-sec/kg), is based on 94% $I_{vac}$ efficiency and a calculated leakage loss of 0.069 lb/sec (0.031 kg/sec).

Table XXVIII summarizes the engine operating parameters at design thrust, uprated to 8000-lb (35.59 kN) thrust, and throttled to 10% of design thrust. The engine conditions at all three points are well within the limits established in Task I.

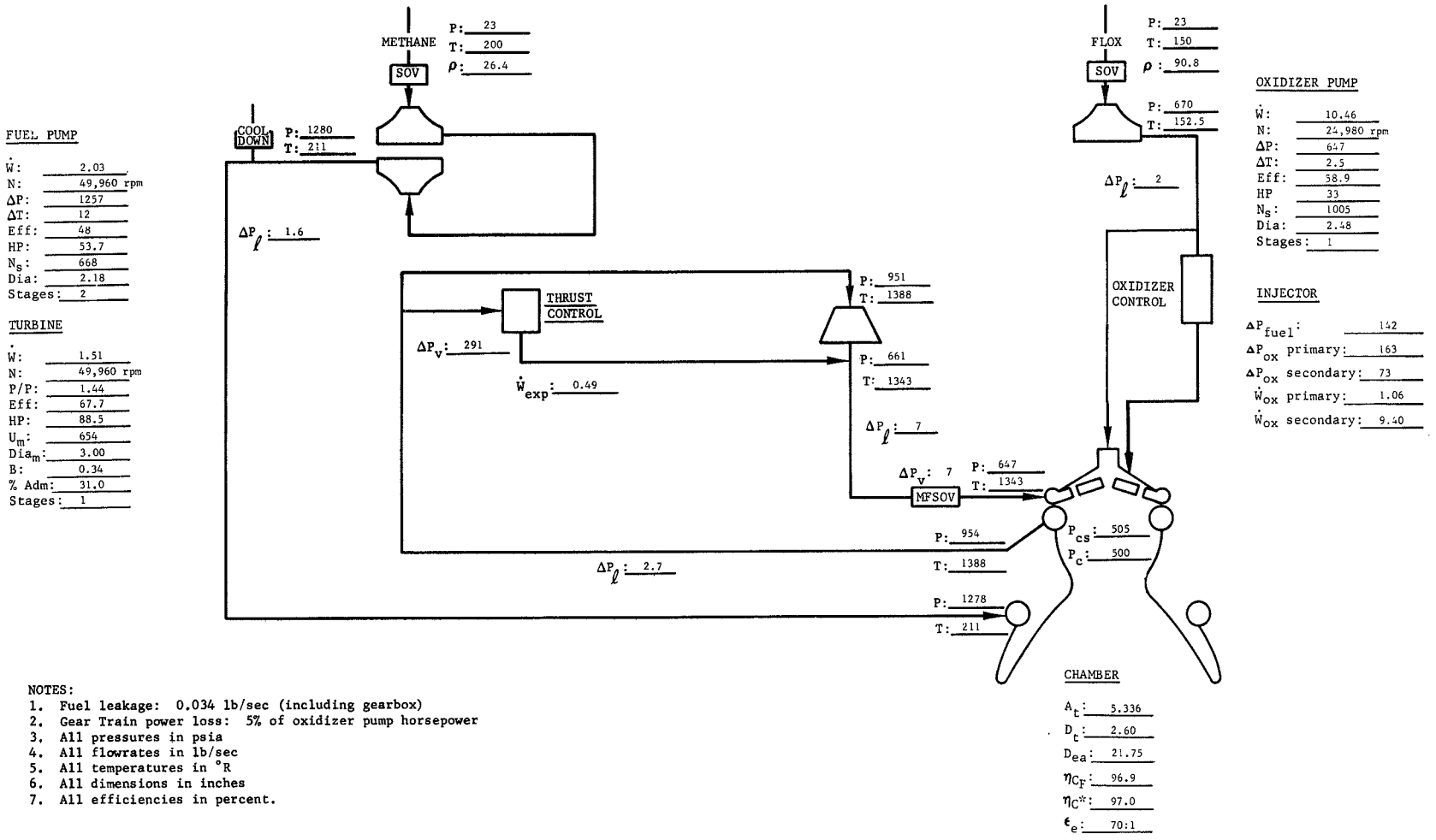


NOTES:
1. Fuel leakage: 0.034 lb/sec (including gearbox)
2. Gear Train power loss: 5% of oxidizer pump horsepower
3. All pressures in psia
4. All flowrates in lb/sec
5. All temperatures in °R
6. All dimensions in inches
7. All efficiencies in percent.

Figure 80. 5000-lb (22240-N) Flox/Methane Engine Cycle Schematic FD 27375B

Table XXVIII. Engine Design

| | Design Point | Uprated | 10% Thrust |
|---|---|---|---|
| Performance Summary | | | |
| Thrust, lb (N) | 5000 (22240) | 8000 (35590) | 500 (2224) |
| Chamber Pressure-Throat Total, psia ($N/cm^2$) | 500 (344.7) | 800 (551.6) | 50 (34.47) |
| Thrust Chamber Mixture Ratio | 5.25 | 5.25 | 5.25 |
| Theoretical Vaccum Specific Impulse, $lb_f$-sec/$lb_m$ (N-sec/kg) | 425.5 (4173) | 426.1 (4187) | 421.2 (4131) |
| Nominal Specific Impulse, $lb_f$-sec/$lb_m$ (N-sec/kg) | 399.4 (3917) | 399.9 (3922) | 374.4 (3672) |
| Fuel Flow, lb/sec (kg/sec | 2.06 (0.95) | 3.31 (1.50) | 0.219 (0.0995) |
| Oxidizer Flow, lb/sec (kg/sec | 10.46 (4.75) | 16.70 (7.58) | 1.116 (0.506) |
| Engine Mixture Ratio | 5.076 | 5.051 | 5.083 |
| Fuel Leakage (total), lb/sec (kg/sec) | 0.0685 (0.311) | 0.125 (0.0567) | 0.007 (0.00506) |
| Oxidizer Pump | | | |
| Inlet Total Pressure, psia ($N/cm^2$) | 23 (15.86) | 31 (21.37) | 23 (15.86) |
| Inlet Temperature, °R (°K) | 150 (83.33) | 150 (83.33) | 150 (83.33) |
| Inlet Density, $lb/ft^3$ ($kg/m^3$) | 90.8 (1454) | 90.8 (1454) | 90.8 (1454) |
| Flow Rate, gpm ($m^3$/sec) | 51.6 (11.72) | 82.0 (42.30) | 5.50 (2.84) |
| Head Rise, ft (m) | 1023 (311.8) | 1775 (541.0) | 86.5 (26.37) |
| Speed, rpm (rad/s) | 24,980 (2616) | 34,450 (3608) | 6620 (693.3) |
| Efficiency, (%) | 58.9 | 62.2 | 29.3 |
| Horsepower, hp (W) | 33.0 (24600) | 86.4 (6473) | 0.579 (431.8) |
| Specific Speed | 1005 | 1150 | 541 |
| Discharge Pressure, psia ($N/cm^2$) | 670 (461.95) | 1157 (797.73) | 77.5 (53.43) |
| Fuel Pump | | | |
| Inlet Total Pressure, psia ($N/cm^2$) | 23 (15.86) | 27 (18.62) | 23 (15.86) |
| Inlet Temperature, °R (°K) | 200 (111.1) | 200 (111.1) | 200 (111.1) |
| Inlet Density, $lb/ft^3$ ($kg/m^3$) | 26.4 (422.9) | 26.4 (422.9) | 26.4 (422.9) |
| Flow Rate, gpm ($m^3$/sec) | 35.1 (7.97) | 56.1 (12.75) | 3.74 (0.850) |
| Head Rise per Stage, ft (m) | 3436 (1047) | 5929 (1807) | 282 (85.95) |
| Speed, rpm (rad/s) | 49,960 (5232) | 68,900 (7215) | 13,240 (1386) |
| Efficiency, (%) | 48.0 | 50.7 | 23.0 |
| Horsepower, hp (W) | 53.7 (40040) | 140.2 (104500) | 0.95 (708.4) |
| Specific Speed | 668 | 760 | 370 |
| Discharge Pressure, psia ($N/cm^2$) | 1280 (882.5) | 2201 (1517) | 126 (86.87) |

Table XXVIII. Engine Design (Continued)

| | Design Point | Uprated | 10% Thrust |
|---|---|---|---|
| Turbine | | | |
| Inlet Total Pressure, psia ($N/cm^2$) | 951 (655.7) | 1730 (1193) | 80.8 (55.70) |
| Inlet Total Temperature, °R (°K) | 1388 (711.1) | 1311 (728.3) | 1702 (945.6) |
| Discharge Total Pressure, psia ($N/cm^2$) | 661 (455.7) | 1040 (717.0) | 70.2 (48.40) |
| Discharge Total Temperature, °R (°K) | 1343 (746.1) | 1248 (693.3) | 1692 (940.0) |
| Speed, rpm (rad/s) | 49,960 (5232) | 68,900 (7215) | 13,240 (1386) |
| Efficiency % | 67.7 | 70.5 | 36.6 |
| Horsepower, hp (W) | 88.5 (66870) | 231 (172300) | 1.55 (1156) |
| Turbine Flow, lb/sec (kg/sec) | 1.51 (0.686) | 2.90 (1.318) | 0.108 (0.0491) |
| Bypass Flow % | 25.3 | 10.2 | 48.0 |
| Thrust Control Bypass Area, $in.^2$ ($cm^2$) | 0.0564 (0.364) | 0.0187 (0.121) | 0.1947 (1.256) |
| Thrust Chamber | | | |
| Chamber Pressure (injector Static), psia ($N/cm^2$) | 505 (348.2) | 808 (557.1) | 50.5 (34.81) |
| Coolant Flow Rate, lb/sec (kg/sec) | 2.03 (0.921) | 3.24 (1.470) | 0.215 (0.0976) |
| Coolant Jacket Pressure Drop, psi ($N/cm^2$) | 324.3 (223.6) | 463 (319.2) | 44.8 (30.88) |
| Coolant Jacket Temperature Rise, °R (°K) | 1176 (653.3) | 1093 (607.2) | 1499 (832.8) |
| Injector | | | |
| Fuel, lb/sec (kg/sec) | 1.99 (0.904) | 3.18 (1.443) | 0.212 (0.0964) |
| Fuel Injector, ΔP | 142 | 209 | 19.2 |
| Oxidizer Flow, lb/sec (kg/sec) | 10.46 (4.55) | 16.70 (7.56) | 1.116 (0.507 |
| Oxidizer Secondary, ΔP | 73 | 189 | 0.3 |
| Oxidizer Primary, ΔP | 163 | 343 | 27.0 |
| Lines and Valves | | | |
| Fuel line to coolant inlet manifold ΔP, psi ($N/cm^2$) | 1.6 (1.10) | 4 (2.75) | NIL |
| Fuel line to turbine ΔP, psi ($N/cm^2$) | 2.7 (1.86) | 4 (2.75) | 0.3 (0.20) |
| Fuel line to injector ΔP, psi ($N/cm^2$) | 7 (4.82) | 13 (8.96) | 0.6 (0.41) |
| Main Fuel Shutoff Valve ΔP, psi ($N/cm^2$) | 5 (3.44) | 10 (6.89) | 0.4 (0.27) |
| Oxidizer line ΔP psi, ($N/cm^2$) | 2 (1.37) | 6 (4.13) | NIL |
| Oxidizer flow control valve ΔP, psi ($N/cm^2$) | 89 (61.36) | 153 (105.49) | 27 (18.61) |

Additional off-design cycle data showing the effect of heat flux ($Q_m/Q_p$) and mixture ratio on the cycle operating parameters are presented in table XXIX. The results shown are consistent with the preliminary results shown in table XX, and show a satisfactory cycle balance over a wide range of conditions.

As discussed in Section IV paragraph B, the turbomachinery efficiencies used for the cycle analysis are believed to be conservative. However, the low volumetric flow rates, combined with the high operating pressures, are outside the range of available experimental data, and the accuracy of the turbomachinery efficiencies must be of concern. The effects of deviations from assumed efficiencies were therefore evaluated with the results shown in figure 81. Only the effects of reductions in turbomachinery efficiency below the values used in analysis were considered; it was found that a loss in oxidizer pump efficiency of 10% results in a reduction of 2.5% in power margin (bypass flow), while a 10% loss in either fuel pump or turbine efficiency would cause approximately 6% loss in bypass flow. Even if all three components operated at 10% below their predicted efficiency, a bypass flow of over 10% would be maintained. Any single efficiency deviation might be expected, but combined effects this extensive would be unlikely. If they were encountered, uprating capability might be limited, but satisfactory design point operation would be assured.

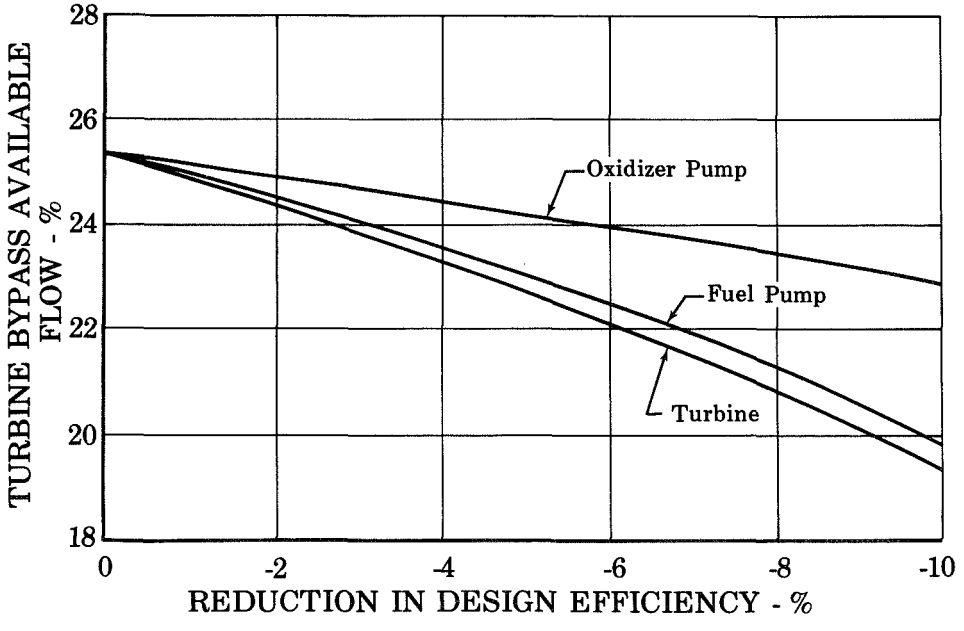


Figure 81. Effect of Component Efficiency on Excess Power FD 29208

Table XXIX. Space Storable Engine, Off-Design Operation

| | 1 | 2 | 3 | 4 | 5 | 6 | 7 | 8 | 9 | 10 |
|---|---|---|---|---|---|---|---|---|---|---|
| Chamber Pressure, psia ($N/cm^2$) | 500 (344.7) | 500 (344.7) | 500 (344.7) | 500 (344.7) | 500 (334.7) | 800 (551.6) | 800 (551.6) | 800 (551.6) | 200 (137.9) | 50 (34.47) |
| Mixture Ratio | 5.25 | 5.25 | 5.25 | 4.75 | 5.75 | 5.25 | 5.25 | 5.25 | 5.25 | 5.25 |
| $Q_m/Q_p$ | 0.9 | 1.0 | 0.76 | 0.9 | 0.9 | 0.9 | 1.0 | 0.76 | 0.9 | 0.9 |
| Turbine Bypass Flow, % | 25.2 | 27.0 | 21.8 | 24.6 | 25.2 | 9.9 | 12.6 | 5.5 | 39.6 | 50.6 |
| Turbine Speed, rpm (rad/s) | 49,480 (5182) | 49,900 (5226) | 48,900 (5121) | 51,840 (5429) | 47,810 (5007) | 68,150 (7137) | 68,620 (7186) | 67,550 (7074) | 28,600 (2995) | 12,110 (1268) |
| Turbine Inlet Temperature, °R (°K) | 1389 (771.7) | 1483 (823.9) | 1249 (693.9) | 1312 (728.9) | 1459 (870.5) | 1312 (728.9) | 1411 (783.9) | 1187 (659.4) | 1546 (858.9) | 1702 (945.5) |
| Turbine Pressure Ratio | 1.43 | 1.42 | 1.44 | 1.47 | 1.40 | 1.64 | 1.63 | 1.67 | 1.23 | 1.12 |
| Fuel Pump Discharge Pressure, psia ($N/cm^2$) | 1274 (878.4) | 1300 (896.3) | 1240 (854.9) | 1360 (937.7) | 1215 (837.7) | 2184 (150.6) | 2220 (1531) | 2130 (1469) | 499 (344.0) | 126 (86.87) |
| Oxidizer Pump Discharge Pressure, psia ($N/cm^2$) | 662 (456.4) | 676 (466.1) | 644 (444.0) | 742 (511.6) | 605 (417.1) | 1113 (767.4) | 1134 (781.9) | 1090 (751.5) | 276 (190.3) | 85 (58.60) |
| Hex ΔP, psid ($N/cm^2$) | 305 (210.3) | 324 (223.4) | 274 (188.9) | 322 (222.0) | 295 (203.4) | 430 (296.5) | 465 (320.6) | 377 (259.9) | 152 (104.8) | 44 (30.33) |
| Hex ΔT, °R (°K) | 1176 (653.3) | 1270 (705.5) | 1037 (576.1) | 1099 (610.5) | 1247 (692.8) | 1093 (607.2) | 1192 (662.2) | 968 (537.8) | 1339 (743.9) | 1499 (832.8) |
| Fuel Injector ΔP, psid ($N/cm^2$) | 142 (97.91) | 152 (104.8) | 127 (87.56) | 162 (111.7) | 128 (88.25) | 209 (144.1) | 226 (115.8) | 188 (129.6) | 66 (45.51) | 19 (13.10) |
| Oxidizer Injector ΔP (Primary), psid ($N/cm^2$) | 155 (106.9) | 168 (115.8) | 136 (93.77) | 234 (161.3) | 98 (67.57) | 299 (206.1) | 320 (220.6) | 273 (188.2) | 74 (51.02) | 34 (23.44) |
| Oxidizer Injector ΔP (Secondary), psid ($N/cm^2$) | 75 (51.71) | 74 (51.02) | 76 (52.40) | 69 (47.57) | 80 (55.16) | 194 (133.8) | 193 (113.1) | 197 (135.8) | 10 (6.89) | 24 (16.55) |
| WP/WT Oxidizer Injector, % | 11.2 | 11.7 | 10.6 | 13.9 | 8.8 | 9.8 | 10.2 | 9.4 | 19.1 | 51.3 |
| Injector Momentum Ratio | 3.14 | 3.35 | 2.83 | 3.50 | 2.80 | 1.85 | 1.99 | 1.66 | 7.73 | 11.4 |
| Thrust Control Effective Area, $in.^2$ ($cm^2$) | 0.0561 (0.362) | 0.0619 (0.399) | 0.0460 (0.27) | 0.0539 (0.38) | 0.0565 (0.35) | 0.0180 (0.116) | 0.0238 (0.14) | 0.0096 (0.019) | 0.1210 (0.781) | 0.2170 (1.400) |
| Oxidizer Control Effective Area, $in.^2$ ($cm^2$) | 0.1634 (1.055) | 0.1497 (0.65) | 0.1898 (1.22) | 0.1097 (0.708) | 0.3678 (2.35) | 0.2308 (1.490) | 0.2087 (1.348) | 0.2721 (1.755) | 0.0679 (0.9438) | 0.0142 (0.0915) |

## B. TURBOMACHINERY

The turbopump for the 5000-lb (22.24 kN) flox-methane engine preliminary design consists of a two-stage centrifugal liquid methane pump which is driven directly by a single stage partial admission impulse turbine, and a single stage centrifugal flox pump that is geared from the fuel pump-turbine shaft through an idler at a gear reduction of 2:1. A cross section view of the turbopump assembly is shown in figure 82. The complete assembly is less than 15.0 in. (38.10 cm) long and weighs only 24.2 lb (10.98 kg).

Data on pump and turbine efficiencies and primary operating variables were given in table XXVII for the engine design point and for the uprated and 10% thrust conditions. To assure that the turbopump could be operated at the speeds, flowrates, and pressures required for uprating, the turbomachinery was optimized at the 8000-lb (35.59 kN) thrust condition; thus, it is derated at the 5000-lb (22.24 kN) thrust design point. In addition to providing uprating capability, this design approach assures that a substantial operating margin is available at the design point, e.g., bearing and seal velocities are well below limiting values and pump and turbine efficiencies are not critical, so that confidence of success in an initial development program for a fixed thrust, design point engine will be high.

### 1. Fuel Pump

Performance of dynamic type pumps in conventional size ranges can be reliably predicted using well established similarity relationships based on correlation of data from many existing water pumps. The propellant pumps for the 5000-lb (22.24 kN) flox/methane engine are in a size range for which similarity relationships have not been confirmed. This necessitates attention to details of design to avoid losses. Some of the unique problems presented relative to obtaining high efficiency because of the small sizes are:

1. Extremely small leakage clearances are required to maintain the similarity relationships implied in the conventional prediction techniques.

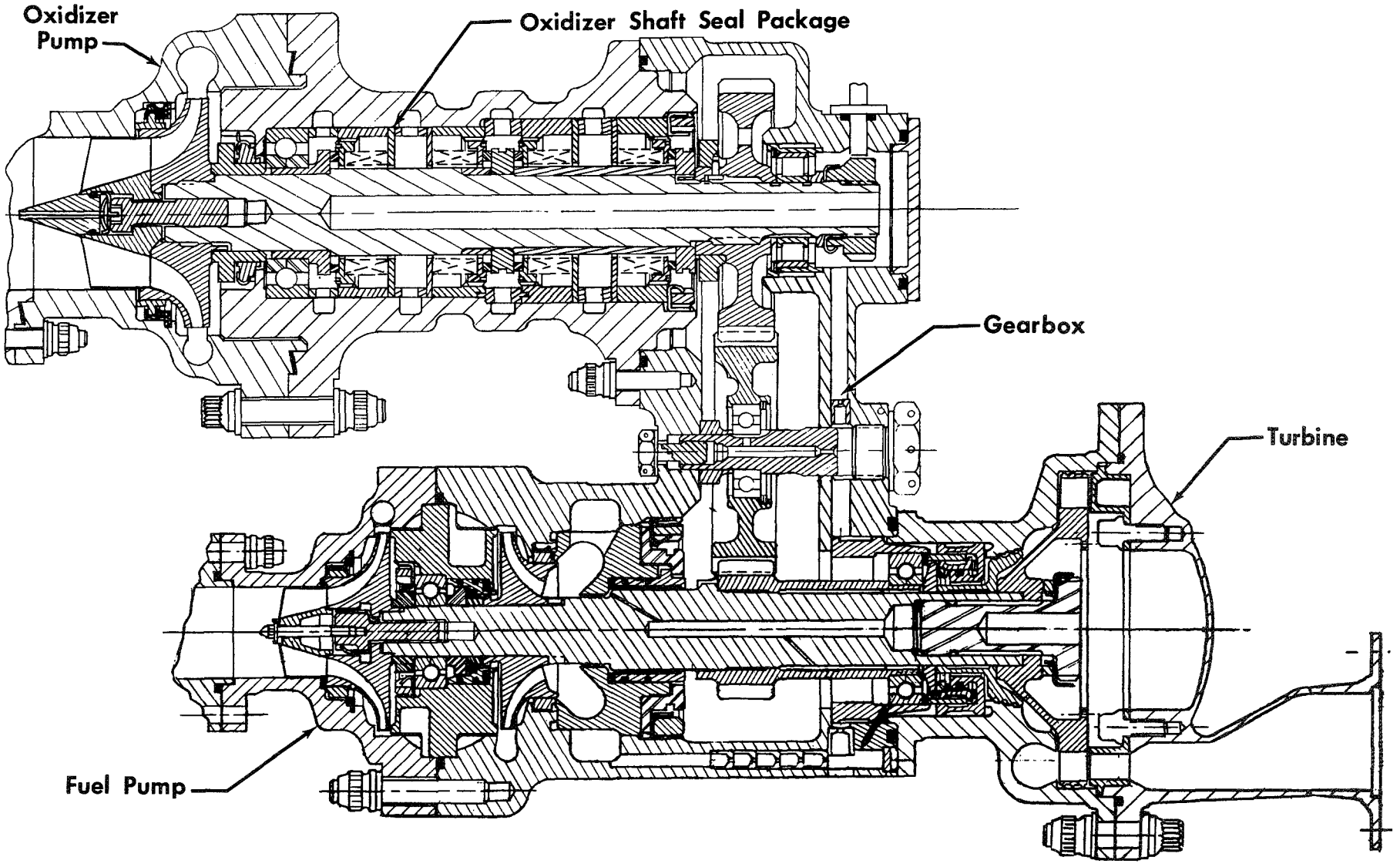


Figure 82. Turbopumps

GS 11172A

2. Small dimensions (blade heights, impeller diameters, etc.) can increase viscous losses because of the reduced characteristic dimension included in the Reynolds Number calculation. An opposite effect results from the lower viscosity of the fluid being pumped. Conventional prediction methods are commonly based on the viscosity of water. The viscosity of methane is $7 \times 10^{-5}$ $lb_m$/ft-sec ($13.38 \times 10^{-4}$ N-sec/$m^2$) as compared to $6.7 \times 10^{-4}$ $lb_m$/ft-sec ($9.97 \times 10^{-4}$ N-sec/$m^2$) for water; therefore the viscous losses are reduced when pumping methane. Increased efficiency with cryogenic fluids has been demonstrated by experimental data for RL10 oxidizer pumps tested with liquid fluorine. Efficiencies 6 to 8 points higher than were predicted by water pump correlations were obtained.

3. Bearing and seal losses, which are normally very small when compared to the total pump power, represent a larger proportion of the total and can represent an appreciable percentage loss.

4. Losses associated with shroud back vanes incorporated to obtain axial thrust balance can become appreciable.

The 5000-lb (22.24 kN) pumps were designed to avoid, where possible, losses resulting because of these problems. A cross sectional view of the methane pump is shown in figure 83. It is a two-stage centrifugal design with the stages mounted back-to-back to minimize axial thrust unbalance. The specific speed, per stage, is 760 at the 8000-lb (35.59 kN) thrust design point. Features incorporated to maximize efficiency are discussed in the following description of individual elements and performance of the pump.

a. Inducer

A three blade, unshrouded inducer of 347 stainless steel is provided upstream of the first-stage impeller to reduce the required net positive suction pressure at the pump inlet. The inducer was designed for a suction specific speed of 25,000. The resulting net positive suction pressure required at the design point is 5 psi (3.45 N/$cm^2$) as compared to the 8 psi (5.52 N/$cm^2$) specified in table XXVI. The

inducer blade inlet angle is 9° (0.157 rad). In view of the fact that it satisfied the design requirement, and should be adequate since the tank-tankage thicknesses in stages suitable for the engine will likely be established by minimum gage rather than stress considerations, the 25,000 $N_{ss}$ level should be adequate. $N_{ss}$ could be increased, and the net positive suction pressure requirement could be reduced, through a reduction in the blade inlet angle (to a minimum of approximately 6° (0.105 rad); however, an increase in the pump inlet diameter and a contoured blade tip diameter would be required if this were done. These changes could be incorporated, if required, at the cost of a minor pump efficiency degradation and slightly increased complexity of the inducer and its housing.

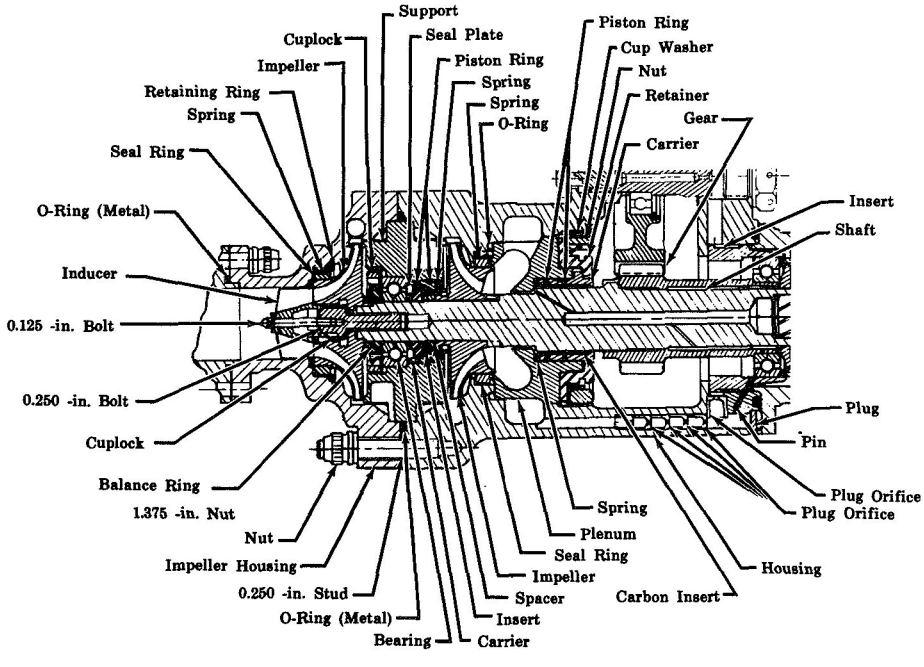


Figure 83. Fuel Pump FD 31591

b. Impellers

The impellers are designed to provide equal headrise across each stage. The blades are swept to an exit angle of 22.5° (0.393 rad), the tip diameter is 2.18 in. (5.54 cm), and the blade height at the impeller tip is 0.078 in. (0.198 cm). The 22.5° (0.393 rad) sweep angle provides a drooping head-flow characteristic which, as shown by experience with the RL10 expander cycle engine, is desirable from a system stability standpoint. The low sweep angle also permits maximum blade height and consequently a more optimum channel shape and minimum sensitivity to boundary layer thickness. Because of the low blade heights, impeller front shrouds were incorporated to prevent blade tip leakage; shroud back vanes were not required to obtain a satisfactory axial thrust balance, and therefore were not incorporated in the interest of reducing shroud disk friction.

The pump impellers are machined from 347 stainless steel and the shrouds are attached with gold-nickel braze. Calculated tangential stresses in the more highly stressed impeller, the second stage at the uprated design condition (8000-lb, 35.59 kN thrust) are shown in figure 84. The calculated maximum shear stress at the brazed blade-shroud interface was 2700 psi (1862 $N/cm^2$), compared to an allowable 32,000 psi (22050 $N/cm^2$) at the operating temperature.

c. Impeller Shroud Seals

The diametral clearance for typical wear ring seals at the shroud front seal position, as limited by tolerances, was estimated to be approximately 0.010 in. (0.0254 cm). The leakage through wear ring seals with this clearance was estimated to be greater than 20% of the total pump inlet flow, which would have an extremely adverse effect on efficiency. In order to reduce the penalty, floating ring seals were selected for both the first-and second-stage impellers. Seal details are shown in figure 85. These seals are free to move in a radial direction relative to the shaft; this floating characteristic permits very close diametral clearances to be maintained. The sealing element material is carbon; the pressure differential across the seal provides the force to seat the vertical sealing surface against

the pump housing. The maximum diametral clearance was specified to be 0.0012 in (0.0030 cm). With clearances of this magnitude, the calculated leakage was less than 5% of the inlet flow.

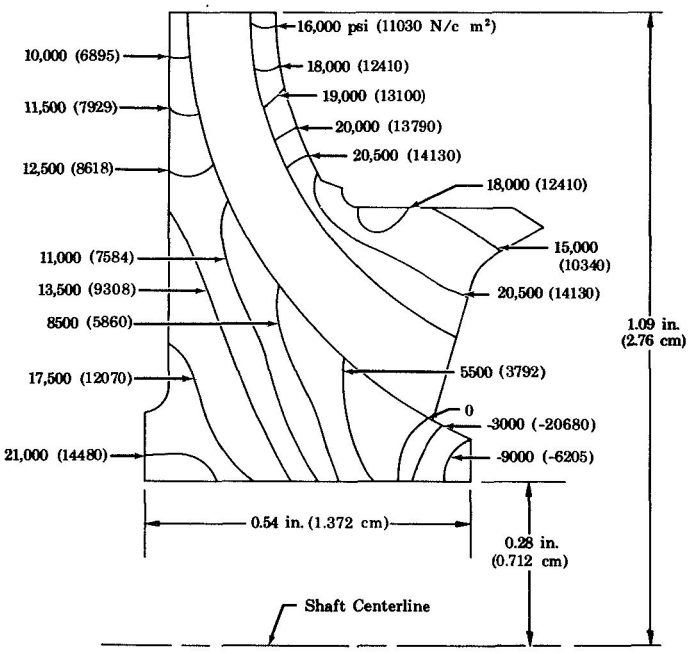


Figure 84. Fuel Pump Second Stage Impeller Tangential Stress Distribution Contours at 68,000 rpm (7121 rad/s) FD 31617

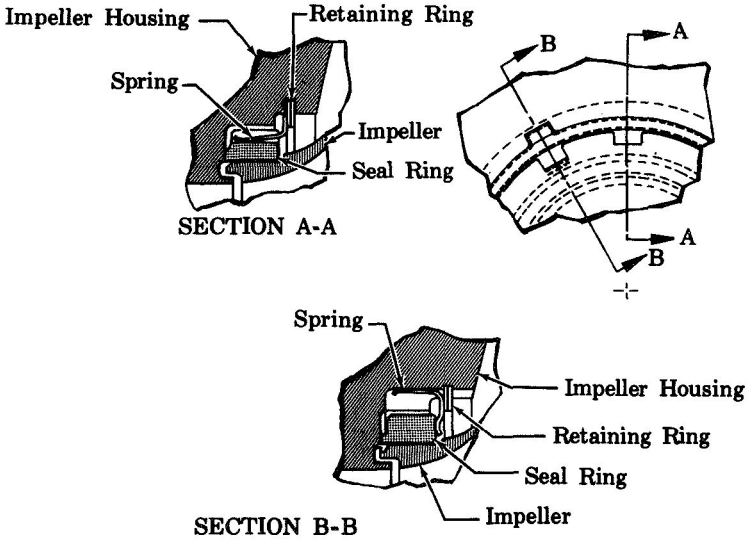


Figure 85. Fuel Pump Shroud Seal FD 31680

d. Impeller Interstage Seal

Shaft critical speed considerations mentioned in a later paragraph made it important to restrict the axial distance allowed for the impeller interstage seal. This requirement was in conflict with the desirability of using a balanced seal design, which would have necessitated some length. The shaft length restriction was given preference. A floating ring seal design can be adapted in short lengths, and would be suitable. However, it is felt that this area is one which requires further study, and for which alternative approaches would be desirable during development. The design of figure 83 shows a controlled wear, spring loaded, face seal. Details are shown in figure 86; the stationary nosepiece is carbon and the rotating mating ring is chrome plated 347 stainless steel. This might also be called a "wear-in" seal. Because of the magnitude of the pressure loading, the nosepiece will wear rapidly (for 0.002-0.007 in.; 0.00508-0.0178 cm) until contact is made between the outer bearing race and the seal carrier. At this point, no further wear is incurred; the maximum resulting clearance, calculated on the basis of the maximum shaft misalignment within tolerances, would allow leakage of the same magnitude as that resulting with a 0.0005 in. (0.00127 cm) radial clearance floating ring seal. Note in figure 86 that a series of labyrinths are provided on the shaft upstream of the seal. These serve as a back-up in the event of excessive seal wear or seal failure.

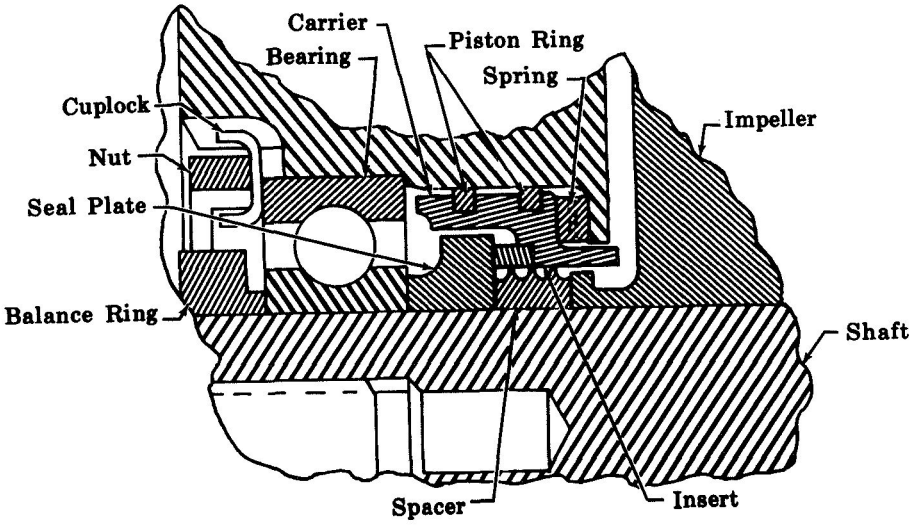


Figure 86. Fuel Pump Interstage Seal FD 31652

e. Fuel Pump Shaft Seal

A floating bushing seal is used to limit shaft leakage into the gearbox. An enlarged view of the seal is shown in figure 87. The seal insert is carbon and the retainer is Invar. The Invar material was chosen because its coefficient of thermal expansion is compatible with the carbon and excessive loading of the carbon as the seal cools to operating temperature can be avoided. Two Beryllium 25 piston rings are provided to prevent leakage around O.D. of the seal, and a series of labyrinths are provided on the shaft upstream of the seal as an emergency back-up.

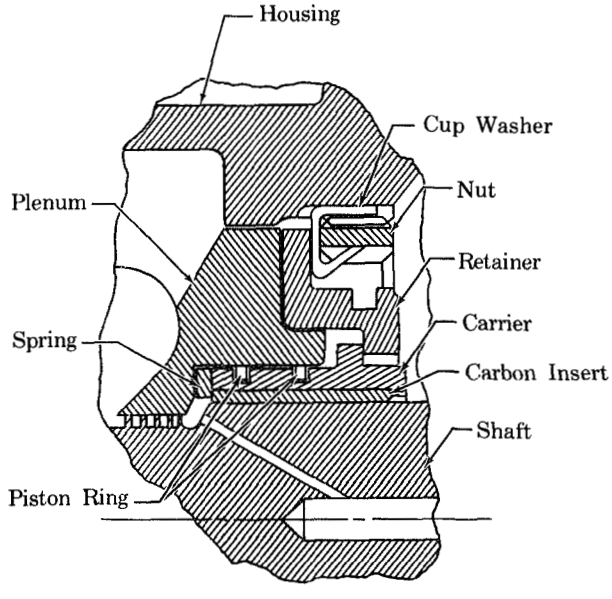


Figure 87. Fuel Pump Shaft Seal FD 31585

f. Shaft Support System

The common fuel pump/turbine shaft is made of Inconel 718 material and is mounted on two ball bearings. Inconel 718 material was chosen to withstand the operating environment at the turbine end. The calculated axial thrust load, based on the unbalanced forces on the impellers and turbine wheel was 344 lb (15.30 kN) in a direction toward the pump inlet. This load is transferred to the pump housing by the front bearing, which is located between the two pump stages. The rear bearing outer race is loaded in the thrust direction by a spring washer.

Analysis indicated a calculated shaft critical speed of 90,000 rpm (9425 rad/s), for the design shown in figure 83 giving a critical speed margin of 33%. The particular arrangement of the pump, turbine, and gearing, with dimensional requirements for assembly, did not provide acceptable critical speed characteristic in the initial layout. Iterations were necessary to achieve the final result. It was found necessary to minimize the overhang at the turbine end, consistent with dimensions required for seals and manifolding, and to reduce the distance between bearings as much as possible. The bolt circle for attachment of the turbine inlet housing to the pump housing was restricted to provide clearance at the idler gear through-bolt, so it was necessary to allow axial clearance at the gear train opening for assembly of the second-stage pump inlet plenum. This complicated the problem, forcing measures to conserve length, as noted in the above discussion of the pump interstage seal.

The front bearing is cooled and lubricated by methane interstage leakage flow. Liquid methane is supplied to the rear bearing through drilled passages in the shaft. The calculated flowrate to cool the rear bearing at the 8000-lb (35.59 kN) thrust design point was 0.012 lb/sec (0.00545 kg/sec) based on the heat generated due to thrust load and friction forces. The front bearing DN (diameter in millimeters x rotative speed in rpm) was calculated to be $1.02 \times 10^6$ and the rear bearing DN was calculated to be $1.7 \times 10^6$. The material for the bearings and races is consumable-electrode, vacuum-melted AMS5630. The separator material for the ball bearings is aluminum armored plastic of the type used in the RL10 engine turbopump, selected on the basis of demonstrated suitability, in a modified RL10A-1 engine tested with flox/methane (Reference 4).

A balance ring is provided at the fuel pump end of the shaft and weights are added to the turbine disk at the other end for dynamic balancing.

g. Housings

The fuel pump is encased in two aluminum housings. Machined volute collectors and straight tangential nozzle diffusers are used for

recovery of the velocity head in each stage. The housing stress limitation was established at 85% of the 0.2% offset yield strength. The flanges at the pump inlet and at the interface between the two housing were designed for a maximum deflection of 0.0001 in. (0.000254 cm) to insure good sealing. The metal O-ring flange seals shown were selected based upon experience to-date in an extensive investigation being conducted by Pratt & Whitney Aircraft under Air Force Contract F-04611-68-G-0002 to define the leakage characteristics for a large number of flange seal types. Work in the investigation is continuing, and the flange seal selection can be reviewed as more data become available.

h. Performance

The predicted pump operating characteristics are shown in figure 88. The predictions were generated using conventional techniques for head-rise and similarity relations for efficiency. Because of questions regarding the accuracy of similarity relations for pumps of this size, a pump loss analysis was conducted to provide an independent prediction of efficiency.

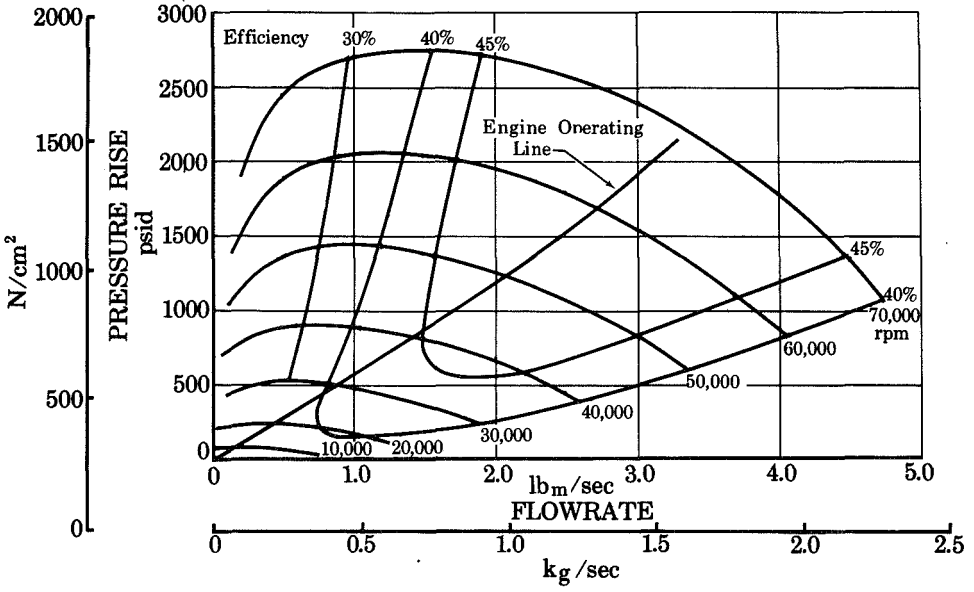


Figure 88. Space Storable Engine Fuel Pump FD 31587

Pump losses are grouped into three categories: (1) volumetric losses, (2) hydraulic losses, and (3) mechanical losses. Volumetric losses take into account the power absorbed by fluids recirculating within the pump or leakage overboard after passing through the impeller. The hydraulic losses take into account pump inlet losses, losses in the impeller flow channels, due to friction, turbulence, and separation, and collector and diffuser losses. Mechanical losses account for the remaining sources of power absorption i.e., disk friction, and bearing and seal losses. The very tight clearances required with conventional pump design to obtain acceptable leakage values was found to be a serious problem. Leakage sources include:

1. Recirculation of fuel from the impeller discharge to the pump inlet (both stages).
2. Recirculation of fuel from the second-stage of the pump to the first-stage.
3. Leakage along the shaft into the gearbox.
4. Bearing coolant flow extraction.

A summary of the calculated pump losses is shown in table XXX.

Table XXX. Calculated Fuel Pump Losses

| | 1st-Stage | 2nd-Stage |
|---|---|---|
| Volumetric Efficiency, % | 96 | 93 |
| Shroud Recirculation Flow, lb/sec (kg/sec) | 0.070 (0.0318) | 0.144 (0.0654) |
| Interstage Leakage Flow, lb/sec (kg/sec) | | 0.09 (0.0409) |
| Shaft Leakage Flow, lb/sec (kg/sec) | 0.042 (0.0191) | |
| Bearing Coolant Flow, lb/sec (kg/sec) | 0.023 (0.0104) | |
| Mechanical Efficiency,% | 86 | 86 |
| Disk Friction, hp (W) | 9.3 (6935) | 9.3 (6935) |
| Bearing Loss, hp (W) | 0.03 (22.77) | |
| Hydraulic Efficiency, % | 76 | 76 |
| Impeller Flow Channel Efficiency, % | 85 | 85 |
| Collector and Diffuser Efficiency, % | 90 | 90 |
| Pump Efficiency, % | 62.5 | 60.8 |

The indicated average efficiency for the two stages based on calculated losses was 61.6%. The efficiency predicted by similarity using the Worthington curve was 50.7%. Thus the efficiency indicated by loss calculations was 11% higher than Worthington, indicating that the latter prediction was not necessarily optimistic. The pump leakages were calculated based on perfect seal concentricity, and the leakage through the vertical sealing surfaces of the floating ring seals was assumed to be zero, which tends to make the calculated volumetric efficiency somewhat high. If more conservative assumptions were made, the calculated value would be closer to the Worthington efficiency, so it appears to be a reasonable estimate.

2. Oxidizer Pump

A cross section view of the oxidizer pump is shown in figure 89. The problems imposed on the fuel pump because of size considerations also apply to the oxidizer pump, and therefore similar design approaches were followed where possible. The pump is a single stage centrifugal design with a specific speed of 1150 at the design point. The pump components and performance are discussed below.

a. Inducer

A three blade unshrouded inducer design similar to that for the fuel pump is incorporated in the oxidizer pump. It, too, was designed for a suction specific speed of 25,000, and provides net positive suction pressure capabilities at the design point of 9 psi (6.21 $N/cm^2$), compared to the contractural requirement of 12 psi (8.27 $N/cm^2$). The inducer blade inlet angle is the same as that of the fuel pump, 9° (0.3142 rad), and again a reduction in this angle to approximately 6°R (0.2037 rad) could provide improved suction performance, but at the expense of slightly more complex parts. The inducer is 347 stainless steel and is attached to the shaft with a locked bolt. Similar threaded attachments were used in the RL10 oxidizer pumps that were successfully tested in liquid fluorine and liquid flox (References 4, 8, and 13, and these are therefore considered acceptable for fluorine service.

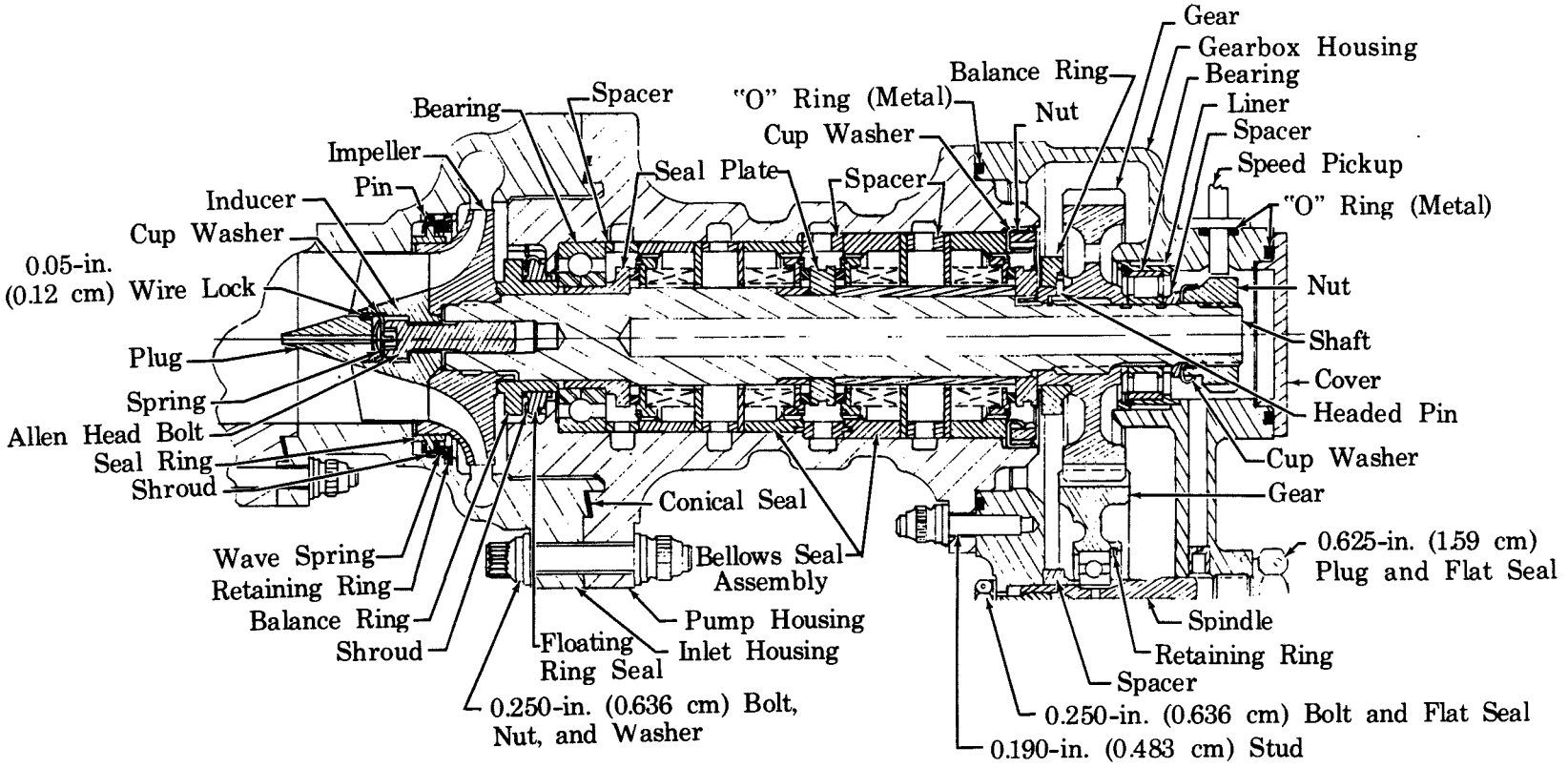


Figure 89. Oxidizer Pump Cross Section

FD 31614

b. Impeller

The impeller blades are swept back to the same exit angle as the fuel pump, 22.5° (0.3927 rad). Impeller tip diameter is 2.48 in. (6.30 cm), and the blade height at the tip is 0.132 in. (0.335 cm). The blade sweep was selected to provide characteristics similar to those of the fuel pump for off-design operation, and to take advantage of maximized blade height. An impeller front shroud was incorporated to prevent blade tip leakage, and because shroud back vanes were not required to obtain a satisfactory axial thrust balance, they were not used. The pump impeller is machined from 347 stainless steel and the front shroud is attached with gold-nickel braze. The impeller stresses at the 8,000-lb (35.59 kN) thrust uprated design point are shown in figure 90. The maximum shear stress in the braze joint at the blade shroud interface was 6,500 psi (4482 $N/cm^2$), as compared to an allowable value of 140,000 psi (96530 $N/cm^2$). The materials and fabrication methods are the same as those for RL10 oxidizer pumps that have been tested in fluorine and flox.

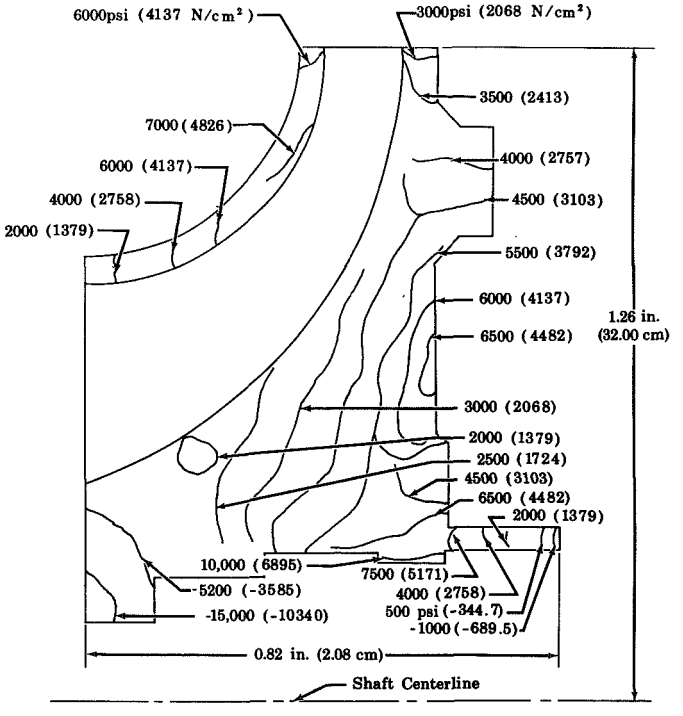


Figure 90. Flox/Methane Oxidizer Pump Impeller Tangential Stress Distribution Contours at 34,000 rpm (3560 rad/s) FD 31616

c. Impeller Front Shroud

It was estimated that the diametral clearance for a typical wear ring seal at the impeller front shroud would be approximately the same as in the case of the fuel pump, 0.010 in. (0.0254 cm). The maximum leakage of flox through such a clearance was calculated to be approximately 9% of the total oxidizer flow, so again, a need for a floating ring seal was indicated. The oxidizer shroud seal is shown in detail in figure 91. The seal is held in place by a spring wave washer, a retaining ring, and a seal shroud. Maximum diametral clearance was specified as 0.0012 in. (0.0005 cm); a tab on the seal shroud, that fits into a slot machined into the pump housing, prevents rotational motion. Ilkoloy* (80% Ni, 20% CaF) was selected as the material for this seal because of its expansion coefficient and because of its demonstrated performance when tested in a liquid fluorine rubbing seal rig at P&WA (Reference 8). Its coefficient of linear expansion is approximately equal to the expansion coefficient of the stainless steel impeller so that changes in the seal annular clearance will be minimal as pump temperature stabilizes.

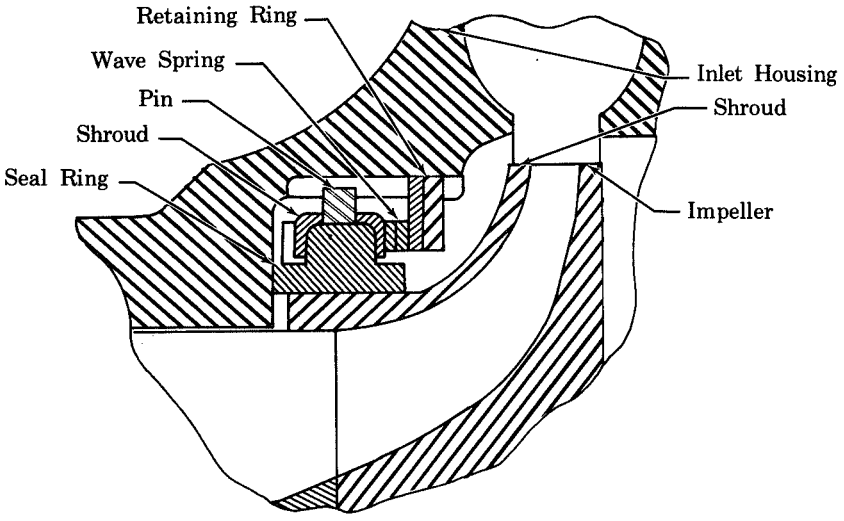


Figure 91. Oxidizer Pump Shroud Seal FD 31615

*Ilkoloy is a designation of the Ilkon Corporation, Natick, Massachusetts.

d. Bearing Upstream Seal

A floating ring seal as shown in figure 92 was incorporated between the impeller and the bearing, to provide controlled leakage that would insure a positive flow of coolant to the bearing. The seal also serves to reduce the pressure upstream of the primary shaft seal to approximately the value of pump inlet pressure. The material for the seal (Ilkoloy), is identical to that of the impeller front shroud seal. Leakage was calculated to be 0.108 lb/sec (0.00491 kg/sec), at the 8000-lb (35.59 kN) thrust operating point, a level which is considered conservative for bearing cooling. The coolant flow is recirculated to the pump inlet; it represents approximately 0.7% of the total oxidizer flow and will be reflected in pump efficiency. The low pressure downstream of the bearing insures minimum flox overboard leakage through the primary shaft seal and permits reduced face loading of the primary shaft seal for reliability and long life.

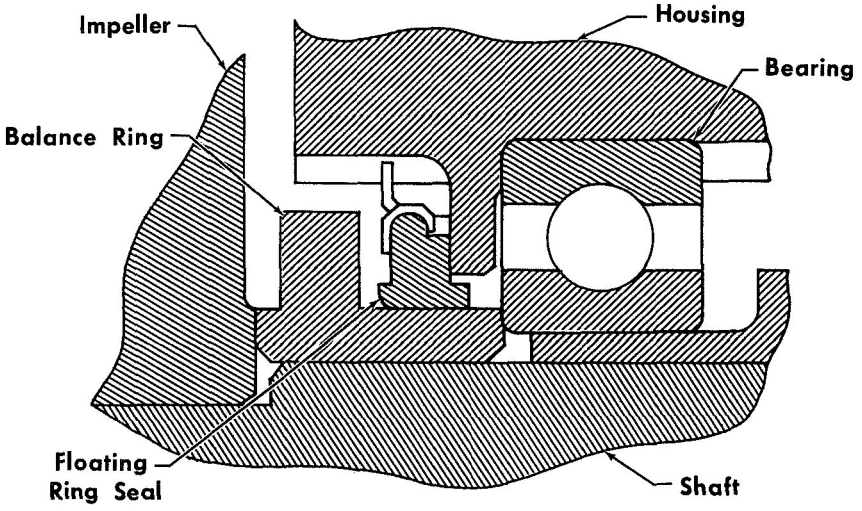


Figure 92. Oxidizer Bearing Upstream Shaft Seal GS 11217

e. Shaft Seal Package

The oxidizer pump shaft seal package is shown in figure 93. The package incorporates primary seals at either end, one for flox at the pump end, and one for methane at the gearbox end. Secondary seals are provided behind each primary seal, and the cavities between the primary and secondary seals are vented overboard (through nonpropulsive vents when the engine is operating in space) to prevent mixing of the

hypergolic propellants that leak through the primary seals. There is a third cavity between the secondary seals, which is also vented to space; however, use of a helium purge at this center cavity is recommended for ground testing to assure positive separation of the propellants.

The general configuration of the seal package is identical to that of the RL10 oxidizer pump. The four seal arrangement has proved extremely effective in fluorine/hydrogen and flox/methane testing of modified RL10 engines. On one occasion, a modified RL103-3 engine survived the failure of a primary fluorine seal with the only damage sustained being limited to the oxidizer pump seal package. All of the seals in the 5000-lb (22.24 kN) oxidizer pump shaft seal package are bellows type face seals whereas intermediate seals in the RL10 pump are split ring type seals. The all-bellows seal arrangement is similar to that of fluorine pumps, designed to provide more positive sealing. Use of all bellow seals increased the length of the seal package slightly, but the additional length was considered justified.

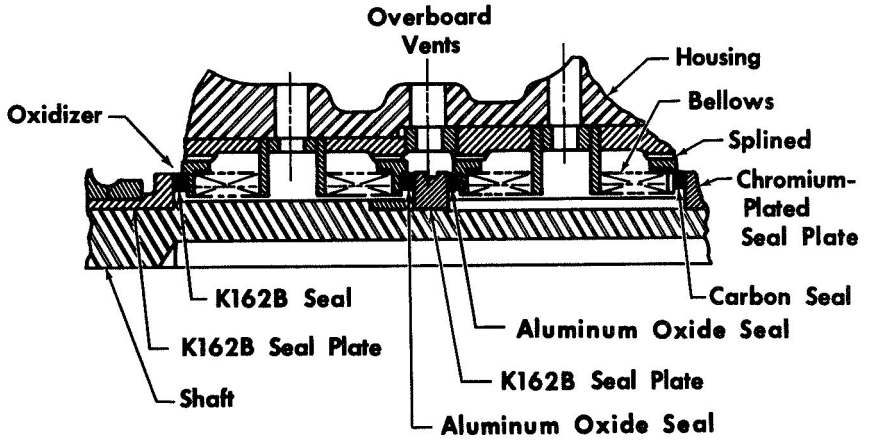


Figure 93. Oxidizer Pump Shaft Seal Package GS 11183B

Inconel X was specified for seal bellows; it was believed that this material would overcome deficiencies of the stainless steel and Inconel 718 materials used in seals of modified RL10 pumps, tested in fluorine and flox. Splined retainers were incorporated to isolate torque and provide damping while permitting axial travel. Materials selected for rubbing seal surfaces duplicated those used in modified RL10A-1 oxidizer pumps, tested in liquid flox. The primary oxidizer

seal incorporates Kentanium K162B* for both the nosepiece and the mating ring. The common mating ring for the secondary seals is Kentanium K-162B; the stationary nosepiece of oxidizer seal is aluminum oxide and that of the fuel seal is aluminum oxide. The fuel primary seal uses a conventional carbon stationary nosepiece and chromium plated stainless steel rotating mating ring.

In Section III, it was stated that seal rubbing velocities up to 145 ft/sec (44.20 m/sec) had been demonstrated with fluorine compatible seal materials, and that it was believed that rubbing velocities up to approximately 190 ft/sec (57.91 m/sec) were possible with existing materials. This increase in rubbing velocity was predicted on the basis of attainable seal loading. An important criterion in determining limitations of seal face materials is the PV factor, the product of the unit pressure acting on the seal face junction (psi) and the rubbing velocity (fpm). The unit pressure is the total load resulting from the bellows preload and the unbalanced pressure-area force on the seal face, divided by the contact area. Although most experience with fluorine pump seal materials tested by Pratt & Whitney Aircraft was at the operating conditions of the RL10 oxidizer pump, a few tests were conducted with varied seal preloads and rubbing velocities. A summary of the data from these tests, including PV factors, for K162B rubbing on K162B is given in table XXX. It will be noted that PV factors up to 855,000 were demonstrated successfully while failures occurred at a PV factor of 1,300,000.

The total pressure loading on the main oxidizer seal face for the 5000-lb (22.24 kN) flox/methane engine pump was calculated to be 10.6 psi (7.31 $N/cm^2$) with a 50 psi (34.47 $N/cm^2$) pressure differential across the seal. With 600 psi (413.7 $N/cm^2$) pressure differential across the seal, a condition which would exist if the bearing upstream seal were not incorporated, the total pressure loading would be 70.4 psi (48.54 $N/cm^2$). The rubbing speed at the uprated thrust level was 11,500 ft/min (3505 m/m); thus, the PV factor would be 122,000 with the bearing upstream seal, and 810,000 without it. Therefore, the seal material combination would be satisfactory even if the bearing upstream seal were to fail.

*Kentamium K-162B is a designation of the Kennametal Company, Latrobe, Pennsylvania.

Table XXXI. Seal Rig Test Data for K162B on K162B

| Test duration, min. | 30 | 30 | 30 | 2 |
|---|---|---|---|---|
| Speed, rpm (rad/s) | 11,000 (1152) | 18,000 (1885) | 11,000 (1152) | 18,000 (1885) |
| Rubbing Velocity, Fpm (m/m) | 5,300 (1615) | 8,700 (2652) | 5,300 (1615) | 8,700 (2652) |
| Spring Loading, lb (kg) | 14 (6.35) | 14 (6.35) | 40 (18.14) | 40 (18.14) |
| Pressure Loading, lb (kg) | 36 (16.33) | 36 (16.33) | 36 (16.33) | 36 (16.33) |
| Seal Pressure x Velocity | 520,000 | 855,000 | 793,000 | 1,300,000 |
| Nosepiece Wear, in. (cm) | 0.0001 (0.000254) | Nil | 0.0013 (0.00330) | 0.0021 (0.00534) |
| Mating Ring Wear, in. (cm) | Nil | Nil | 0.0004 (0.00102) | 0.0015 (0.00381) |
| Remarks | Successful | Successful | Successful | Failed |

It was not possible to make a straightforward assessment of the capabilities of the secondary seal materials selected on the basis of experience. The materials were demonstrated in the intermediate seal locations of the RL10 seal package in fluorine tests at rubbing velocities up to 170 ft/sec (51.82 m/sec), but as noted above, this was in split ring type seals. Unit face loading for this split ring seal, is difficult to assess because a portion of the axial load is transmitted to the pump housing by friction. Therefore, the equivalent PV factor for the secondary seal position cannot be directly calculated. The face loading on the secondary seals is low, however, because of the low pressure differential across the seal, and therefore is of reduced importance. Considering rubbing velocity along, the velocity required for the 5000-lb (22.24 kN) flox/

methane engine is 192 ft/sec (58.52 m/sec) at the 8000-lb (35.59 kN) thrust level and 139 ft/sec (42.37 m/sec) at the 5000-lb (22.24 kN) thrust level. Since 170 ft/sec (51.82 m/sec) was demonstrated, no seal material problems at the intermediate location are anticipated at the design point, and it is reasonable to believe that trouble-free operation at the uprated thrust level is feasible.

f. Shaft and Support System

The oxidizer pump shaft is made of 347 stainless steel and is mounted on a front ball bearing and a rear roller bearing. The thrust load is transferred to the oxidizer pump housing by the front ball bearing which is located between the oxidizer shaft seal package and the impeller. Balance rings are provided on both ends of the shaft to allow for dynamic balancing. The calculated critical speed for the shaft was 85,900 rpm (8995 rad/s). This provides a critical speed margin of 150%. The bearing thrust load was calculated from the unbalanced forces on the impeller to be 823 lb (36.70 kN) at the 8000-lb (35.59 kN) thrust design point. At the 5000-lb (22.24 kN) thrust level this load is reduced to 700 lb (31.14 kN).

This ball bearing is cooled and lubricated by flox. The calculated minimum flow rate required to cool the bearing at the 8000-lb (35.59 kN) design point was 0.013 lb/sec (0.00590 kg/sec) based on the heat generated due to the thrust loads and friction forces. The bearing coolant flow that will be allowed by a ring type bearing upstream seal was estimated at 0.108 lb/sec (48.99 kg/sec), which should provide adequate margin. The materials for the flox bearing were not selected. It is understood that there are a few candidate materials for such bearings that are still being evaluated by another investigator under NASA contract, and it was felt that selection should be deferred until the results of this work become available. The bearing DN was calculated to be 850,000, which is believed to be well within demonstrated values.

The rear roller bearing is mounted in the gearbox housing, where it is cooled by liquid methane supplied through drilled passages in

the housings. The coolant flowrate was calculated to be 0.008 lb/sec (0.00365 kg/sec) and the bearing DN was calculated to be 510,000. The bearing rollers and races are consummable-electrode, vacuum-melted AMS 5630 material. The bearing separator is aluminum-armored plastic.

g. Housings

There are two forged aluminum housings for the oxidizer pump. The inlet housing includes a machined volute collector and a straight tangential nozzle diffuser for the recovery of the velocity head. The housing stress limitation was established at 85% of the 0.2% offset yield strength. The flange was designed for a maximum deflection of 0.0001 in. (0.0254 cm) to ensure low leakage. The flange is sealed with an uncoated aluminum angle gasket, rather than the metal O-rings used in the fuel pump. This type flange joint was selected on the basis of effective sealing RL10 oxidizer pumps tested in fluorine.

h. Performance

Predicted pump operating characteristics are shown in figure 94 for the required ranges of flowrates and pressure rises. The limitations imposed by a lack of experimental background data for pumps of the sizes being considered apply to the oxidizer pump as well as the fuel pump; therefore, a loss analysis was conducted for this pump also; the results are shown in table XXXII.

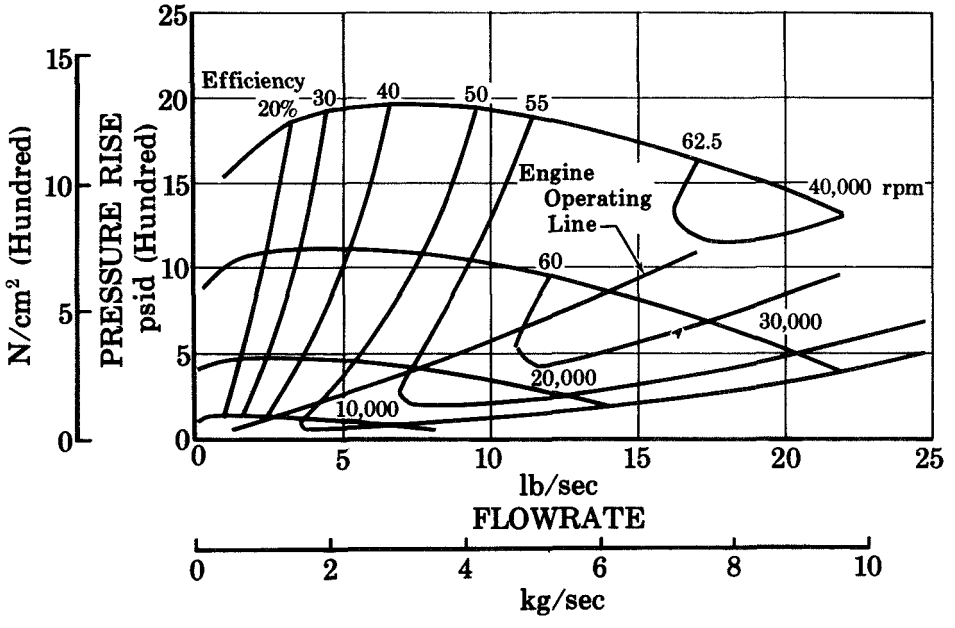


Figure 94. Space Storable Engine Oxidizer Pump FD 31588

Table XXXII. Calculated Oxidizer Pump Losses

| | |
|---|---|
| Volumetric efficiency, % | 98.0 |
| Shroud Recirculation Losses, lb/sec (kg/sec) | 0.212 (0.0962) |
| Bearing coolant loss, lb/sec (kg/sec) | 0.108 (0.0490) |
| Shaft Leakage Loss, lb/sec (kg/sec) | Nil |
| Mechanical efficiency, % | 89.5 |
| Bearing Load, hp (W) | 0.16 (119.3) |
| Disk Friction Loss, hp (W) | 7.35 (5481) |
| Rubbing Seal Losses (Shaft Seal Package), hp (W) | 0.7 (552) |
| Hydraulic efficiency, % | 77.6 |
| Impeller Flow Channel efficiency, % | 85.0 |
| Collector and Diffuser efficiency, % | 91.5 |

The indicated pump efficiency based on the above losses was calculated to be 68%. The efficiency predicted by the Worthington curve of figure 17 is 62.1%. The indicated value of pump efficiency is approximately 6% higher than Worthington. As in the case of the fuel pump, the ring seal leakages were calculated on the basis of complete concentricity, and zero leakage was assumed across the vertical sealing surfaces. When allowance is made for these assumptions, the predicted efficiency level based on similarity appears to be quite reasonable.

3. Turbine

A cross section view of the turbine, which is a single-stage, partial-admission, impulse type, is shown in figure 95.

a. Rotor

There are 38 blades incorporated on the rotor; the mean diameter is 3 in. (7.62 cm), and the blade height is 0.34 in. (0.0864 cm). The rotor blades are machined integral with the rotor and are fully shrouded to prevent blade tip leakage. The shroud is attached with gold-nickel braze, and a 3-step labyrinth seal with a maximum radial

clearance of 0.005 in. (0.0127 cm) is provided between the shroud and the housing to reduce leakage. The rotor and shroud are made from a forged nickel based alloy with a composition comparable to that which International Nickel Company identifies as IN100. This material is currently being developed by Pratt & Whitney Aircraft for high temperature turbine disks. Calculated rotor stresses are shown in figure 96. Allowable stresses are shown for comparison, and it will be noted that significant margins are available.

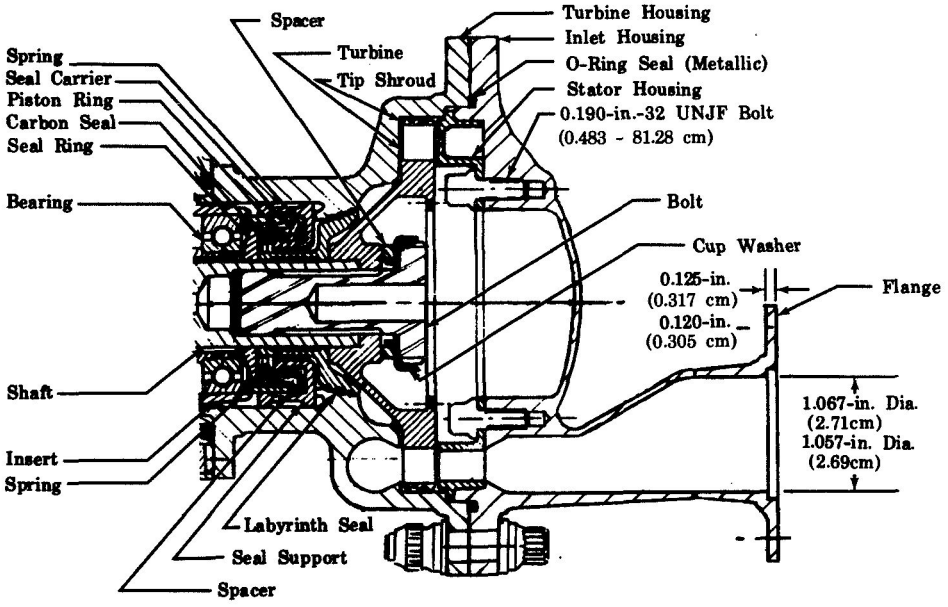


Figure 95. Turbine Cross Section FD 31590

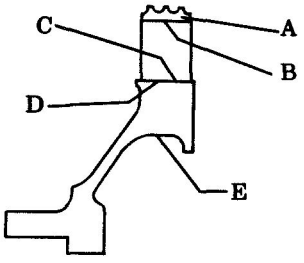


| | | Calculated Stress, psi ($N/cm^2$) | | Allowable Stress, psi ($N/cm^2$) | |
|---|---|---|---|---|---|
| A | Tangential Stress | 33,700 | (23240) | 84,500 | (58260) |
| B | Braze Tensile Stress | 6,470 | (4461) | 13,000 | (8963) |
| C | Blade Root Stress | 25,700 | (17720) | 84,500 | (58260) |
| D | Tangential Stress | 50,350 | (34715) | 84,500 | (58260) |
| | Radial Stress | 5,840 | (4027) | 84,500 | (58260) |
| E | Tangential Stress | 68,730 | (47390) | 84,500 | (58260) |

Figure 96. Turbine Rotor Stresses FD 31586

b. Stator

Eight vanes are incorporated on the turbine stator. Only six of these are used to provide the nominal arc of admission (31%); the remainder are plugged, but are available for turbine area adjustments. A single nozzle can be partially plugged for more precise adjustments. The stator is Inconel 718, and the vanes are attached with gold-nickel braze.

c. Shaft

The suspension system for the fuel pump-turbine shaft was described in the fuel pump discussion (paragraph B.1). The turbine rotor is attached to the shaft with a locked bolt, and torque is transmitted from the rotor to the shaft through a 4-tooth spline.

The turbine shaft seal package is shown in figure 97. The primary shaft seal is a rubbing face seal. A four step labyrinth seal (0.005 in., 0.127 cm, maximum radial clearance) is provided upstream of the face seal to provide a measure of redundancy in the event of a face seal failure, and to provide an additional restriction to leakage flow. An additional single step labyrinth seal is provided downstream of the face seal. The cavity between this seal and the face seal is vented overboard to prevent the hot turbine gases from entering the gearbox. The total overboard turbine leakage was calculated to be 0.06 lb/sec (0.23 kg/sec) at the uprated design point and 0.029 lb/sec (0.013 kg/sec) at the 5000-lb (22.24 kN) thrust design point. With the exception of the carbon face, shaft seal components are Inconel 718 material.

d. Housings

Turbine inlet and discharge housings are configured as shown in figure 95. Manifolds are designed to provide constant velocity. The housings are Inconel 718 and are connected with a bolted flange joint. The flanges were designed for a maximum deflection of 0.0001 in. (0.000254 cm) to ensure low leakage values. A metal O-ring seal is shown in figure 98, but this selection should be reevaluated when results from the static seal evaluation program being conducted under Air

Force Contract F04611-68-C-0002 become available. The maximum housing stress limitation was established at 85% of the 0.2% offset yield strength; however, the actual stress levels were much less than this because of minimum dimension considerations.

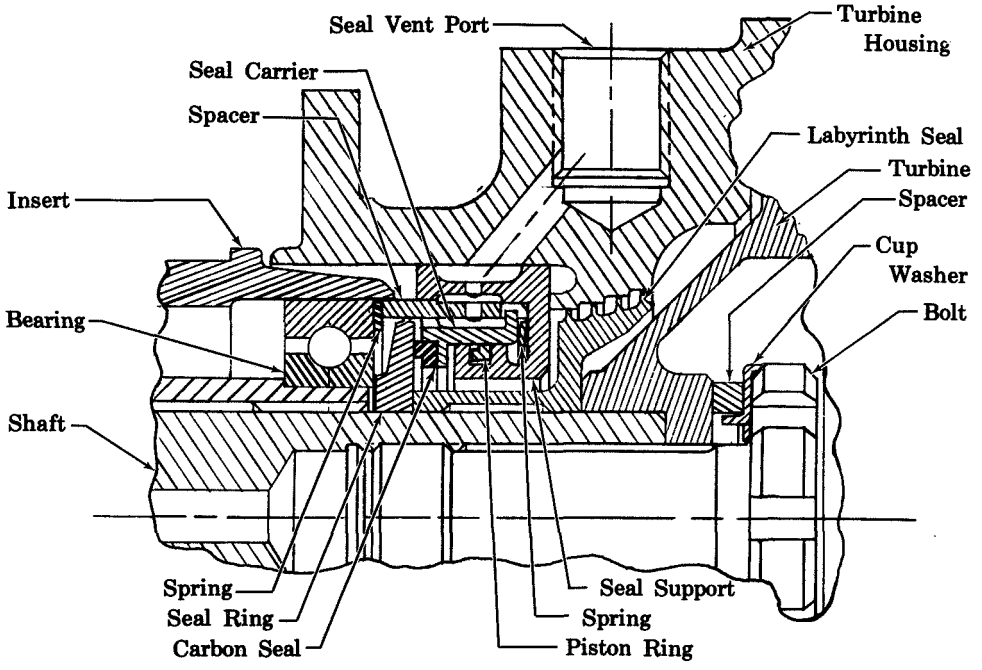


Figure 97. Turbine Shaft Seal Package FD 31583

e. Performance

The predicted turbine efficiency at the 5000-lb (22.24 KN) design point is 68.8%. Predicted turbine efficiency is shown vs turbine isentropic velocity ratio in figure 98. The calculated turbine loss coefficients at the design point are shown in table XXXIII.

Table XXXIII. Turbine Loss Coefficients

| | End Loss Coefficient | Profile Loss Coefficient | Trailing Edge Coefficient |
|---|---|---|---|
| Vane | 0.942 | 0.962 | 0.996 |
| Rotor | 0.865 | 0.876 | 0.990 |

In addition to these losses, the partial admission degradation was calculated to be 9 percentage points, and the shroud leakage was calculated to be 5% of the turbine flow.

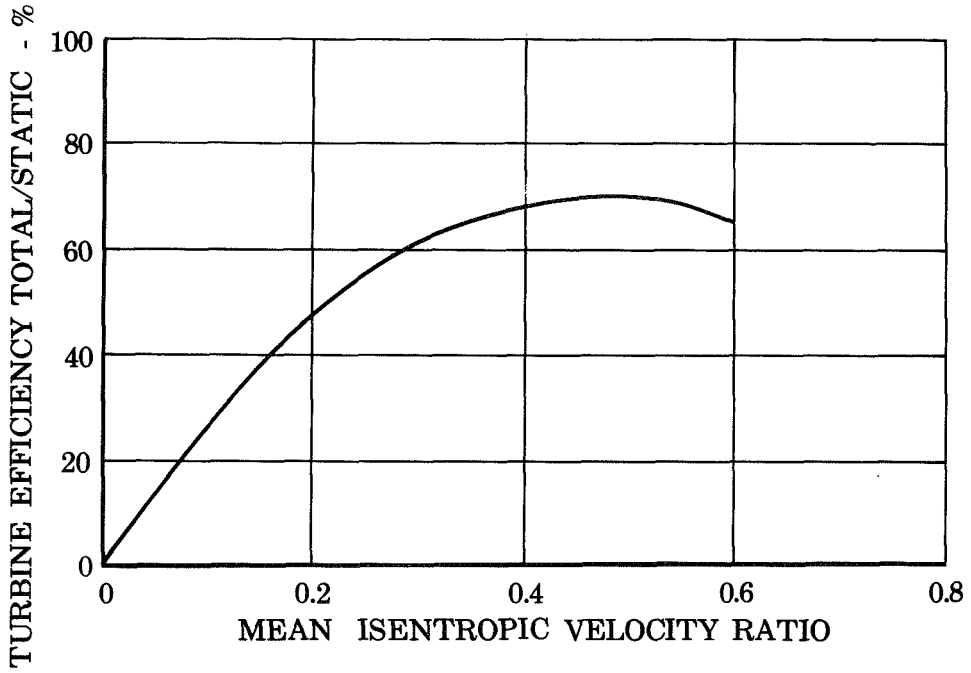


Figure 98. Turbine Efficiency vs Mean Isentropic Velocity Ratio FD 31589

f. Gear Train

Spur gears on the main drive shaft, idler shaft, and oxidizer pump shaft transmit power from the turbine to the oxidizer pump. Gear cooling and lubrication are provided by the gaseous methane atmosphere in the housing. The gears are machined from forged AMS 6260 material and the teeth are carburized and coated with an antiscuffing coating (Molybdenum Disulfide-Graphite varnish) to provide dry lubrication. The gear loading characteristics at the 8000-lb (35.59 kN) thrust condition are shown in table XXXIV; comparable RL10 values are included for comparison.

It will be noted from table XXXIV that the gear loading for the uprated flox/methane engine is much less than that of the RL10; however, the pitch line velocity is higher. Pitch line velocities greater than 27,000 ft/min (8230 m/min) are considered state-of-the-art for long-life conventionally lubricated gears. Extensive data for gears without conventional lubrication are not available, but shorter life and greater wear must be expected at high pitch line velocities. Gears from uprated RL10 engines have demonstrated very low wear characteristics at pitch

RL10 engines used bill-of-material gear trains in which the idler gear is mounted on two roller bearings, and the gear wear in 965 seconds of operation at pitch line velocities of approximately 19,000 ft/min (5974 m/min) was 0.006 in. (0.1525 cm) for this configuration. The idler gear was mounted on a single roller bearing, and hence more freedom of motion was provided for gear self alignment in later uprating tests. With this modification, an updated engine was tested for a total of 2400 seconds, of which 1683 seconds were accumulated at the 20,000-lb (88.96 kN) thrust level. Pitch line velocities ranged from 18,700 ft/min (5700 m/min) to 20,400 ft/min (6218 m/min), and the gear wear was negligible.

Table XXXIV. Gear Loading Characteristics

| | Fuel Pump Shaft Gear and Idler Gear Mechanism 8000 lb (35.59 kN) | | Oxidizer Pump Shaft Gear and Idler Gear Mechanism 8000 lb (35.59 kN) | |
|---|---|---|---|---|
| | Flox/Methane | RL10A3-3 | Flox/Methane | RL10A3-3 |
| Pitch Line Velocity, ft/min (m/min) | 24,176 (7369) | 15,570 (4746) | 24,176 (7369) | 15,570 (4746) |
| Tangential Load, lb (N) | 109 (484.8) | 295 (1313) | 109 (484.8) | 295 (1313) |
| Hertz Stress, psi ($N/cm^2$) | 63,500 (43820) | 76,900 (53060) | 75,000 (51750) | 73,000 (50370) |
| Dynamic Load, lb (N) | 449 (199700) | 1,545 (6872) | 751 (3340) | 1,460 (6494) |
| Beam Fatigue Strength, lb (N) | 860 (3825) | 1,865 (8296) | 1,287 (5725) | 1,857 (8260) |
| Stator Beam, Strength, lb (N) | 1,775 (7895) | 3,849 (17120) | 2,655 (11810) | 3,832 (17040) |

Based upon the RL10 engine experience, the idler gear mount for the 5000-lb (22.24 kN) flox methane engine was designed as a single ball bearing to provide the self alignment feature. The pitch line

velocity for the gears at the 5000 lb (22.24 kN) design point is 17,500 ft/min (5334 m/min). Thus, the feasibility of unlubricated gears operating at this level of pitch line velocity has definitely been established, and a reasonable extrapolation would indicate that uprating to 8000 lb (35.59 kN) is completely feasible.

The idler gear ball bearing is cooled with liquid methane supplied through drilled passages in the housings and in the idler gear shaft. The required bearing coolant flow rate was calculated to be 0.003 lb/sec (0.00136 kg/sec); to meter this small flow, a series of orifices was used in the housing passage as shown earlier in the fuel pump sketch of figure 83. The bearing DN is 375,000; balls and races are consumable electrode, vacuum-melted AMS5630 material. The idler shaft is made of 347 stainless steel material.

The gearbox housing is made of aluminum; internal pressure is maintained at 50 psia (34.47 $N/cm^2$) with a pressure relief valve of the type shown in figure 99.

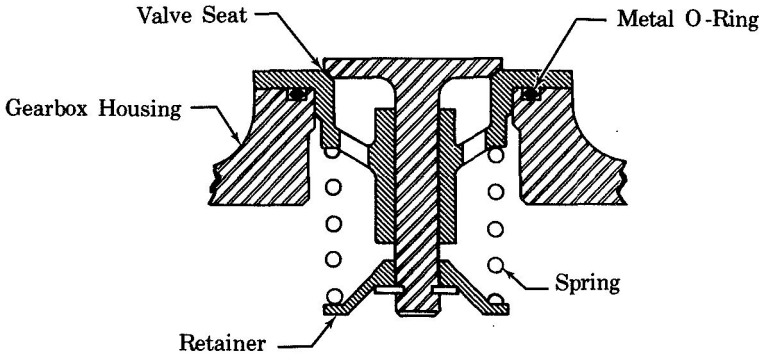


Figure 99. Gearbox Relief Valve FD 31584

C. INJECTOR

A dual-orifice injector was selected for the 5000 lb (22.24 kN) engine preliminary design to provide high performance and stable combustion over a wide thrust range so that the desired uprating and throttling capabilities would be inherent in the basic hardware. The basis for the selection of a dual-orifice for throttling capability was given in Section III, paragraph F. The dual-orifice injector concept is classified, and the confidential aspects of the design will

not be described in this report. Reference 15 provides a detailed description of the dual-orifice concept as applied to a gaseous fuel-liquid oxidizer injection application such as that considered here.

A relatively conventional coaxial injector would provide high performance and stable combustion for fixed thrust operation, and the dual-orifice feature would not be required. A new fixed thrust injector was not designed in this effort because a basic design was available from Contract NAS3-11190. In that program, a coaxial injector with tangential entry swirlers demonstrated over 97% c* efficiency at the 5000 lb (22.24 kN) engine design conditions; the design is described in Reference 6.

In the Task I studies, the requirement for a dual-orifice injector for throttled operation was based on analysis of off-design injector pressure drops that recognized a contract requirement that the oxidizer injector pressure drop be less than 25% of chamber pressure at the design point. The use of higher design point pressure drops would provide more throttling potential for a fixed geometry injector, but the higher design pressure drops would reduce the fuel-to-oxidizer momentum ratio at the design point, making high c* efficiency difficult to attain, and would increase required pump power. In the oxygen/hydrogen RL10 program, it has been demonstrated that 10:1 throttling is feasible with conventional coaxial injectors and design point oxidizer injector pressure drops of less than 20%. However, with flox/methane, performance requirements are known to be more severe than for oxygen-hydrogen. It is reasonable to assume that requirements for combustion stability may also be more critical. Thus it was concluded that, because the dual-orifice injector offered a means of tailoring performance and assuring system stability through adjustment of flow split (as is explained in the following paragraphs) without hardware changes and with little increase in injector cost or complexity, its use was justified.

1. Estimated Performance

The dual-orifice injector concept has demonstrated excellent performance and stability over a wide throttling range under three Air Force contracts (References 15, 16, and 17). Dual-orifice injectors

incorporate parallel propellant paths for one or both propellants; stability and high performance are obtained over a range of thrust levels by varying the flow split between the paths, which are identified as primary and secondary. In gas-liquid systems, dual flowpaths are provided only for the liquid which in this case is the oxidizer. Based upon results obtained in tests of such injectors, the split in oxidizer flow is believed to benefit performance because oxidizer atomization is increased through an interchange of momentum between the primary and secondary oxidizer streams. One major advantage of the dual-orifice injector is the capability of optimizing flow split and fuel-to-oxidizer momentum ratio independently to obtain maximum performance.

A dual-orifice injector designed for and tested with fluorine-hydrogen propellants under Air Force Contract AF04(011)-9965 was tested with flox-methane by P&WA in an independently sponsored program. The injector was tested at chamber pressure levels of 250, 500, and 750 psia (172.4, 345.7, and 518.1 $N/cm^2$). At 500 and 750 psia (345.7 and 518.1 $N/cm^2$), it was not possible to vary oxidizer flow split because of injector geometry limitations; however, variations were possible at 250 psia (172.4 $N/cm^2$) chamber pressure. The combustion efficiency was found to be a function of chamber pressure and oxidizer flow split for a given level of fuel-to-oxidizer injection momentum ratio, which has been found to be a reasonable parameter for correlation of results in previous investigations with gas-liquid injectors. Chamber pressure effects are apparent from figure 100 which shows that high performance was obtained at lower injection momentum ratios as chamber pressure was increased. Flow split effects were found to be similar to those demonstrated for fluorine-hydrogen in the contract program. These were correlated using the parameter oxidizer momentum interchange (per pound of oxidizer flow per second), which is defined as:

$$M_I = \frac{\Delta V_{po} \left(\dot{W}_p\right)}{\dot{W}_{ox}}$$

where:

$\Delta V_{po}$ = change in primary oxidizer velocity, ft/sec (m/sec)

$\dot{W}_p$ = primary oxidizer flow, lb/sec (kg/sec)

$\dot{W}_{ox}$ = total oxidizer flow, lb/sec (kg/sec)

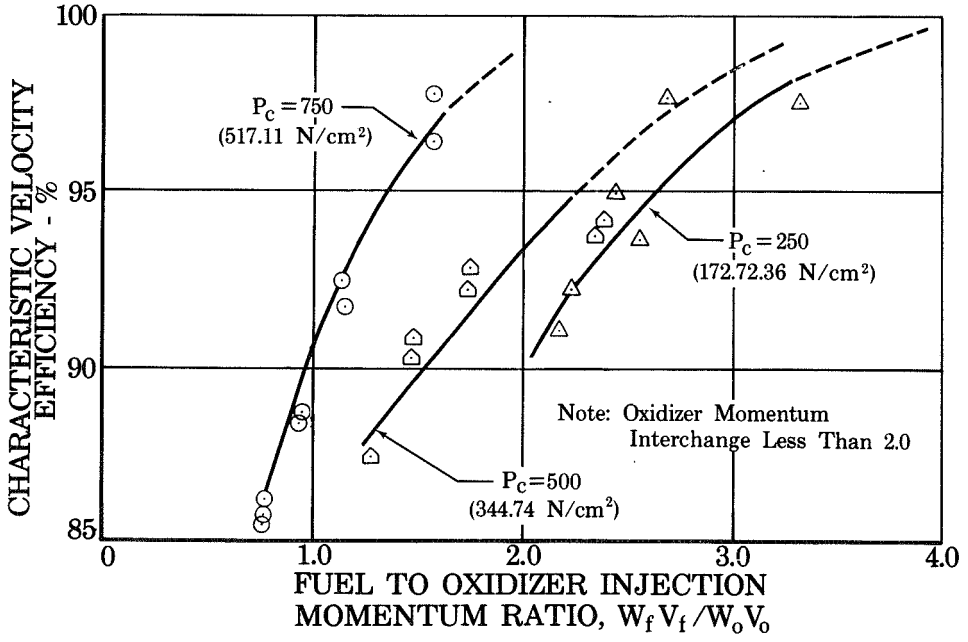


Figure 100. Dual Orifice Injector Performance FD 29220

The effect of momentum interchange on performance is shown in figure 101, which presents c* efficiency vs momentum ratio for various levels of momentum interchange. It can be seen that increasing the oxidizer momentum interchange can greatly facilitate obtaining high performance by reducing the momentum ratios required. The ability to increase performance through oxidizer momentum interchange is particularly important for high chamber pressure operation where high fuel-to-oxidizer momentum ratios are difficult to achieve because of geometric limitations on the injector.

One effect of the momentum interchange is to improve atomization, which has been found to be important for the flox/methane combination. Figure 102 compares the performance of coaxial injectors that have been tested with flox-methane; modified RL10A-1 and RL10A-3 types, and a tangential entry swirler type (tested under Contract NAS3-11190). The RL10A-1 injectors had straight concentric jets, and the RL10A-3 injec-

tor elements included ribbon type swirlers in the liquid oxidizer spuds. The increase in performance with swirlers is obvious when the two RL10 injectors are compared. The Contract NAS3-11190 injector including tangential entry swirlers demonstrates another effect; each oxidizer element in this injector was calibrated prior to installation to ensure even mass and mixture ratio distribution across the face of the injector. The increase in performance over the RL10A-3 injector is attributed mostly to the better propellant distribution that resulted, but the higher chamber pressure and the high oxidizer pressure drops used also contributed.

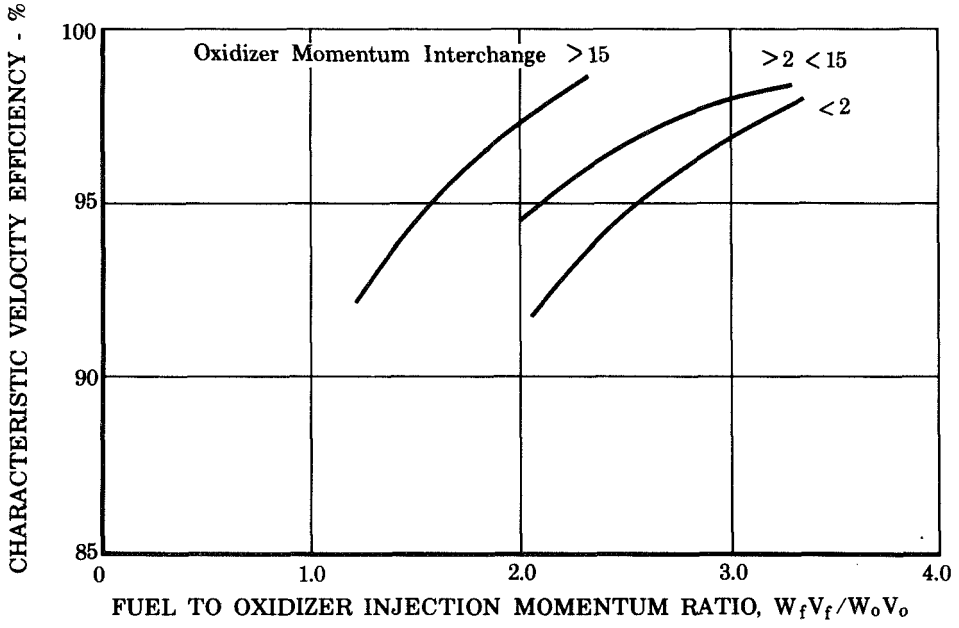


Figure 101. Effect of Oxidizer Momentum Interchange on Dual Orifice Injector Performance FD 29207

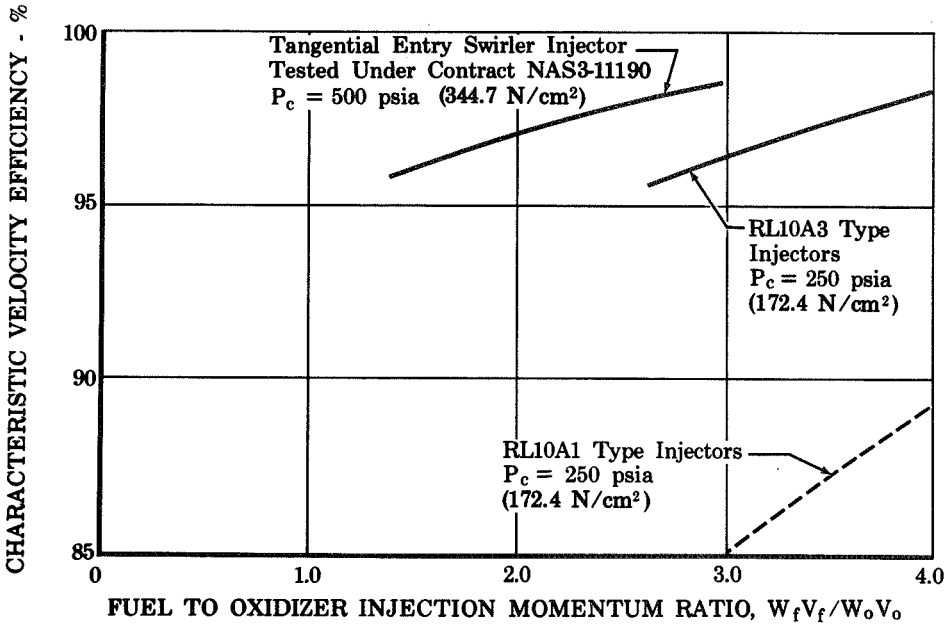


Figure 102. Flox/Methane Injector Performance FD 29191

The capability for affecting performance with flow split can be seen by comparing figures 103 and 104. At the low levels of oxidizer momentum interchange, higher momentum ratios are required to achieve good performance with the dual-orifice injector as compared to the tangential entry swirler injector; however, when higher levels of oxidizer momentum interchange are considered the dual-orifice injector is superior. For example, figure 103 compares the tangential entry swirler injector with the dual-orifice injector at high flow splits on the basis of momentum ratio and figure 104 compares the two injectors on the basis of mixture ratio using an optimized flow split for the dual-orifice injector. It can be seen that the dual-orifice injector which was designed for fluorine/hydrogen shows slightly better performance than the fixed geometry unit designed specifically for flox/methane, even though the data for it were taken at lower pressures. (Figure 100 showed the beneficial effect of high chamber pressure on performance.)

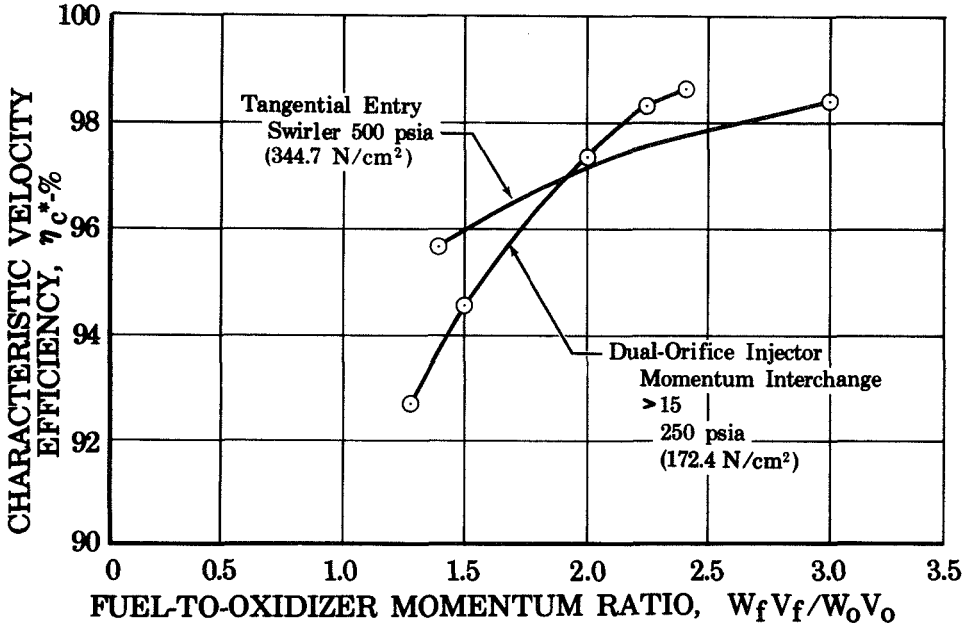


Figure 103. Comparison of Dual-Orifice and Tangential Entry Injectors Based On Momentum Ratio FD 29210

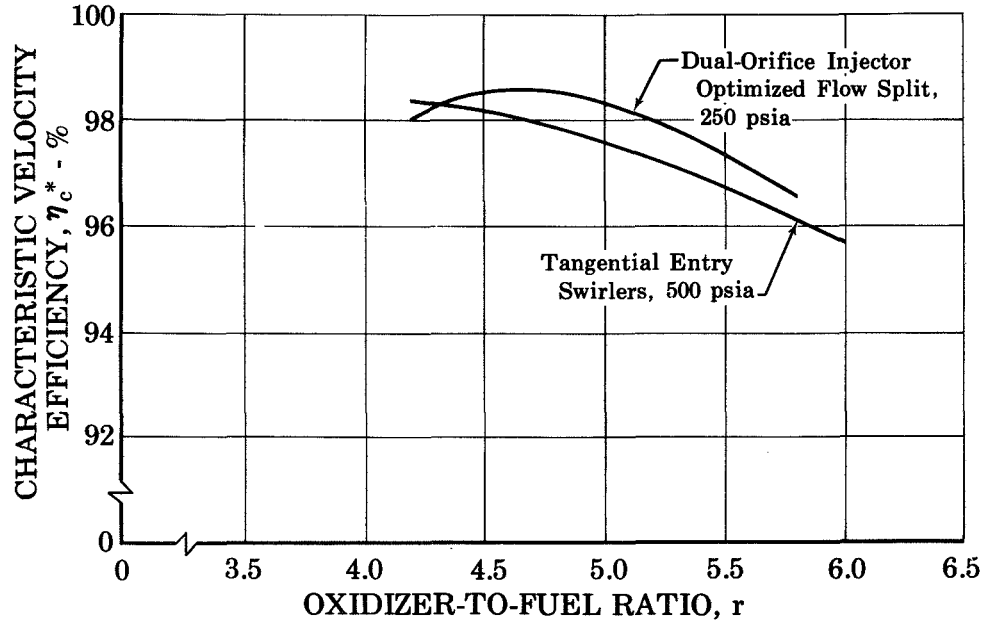


Figure 104. Comparison of Dual-Orifice and Tangential Entry Injectors Based On Mixture Ratio FD 29209

If provided the necessary fuel-to-oxidizer momentum ratio and oxidizer momentum interchange, the dual-orifice injector will provide high c* efficiency over the entire 10:1 thrust range and for the

uprated engine operating point. Table XXXV shows the calculated values of momentum ratio and momentum exchange for the design used in the 5000 lb (22.24 kN) engine. A predicted c* efficiency, based on extrapolation of the data in figures 100, 101, and 102 is also included. Even if the prediction is slightly optimistic, it appears that c* efficiencies in excess of 98% over the entire thrust range should be readily achievable.

Table XXXV. Injector Characteristics

| Thrust, lb (N) | Chamber Pressure, psia ($N/cm^2$) | Fuel-to-Oxidizer Momentum Ratio | Oxidizer Momentum Interchange | Predicted Characteristic Velocity Efficiency, % |
|---|---|---|---|---|
| 8000 (35.59 kN) | 800 (551.6) | 1.9 | 1.4 | 98.7 |
| 5000 (22.24 kN) | 500 (334.7) | 3.2 | 2.3 | 99 |
| 500 (2.224 kN) | 50 (34.47) | 11.7 | 13.8 | 99+ |

2. Injector Description

The injector has 65 dual-orifice elements arranged concentrically on four diameters. To provide a uniform mass flux over the face of the injector, uniform element spacing is used and the flow-per-element in the outer diameter is increased to compensate for the unused peripheral zone resulting from not locating the elements too close to the thrust chamber wall. A transpiration-cooled porous faceplate is incorporated. A 40 scfm (1.13 $m^3$) flowrate porosity (40 standard cubic feet, 1.13 $m^3$, of air per square foot per minute when exhausted to 14.7 psia, 10.13 $N/cm^2$, with a 2 psi, 1.38 $N/cm^2$, pressure drop) was specified based on results of flox/methane tests at 500 psia (344.7 $N/cm^2$) chamber pressure under Contract NAS3-11190 (Reference 6). The secondary oxidizer spuds are machined from nickel 200 to provide maximum material compatibility with flox and to minimize potential spud burning. The primary spuds are fabricated from Hastelloy X.

The combination of high fuel inlet temperature and cryogenic flox temperatures in the injector create the possibility for significant relative changes in dimensions as thermal equilibrium is achieved dur-

ing operation. To prevent distortion of the injection pattern, provision has been made for mechanically centering oxidizer spuds in the injector elements. The high fuel temperature also led to incorporation of a titanium insulating plate between the fuel cavity and oxidizer divider plate to reduce internal heat transfer. The titanium plate would not be required for full thrust operation, but is needed to reduce oxidizer boiling at reduced thrust.

## D. THRUST CHAMBER

The Thermal Skin thrust chamber and coolant passage geometries for the preliminary engine design were similar to those used in the Task I studies except for the change in the exhaust nozzle expansion ratio and contour. Pass-and-one-half counterflow cooling was used to provide optimum cooling with minimum manifold weight. The design was based heavily on experience gained under Contract NAS3-11190 and is similar to experimental regeneratively cooled chambers being built under that contract. The most significant differences between the two designs are (1) changes in the combustion chamber geometry as discussed in Section III, (2) a moderate improvement in coolant channel dimensional limitations, justified primarily on the basis of Contract NAS3-11190 experience, and (3) all-flight-weight construction chamber compared to the use of "workhorse" flanges, manifolds, etc., on the experimental chamber. Thrust chamber design characteristics are summarized in table XXXVI.

Table XXXVI. Preliminary Design Thrust Chamber Characteristics

| | |
|---|---|
| Contraction Ratio | 4:1 |
| Chamber Length (injector face to nozzle throat), in. (cm) | 13.0 (33.02) |
| Characteristic Length | 36.0 |
| Throat Diameter, in. (cm) | 2.60 (6.60) |
| Nozzle Expansion Ratio | 70:1 |
| Nozzle Exit Diameter, in. (cm) | 21.75 (55.25) |
| Nozzle Length, in. (cm) | 26.25 (66.68) |
| No. of Thermal Skin Staves | 6 |
| Weight, lb (kg) | 32.7 (14.83) |

1. Coolant Passage Geometry

The thrust chamber coolant passage geometry is described graphically in figure 105. The combustion chamber and throat have 168 cooling channels nominally 0.052 in. (0.1322 cm) deep. The number of passages doubles in the nozzle divergent section at the coolant inlet manifold 20 in. (50.80 cm) downstream of the injector face, and again 34 in. (86.36 cm) downstream at a nozzle area ratio of 52. The passage width is 0.077 in. (0.1955 cm) at the injector face and diminishes to a minimum value of 0.026 in. (0.06611 cm) at the nozzle throat for a maximum depth-to-width ratio of 2.0. A nearly constant land width of 0.024 to 0.025 in. (0.0610 to 0.0636 cm) is maintained throughout the length of the chamber.

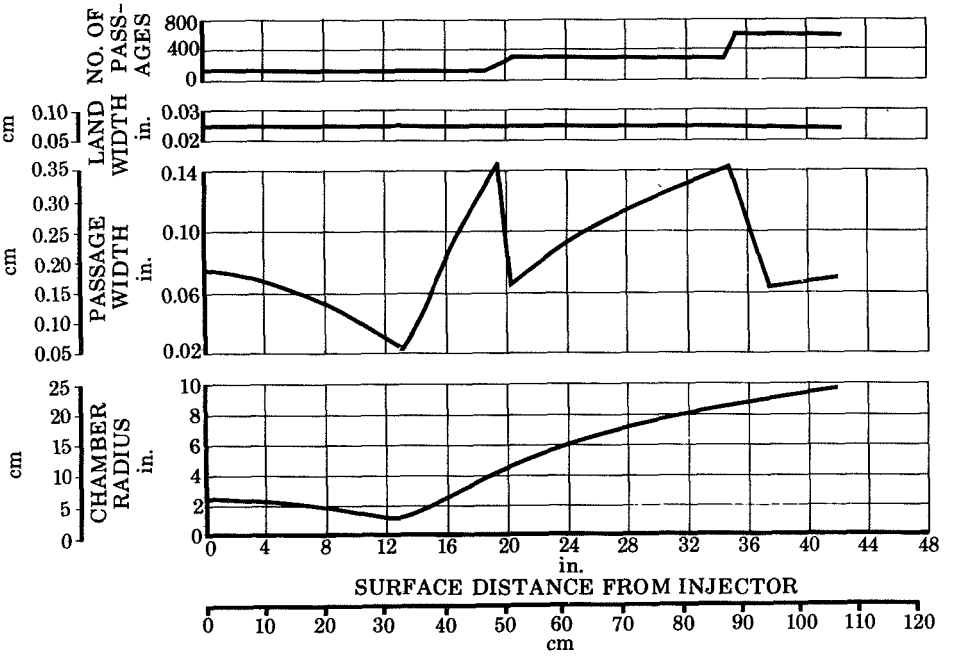


Figure 105. Thrust Chamber Cooling Passage Geometry Auxiliary Hex Cycle Design 2 FD 27934A

Figure 106 shows the layout of the cooling passages on one of the flat plates used to form the individual staves. The coolant enters 20.0 in. (50.80 cm) downstream of the injector, flows to the nozzle exit, and returns through a separate set of passages to the exit manifold at the injector face. Two mating plates are engraved to a depth of 0.026 in. (0.0661 cm) to provide the required 0.052 in. (0.1322 cm)

passage depth in the brazed assembly or stave. At the nozzle exit, the plates are engraved so that the flow from each passage being fed by the inlet manifold is restricted to a single passage flowing toward the injector. This arrangement eliminates one potential source of coolant maldistribution, i.e., vapor-liquid separation when two-phase flow is present at the turn around manifold.

2. Construction

The complete thrust chamber assembly consisting of six brazed staves is shown in figure 107. The inner plate of each stave is fabricated from nickel 200 to provide high thermal conductivity and maximum compatibility with the fluorinated combustion products. The outer plate of the stave is Inconel 600. Inconel 600 provides high temperature strength with good engraving characteristics. Inconel 625 would provide somewhat higher strength, but engraving difficulties were encountered with this alloy under Contract NAS 3-11190, and the potential weight reduction is not vital. Inconel 625 is used for the pressure shell and manifolds. In addition to good high temperature tensile strength, the Inconel alloys provide compatible thermal expansion with the nickel liner.

The brazing techniques used in the chamber are based heavily on Thermal Skin technology developed under Contract NAS3-11190. The individual staves are gold-nickel brazed before forming. The formed staves are then welded in place on a mandrel. A four piece pressure shell is then brazed around the staves in the combustion chamber from the axial location of the injector face to approximately 1-in. (2.54-cm) downstream of the nozzle throat. Silver braze is used to attach the shell. Reinforcing strips are welded to the pressure shell at mating seams as shown in figure 106. The manifolds, which are welded assemblies, are then welded to the chamber.

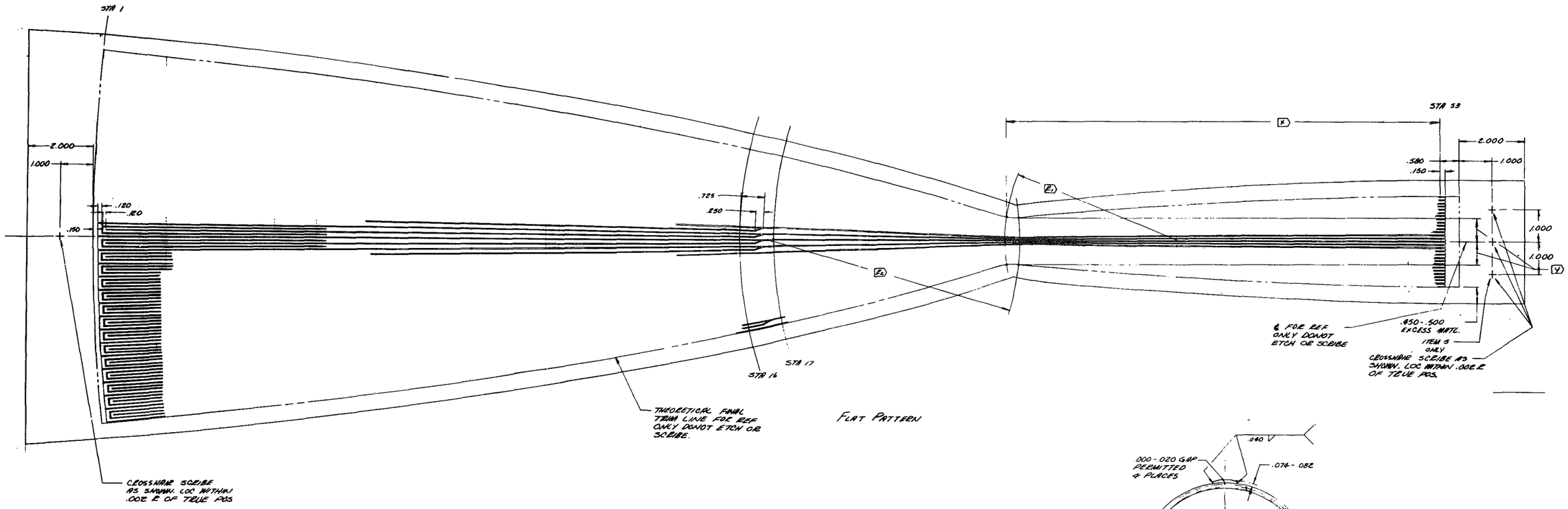


FLAT PATTERN

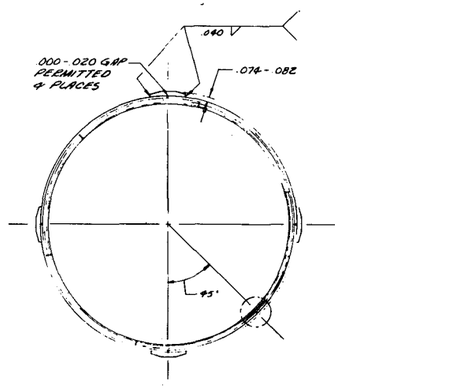


| STA | X | Y | ANG SLOPE | Z | L | A | J |
|---|---|---|---|---|---|---|---|
| 1 | 40.982 | 5.719 | 112 | 84.377 | .025 | .077 | .080 |
| 2 | 39.029 | 5.845 | | 31.364 | | .073 | .076 |
| 3 | 37.399 | 5.883 | | 47.376 | | .070 | .072 |
| 4 | 35.987 | 5.139 | | 43.226 | | .067 | .069 |
| 5 | 34.135 | 4.945 | 118 | 39.877 | | .068 | .065 |
| 6 | 32.603 | 4.743 | 56 | 35.650 | | .146 | .149 |
| 7 | 31.189 | 4.535 | | 36.503 | | .137 | .182 |
| 8 | 29.708 | 4.326 | | 29.866 | | .130 | .134 |
| 9 | 28.334 | 4.184 | | 26.310 | | .125 | .127 |
| 10 | 27.020 | 3.911 | | 88.878 | | .115 | .119 |
| 11 | 25.754 | 3.706 | | 21.458 | | .108 | .111 |
| 12 | 24.539 | 3.487 | | 19.163 | | .140 | .103 |
| 13 | 23.369 | 3.255 | | 16.962 | | .098 | .093 |
| 14 | 22.268 | 3.020 | | 14.946 | | .086 | .086 |
| 15 | 21.191 | 2.791 | | 13.285 | | .078 | .078 |
| 16 | 20.183 | 2.570 | 56 | 11.913 | .025 | .068 | .070 |
| 17 | 19.259 | 2.384 | 58 | 10.087 | .019 | .144 | .189 |
| 18 | 18.347 | 2.140 | | 8.716 | | .129 | .183 |
| 19 | 17.508 | 1.925 | | 7.516 | | .114 | .143 |
| 20 | 16.719 | 1.714 | | 6.480 | | .099 | .102 |
| 21 | 15.984 | 1.518 | | 5.592 | | .089 | .087 |
| 22 | 15.309 | 1.330 | | 4.781 | | .071 | .073 |
| 23 | 14.692 | 1.188 | | 3.962 | | .057 | .058 |
| 24 | 14.185 | .964 | | 3.901 | | .040 | .044 |
| 25 | 13.715 | .839 | | 3.047 | | .036 | .037 |
| 26 | 13.301 | .730 | | 3.018 | | .031 | .036 |
| 27 | 12.898 | .732 | | 2.884 | | .027 | .028 |
| 28 | 13.077 | .714 | | — | | .032 | .027 |
| 29 | 12.930 | .782 | | 7.503 | | .027 | .027 |
| 30 | 12.648 | .759 | | 2.110 | | .029 | .030 |
| 31 | 12.118 | .799 | | 2.842 | | .033 | .033 |
| 32 | 11.689 | .850 | | 9.799 | | .036 | .037 |
| 33 | 10.967 | .899 | 58 | 10.881 | .024 | .089 | .090 |

| STA | X | Y | ANG SLOPE | Z | L | A | J |
|---|---|---|---|---|---|---|---|
| 34 | 10.394 | .945 | 58 | 11.980 | .029 | .042 | .044 |
| 35 | 9.852 | .989 | | 13.197 | | .046 | .047 |
| 36 | 9.291 | 1.031 | | 14.517 | | .049 | .050 |
| 37 | 8.680 | 1.070 | | 15.956 | | .051 | .053 |
| 38 | 8.109 | 1.107 | | 17.546 | | .034 | .036 |
| 39 | 7.538 | 1.142 | | 19.300 | | .057 | .058 |
| 40 | 6.968 | 1.173 | | 21.267 | | .059 | .061 |
| 41 | 6.398 | 1.205 | | 23.493 | | .061 | .063 |
| 42 | 5.828 | 1.233 | | 26.042 | | .063 | .065 |
| 43 | 5.258 | 1.259 | | 29.002 | | .065 | .067 |
| 44 | 4.689 | 1.283 | | 32.498 | | .066 | .069 |
| 45 | 4.120 | 1.306 | | 36.707 | | .068 | .070 |
| 46 | 3.551 | 1.328 | | 41.896 | | .069 | .072 |
| 47 | 2.982 | 1.340 | | 48.449 | | .071 | .073 |
| 48 | 2.413 | 1.354 | | 57.183 | | .072 | .074 |
| 49 | 1.845 | 1.367 | | 69.241 | | .072 | .073 |
| 50 | 1.276 | 1.377 | | 87.188 | | .073 | .076 |
| 51 | .708 | 1.385 | | 116.910 | | .074 | .074 |
| 52 | .139 | 1.390 | | 174.067 | | .074 | .073 |
| 53 | .000 | 1.391 | 58 | 199.891 | .006 | .074 | .077 |

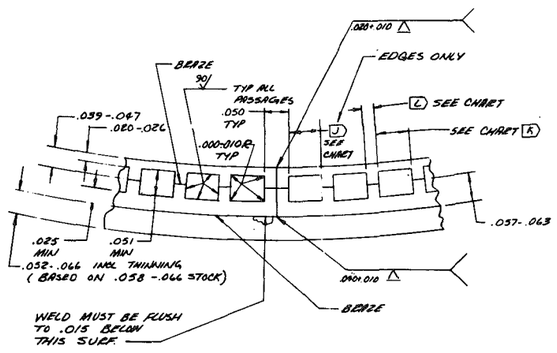


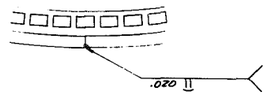


Figure 106. Chamber Segment Cooling Passage Layout

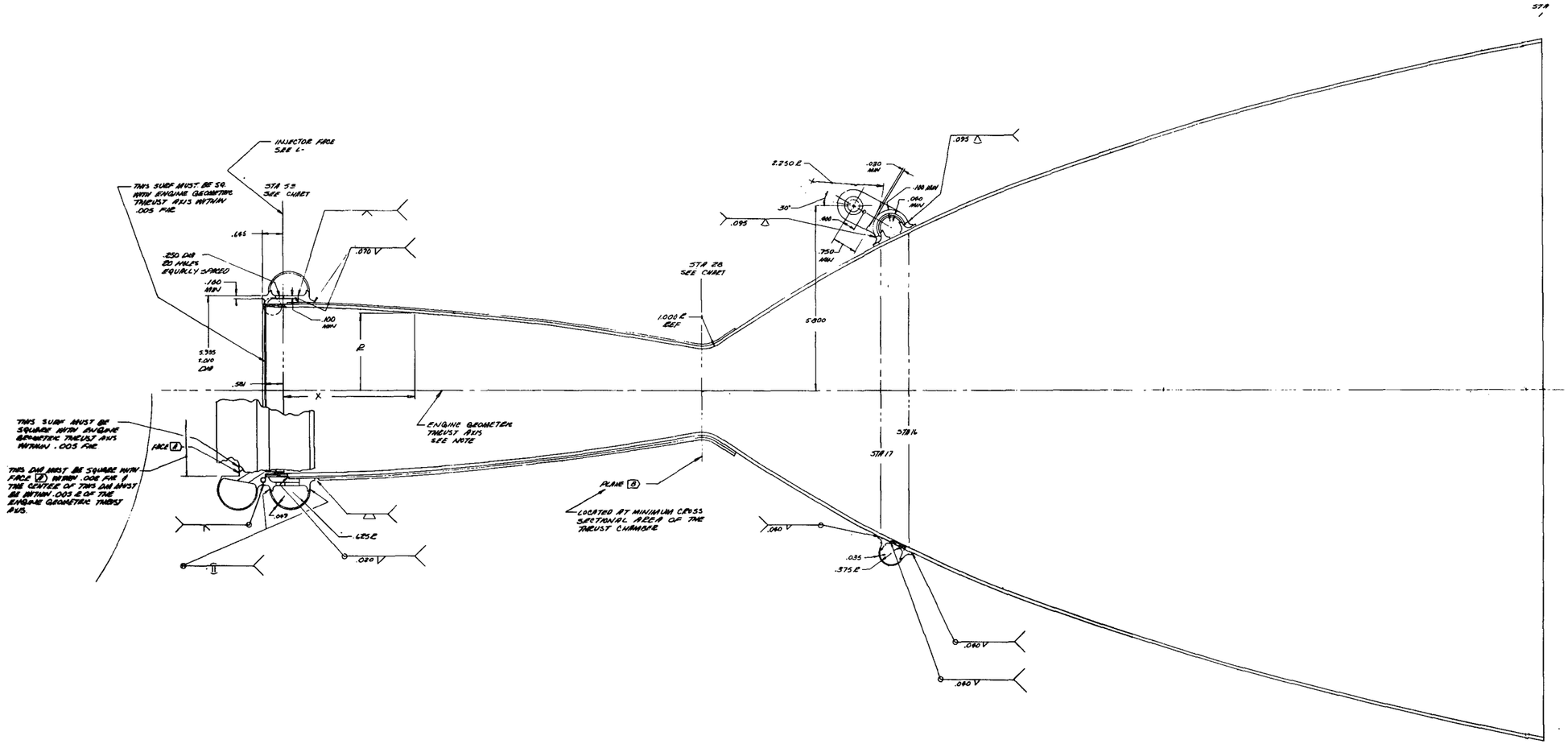


Nozzle Contour

| STA | X | R | STA | X | R |
|---|---|---|---|---|---|
| 1 | 39.833 | 10.875 | 31 | 12.591 | 1.969 |
| 2 | 37.966 | 10.698 | 32 | 12.026 | 1.561 |
| 3 | 36.386 | 10.165 | 33 | 11.448 | 1.654 |
| 4 | 34.740 | 9.783 | 34 | 10.895 | 1.766 |
| 5 | 33.207 | 9.411 | 35 | 10.369 | 1.826 |
| 6 | 31.731 | 9.052 | 36 | 9.764 | 1.906 |
| 7 | 30.313 | 8.695 | 37 | 9.198 | 1.981 |
| 8 | 28.949 | 8.351 | 38 | 8.639 | 2.058 |
| 9 | 27.633 | 7.650 | 39 | 8.067 | 2.113 |
| 10 | 26.380 | 7.993 | 40 | 7.501 | 2.181 |
| 11 | 25.179 | 7.030 | 41 | 6.936 | 2.239 |
| 12 | 24.039 | 6.673 | 42 | 6.370 | 2.295 |
| 13 | 22.944 | 6.192 | 43 | 5.805 | 2.348 |
| 14 | 21.915 | 5.767 | 44 | 5.239 | 2.386 |
| 15 | 20.957 | 5.391 | 45 | 4.676 | 2.417 |
| K | 20.017 | 4.864 | 46 | 4.108 | 2.463 |
| 17 | 19.154 | 4.488 | 47 | 3.563 | 2.493 |
| 18 | 18.363 | 4.065 | 48 | 2.977 | 2.528 |
| 19 | 17.593 | 3.647 | 49 | 2.412 | 2.547 |
| 20 | 16.895 | 3.238 | 50 | 1.846 | 2.562 |
| 21 | 16.259 | 2.892 | 51 | 1.281 | 2.581 |
| 22 | 15.666 | 2.446 | 52 | .715 | 2.591 |
| 23 | 15.196 | 2.117 | 53 | .581 | 2.593 |
| 24 | 14.671 | 1.810 | 54 | 0.000 | 2.593 |
| 25 | 14.298 | 1.559 | | | |
| 26 | 14.030 | 1.434 | | | |
| 27 | 13.846 | 1.336 | | | |
| 28 | 13.581 | 1.300 | | | |
| 29 | 13.397 | 1.317 | | | |
| 30 | 13.015 | 1.388 | | | |

Nozzle Contour tol ±.005

■ Prior to machining pilot

Figure 107. Thermal Skin Chamber Assembly

GS 11038

3. Alternate Fabrication Methods

As discussed in Section III, paragraph B, Thermal Skin was selected for the Task I analysis primarily on the basis of being able to use a high temperature alloy on the chamber outer wall and provide greater versatility for passage branching in the exhaust nozzle. Another strong factor in the selection of Thermal Skin was the experience level. Regeneratively cooled Thermal Skin chambers have been successfully built and tested by P&WA with fluorine/hydrogen and oxygen/hydrogen propellants. Under Contract NAS3-11190 a water-cooled Thermal Skin thrust chamber was successfully fabricated and tested with flox/methane at conditions nearly identical to the requirements of this design, i.e., 5000-lb (22.24 kN) thrust and 500-psia (344.7 $N/cm^2$) chamber pressure. A regeneratively cooled 5000-lb (22.24 kN) thrust chamber was designed using experimental heat flux data from the water-cooled unit. Chambers being fabricated to this design will be tested in the spring of 1969. This experience has provided a high degree of confidence in the feasibility of the design established for the 5000-lb (22.24 kN) engine. However, should another fabrication method prove to be advantageous in cost of simplified manufacturing, the alternative technique could be investigated.

The coolant passage design of figure 105 is compatible for electroformed construction as it is described in Reference 7. In this technique, the lands between coolant passages are formed in voids cut in a filler material. The constant land width of 0.025 in. (0.0636 cm) used may be more readily machined than variable land widths that have been used in most previous Thermal Skin designs. The primary design changes that would be necessary for electroforming would be: (1) modification of the land geometry at points where passages branch to facilitate machining of the filler; (2) changing the passage backside thickness to provide the required strength with pure nickel; and (3) reducing the coolant passage dimensions to compensate for the reduction of surface roughness in electroformed, as compared to Thermal Skin channels.

## E. ENGINE CONTROLS

Several factors make the preliminary design of an engine control system more tentative than that for major system components such as the turbopump, thrust chamber, and injector. First, because a major function of the control system is to integrate the operation of the major components, the control system cannot completely be finalized until the operating characteristics of the other components have been firmly established. Second, control requirements are heavily dependent on mission and vehicle requirements, which have not been specified for this study. Finally, control requirements for special engine operating modes that might be required (throttling, etc.) must be anticipated, and an optimized system design must include consideration of the best way to integrate the controls for all modes of operation.

Because of these uncertainties, the designs for control components in the engine study were not subject to study in the same detail as were those of the major components. Analytical effort was directed toward selection of control points, study of starting and shutdown requirements, and consideration of control requirements for special cases such as uprating, throttling, and tank head idle, etc. In the area of actual board design, preliminary designs were made and specifications were generated for engine control valves for fixed thrust operation in accordance with contract requirements.

The studies of engine control points showed that controls similar to those used in the RL10 expander cycle engine would provide a very satisfactory arrangement. Furthermore, experience in testing a modified RL10 engine with flox and methane under Contract NAS3-7950 (Reference 4) showed that the basic cycle and control system were suitable for use with the propellant combination. Therefore, the designs generated were basically scaled down RL10 components. Minimal mechanical design effort was expended, and features of the RL10 control components which have been proved in service, but which could not otherwise be recognized and used in a preliminary effort of this type, were incorporated. Thus, the designs would provide a sound base for

the start of development, although modifications might be required as engine operating requirements were crystallized.

The scope of the study did not permit dynamic simulation to identify transient problems or to evaluate engine stability. The fundamental control system operation for fixed thrust operation, which is discussed in paragraph 3, relied heavily on RL10 experience to define transient requirements of a cryogenic expander cycle engine. A conventional smooth start following a prestart cooldown typical of most cryogenic engines currently in use or under development, was assumed.

1. Control Point Selection

Functional requirements for the 5000-lb (22.24 kN) engine control system include:

1. Propellant shutoff
2. Start-up and space restart, encompassing the cooldown and fill transients, turbopump acceleration, and thrust buildup
3. Steady-state control of thrust and mixture ratio, including the necessary controls to vary thrust over the required throttle range
4. Shutdown, including the deceleration of the turbopumps, thrust decay, and propellant shutoff

As noted above, transient start-up and shutdown problems could not be examined in detail because dynamic simulations were beyond the scope of the program. Therefore, the primary consideration in the selection of control points were mixture ratio and thrust control under steady-state conditions. These were evaluated using the mathematical engine model developed for the steady-state analysis. Figure 108 shows possible control points, which were premised upon the approach of regulating thrust by controlling fuel flow, which provides turbopump power and adjusting mixture ratio by varying oxidizer flow. Six fuel-side points were evaluated for thrust control: (1) fuel bypass (for pump recirculation), (2) fuel pump discharge, (3) turbine bypass, (4) turbine upstream (line), (5) turbine inlet (variable area stator),

and (6) turbine downstream. Four locations were suggested in the oxidizer system for mixture ratio control: (1) oxidizer pump bypass (for recirculation), (2) oxidizer pump discharge, (3) oxidizer injector primary line, and (4) oxidizer injector secondary line.

A number of possible control points were eliminated by examination. Variable turbine inlet area was not evaluated for thrust control because of system complexity, and a fuel pump discharge throttle was not evaluated because no potential advantages were apparent. The oxidizer injector secondary flow throttle (location D in figure 108) was found to be capable of fulfilling all requirements for mixture ratio control and no other controls were evaluated on the oxidizer side. Thus, four thrust control schemes and a single mixture ratio control technique were analyzed. Off-design operation was considered, and factors that were evaluated in the analysis included (a) cooling jacket stability, (b) fuel system stability, (c) chamber pressure stability and injector performance, (d) pump suction requirements, (e) control valve sizes and turndown ratios, and (f) thrust trimming.

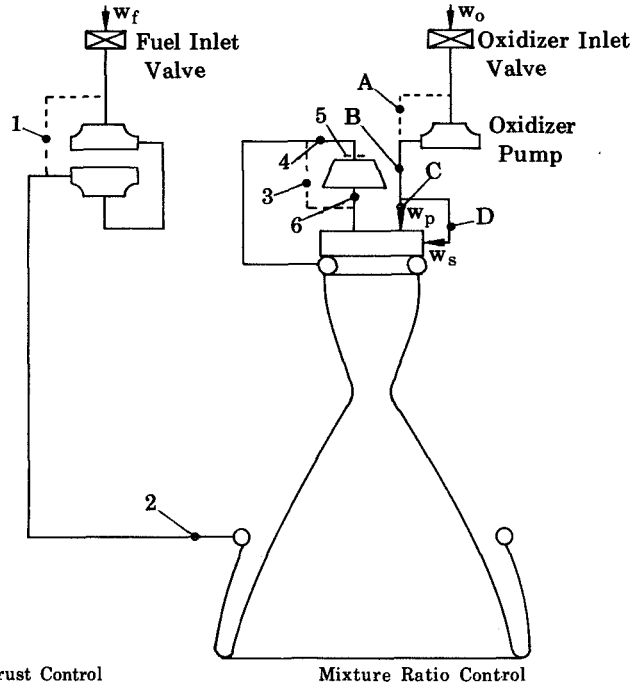


1. Fuel Pump Recirculation
2. Fuel Pump Discharge Throttle
3. Turbine Bypass
4. Turbine Upstream Throttle
5. Variable Inlet Area Turbine
6. Turbine Downstream Throttle

A. Oxidizer Pump Recirculation
B. Oxidizer Pump Discharge Throttle
C. Oxidizer Injector Primary Throttle
D. Oxidizer Injector Secondary Throttle

Figure 108. Possible Control Schemes FD 27846

a. Cooling Jacket Stability

Under some conditions, boiling instabilities of sufficient magnitude to cause failures can be initiated in thrust chamber coolant passages. These instabilities can be minimized by maintaining the jacket pressure at levels greater than the critical pressure of the coolant. Figure 109 shows the cooling jacket exit pressure vs thrust for each of the fuel-side controls considered. These exit pressures would be experienced during engine throttling at constant mixture ratio when using the various fuel-side control valves in conjunction with the oxidizer secondary throttle control. The calculated pressure at which the jacket wall would fail is shown in the plot for reference.

In figure 109, the turbine upstream throttle control is indicated to be superior from the standpoint of cooling jacket stability, i.e., the jacket exit pressure is above critical pressure over all but the lowest thrust portion of the operating range, whereas pressures below critical occur in the 30 to 50% thrust range with other control methods. However, coolant jacket failures are possible over a large thrust range with the turbine upstream throttle, while a safe margin is available with the other approaches. Thus, none of the control methods considered were completely satisfactory, and it was necessary to select one that permitted jacket pressures below critical to occur, or to consider some combination control system.

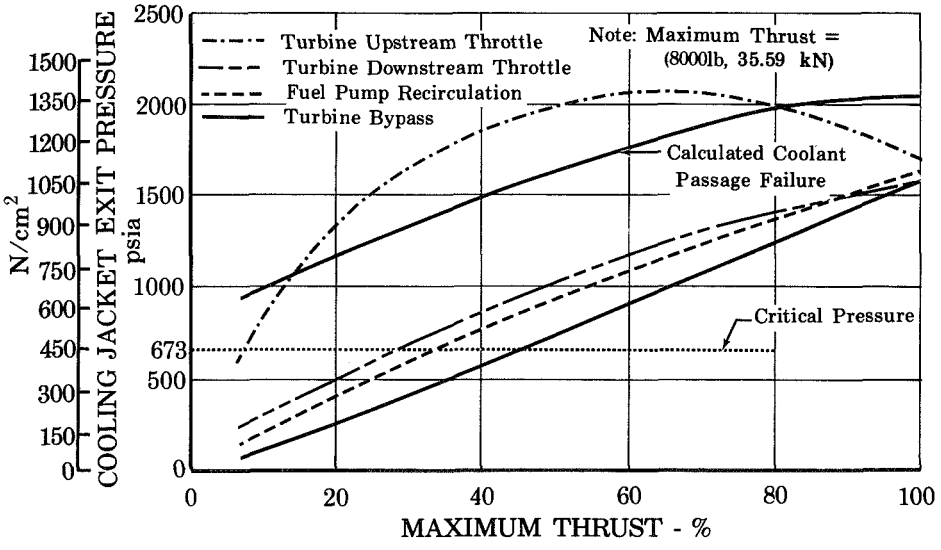


Figure 109. Effect of Thrust Control on Cooling Jacket Exit Pressure FD 27845

A modified RL10 thrust chamber has been operated using flox and methane with subcritical pressures in the cooling jacket, and there were no apparent instabilities. Therefore, operation with cooling jacket pressures less than critical pressure is an acceptable alternative. The severity of boiling instability, when it occurs, is a function of heat flux level, local coolant properties, and the geometric configuration of the fuel system. If problems are encountered, modifications to the geometric configuration of the fuel system (the addition of orifices, volumes, etc.) can be accomplished to reduce the severity to an acceptable level.

If it were considered important to avoid pressures below critical, it would be necessary to use a turbine upstream throttle control, but in conjunction with one of the other fuel-side controls. This solution would allow the cooling jacket pressure to be maintained above critical pressure over most of the thrust range, with the controls scheduled to maintain safe operating pressures in the cooling passages.

b. Fuel System Stability

A map of the fuel pump characteristics, with curves showing the operating lines of the engine for the various thrust control modes, is presented in figure 110. It can be assumed that, as a component, the pump will operate in a stable condition over the entire flow range. However, phenomena, introduced by system effects, might drive the pump into stall when it is a part of the engine system. The degree of instability that can be experienced is a function of the fluid properties, the geometric configuration of the fuel system, the slope of the fuel pump pressure rise vs flow curve, and the severity of any instabilities superimposed on the fuel pump, such as boiling instability or chamber pressure instability.

Requirements for system stability are not rigorously defined. However, experience with the oxygen-hydrogen RL10 engine has shown that it is desirable to operate on a negative slope portion of the pressure rise vs flowrate curve. Figure 110 shows that the fuel pump recirculation, turbine bypass, and turbine downstream throttle controls will meet this requirement over the entire thrust range. The turbine

upstream control has the most undesirable characteristics, with the operating line located near the inflection points of the pump's characteristic curves over much of the thrust range.

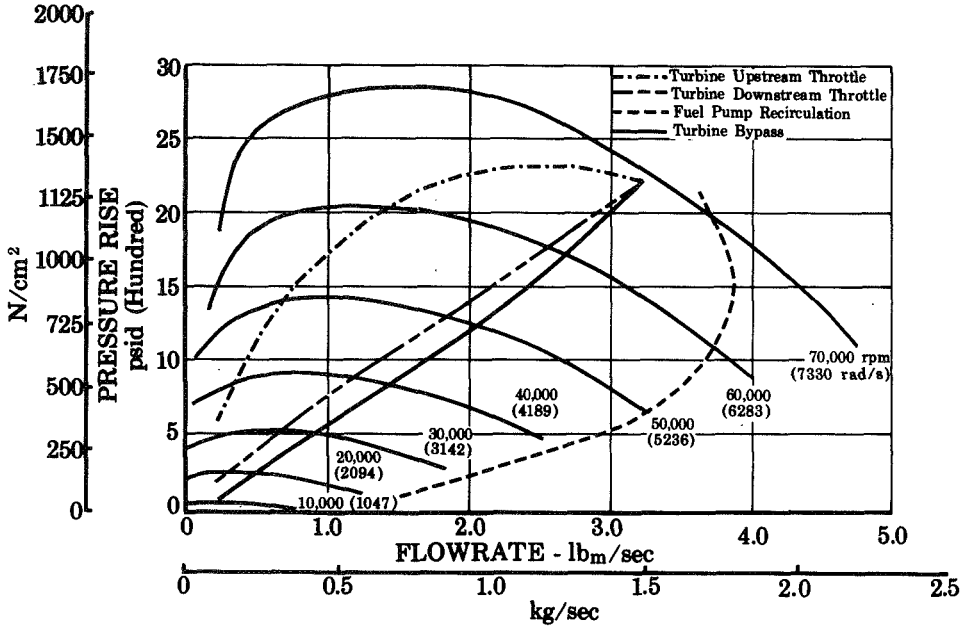


Figure 110. Fuel Pump Operating Characteristics FD 27844A

In the event that system stability proves marginal, the geometry of the fuel system can be altered slightly to correct the condition. In the RL10 engine, an orifice was added at the fuel pump discharge during development to improve the system characteristics during the starting transient. For throttled operation, it was necessary to add a cavitating venturi downstream of the fuel pump to prevent boiling instabilities at low thrust from feeding back to the fuel pump.

c. Chamber Pressure Stability and Injector Performance

As explained in paragraph C, a dual orifice injector was incorporated in the preliminary engine design to provide throttling capability. With this type of injector, throttling of the injector secondary oxidizer flow for mixture ratio control (location D in figure 108) is particularly convenient and was selected. In the secondary oxidizer flow control scheme, the oxidizer primary pressure is set by pump speed, and the secondary flow is varied to achieve the desired flowrate (mixture ratio). Thus the primary-to-secondary flow split and the oxidizer injection momentum are set by turbopump speed.

In contract testing of dual orifice injectors with fluorine/hydrogen, it was found that an oxidizer flow split of 8 to 10% at full thrust and a minimum of 50% at the 10% thrust level were required to obtain optimum performance with stable combustion. Figure 111 indicates that these levels can be obtained with any of the thrust control methods considered. Figure 112 shows that fuel-to-oxidizer momentum ratios exceed 2 at reduced thrust for all control methods which, based upon experience with coaxial-type dual orifice injectors, should provide good combustion efficiency.

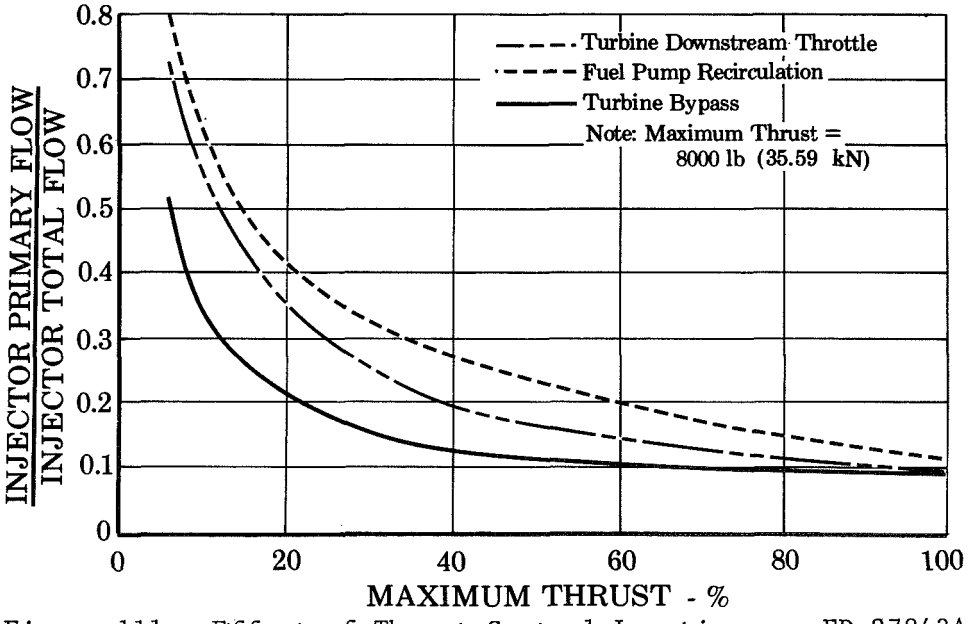


Figure 111. Effect of Thrust Control Location On Oxidizer Injector Flow Split FD 27843A

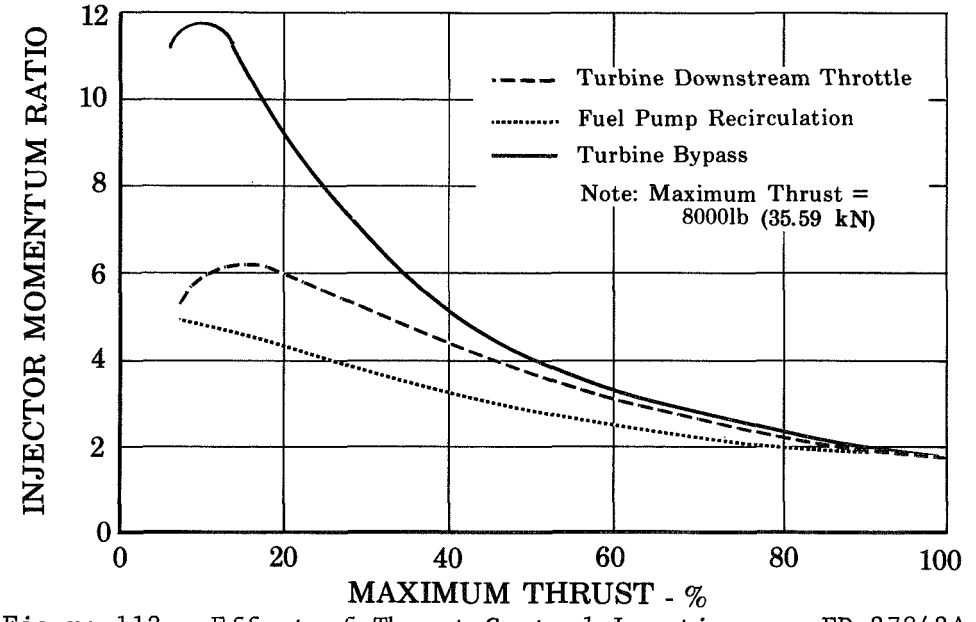


Figure 112. Effect of Thrust Control Location On Injector Momentum Ratio FD 27842A

d. Pump Suction Requirements

Table XXXVII shows the pump net positive suction pressure requirements at the design point (5000 lb; 22.24 kN) thrust for the various control schemes considered.

Table XXXVII. Pump Inlet Head Requirements

| | Turbine Downstream Throttle | Fuel Pump Recirculation | Turbine Bypass |
|---|---|---|---|
| Fuel Pump Net Suction Pressure, psi ($N/cm^2$) | 6.4 (4.41) | 32.0 (22.06) | 6.2 (4.28) |
| Oxidizer Pump Net Suction Pressure, psi ($N/cm^2$) | 11.2 (7.72) | 17.0 (11.72) | 10.7 (7.38) |

One design requirement was operation at net positive suction pressures of less than 8 psi (5.52 $N/cm^2$) for the fuel pump and less than 12 psi (8.27 $N/cm^2$) for the oxidizer pump. Based upon comparable pump design requirements and a suction specific speed of 25,000, either the throttle downstream control or turbine bypass schemes permit engine operation within these limits. However, note that the maximum values are exceeded for both propellant pumps when the fuel pump recirculation control is used. This control scheme requires higher pump speeds than do the other alternatives; increased speed, increased pump flow due to recirculation, and increased temperature of the recirculated flow at the pump inlet all contribute to the high fuel pump NPSP. The high oxidizer pump NPSP results solely from the higher pump speed.

e. Control Valve Sizes and Turndown Ratios

The required effective flow areas of the fuel side valves for thrust control are shown as a function of thrust in figure 113. The oxidizer control areas are shown in figure 114. All the thrust control valves appear to be feasible with respect to area and turndown ratio. The required turndown ratios for the oxidizer control valves used in conjunction with the turbine downstream throttle or with the fuel pump recirculation control are high and would complicate valve design.

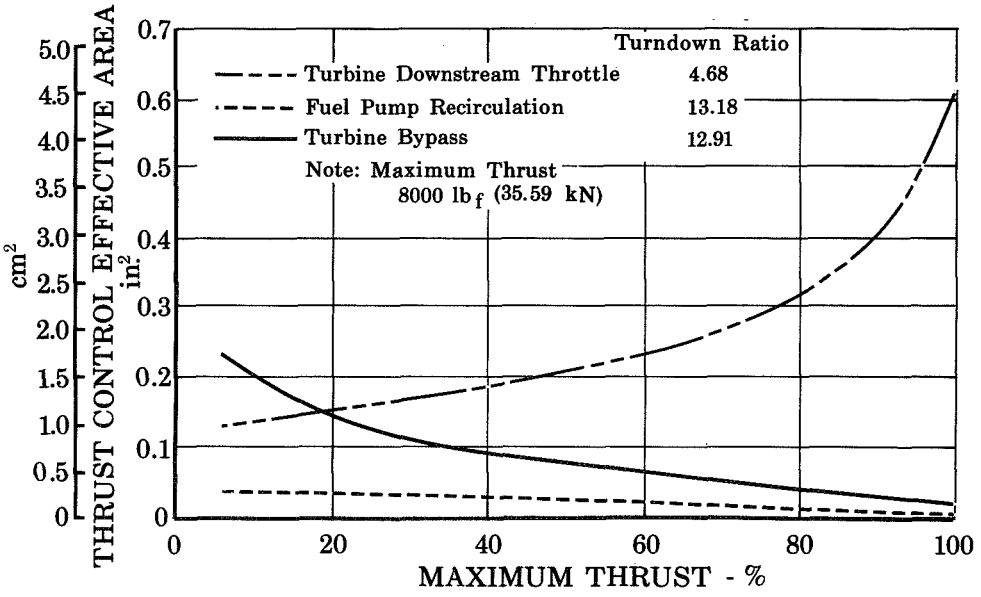


Figure 113. Thrust Control Area Schedules For Candidate Control Locations FD 27841A

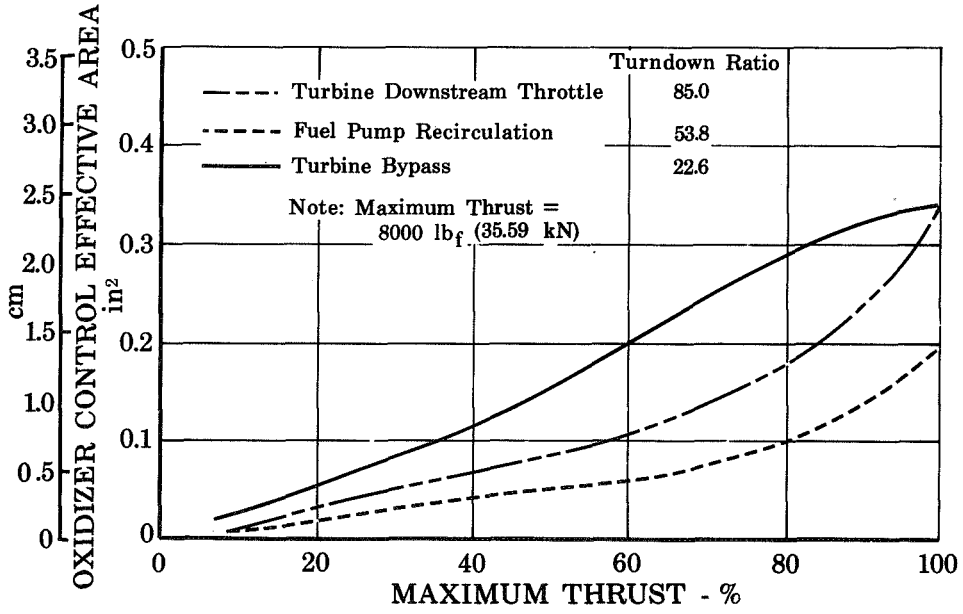


Figure 114. Effect of Thrust Control Location On Oxidizer Control Area Schedule FD 27821A

f. Control Trimming

The relative capability of controls (at the candidate locations) to trim thrust, without significantly altering mixture ratio, is a primary factor in achieving control stability by minimizing interactions between the two control valves. Figures 115 and 116 at 8000 and 500-lb (35.59 kN and 22.24 kN) thrust, respectively, show the

effect of thrust control trim on mixture ratio if the oxidizer valve position is held constant. At high thrust, the turbine by-pass control has nearly ideal trim characteristics and is superior, while at low thrust, the fuel pump recirculation has a slight advantage over the turbine bypass control. The turbine downstream control is inferior to the turbine bypass control at both thrust levels.

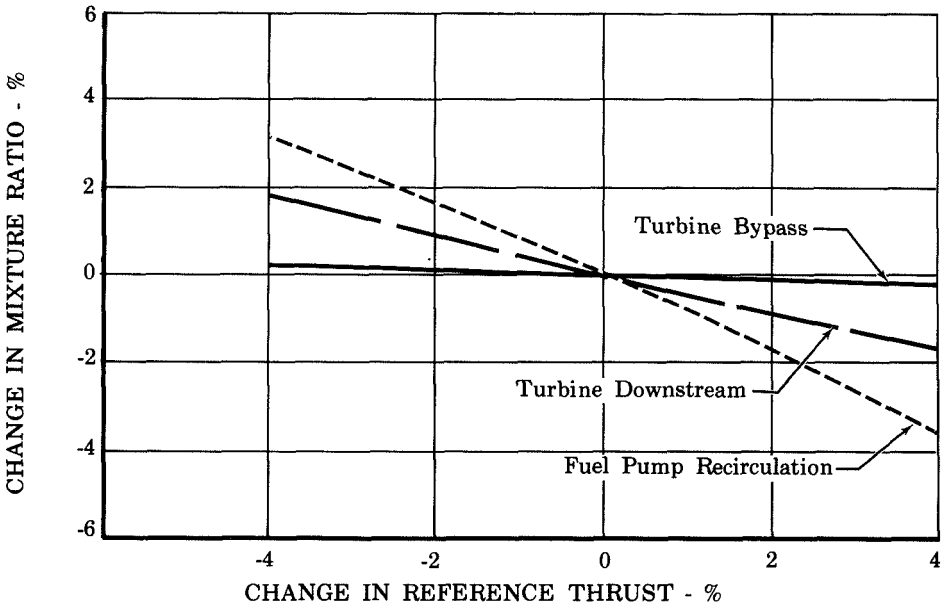


Figure 115. Effect of Thrust Trimming On Mixture Ratio
Reference Thrust = (8000 $lb_f$; 35.59 kN) FD 29226

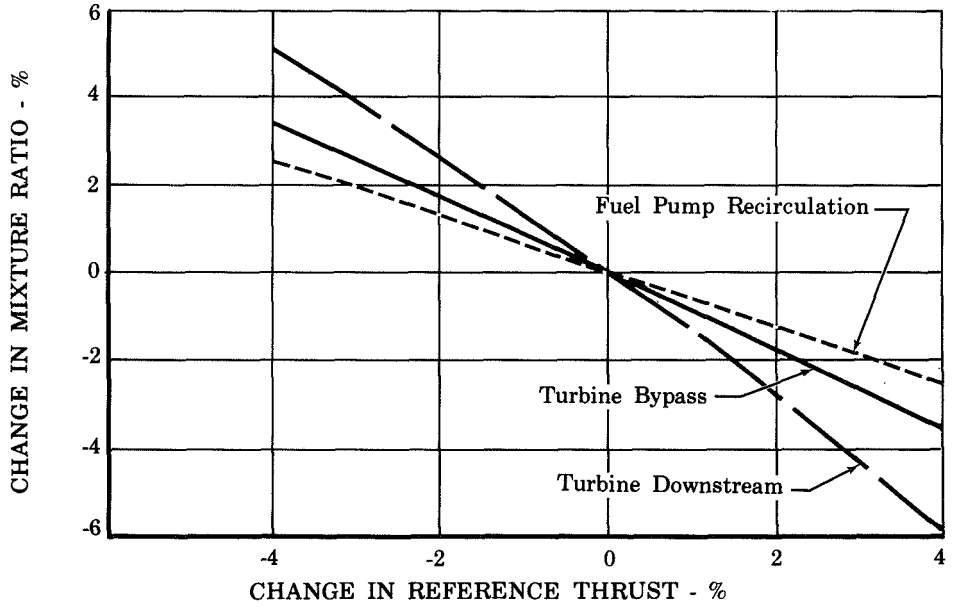


Figure 116. Effect of Thrust Trimming On Mixture Ratio
Reference Thrust = (500 $lb_f$; 2.224 kN) FD 31517

g. Final Selection

Based on the preceding considerations, the turbine fuel bypass was selected for thrust control. The turbine upstream control was eliminated because of high coolant jacket pressures that would be predicted to cause chamber failure, and the fuel pump recirculation control was eliminated because of excessive pump inlet pressure requirements. This restricted the choice to the turbine bypass and the turbine downstream throttle, and the bypass was chosen because of the lower required oxidizer control turndown ratio, the experience level with this type of control in the RL10 engine, and a slight advantage in system stability.

2. Control Components

The basic 5000-lb (22.24 kN) propellant control system, based on the control points selected, is shown schematically in figure 117. It consists of (a) two solenoid valves, (b) fuel and oxidizer inlet shutoff valves, (c) the fuel pump cooldown valve, (d) the main fuel shutoff valve, (e) the thrust control, and (f) the oxidizer flow control valve. These controls are applicable to a fixed thrust engine without tank head start, autogenous pressurization, or propellant utilization. Control requirements for the special cases are discussed in later sections.

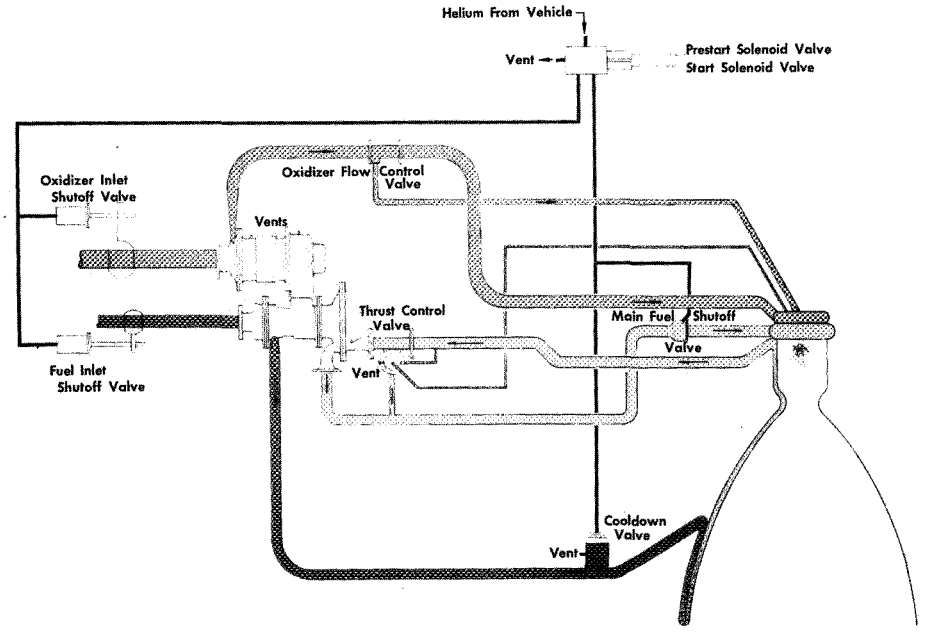


Figure 117. Engine Control Schematic GS 11153A

As noted in the introductory remarks at the beginning of this section, the similarity of the control system to that of the RL10 expander cycle engine led to designs that are basically scaled-down RL10 components. Many of the special features of the RL10 controls that were incorporated in development over the operational period of that engine, and which otherwise might not be considered in a preliminary design, have been incorporated.

a. Prestart and Start Solenoid Valves

The prestart and start solenoid valves control the helium supply from the vehicle storage tank to the propellant control valves. The two valves are mounted in an integral housing and are identical in operation and construction. The prestart valve controls the helium supply to the fuel and oxidizer inlet valve actuators, which open before start to permit conditioning of the fuel and oxidizer pumps. The start solenoid controls the helium supply to the main fuel shutoff valve and the fuel pump cooldown valve.

A schematic of the solenoid valve design is shown in figure 118. In the de-energized position, valve port A is closed and valve port B is open. The balanced poppet is positioned by the force of the valve spring. At either the prestart or start signal, the respective solenoid is energized by the vehicle electrical supply, and the plunger rod moves the poppet valve to a position such that the port A is open and port B is fully closed. Helium is supplied to the respective control system component through valve port A. At shutdown, the solenoid is de-energized and the valve spring returns the valve poppet to a position that closes A and vents the pressure through port B.

b. Propellant Inlet Shutoff Valves

The propellant inlet shutoff valves provide a seal between the vehicle tanks and the engine pumps during nonfiring periods, and open fully upon application of the prestart signal. The propellant pump inlet shutoff valves are helium operated, two-position, ball-type normally closed valves. (See figure 119.) The ball valve design was selected to provide minimum pressure drop and flow distortion at the

engine inlet. The fuel and oxidizer valves are essentially the same in design; the oxidizer valve is significantly larger and subject to restrictions in material selection that do not apply to the fuel valve.

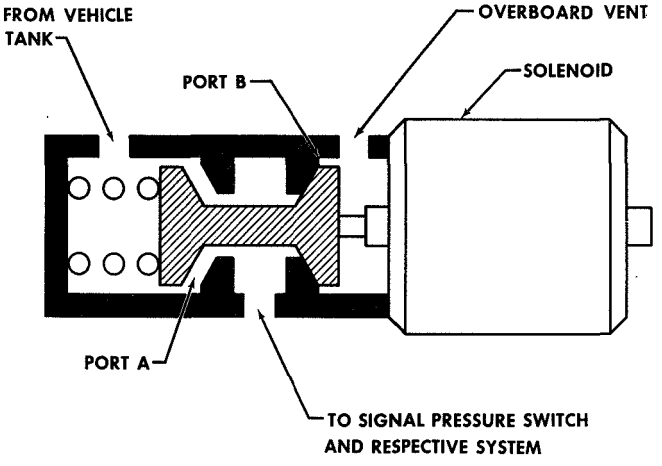


Figure 118. Solenoid Valve Schematic FD 4444

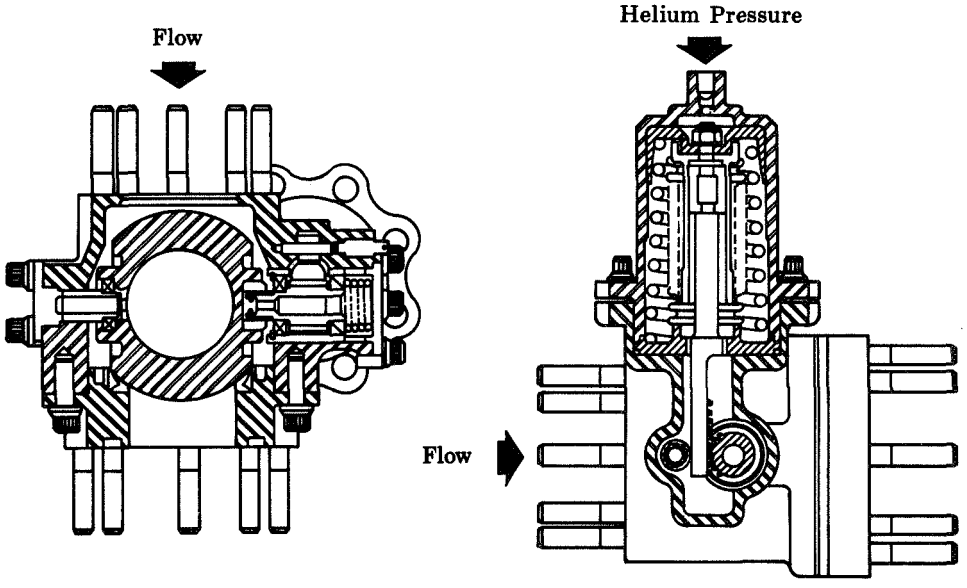


Figure 119. Propellant Inlet Valve FD 29222

At the prestart signal, vehicle-supplied helium pressure acts upon the actuator piston to overcome the resistance of the valve spring and to provide a linear motion of the rack. This produces rotational motion of the ball. As the ball is rotated to the open position, propellants are allowed to pass through the valves into the pumps.

The elapsed time from closed to fully open position is estimated at less than 100 milliseconds, based on RL10 experience.

After removing the helium pressure, the ball valve is returned to its normally closed position by the compressed spring and the helium boosted piston, which gets its boost by leakage past the piston ring seal. The elapsed time from fully open to closed position is estimated to be 130-180 milliseconds for both valves. As shown in figure 119, an orifice, or one-way check valve-orifice arrangement, can be provided at the actuator fitting to alter response between the two valves if desired.

The bellows assembly acts as a seal between the rack and gear chamber, which is exposed to propellant, and the spring chamber, which is exposed to helium. The drive gear and valve ball are ball-bearing mounted and are positioned axially by springs that maintain a constant thrust load for longer bearing life. The gear arrangement and actuator bellows have been used in modified RL10 inlet valves of this type in both liquid fluorine and liquid flox (References 4, 8, and 13).

The inlet valve bodies are aluminum, and the valves have anodized (hard coat) aluminum balls. In figure 119, a single downstream Teflon seal is shown. This is similar to the seals in RL10 engine valves, and is considered suitable for the fuel valve. A large number of RL10 fuel valves have been fabricated and tested; as would be expected, there have been variations in leakage. A number of valves have demonstrated very low leakages, so it is felt that with development, satisfactory valve sealing for long term space storage can be achieved.

In the fluorine-hydrogen and flox/methane RL10 engine programs, gold-plated stainless steel seals were substituted for the Teflon used in oxygen valves because Teflon has been considered unsuitable for fluorine service. The metal-to-metal seals, one at each side of the valve, were used in the modified units. These were effective in preventing through leakage, but there were losses from a vent between the seals. This arrangement would not, therefore, be suitable if the engine inlet valves are to be relied upon to seal against the tank pressure during non-firing periods. It was not felt that a valve configuration which overcame the deficiencies of past units could be

established with any certainty during the preliminary design, and therefore, this appears to be an item which must be deferred for further evaluation or for pursuit of parallel approaches if development were undertaken. Available information (Reference 14) indicates that Teflon of the proper type may be more suitable for fluorine applications than was earlier thought, but this approach has not been exploited. The problems associated with finding a suitable grade of Teflon and establishing its compatibility in this application might be less severe than development of metallic seals with acceptable leakage rates for two year storage in space. Another alternative might be to use a valve of a different type that would be more readily developed, but to locate it remotely from the engine so that flow disturbances would be dissipated upstream of the pump.

c. Fuel Pump Cooldown Valve

The fuel pump cooldown valve (figure 120) provides overboard venting of fuel during prestart to cooldown both fuel pump stages and during shutdown to prevent an excessive pressure buildup in the coolant jacket. The valve is a pressure-boosted, sleeve-type, normally open valve. The pressure boosted feature of the valve was found to be necessary to ensure that the cooldown valve would open before the fuel inlet and main fuel shutoff valves closed. Late opening of the cooldown valve would permit liquid fuel to be trapped in the engine flow system and could cause an excessive pressure buildup in the fuel pump.

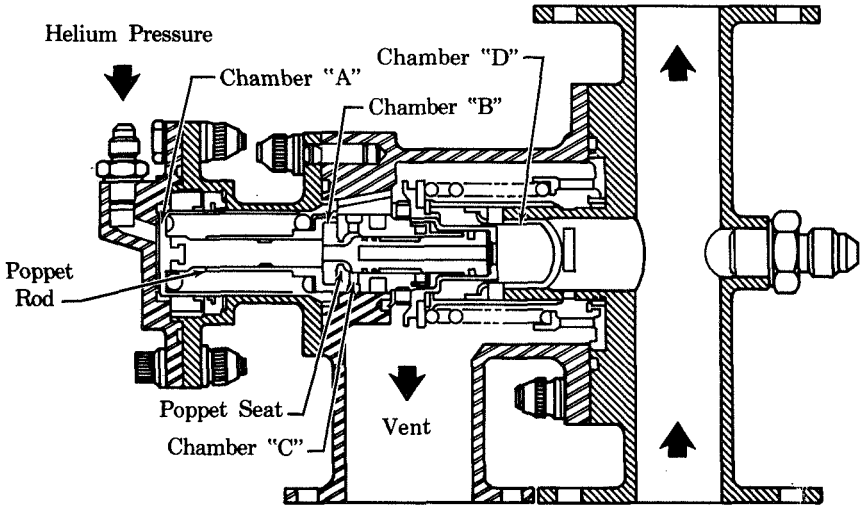


Figure 120. Fuel Pump Cooldown Valve FD 29221

When the fuel prestart helium pressure signal initiates the cooldown cycle, the fuel inlet valve opens and allows fuel to pass through the fuel pump and overboard through the cooldown valve. At the start signal, chamber A of the cooldown valve is pressurized with helium, causing the helium actuator piston to move the piston and the sleeve valve. The sleeve valve travels to a position that covers the vent ports and prevents any further bleed flow. This initial movement of the helium actuator piston also serves to seat the poppet rod against the poppet seat. This provides venting for chamber B and chamber D via internal passages and allows fuel pump discharge pressure to build up in chamber C against the piston.

As the engine accelerates in the early part of the start transient, the fuel pump discharge piston moves the sleeve valve against a Teflon seat and provides a positive seal during steady-state engine operation. At engine shutdown, the helium pressure is vented from chamber A, the poppet rod is lifted off the poppet seat and blocks the vent to chamber B. Fuel pump discharge pressure enters chamber D through chamber B and the internal connection. This pressure "boosts" the sleeve valve open rapidly. The valve is in the full open position approximately 20 milliseconds after the poppet valve is unseated. This fast response provides the pressure relief function prior to inlet and main fuel shutoff valve closure.

d. Main Fuel Shutoff Valve

The function of the main fuel shutoff valve (figure 121) is to prevent flow of fuel into the thrust chamber during cooldown periods and to stop fuel flow into the thrust chamber at shutdown. During engine operation at the design point, the valve pressure drop is only 7 psi (4.83 $N/cm^2$) at a fuel flow rate of 2.0 lb/sec (0.910 kg/sec).

The valve is a helium-operated, two-position, normally closed bullet-type unit. The bullet valve configuration was selected because it is light in weight and because it provides the fast response necessary for adequate control of shutdown impulse. At the start signal, vehicle supplied helium pressure acts upon the internal

effective area of the bellows to overcome the resistance of the valve spring and actuates the valve gate. The exterior of the bellows is vented overboard, and sealed from fuel by a lip seal. When the valve gate is actuated, a flow passage through the valve housing is opened, permitting fuel to flow into the injector. After removing the helium pressure, the valve gate is returned to its normally closed position by the compressed spring. Sealing is effected by spring loading a spherical surface on the gate against a conical surface on the valve housing and by the gate seal ring. The fuel inlet shutoff valve provides the necessary sealing between the vehicle and the fuel pump; therefore, zero leakage of the main fuel shutoff valve is not required.

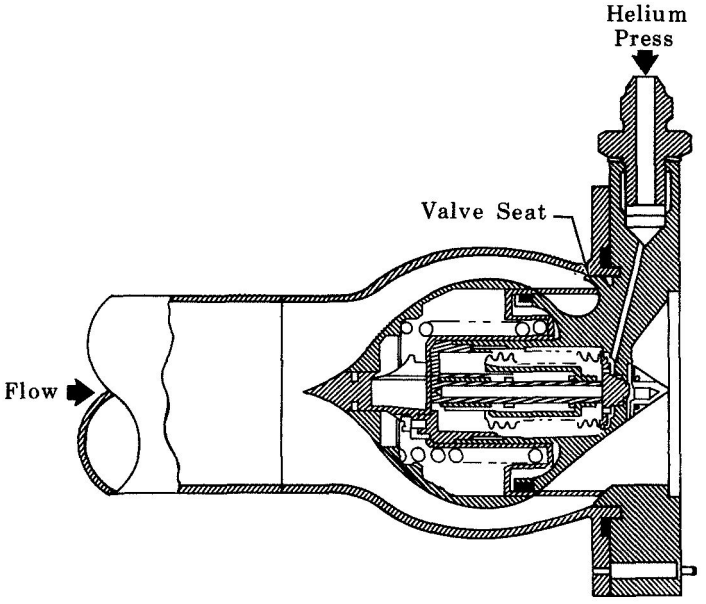


Figure 121. Main Fuel Shutoff Valve FD 29223

e. Thrust Control Valve

The thrust control valve (figure 122) is a reduced scale RL10 design. It is a servo-operated variable-position valve that controls engine thrust by regulating the amount of fuel that bypasses the turbine as a function of combustion chamber pressure. This, in turn, controls the speed of the turbopump.

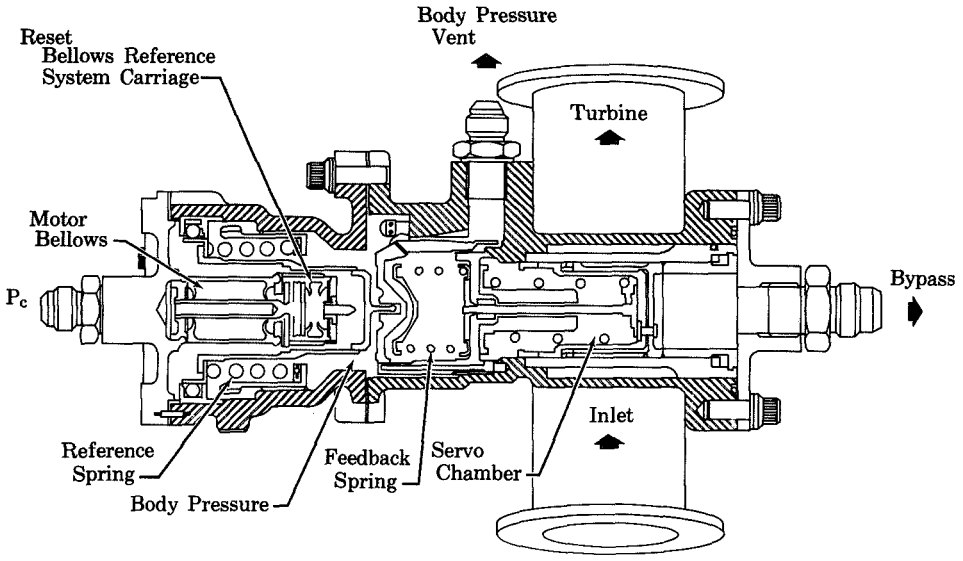


Figure 122. Thrust Control FD 29224

Referring to figure 122, the reference system carriage position is determined by: (1) the combustion chamber pressure acting on the area of the motor bellows; (2) the reference spring preload, which can be remotely adjusted during engine calibration to provide the nominal combustion chamber pressure of 500 psia; and (3) by pressure differential acting on the reset bellows area. The reset bellows internal pressure is supplied from body pressure through a pneumatic reset volume orifice into the reset bellows. This causes reset pressure to lag body pressure during engine acceleration, thus producing a force that allows the carriage to be positioned to a nominal position before chamber pressure reaches the 500 psia (344.7 $N/cm^2$) set-point. This actuates the servo lever, which bleeds off servo chamber pressure and opens the turbine bypass area before engine nominal conditions are reached, to reduce thrust overshoot.

The bypass valve is spring-loaded in the closed position and senses turbine discharge pressure and servo chamber pressure. Servo chamber pressure is supplied through an orificed line from the heat exchanger discharge passage and is bled into the body through a shear orifice servo valve, which was selected for its stability. Body pressure is bled overboard through an orifice sized to give the desired pressure. When servo chamber pressure is reduced by the opening of the servo valve, the increased pressure differential acting on the bypass valve

is sufficient to overcome the valve spring force and the valve is repositioned. This uncovers the contoured bypass ports that permit flow to bypass the turbine.

The servo valve lever position is maintained by a force balance of the reference system, which reflects chamber pressure, and the feedback spring, which reflects bypass valve position. A change in chamber pressure will produce a force unbalance that varies the position of the servo valve, thereby producing proportional variation in servo chamber pressure. This pressure variation repositions the bypass valve, which alters the feedback spring force until the force balance is regained. Repositioning of the bypass valve varies turbine power which establishes total propellant flow, chamber pressure, and thrust.

f. Oxidizer Flow Control Valve

The oxidizer flow control valve acts only on the oxidizer secondary flow while the primary flow goes directly to the injector. The functions of the oxidizer flow control and pressure relief valve shown in figure 123 are as follows:

1. Maintain the required oxidizer flow during the cooldown cycle
2. Control the oxidizer flow to provide an acceptable oxidizer-to-fuel ratio during the start cycle
3. Permit ground trim of mixture ratio.

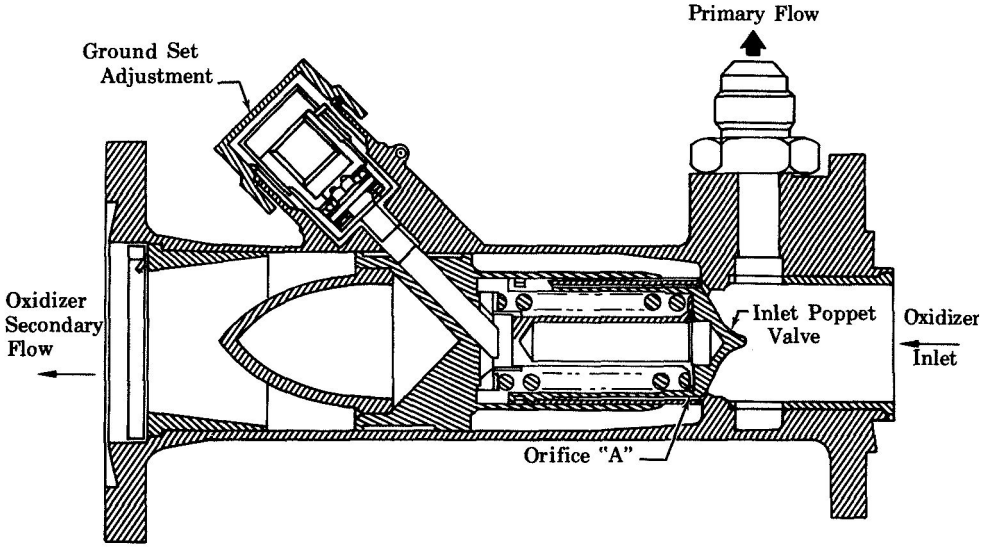


Figure 123. Oxidizer Flow Control Valve FD 29225

The oxidizer secondary flow during engine cooldown is controlled by fixed area orifices built into the valve. The controlled oxidizer flow is necessary to maintain a satisfactory oxidizer-to-fuel ratio for engine acceleration. An additional orifice ("A" in figure 123), which is controlled by the inlet poppet valve, is fully closed during cooldown and during the initial portion of the start cycle.

The back face of the inlet poppet valve senses pump inlet pressure and the upstream surface is subjected to pump discharge pressure. The area opened at orifice "A" during acceleration is a function of the valve contour and the oxidizer pump pressure rise. During testing of a modified RL10A-1 engine with flox-methane under Contract NAS3-7950 (Reference 4), it was found that scheduling of the oxidizer flow during acceleration was critical. However, the large volume of the engine system designed for hydrogen contributed to the criticality of this function, and it is believed that the severity of the problem will be reduced in the 5000-lb (22.24 kN) engine designed for methane. As mentioned earlier, the exact requirements can only be established after the performance of the major engine components have been established.

The maximum area of the oxidizer flow control is regulated by an adjustment stop that can be remotely controlled during an acceptance test. The flow requirements are 9.4 lb/sec (4.26 kg/sec) at a design pressure drop across the oxidizer flow control valve of 70 psi (48.26 $N/cm^2$).

g. Valve Specifications

Preliminary specifications for the nine control valves are provided in table XXXVIII. Total control valve weight is estimated at 14 lb (6.35 kg). Total electrical requirements are a maximum of 1.0 amperes from prestart to start and 2.0 amperes from start to shutdown with a voltage of 18 to 29 volts. From 0.75 to 3.0 standard $ft^3$ (21.23 to 84.93 standard liters) of helium supplied at 1500$\pm$ 100 psia (1034 $\pm$ 68.95 $N/cm^2$) are required for each complete engine operation from prestart to shutdown. The wide variation in helium requirements is based on the potentially high variation in helium temperature at shut-down (150 to 620°R; 83.33 to 344.4°K) which has been provided for.

Table XXXVIII. Control Valves for Fixed Thrust-Cooled Start, Preliminary Specifications

| | Solenoid Valves | Fuel Inlet Shutoff Valve | Oxidizer Inlet Shutoff Valve | Fuel Pump Cooldown Valve | Main Fuel Shutoff Valve | Thrust Control | Oxidizer Flow Control Valve |
|---|---|---|---|---|---|---|---|
| Type of Actuation | Electrical | Helium | Helium | Helium | Helium | Chamber Pressure | Flox Pump, ΔP |
| Normal Position | Closed | Closed | Closed | Open | Closed | Closed | Partially Open |
| Line Fluid | Helium | Methane | Flox | Methane | Methane | Methane | Flox |
| Line Pressure, psia ($N/cm^2$) | 0-1500 (0-1034.21 | 20-125 (13.78-86.18) | 20-125 (13.78-86.18) | 0-1400 (0-965.3) | 0-750 (0-517.1) | 0-700 (0.482.6) | 0-700 (0-482.6) |
| Actuation Pressure, psia ($N/cm^2$) | -- | 1500 ± 100 (1034 ± 68.95) | 1500 ± 100 (1034 ± 68.95) | 1500 ± 100 (1034 ± 68.95) | 1500 ± 100 (1034 ± 68.95) | 0-600 (0-413.7) | 0-750 (0.517.1) |
| Line Fluid Temperature, °R (°K) | 150-620 (83.33-344.44 | 170-260 (94.44-144.4) | 150-200 (83.33-111.1) | 170-300 (94.44-166.7) | 1200-1500 (666.7-833.3) | 1200-1500 (666.7-833.3) | 150-210 (83.33-116.7) |
| Actuator Fluid Temperature, °R (°K) | -- | 150-620 (83.33-344.4) | 150-620 (83.33-344.4) | 150-620 (83.33-344.4) | 150-620 (83.33-344.4) | 1200-1500 (666.7-833.3) | 150-210 (83.33-116.7) |
| Ambient Temperature, °R (°K) | 395-620 (219.4-344.4) | 170-620 (944.4-344.4) | 150-620 (833.3-344.4) | 170-620 (94.4-344.4) | 170-620 (94.4-344.4) | 170-620 (94.4-344.4) | 170-620 (944.4-344.4) |
| Time to Full Open, millisec | 20-30 | 60-100 | 60-100 | 15-50 | 90-120 | -- | -- |
| Time to Full Closed, millisec | 15-25 | 130-180 | 130-180 | 80-100 | 60-100 | -- | -- |
| Shutdown, Repeatability | ±10 | ±20 | ±20 | ±10 | ±10 | -- | -- |
| External Leakage at Ambient Temperature, sccs | Safe | Safe | Safe | Safe | Safe | Safe | Safe |
| Actuator Leakage, sccs | -- | Safe | Safe | 1.25 Cold | 1 Cold | Safe | Safe |
| Closed Valve Leakage at Coast Temperature and Pressure, sccs | 8 | 0.5 | 0.3 | 400 | 4000 | -- | -- |
| Required Voltage, volts | 18-29 | -- | -- | -- | -- | -- | -- |
| Maximum Current, amperes | 1.0 | -- | -- | -- | -- | -- | -- |
| Estimated Weight, lb (kg) | 0.8 (each) (0.363) | 1.6 (0.726) | 2.3 (1.043) | 2.1 (0.953) | 1.7 (0.771) | 3.7 (1.678) | 1.0 (0.454) |
| Valve Body Material | Aluminum | Aluminum | Aluminum | Aluminum | Stainless Steel | Stainless Steel | Aluminum |

The term "safe" leakage as applied to engine overboard leakage in table XXXVIII is meant to infer essentially zero leakage based on conventional detection methods. The propellant inlet valve closed leakage values shown in the table are based on moderate development of the scaled down RL10 type valve shown in figure 123. This leakage rate would result in a propellant loss of approximately 65 lb/year (29.48 kg/year) of storage assuming that the tanks were at their maximum pressure (125 psia; 86.19 $N/cm^2$) for the entire time. With more extensive development the valve leakage could probably be reduced to 10 to 20% of the leakage rates shown. Further reduction in leakage rates would require either a major valve modification or complete valve re-design followed by a major development effort.

The valve designs are premised on meeting the requirements of specification MIL-E-5149, and qualification according to MIL-E-5151 and MIL-E-5272 unless overriding requirements are specified. The specifications MS-33540, MS-33586, MS-33588, and AND-10056 are also employed where applicable. Material specifications are based on ANA Bulletin 343.

3. Basic Control System Operation

a. Starting

The engine starting sequence is divided into a prestart cycle and a start cycle. The prestart cycle is used to thermally condition the turbopumps, and the start cycle is used to accelerate the engine to full thrust. The prestart cycle is initiated by an electrical signal from the vehicle, which energizes the prestart solenoid valve. Pressurized helium flows through the solenoid valve and opens both pump inlet valves. Propellant then flows through and cools the turbopumps. The fuel is discharged overboard through the fuel pump cooldown valve, and the oxidizer flows into the thrust chamber through the oxidizer primary injector supply line and through a bypass orifice incorporated in the oxidizer control valve. The prestart cycle is sequenced for the time interval required to cool the pumps as determined experimentally.

The start cycle is initiated by a second electrical signal from the vehicle. The start solenoid valve is energized, and pressured helium, flowing through the start solenoid valve, closes the fuel cool-

down valve, opens the main fuel shutoff valve and allows fuel from the pump discharge to flow through the thrust chamber coolant passages. The fuel passes through the turbine to the injector where combustion is initiated. Heat is then transferred to the fuel flowing through the cooling jacket providing energy for the turbine to overcome the static friction of the turbopump assembly and start turbopump rotation. The oxidizer control valve area during the starting transient is scheduled as a function of the oxidizer pump pressure rise as discussed under paragraph 2.f. The area schedule must be set to maintain mixture ratio within acceptable limits and prevent an excessive engine acceleration.

Experience with the RL10 flox/methane engine showed that the rate of chamber pressure buildup is a very important factor in the engine starting transient. Too rapid chamber pressure rise can result in localized coolant flow stoppage and passage burnout, because of the rapid change in the coolant density when a sudden heat load is applied. As noted above, the problem was critical in a modified RL10 engine, and required careful scheduling of the oxidizer control valve area to provide a relatively slow start transient. This problem should be greatly reduced in the 5000-lb (22.24 kN) thrust engine because the coolant passages are designed for methane rather than hydrogen. The volume of cold methane that can accumulate is substantially reduced. However, the problem is recognized and the rate of chamber pressure rise can be controlled as required.

The thrust control begins to open during the engine acceleration as was discussed in paragraph 2.e. The timing and area schedule of this valve must be set to complement the oxidizer control valve in controlling mixture ratio during engine acceleration. The thrust control also limits thrust overshoot to an acceptable level.

The engine starting system described is a basic proven approach; however, area schedules must be set based on transient analysis and experimental component data, and some modifications would certainly be required, if implementation of the designs were attempted. To define the engine starting transient in greater detail, a dynamic simulation must be conducted, using actual engine component operating characteristics wherever possible. This is beyond the scope of this contract.

Some of the factors that must be evaluated in such a simulation include:

1. Engine metal temperature at start signal
2. Mixture ratio during start transient
3. Rate of chamber pressure buildup
4. Pump inlet temperatures and pressures
5. Thrust overshoot
6. Line and component filling characteristics
7. Pump stall
8. Propellant phase changes
9. Injector flow reversals
10. Time to accelerate
11. Component cooldown characteristcs

b. Shutdown

The engine shutdown cycle begins when the electrical signal from the vehicle terminates. This permits the solenoid valves to return to their normally vented position, which shuts off the helium supply and vents the helium from all valve actuators. Closing the main fuel shutoff valve stops flow through the turbine, thus stopping the pump rotation and allowing the system to come to rest. The fuel inlet shutoff valve closes, preventing fuel from entering the system. The fuel pump cooldown valve opens, draining fuel from the system to prevent pressure buildup due to trapping fuel between the main fuel shutoff valve and the inlet valve. The oxidizer inlet shutoff valve closes, stopping oxidizer flow into the engine. The remaining oxidizer flow in the system flows through the injector and into the thrust chamber.

4. Modified Control Requirements

The control system described in paragraph E.2 and 3 is well defined based on the analytical effort conducted under this contract and RL10 expander cycle experience. Because of the experience, there is a high confidence level that such a system could be applied to a fixed thrust flox/methane expander cycle engine with minimal control component development. However, the system as defined does not provide for special modes of engine operation. Additionally, it assumes that conventional approaches such as prestart cooldown for pump conditioning, overboard fuel venting at engine shutdown, and ground set mixture ratio

adjustment and thrust adjustment are acceptable. For the deep space missions for which the engine is primarily intended, non-conventional procedures, such as use of non-vented tanks, are likely to be employed. Therefore, in a final design, it would be necessary to re-examine the acceptability of these conventional engine procedures. Such an examination was not possible, since requirements were not defined in great detail, and also, it was not within the scope of a preliminary design study. However, it was considered desirable to examine briefly the possibilities for throttling, propellant utilization, and tank head idle operation.

a. Throttled Operation

To throttle an expander cycle engine with a turbine bypass thrust control, it is only necessary to increase the bypass area to reduce the turbopump power. With fixed ratio geared pumps, it is also necessary to modulate the oxidizer flow control valve to maintain the desired mixture ratio. These steps permit thrust reduction until some component limitation is reached.

The cycle data presented in paragraph A showed that the valve flow areas used for the controls of the fixed thrust engine, matched with acceptable turn-down ratios, were adequate for 10% thrust and for uprating to 8000-lb (35.59 kN) thrust. These data were based on nominal engine inlet conditions. If high tank pressures are to be provided for, several problems are encountered. At fuel tank pressures above 100 psia (68.95 $N/cm^2$), even if the turbine flow were bypassed completely, fuel flow in excess of the 0.22 lb/sec (0.100 kg/sec) required for 10% thrust would be produced by the high tank pressure. Thus the bypass thrust control is inadequate, and a separate fuel throttle valve in addition to the thrust control would be required. A similar problem exists with the oxidizer flow control. The oxidizer control valve in the fixed thrust system throttles only the oxidizer secondary flow; this control point was shown to be adequate for 10% thrust based on nominal tank pressures. However, at higher tank pressures the oxidizer control valve turndown ratios increase prohibitively, and the upper limit tank pressure (125 psia; 86.19 $N/cm^2$) is sufficient to force excessive oxidizer flow through the primary orifice alone, even

if the secondary flow is completely shut off. It must be concluded that, to accommodate high oxidizer tank pressures at 10% thrust, both the oxidizer primary and secondary flow must be throttled.

It has been mentioned that limitations on components other than the controls can be reached. A potential problem with throttled operation of a pump-fed engine is dynamic flow instability in the fuel system resulting from boiling within the cooling jacket. This problem was encountered in throttling tests of RL10 engine, and a cavitating venturi between the fuel pump and thrust chamber coolant inlet was found to be highly successful in stabilizing flow. Since an additional fuel system pressure drop is necessary for adequate throttling at low thrust in the 5000-lb (22.41 kN) engine, cavitating venturi upstream of the jacket inlet could serve both to stabilize the system and provide throttling.

The problems of throttling can also be magnified depending upon the tolerances which must be held on engine operating parameters, since these affect the accuracy required of control system inputs. Under NASA Contract NAS8-11427, control requirements for a cryogenic engine with 10:1 throttling and with relatively close tolerances on thrust and mixture ratios were investigated (AEB Control System Study, Reference 19). Because of the similarity in the engine requirements (10:1 throttling, propellant utilization, tank head idle, etc.) many of the conclusions from that study with respect to control input parameters are applicable to a throttleable version of the 5000-lb (22.41 kN) engine if similar requirements are established. As applied to the 5000-lb (22.41 kN) engine, conclusions from the AEB study are as follows:

1. Thrust Control
    a. Both chamber pressure and total propellant flow senses are sufficiently accurate for steady-state thrust control.
    b. Chamber pressure offers the better transient characteristics.
    c. The relative applicability of the two is not affected by the control points used.

2. Mixture Ratio Control

   a. Flowmeters biased by inlet temperature (i.e., mass flowrate) was the only sense that could provide adequate mixture ratio control at low thrust.

   b. The transient characteristics of an oxidizer flow divided by chamber pressure sense ($W_o/W_p$) are better than those of flowmeters on both propellants ($W_o/W_f$).

   c. The relative applicability of the two methods is not affected by the control points used.

The superiority of flowmeters for providing accurate mixture ratio control at low thrust would far outweigh all other considerations. When flowmeters are used for mixture ratio control, much of the potential advantage of using chamber pressure for thrust control is lost, and an additional sense ($P_c$) would be required. Consequently, propellant flow ($W_o + W_f$) would also be the preferable sense for thrust control.

b. Propellant Utilization

The basic engine control system, described above, provided only for trimming to establish the nominal mixture ratio at nominal inlet conditions. This is accomplished by adjusting the maximum flow area of the oxidizer control valve as was described under paragraph E.2. If the engine is operated with other than nominal conditions, mixture ratio variations will result. Figure 124 shows predicted variations in mixture ratio as a function of pump inlet temperatures, assuming that propellant inlet pressures are adjusted to provide a constant net positive suction pressure over the entire temperature range. Note that an increase in the oxidizer inlet temperature produces a decrease in engine mixture ratio while an increase in the fuel inlet temperature has an opposite effect. In an actual mission the propellants would be loaded cold and both would generally change temperature in the same direction as the mission progresses. An oxidizer temperature increase would cause a decrease in mixture ratio, but a corresponding increase in fuel temperature would have a compensating effect. The two temperature effects are approximately additive; therefore, the mixture ratio can be determined using the curves for any combination of inlet temperatures.

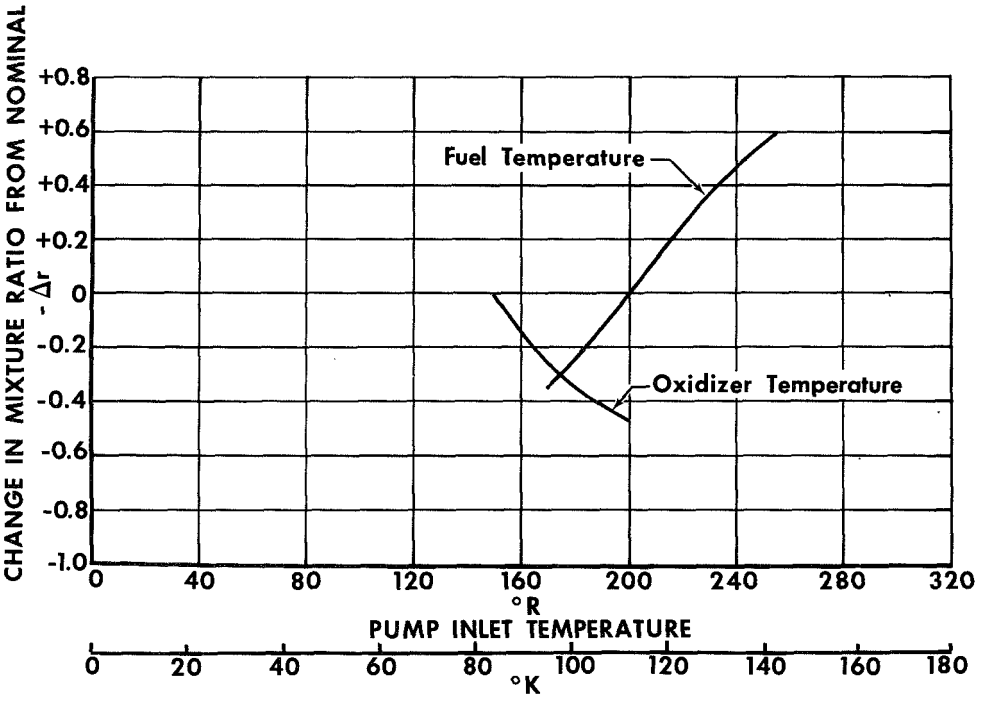


Figure 124. Effect of Pump Inlet Temperature On Mixture Ratio GS 11071B

In all but the earliest model of the RL10 engine (the RL10A-1), capability for varying engine mixture ratio in response to vehicle requirements for propellant utilization is incorporated in the oxidizer flow control valve. The valve has an adjustable restriction adapted to a vehicle system actuator which can vary engine mixture ratio within limits controlled by mechanical stops on the valve adjustment stem. The actuator input is, as noted, provided by a vehicle system; in the Centaur and Saturn vehicles which used the RL10, a conventional arrangement was used in which the tank propellant level was sensed and mixture ratio adjustments were computed to maintain the proper propellant balance in the tank.

In the RL10 valve, the variable restriction feature is incorporated in series with the main regulating piston as a separate section of the valve. This arrangement could readily be incorporated in the valve design for the 5000-lb (22.24 kN) engine.

Possible sources of disproportionate residuals in the tankage are initial loading errors, propellant boiloff or leakage, variations in engine mixture ratio due to propellants being supplied at conditions

different than nominal, or errors in trimming the engine mixture ratio. For the 5000-lb (22.24 kN) engine operating in a vehicle with non-vented tankage, there would be no boiloff losses, and the primary cause of disproportionate propellant consumption during a mission would be engine mixture ratio variations caused by variations in propellant inlet temperature. Consequently, if initial loading was accurate, propellant utilization might be accomplished by accurate control of engine mixture ratio. This could be accomplished by sensing inlet temperature and adjusting the oxidizer control valve, accordingly. This possibility bears investigation from a vehicle standpoint, since it might eliminate the complexity of a propellant utilization system based on liquid level sensing.

c. Tank Head Idle

Tank head idle is defined as operation of the engine at a low thrust level using propellants supplied by tank pressure without benefit of the turbomachinery. Tank head idle may be considered in conjunction with pumped idle operation and autogenous pressurization as a means of eliminating the need for a helium pressurization system. In the combined idle mode with autogenous pressurization, the engine is fired initially in the tank head idle mode to settle the propellants and thermally condition the turbopumps. Operation is then continued into the pumped idle mode where propellants for tank pressurization to the level required for full thrust turbopump operation are extracted from the engine prior to engine acceleration to full thrust. During the pumped idle mode, the pumps operate on essentially zero net positive suction pressure (NPSP) and thus the propellant tanks require no prior externally supplied pressurization gases. The system is known as "autogenous pressurization" because of its ability for self-pressurization. A typical thrust-time curve for the combined system is shown in figure 125.

In the tank head idle mode with liquid propellants supplied to the engine, thrust is limited by the available tank pressure. For the inlet requirements of this investigation, the fuel has a lower minimum vapor pressure than the oxidizer; consequently, the fuel provides the greatest restriction to maximum thrust. Figure 126 shows the maximum

chamber pressure that can be maintained by the fuel as a function of methane tank temperature. The solid line is for zero NPSP corresponding to that available in an autogenous pressurization system, while the dotted line is for typical pump-fed inlet conditions where the necessary pump NPSP is previously provided by external pressurization. In cases where the oxidizer tank pressure drops appreciably below the fuel tank pressure, the oxidizer tank pressure becomes the primary limitation on thrust; however, for the inlet conditions investigated under this study (minimum flox temperature = 150°R, 83.33°K), the oxidizer could always maintain a chamber pressure above 10.0 psia (6.90 N/cm$^2$), even with zero NPSP.

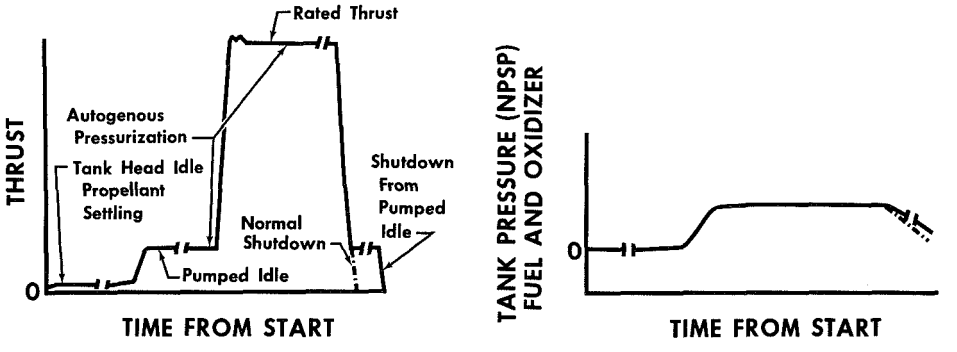


Figure 125. Operational Mode Engine Firing GS 7115

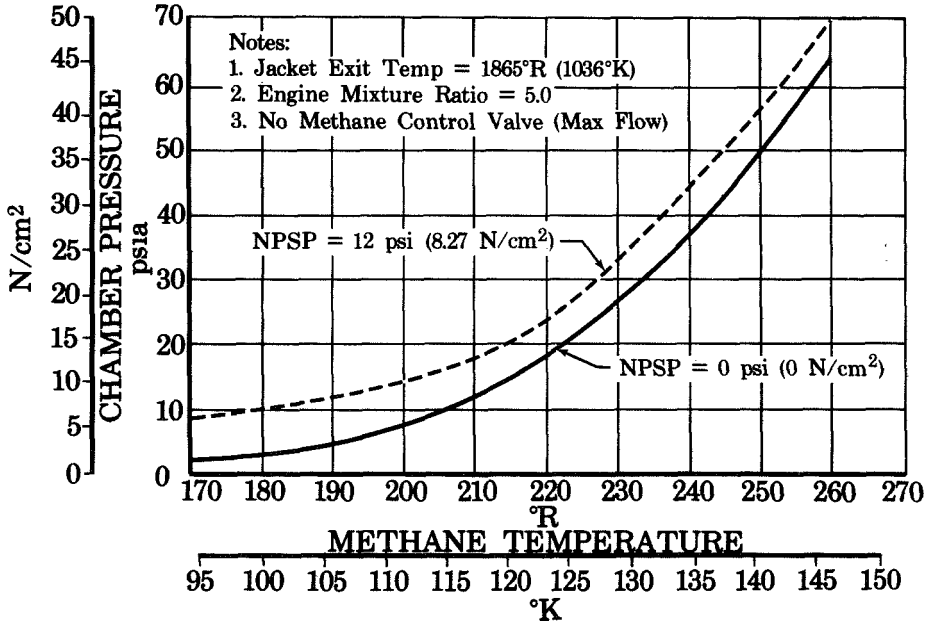


Figure 126. Effect of Methane Temperature On Chamber Pressure FD 31519

Mixture ratio control is the most difficult requirement associated with tank head idle. At 10% thrust (50 psia, or 34.47 $N/cm^2$ chamber pressure), mixture ratio must be maintained below 5.25 to prevent methane cracking. At 1% thrust (5 psia, or 3.45 $N/cm^2$ chamber pressure) the maximum tolerable mixture ratio drops to 5.0. The problems associated with mixture ratio control are:

1. The propellant inlet state may be gas, liquid, or two phase, and the control system must provide adequate response and control valve turndown ratios to account for these phase changes.
2. Variation in inlet pressure will affect propellant flow and increase turndown ratio requirements.
3. There is no simple direct means for determining inlet state; consequently, direct flow measurement becomes virtually impossible until the propellants are settled.

In the RL10A-3-7, tank head idle control was accomplished by sensing chamber pressure and coolant jacket discharge temperature to control the oxidizer flow control valve position. Chamber pressure and thrust are influenced primarily by oxidizer flow, while fuel coolant temperature is influenced primarily by mixture ratio, hence an adequate indirect measure is obtained. Chamber pressure and fuel temperature are fed into a computer which schedules the oxidizer flow control valve area using experimentally determined biases and time constants. A relatively narrow range of inlet pressures was anticipated for a vented tank application, i.e., approximately 23 ± 2 (15.86 ± 1.38 $N/cm^2$) psia for the fuel and 33 ± 2 psia (22.75 ± 1.38 $N/cm^2$) on the oxidizer tank. However, even with this limited range oxidizer flow control valve turndown ratios of approximately 20:1 were required to compensate for the oxidizer inlet state.

In the 5000-lb (22.24 kN) flox-methane engine, control requirements are much more severe because of the much wider variation in propellant pressure for non-vented tanks. The fuel flow is relatively insensitive to the inlet state because most of the fuel system pressure drop occurs in the thrust chamber and injector where the fuel would be vaporized regardless of the inlet conditions; thus, the fuel flow is

almost directly proportional to the fuel tank pressure. The oxidizer flow is sensitive to both inlet pressure and inlet state. The most promising control point for the oxidizer in the tank head idle mode still appears to be the oxidizer flow control valve as in the RL10A3-7. Figure 127 shows the oxidizer control valve requirements to maintain a mixture ratio of 5.0. The curve is based on zero NPSP, as applied to an autogenous pressurization system. It can be seen that for low methane inlet temperatures (and correspondingly low pressures) the control valve turn down ratios would become excessive, particularly with liquid flox at the engine inlet. Furthermore, at these high turn down ratios the oxidizer control valve area is much less than the injector area; consequently, the injector pressure drops would be extremely low, even with a dual orifice injector.

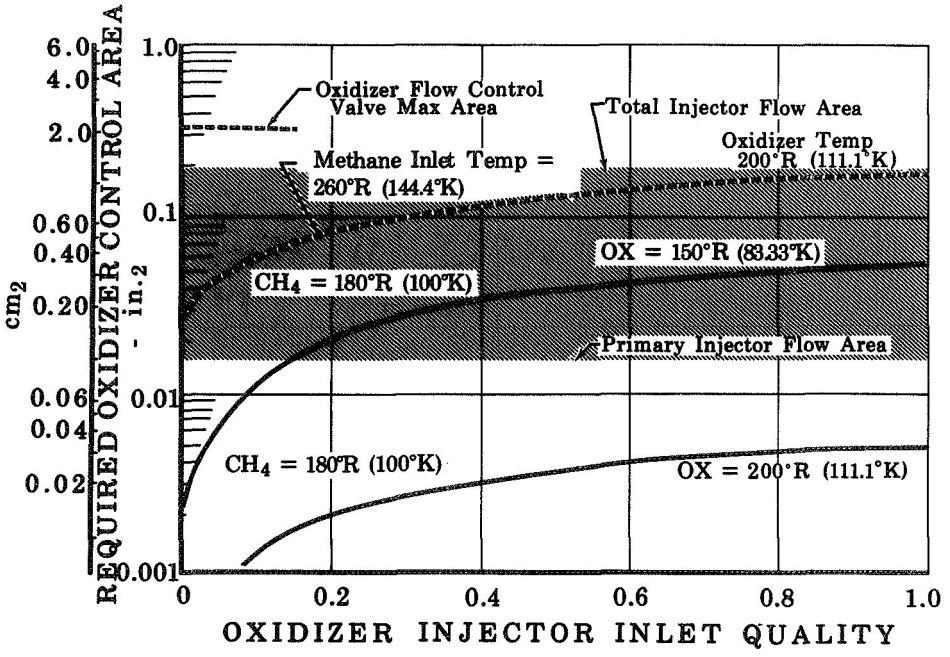


Figure 127. Estimated Oxidizer Control Area Schedules FD 31570

In the event that tank head idle capabilities were desired for minor $\Delta V$ propulsion requirements or as a means of utilizing cooldown propellant flow to produce useful thrust, rather than just as a step in the autogenous pressurization scheme, a different control approach suited to the mode could be taken. This would require tank pressurization and would use cavitating venturi flow meters at the pump inlets.

The latter method provides a unique approach by utilizing a constant tank NPSP to provide a constant tank head idle thrust as well as mixture ratio control. Because cavitating venturis are driven by the available pressure above the fluid vapor pressure, a constant NPSP (as would be desired for nonvented cryogenic tankage) would provide a nearly constant flow regardless of tank pressure. After the propellants are settled, mixture ratio control between 4.0 and 5.0 could be accomplished, with less than 20% variation in engine thrust, without the use of an active control system. The fixed area venturis could be bypassed around a shutoff valve downstream of the propellant inlet valves, or could be fed from an intermediate port on the inlet valves as shown in figure 128. At tank head idle, all flow would be through the venturis and at other thrust levels the venturis would be bypassed.

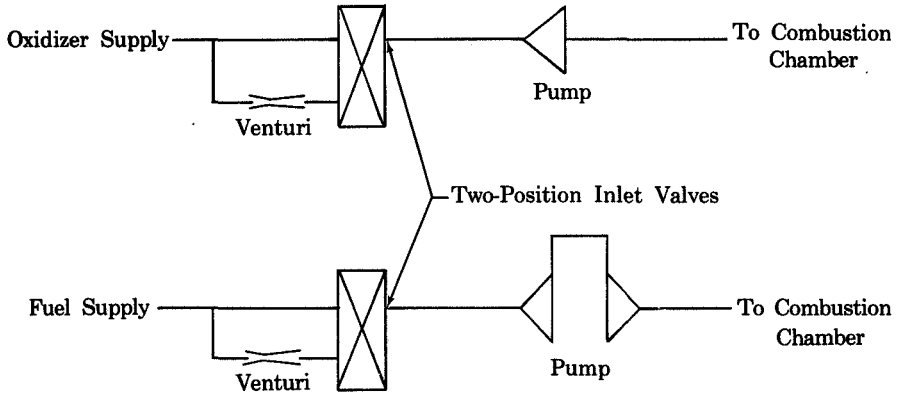


Figure 128. Schematic Tank Head Idle Inlet Controls FD 31518

For a thrust level of 50-lb or 22.24 kN (1% thrust) and an NPSP of 12 psi (8.27 $N/cm^2$) in both tanks, venturi diameters of 0.081 in. (0.206 cm) on the fuel side and 0.051 in. (0.130 cm) on the oxidizer side would be required. For nonsettled propellants, the mixture ratios encountered for various propellant inlet states are given in table XXXIX.

Table XXXIX. Mixture Ratios for Various Propellant Inlet States

| Fuel State | Liquid | Liquid | Gas | Gas |
|---|---|---|---|---|
| Oxidizer State | Liquid | Gas | Liquid | Gas |
| Mixture Ratio Range | 4.0-5.0 | 0.24-0.82 | 25.2-155 | 1.4-25.4 |

Neither the fixed area venturis or the oxidizer flow control throttling can provide the required steady-state mixture ratio for all possible propellant inlet conditions. However, if propellant settling occurs rapidly enough in the small tanks that would be employed, the thrust chamber heat capacity may be sufficient to prevent excessive methane temperatures from being encountered prior to establishing liquid propellant flow into the engine. It is apparent that a narrower range of inlet conditions would simplify the transient requirements. Even more beneficial would be the use of propellant settling devices to assure liquid propellants at the engine inlet.

d. Conceptual Control System for Throttling, Tank Head Idle, etc.

For the reasons discussed earlier, the detailed definition of a control system for all of the various engine operating modes of interest was not attempted. Figure 129 does, however, represent one approach to a control system that would provide throttling, propellant utilization, and tank head idle to eliminate overboard discharge of engine cooldown propellants and provide minor $\Delta V$ propulsion. At the start for nominal engine operation, fixed thrust, fixed mixture ratio, tank head idle flow is metered through fixed area cavitating venturis as shown in figure 128. A solenoid valve advances the inlet valves to the tank head idle position and propellants flow through the venturis and turbomachinery into the thrust chamber. It is assumed that liquid fuel is provided at the engine inlet, or that the fuel is settled before excessively high cooling jacket temperatures are encountered.

Anytime after steady-state tank head idle operation has been achieved, the start solenoid may be activated, advancing the inlet valves to their full open position. Propellant flows are now monitored by turbine flowmeters in each propellant line as the turbomachinery accelerates to the desired thrust level. Flowrates are fed into a closed loop electronic control system which sets the turbine bypass flow area to achieve the desired thrust based on summation of the propellant flows and sets the oxidizer control valve position to maintain the desired mixture ratio. At high thrust, only the oxidizer secondary flow is throttled, while at lower flows a second port in the oxidizer control valve begins to throttle the primary flow. For the upper range of thrust the fuel flow is throttled only by the thrust control regu-

lation of turbopump speeds, but as thrust is reduced to below 40% the variable area cavitating venturi upstream of the cooling jacket also begins to close. The cavitating venturi is tied to the turbine bypass control by a mechanical linkage to prevent control interactions between the two control points.

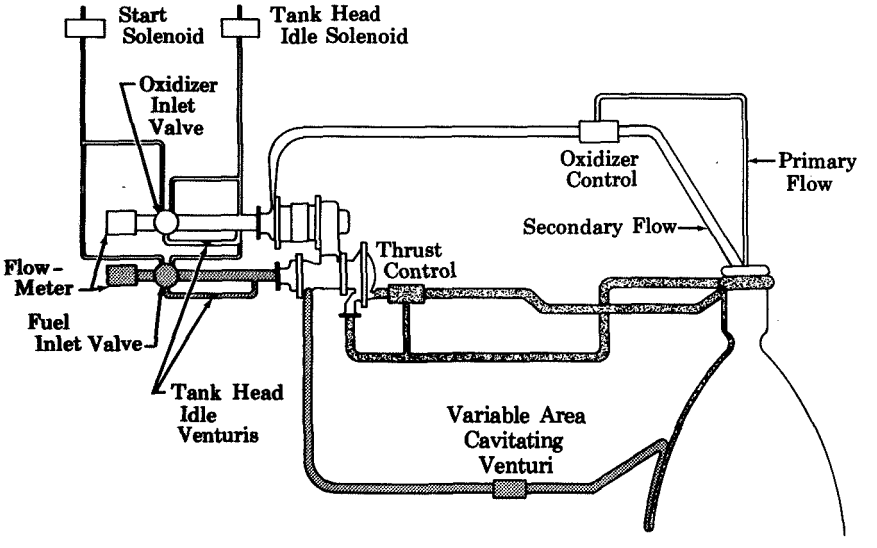


Figure 129. Conceptual Control System for Throttling and Tank Head Idle

FD 31679

Propellant utilization is achieved by sensing propellant tank levels, inlet temperatures, or both, and adjusting the oxidizer flow control valve position accordingly. Since thrust and mixture ratio are computed based on measured flow and controlled to the desired value with a closed loop system, mechanical ground setting of mixture ratio and thrust trim are not required.

## F. PLUMBING AND ENGINE INSTALLATION

The engine component arrangement and installation dimensions are shown in figure 130. The total engine envelope is 46.3 in. (117.6 cm) long and 22 in. (55.88 cm) in diameter. With a 100:1 radiation-cooled skirt, the length would be increased to 59.5 in. (151.1 cm) and the exit diameter would be increased to 26.25 in (66.68 cm).

| | |
|---|---|
| A | ENGINE GIMBAL JOINT, PEDESTAL |
| B | FUEL INLET |
| C | OXIDIZER INLET |
| $D_1$ | ACTUATOR ATTACHMENT LUG |
| $D_2$ | ACTUATOR ATTACHMENT LUG |
| E | HELIUM SUPPLY CONN |
| F | OXIDIZER SEAL VENT |
| G | FUEL SEAL VENT |
| H | GEARBOX RELIEF VALVE VENT |
| J | HELIUM VENT |
| K | ENGINE GIMBAL JOINT PINTLE |
| L | FUEL PUMP COOL DOWN VALVE, VENT |
| M | INSTRUMENTATION BOX |

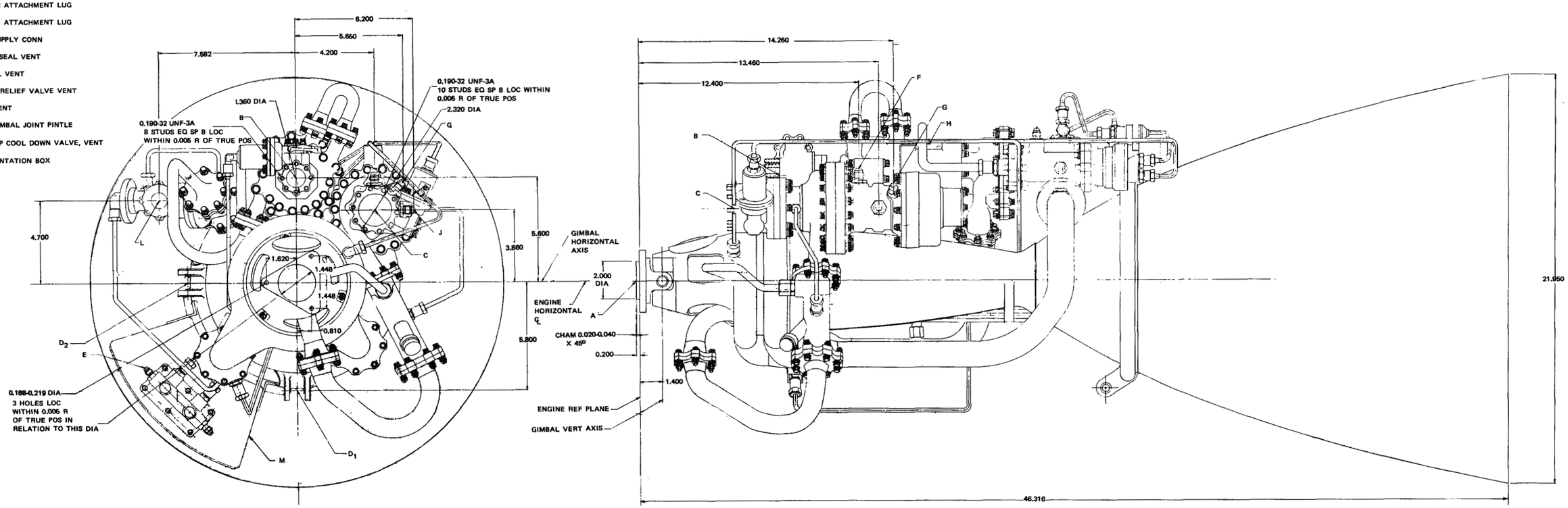


Figure 130. Rocket Engine Installation

FD 31677

1. Engine Plumbing

The engine plumbing is composed of the six propellant lines listed below plus a number of smaller helium, instrumentation, and control valve supply lines:

1. Fuel pump interstage line
2. Fuel pump discharge to thrust chamber inlet manifold
3. Thrust chamber discharge to turbine inlet
4. Turbine discharge to main fuel shutoff valve (fuel shutoff valve is attached to injector inlet)
5. Oxidizer control valve to injector
6. Primary oxidizer flow, pump to injector.

Rigid piping is used throughout the engine with ample contouring to provide for thermal expansion and contraction. AISI 347 stainless steel is used for all of the helium and low temperature propellant lines because of its compatibility with flox, thermal expansion characteristics at cryogenic temperatures (compatible with aluminum valves and pump housings), and high quality welded joints. The turbine inlet and discharge lines are Inconel X750 to provide good high temperature strength. Design practice calls for basing line wall thickness on 0.2% yield strength at the maximum transient pressure; however, using a minimum line gage of 0.020 in. (0.0508 cm), this limit was not achieved. The estimated plumbing weight including flanges is 8.4 lb. (3.81 kg).

The main propellant system connections are sealed with radial-loaded metallic angle gaskets as shown in figure 131. Tolerance control on piping is closely held to maintain the alignment required. The angle gasket seal was selected because of its ability to seal gaseous fluids as well as liquids, its background in liquid fluorine service, and its ability to withstand long-term storage.

2. Gimbal Joint

The engine mount system provides a means of attaching the engine to the vehicle, and also provides a universal bearing system to allow gimballing of the engine. The gimbal mount attachment consists of an

aluminum pedestal with 4-bolt holes as shown in figure 132. The gimbal action is accomplished by means of 4-steel pins and a disk that connect the pedestal to the conical mount. The pins and the disk are coated with a solid lubricant and permit a gimbal movement of well over the design requirement of ±2 deg (0.0349 rad) in both axes. The gimbal joint, conical support, and thrust chamber actuator lugs weight a total of 5.0 lb (2.27 kg).

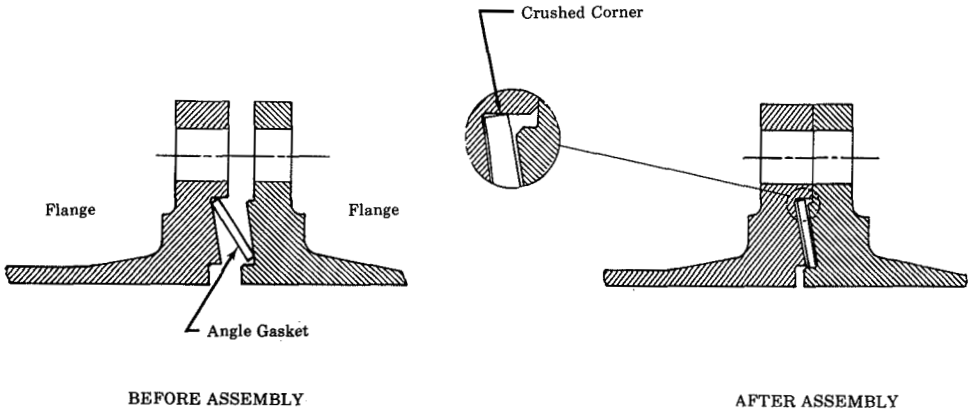


Figure 131. Propellant Pipe Sealing Method FD 1557A

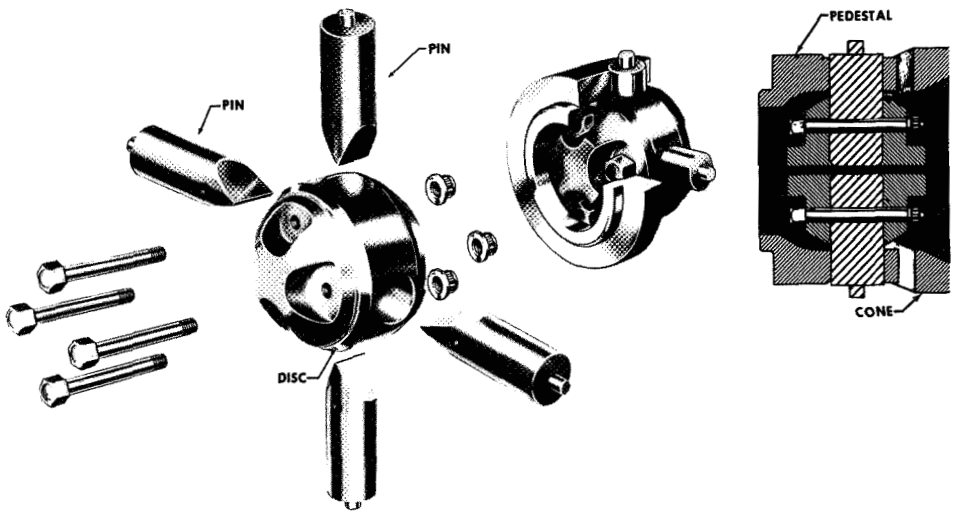


Figure 132. Gimbal Assembly FD 1547D

3. Weight Summary

The engine weight is summarized in table XL. The total engine estimated weight is 98-lb (44.45-kg) dry weight, including solenoid valves and actuator lines. Except for the control system, the component weights are compatible with engine uprating to 8000-lb (35.59 kN) thrust and throttling to 10% thrust. It is anticipated, however, that for a throttling configuration, the control system weight would increase somewhat. The instrumentation box shown in figure 130 is provided as standard equipment for vehicle instrumentation, but, by convention, is not charged to engine weight. The estimated instrumentation box weight is 10 lb (4.54 kg) including supports, but excluding pressure transducers.

Table XL. Component Weight Summary

| | lb | (kg) |
|---|---|---|
| Turbopump | 24.2 | (10.98) |
| Injector | 8.7 | ( 3.95) |
| Thrust Chamber | 32.7 | (14.83) |
| Control Valves | 12.4 | ( 5.63) |
| Lines and Flanges | 8.4 | ( 3.81) |
| Gimbal and Thrust Support | 5.0 | ( 2.27) |
| Attaching Hardware | 5.0 | ( 2.27) |
| Solenoid Valves | 1.6 | ( 0.73) |
| Total Engine Dry Weight | 98.0 | (44.45) |

# SECTION V
# CONCLUSIONS

Under Task I of the "Space Storable Engine Characterization," the expander cycle with a single turbine and geared pumps was determined to be the most desirable configuration for a low-thrust, pump-fed, flox/methane engine. Under Task II a preliminary design of a 5000-lb (22.24 kN) thrust, 500-psia (344.7 $N/cm^2$) chamber pressure, flox/methane engine was completed. The estimated engine vacuum specific impulse is 399.4 $lb_f$-sec/$lb_m$ (3916 N-sec/kg) and approximately 6.0 $lb_f$-sec/$lb_m$ (58.84 N-sec/kg) impulse increase may be achieved with addition of a nozzle extension. The estimated engine weight was 98 lb (44.45 kg). No unanticipated problems were uncovered, and engine development is believed to be completely feasible. Other significant conclusions applicable to low-thrust, pump-fed, flox/methane engines, to be drawn from the study are as follows:

1. Fabrication limitations on coolant passage dimensions significantly influence the limitations on the chamber pressures that can be achieved with the engine cycle, and fabrication research in this area is warranted.

2. Carbon fouling of the turbine could be a significant problem with the gas generator, tapoff, and preburner cycles.

3. Proper propellant distribution for maintaining a satisfactory turbine working fluid temperature without a substantial performance loss with the tapoff cycle would be extremely difficult.

4. Present technology limits on fluorine rubbing seals limit the oxidizer pump speed to less than 40,000 rpm (4189 rad/s).

5. The design chamber pressure and selection of cycles affect the required fuel pump and turbine speeds significantly. Generally, however, both require speeds of 50,000 rpm (5236 rad/s) or higher for satisfactory efficiencies.

6. Turbine admission area requirements are critically low for parallel turbines in closed cycles and result in a substantial loss in available cycle power.

7. For the expander cycle, at 800 psia (551.6 $N/cm^2$) chamber pressure and 5000-lb (22.24 kN) thrust design point, methane cracking in the cooling jacket would probably occur at 10% thrust unless the engine mixture ratio were reduced.

8. The expander cycle at 500 psia (344.7 $N/cm^2$) chamber pressure may be designed for uprating to 8000-lb (35.59 kN) thrust. Uprating of the other cycle/design point combinations, which were considered, appears impractical.

9. Throttling to 10% thrust may be readily accomplished with a variable area or flow-split injector for the oxidizer although other types may be equally applicable. A coaxial dual-orifice injector was found to be well suited to this application.

10. Turbine bypass appears to be the most promising means of thrust control and, with the dual-orifice injector, control of oxidizer secondary flow was judged to be the best method of mixture ratio control.

11. A bootstrap start is feasible with the expander cycle.

# APPENDIX A
# PARAMETRIC HEAT TRANSFER DATA

Presented in this appendix are the parametric data generated under the Task I "Preliminary Regenerative Cooling Analysis" (Section III-B), and the more specific parametric data which describe the thrust chamber cooling characteristics of the four cycle-design point combinations evaluated under the "Cycle Energy Balance," (Section III, paragraph F).

The thrust chamber dimensional requirements are given in Section III, paragraph B.2. Two sets of Thermal Skin dimensional limits were used for the calculations; these are listed in table II (Section III). For both sets of assumed dimensional limits (Case I and II), calculations were made for two inlet pressure to chamber pressure ratios, $P_{in}/P_c$. A $P_{in}/P_c$ of 1.5 was selected as typical of open cycle requirements, such as in a gas generator engine, while a $P_{in}/P_c$ of 3.0 was used to represent closed cycles, such as the expander cycle. The calculated coolant temperature rise and pressure drop for both sets of calculations are presented in figures A-1 through A-24. Figures A-1 through A-12 show the results for Case I, and figures 13 through 24 show the Case II results which were used for the Task IC, "Turbopump Drive Cycle Analysis." Separate curves are presented for two mixture ratios (r = 4.75 and 5.75) at each of the three heat flux levels ($Q_m/Q_p$ = 0.765, 0.90, and 1.0) and the two $P_{in}/P_c$ ratios.

Figures A-25 through A-36 describe the design point and off-design cooling characteristics for the expander and auxiliary heat exchanger cycles at both of the design points used in the Task I analysis. The entire range of coolant pressure drop, coolant bulk temperature rise, and maximum thrust chamber wall temperatures of interest for the four operating variables can be evaluated parametrically with seven sets of curves. The jacket pressure loss can be represented by three sets of curves, as shown in figure A-25, A-28, A-31, and A-34 for each of the four cases. The base $\Delta P/P_c$ data were

calculated at a mixture ratio of 5.25 and a $Q_m/Q_p$ of 1.0. These data are shown in the top set of curves as a function of chamber pressure with lines of constant $P_{in}/P_c$. Influence curves are also shown to provide a correction to the base data for changes in mixture ratio or $Q_m/Q_p$. Similar curves are shown in figures A-26, A-29, A-32, and A-35 for determination of jacket temperature rise, and in figures A-27, A-30, A-33, and A-36 for determination of the maximum wall temperatures. The effect of inlet pressure on jacket temperature rise and on wall temperature is negligible; therefore no influence curves are shown for these variables.

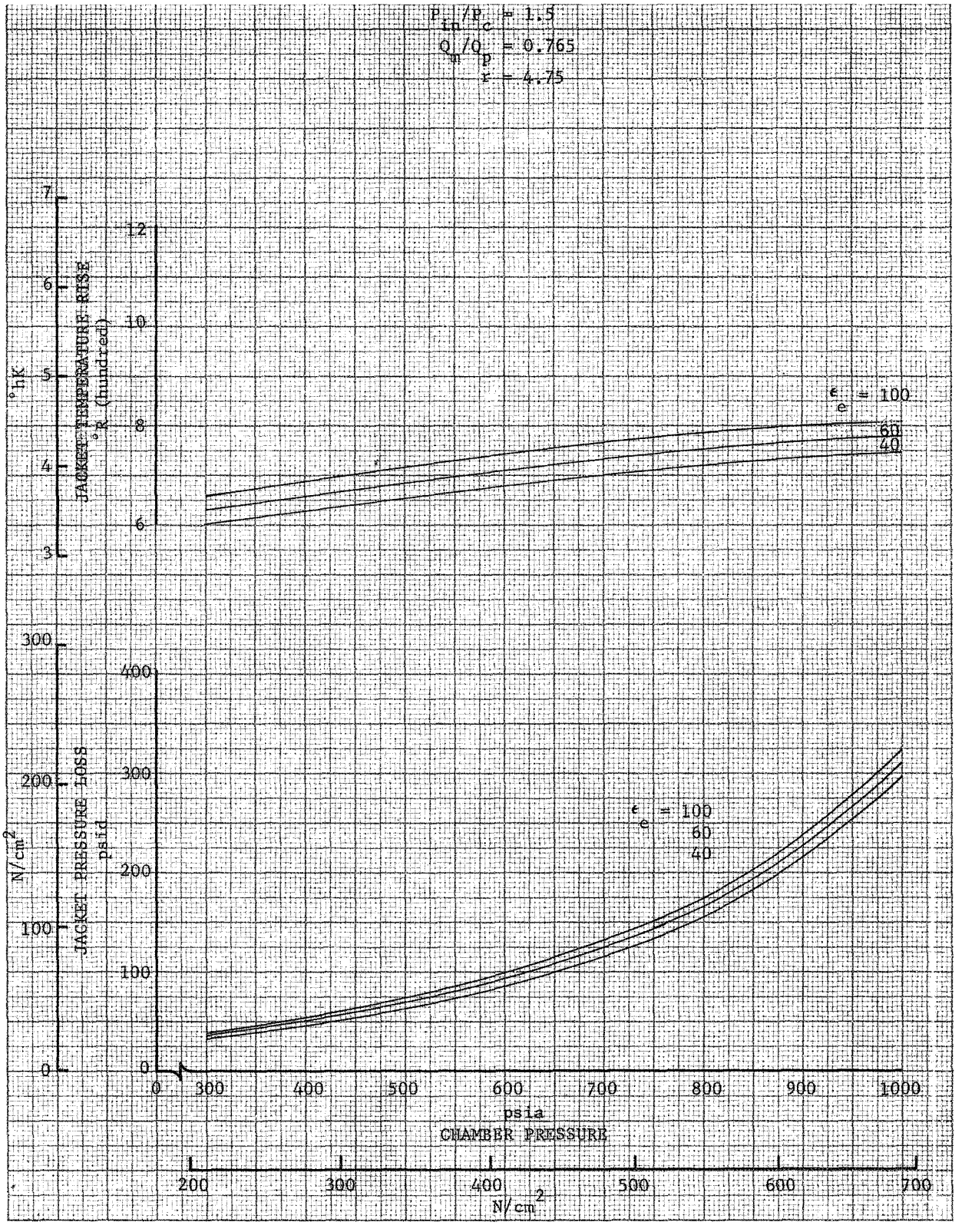


Figure A-1. Flox/Methane 5000-lb (22.24 kN) Coolant Temperature Rise and Pressure Loss - Case I DF 70801

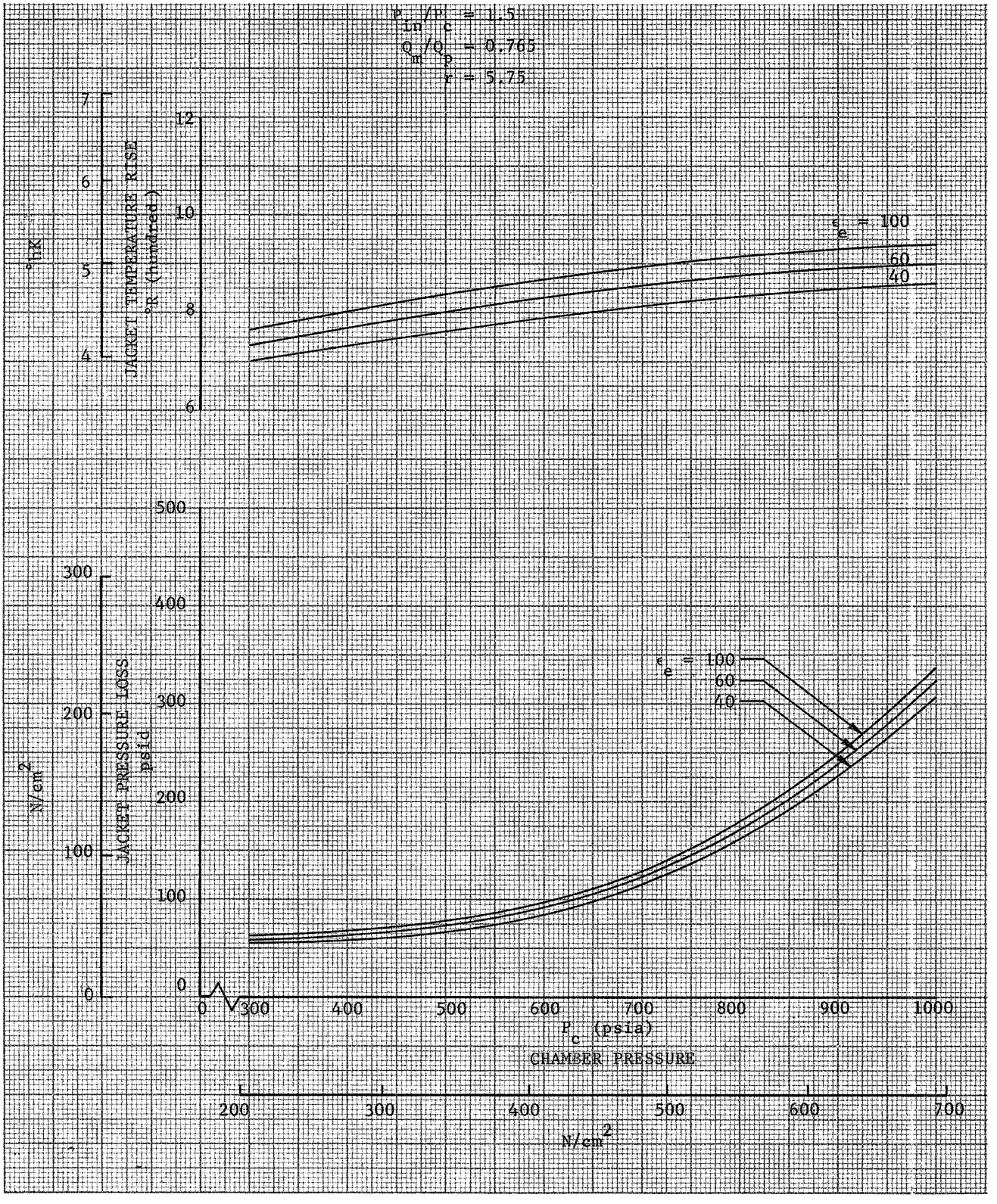


Figure A-2. Flox/Methane 5000-lb (22.24 kN) Coolant Temperature Rise and Pressure Loss - Case I DF 70802

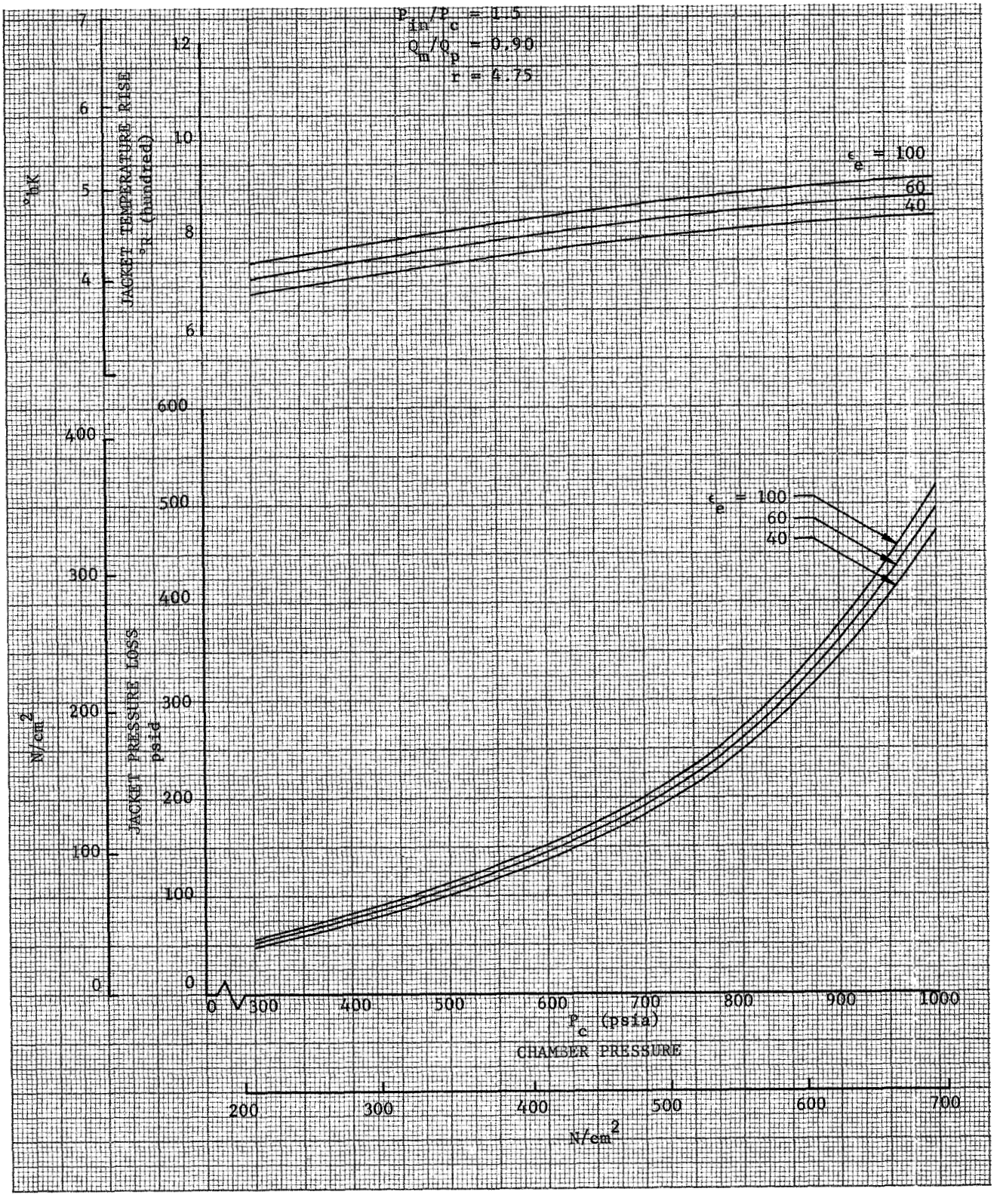


Figure A-3. Flox/Methane 5000-lb (22.241 kN) Coolant Temperature Rise and Pressure Loss - Case I DF 70803

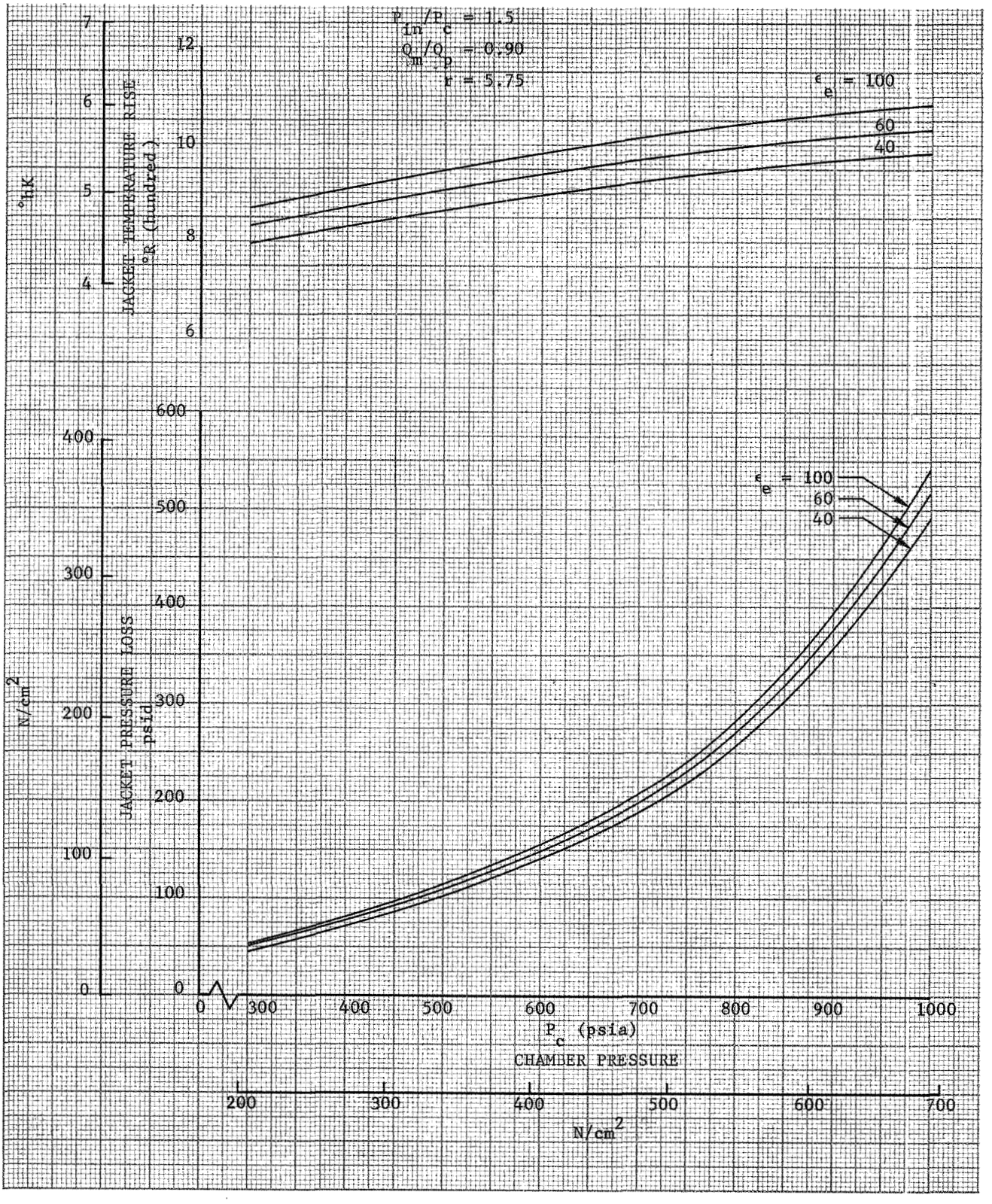


Figure A-4. Flox/Methane 5000-lb (22.24 kN) Coolant Temperature Rise and Pressure Loss - Case I DF 70804

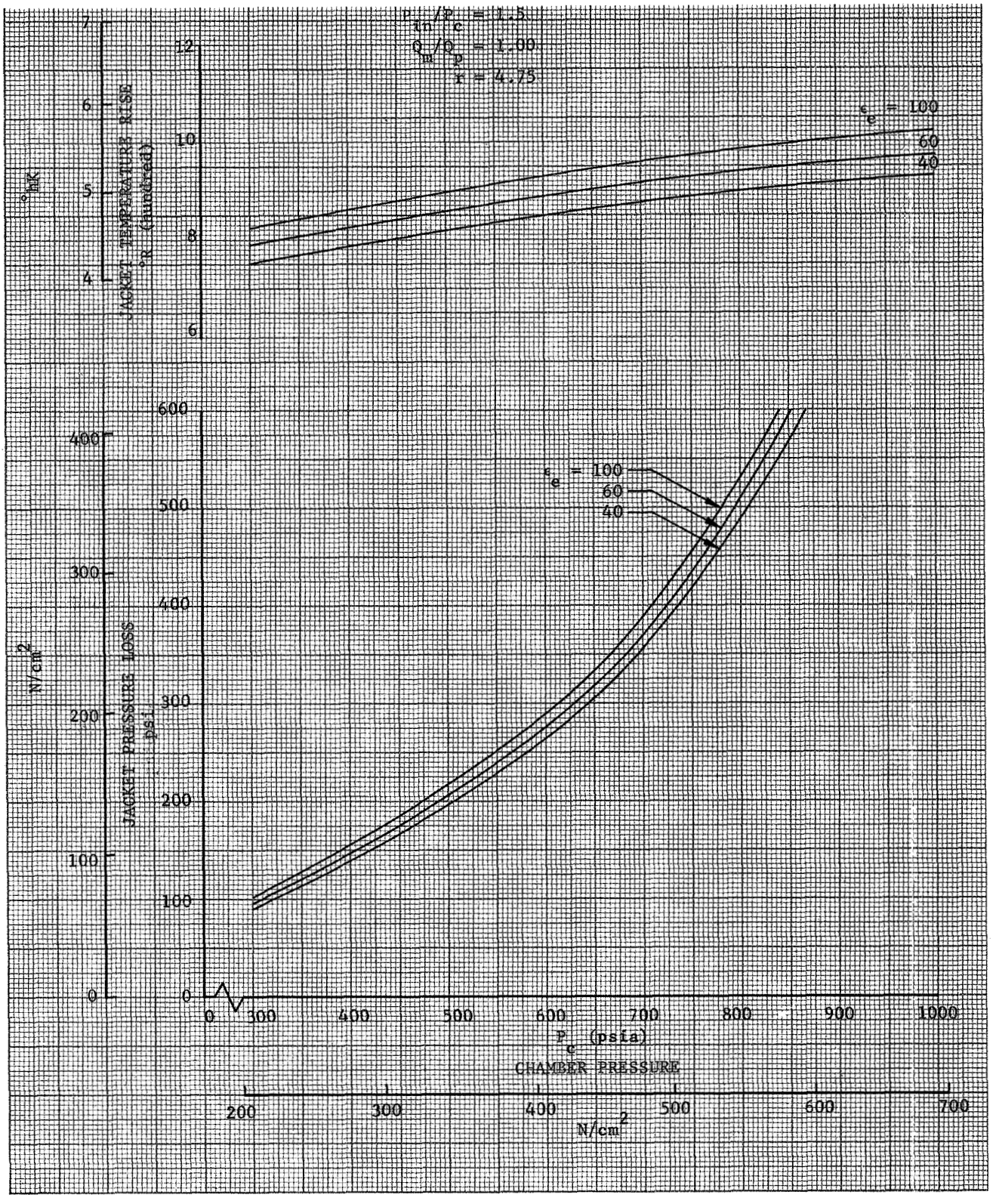


Figure A-5. Flox/Methane 5000-lb (22.24 kN) Coolant Temperature Rise and Pressure Loss - Case I DF 70805

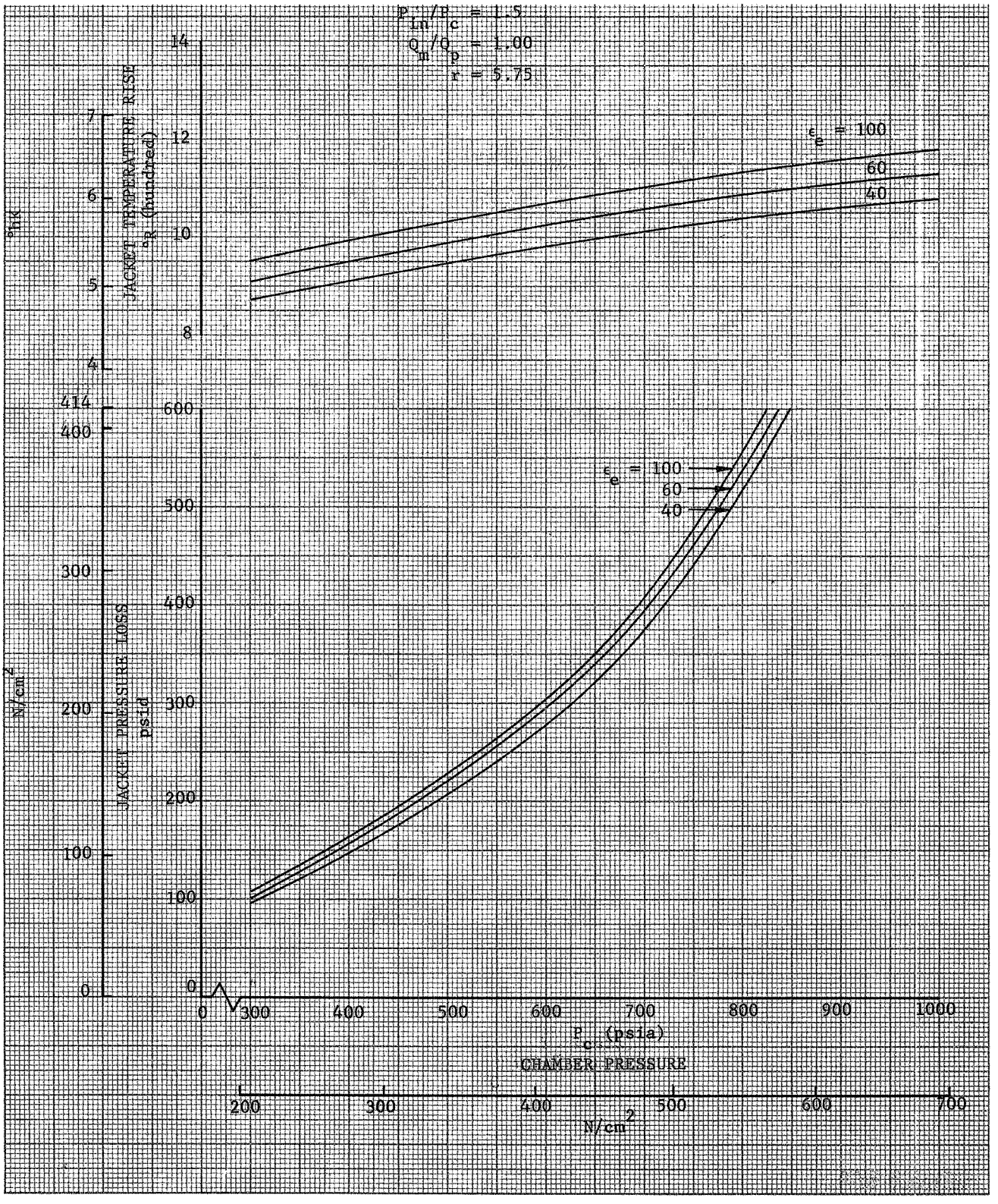


Figure A-6. Flox/Methane 5000-lb (22.24 kN) Coolant Temperature Rise and Pressure Loss - Case I

DF 70806

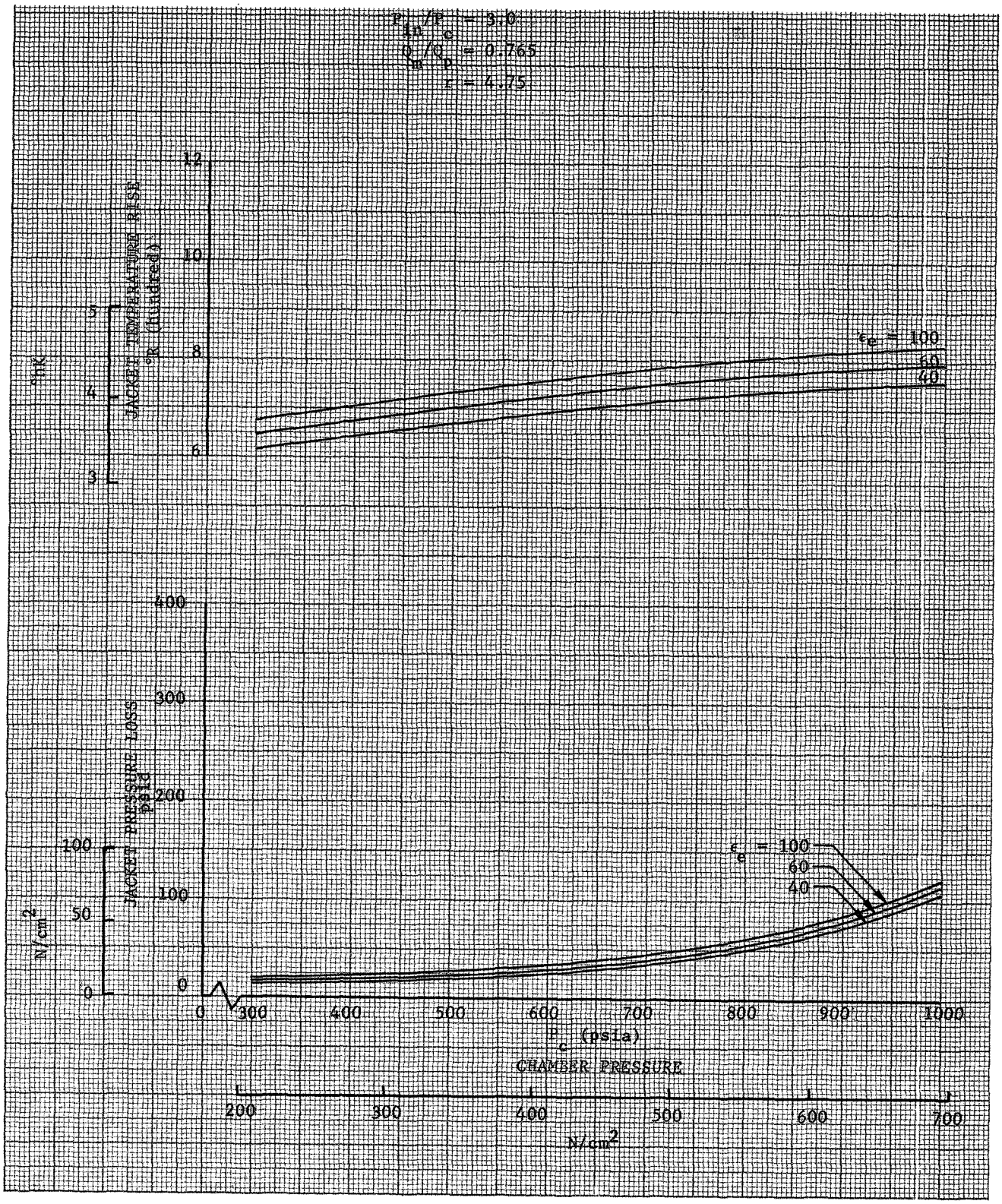


Figure A-7. Flox/Methane 5000-lb (22.24 kN) Coolant Temperature Rise and Pressure Loss - Case I

DF 70807

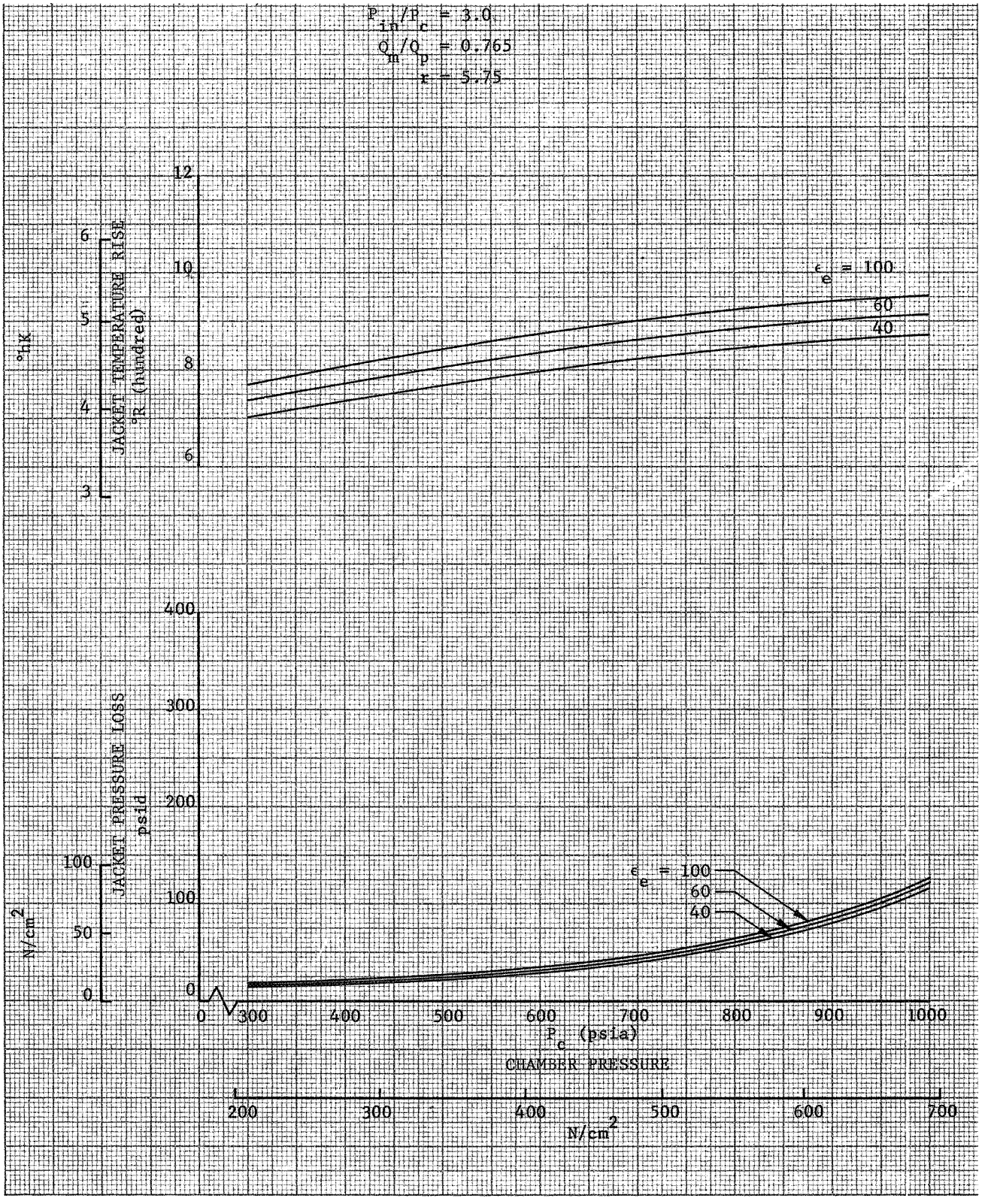


Figure A-8. Flox/Methane 5000-lb (22.24 kN) Coolant Temperature Rise and Pressure Loss - Case I

DF 70808

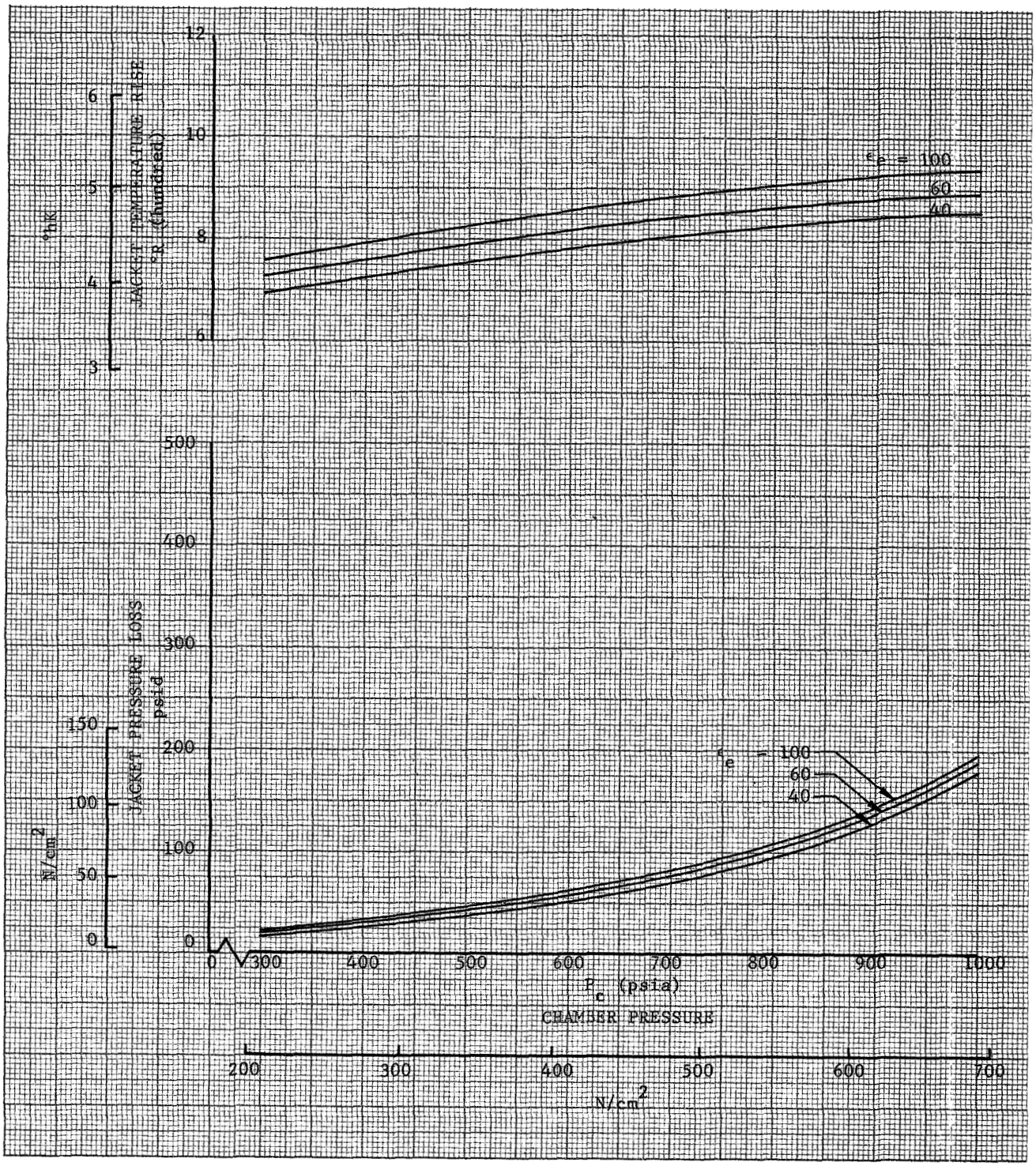


Figure A-9. Flox/Methane 5000-lb (22.24 kN) Coolant Temperature Rise and Pressure Loss - Case I DF 70809

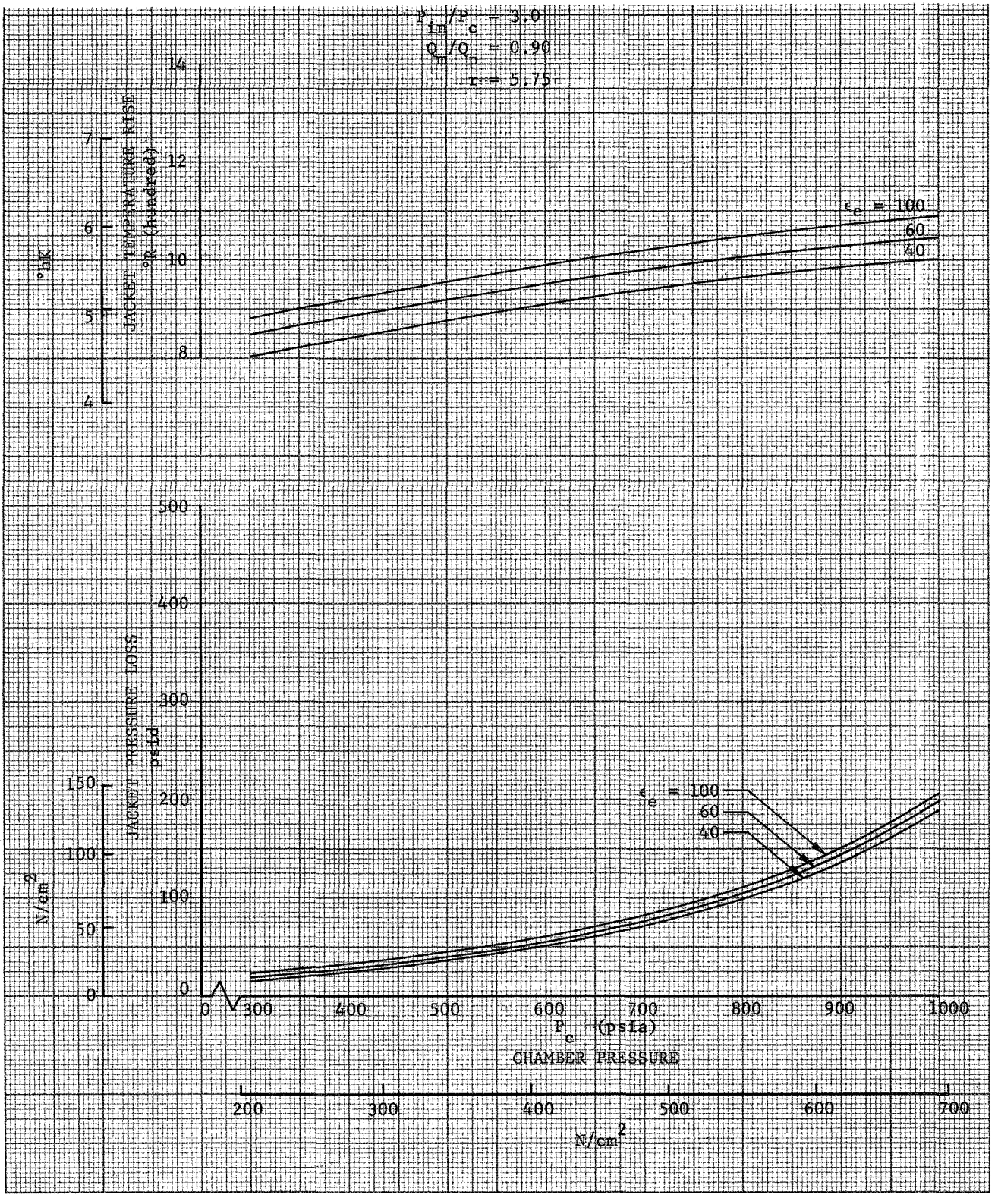


Figure A-10. Flox/Methane 5000-lb (22.24 kN) Coolant Temperature Rise and Pressure Loss - Case I

DF 70810

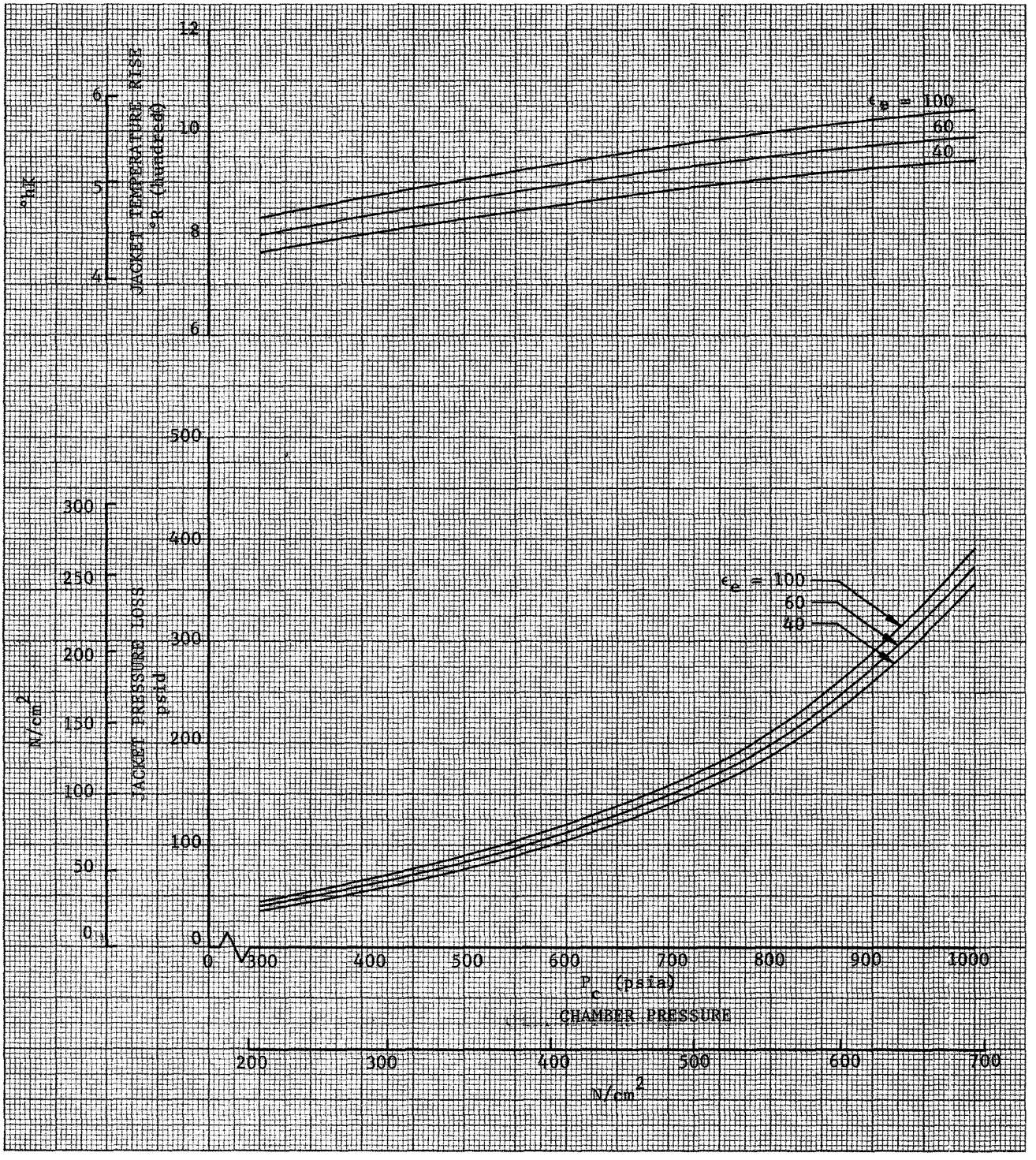


Figure A-11. Flox/Methane 5000-lb (22.24 kN) Coolant Temperature Rise and Pressure Loss - Case I DF 70811

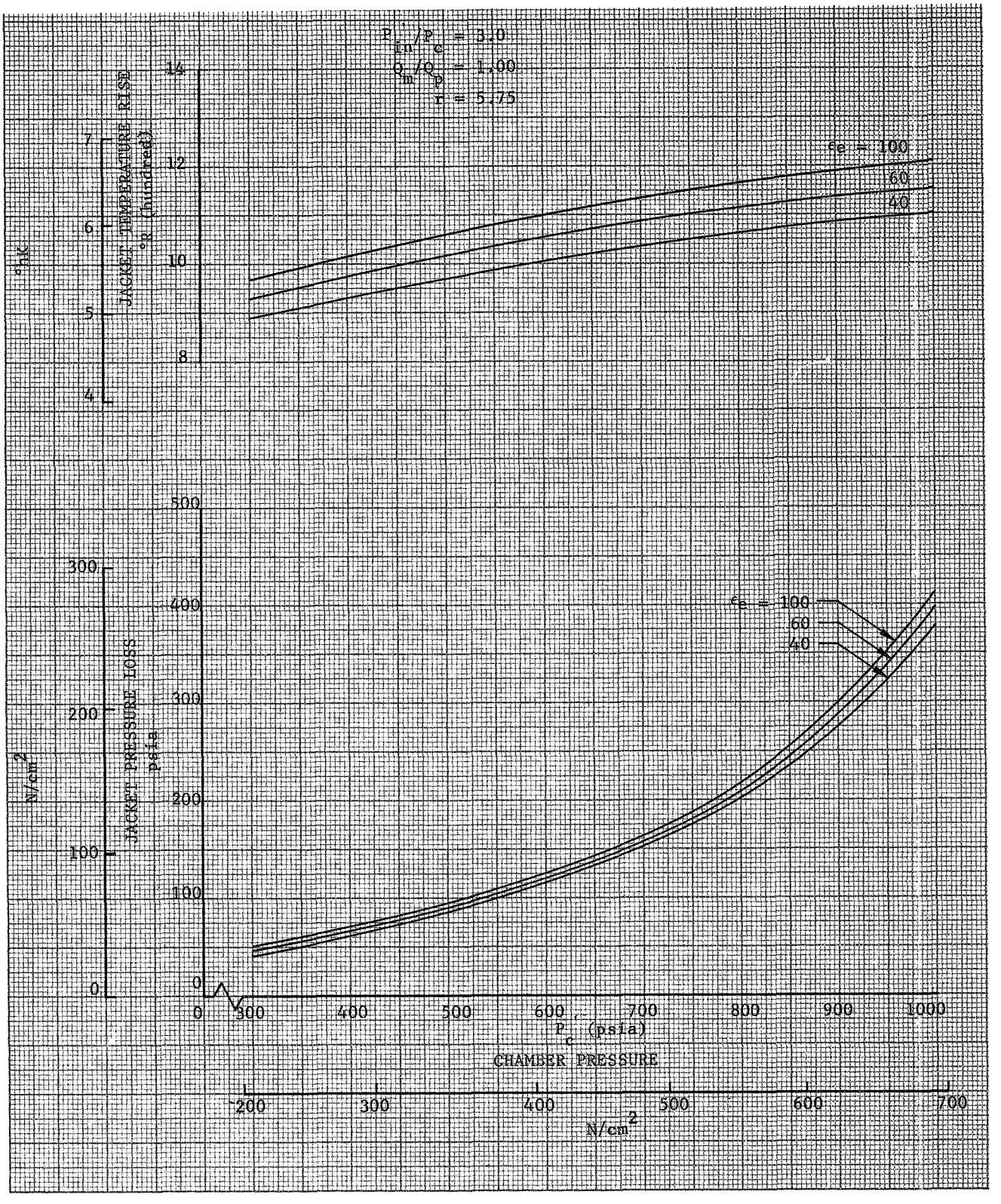


Figure A-12. Flox/Methane 5000-lb (22.24 kN) Coolant Temperature Rise and Pressure Loss - Case I

DF 70812

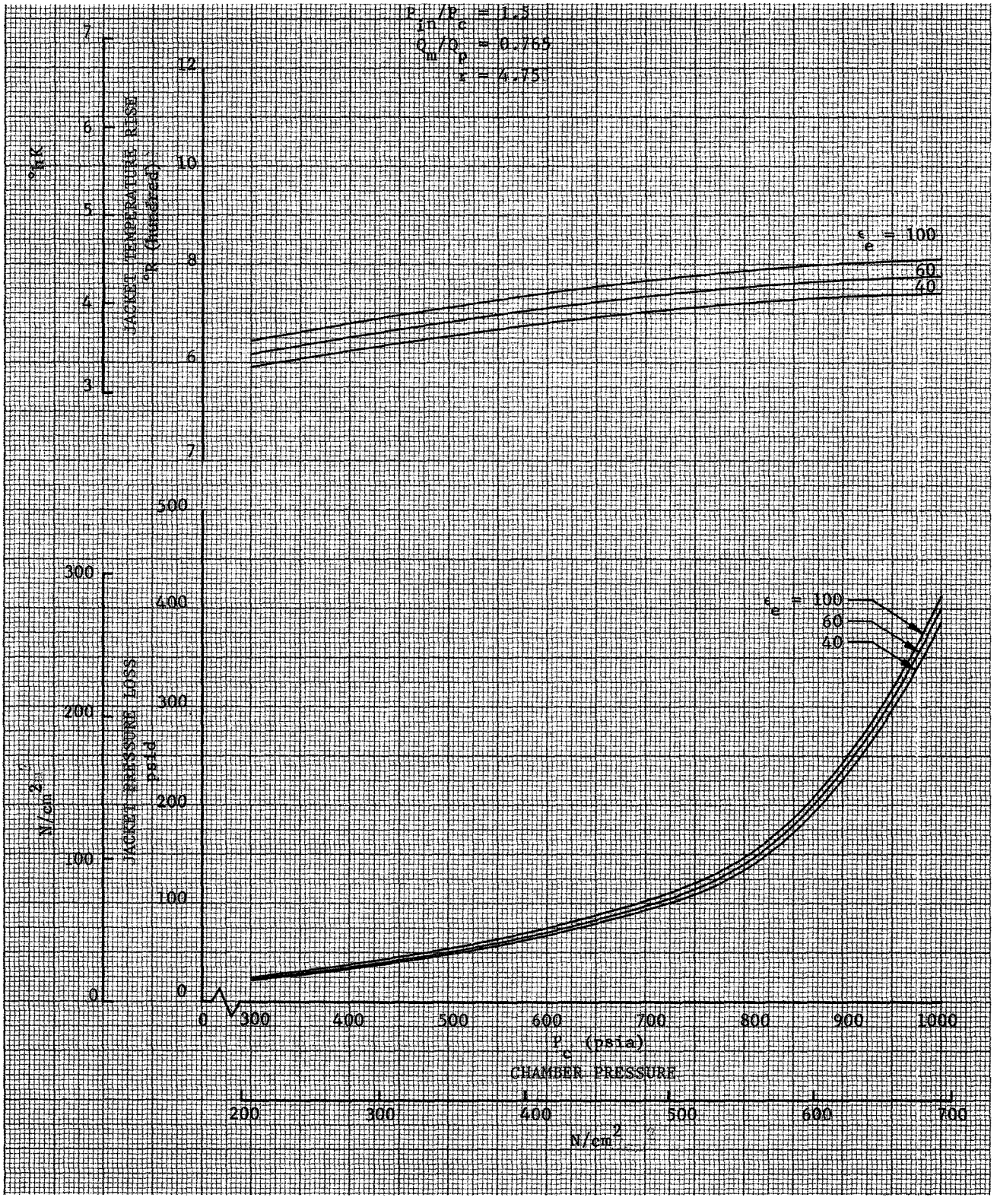


Figure A-13. Flox/Methane 5000-lb (22.24 kN) Coolant Temperature Rise and Pressure Loss - Case II DF 70813

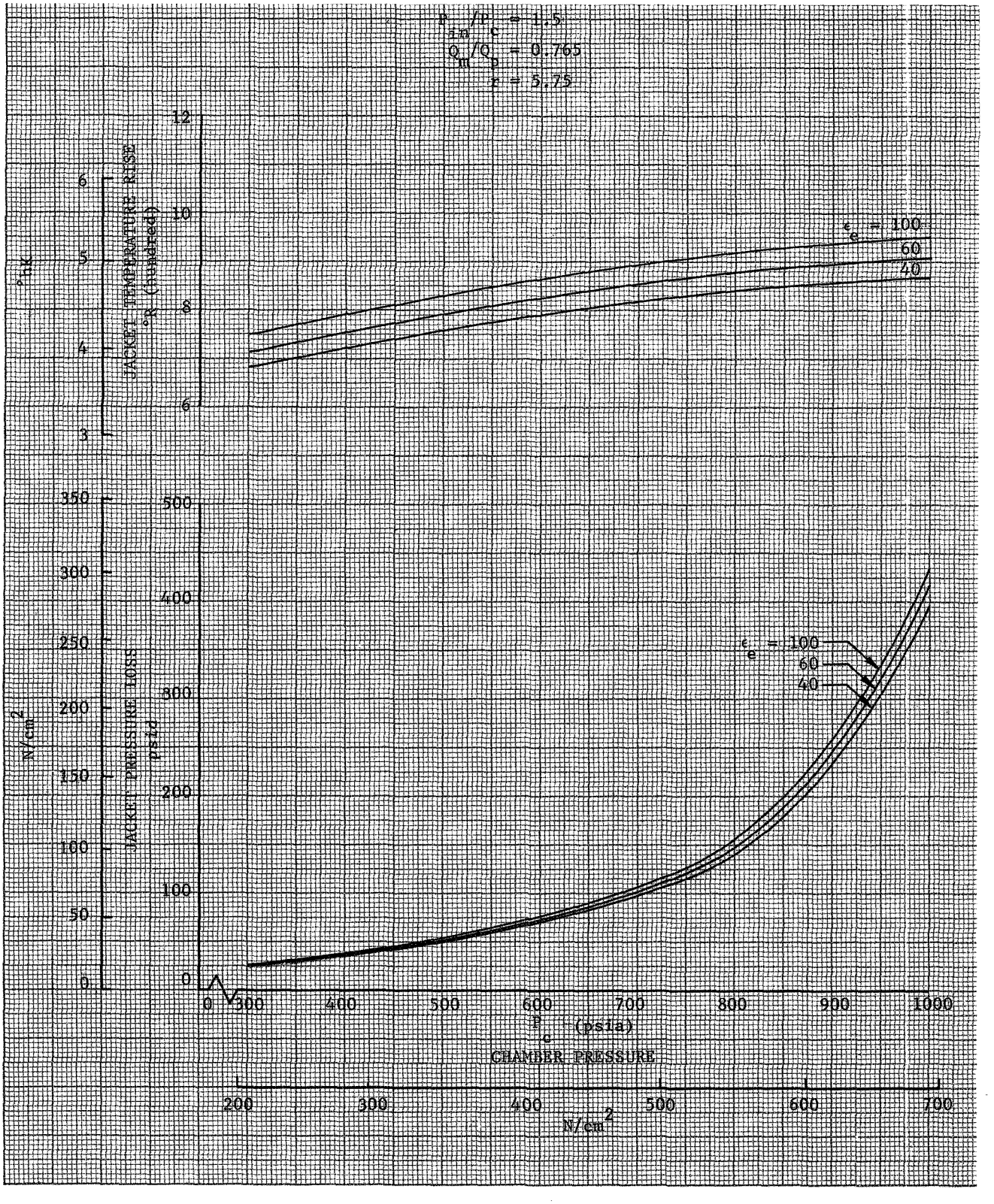


Figure A-14. Flox/Methane 5000-lb (22.24 kN) Coolant Temperature Rise and Pressure Loss - Case II DF 70814

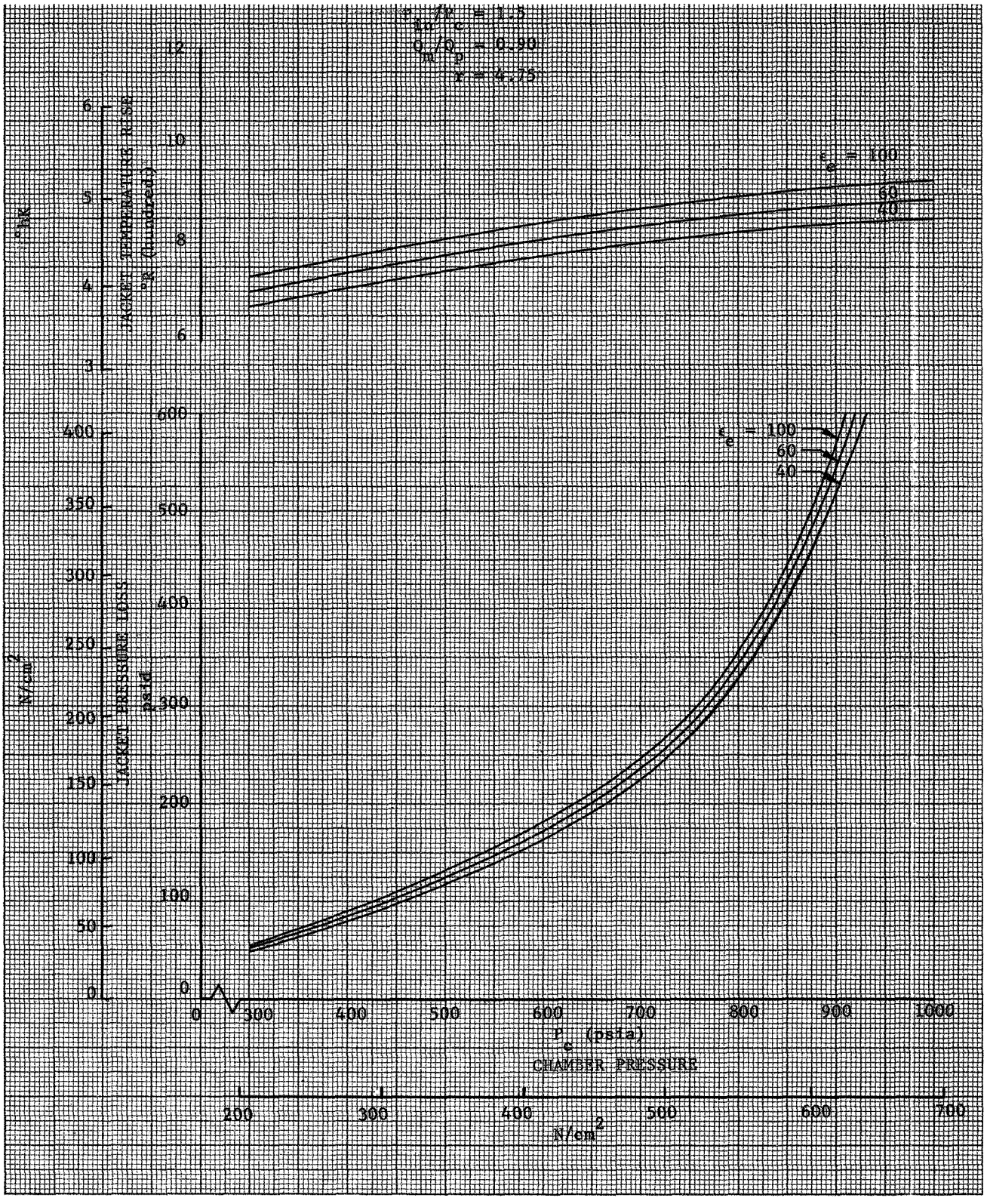


Figure A-15. Flox/Methane 5000-lb (22.24 kN) Coolant Temperature Rise and Pressure Loss - Case II

DF 70815

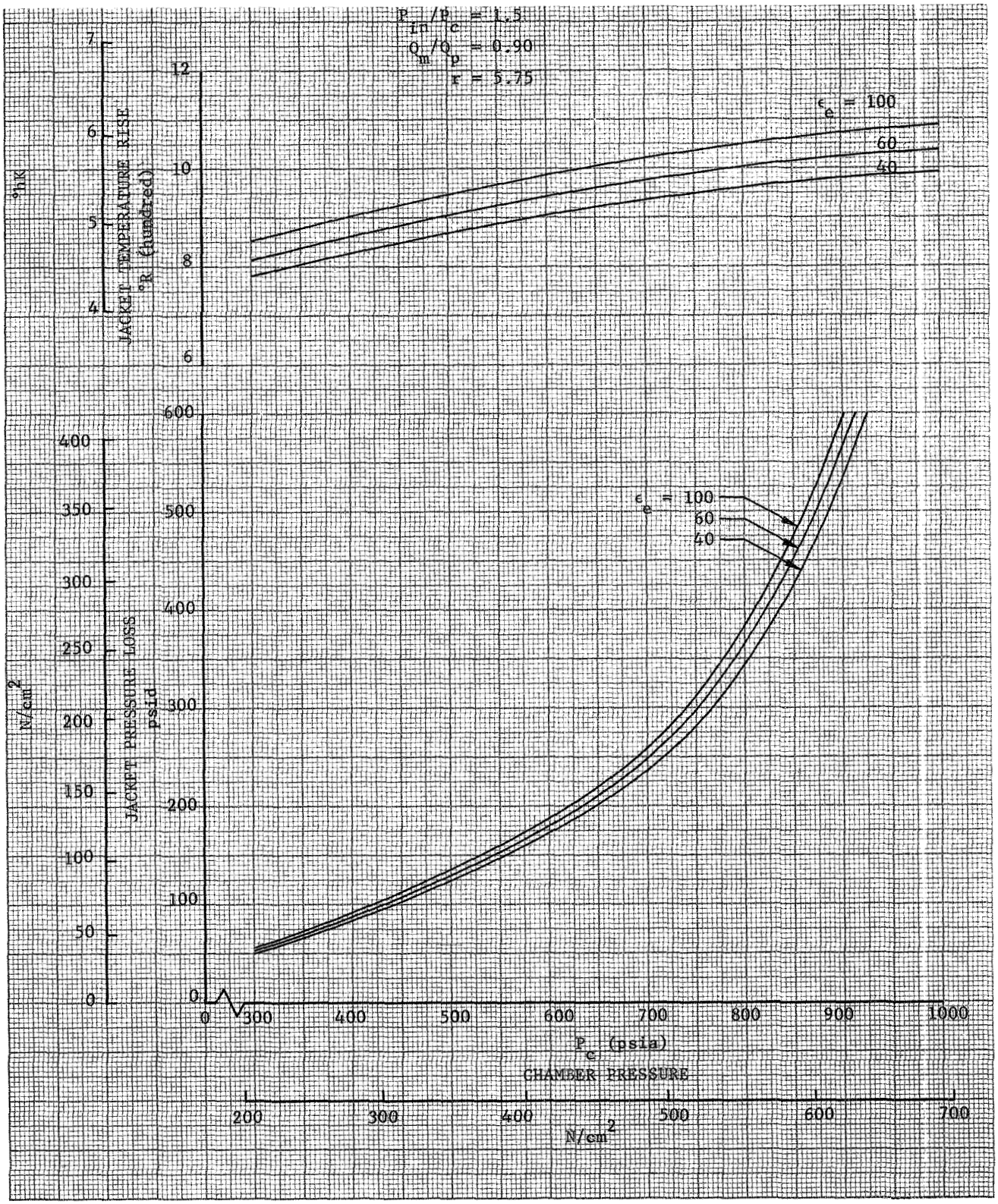


Figure A-16. Flox/Methane 5000-lb (22.24 kN) Coolant Temperature Rise and Pressure Loss - Case II

DF 70816

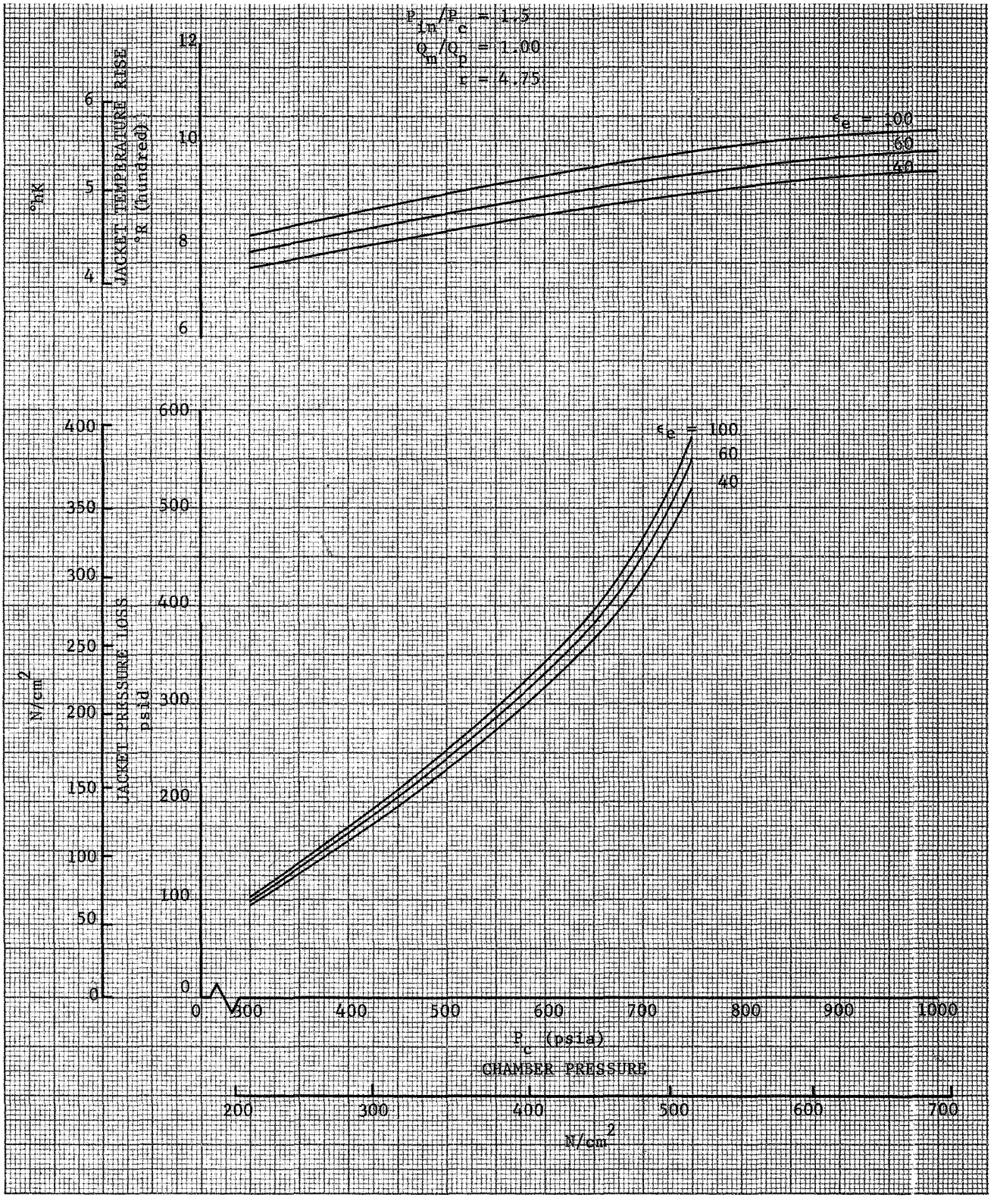


Figure A-17. Flox/Methane 5000-lb (22.24 kN) Coolant Temperature Rise and Pressure Loss - Case II DF 70817

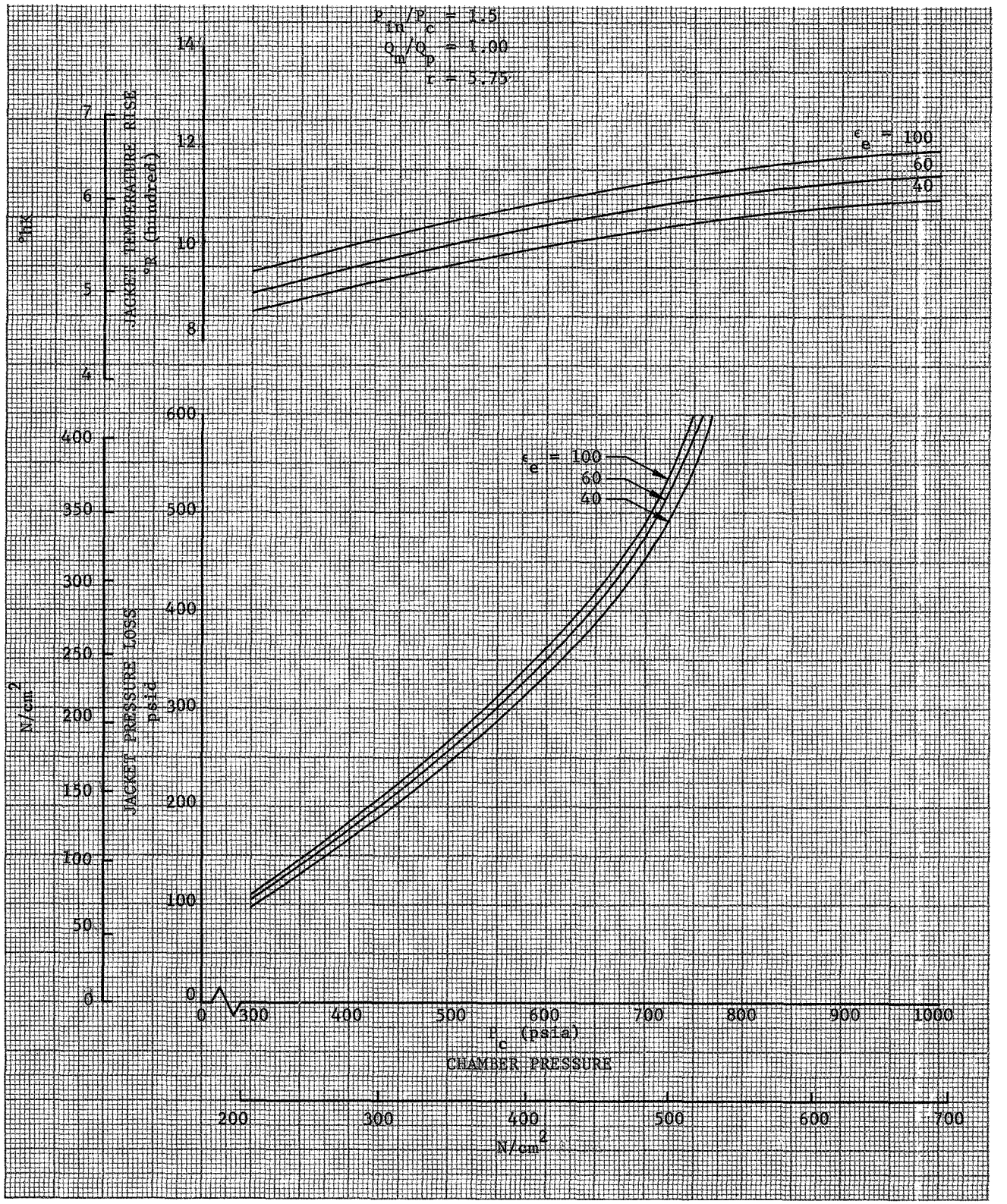


Figure A-18. Flox/Methane 5000-lb (22.24 kN) Coolant Temperature Rise and Pressure Loss - Case II DF 70818

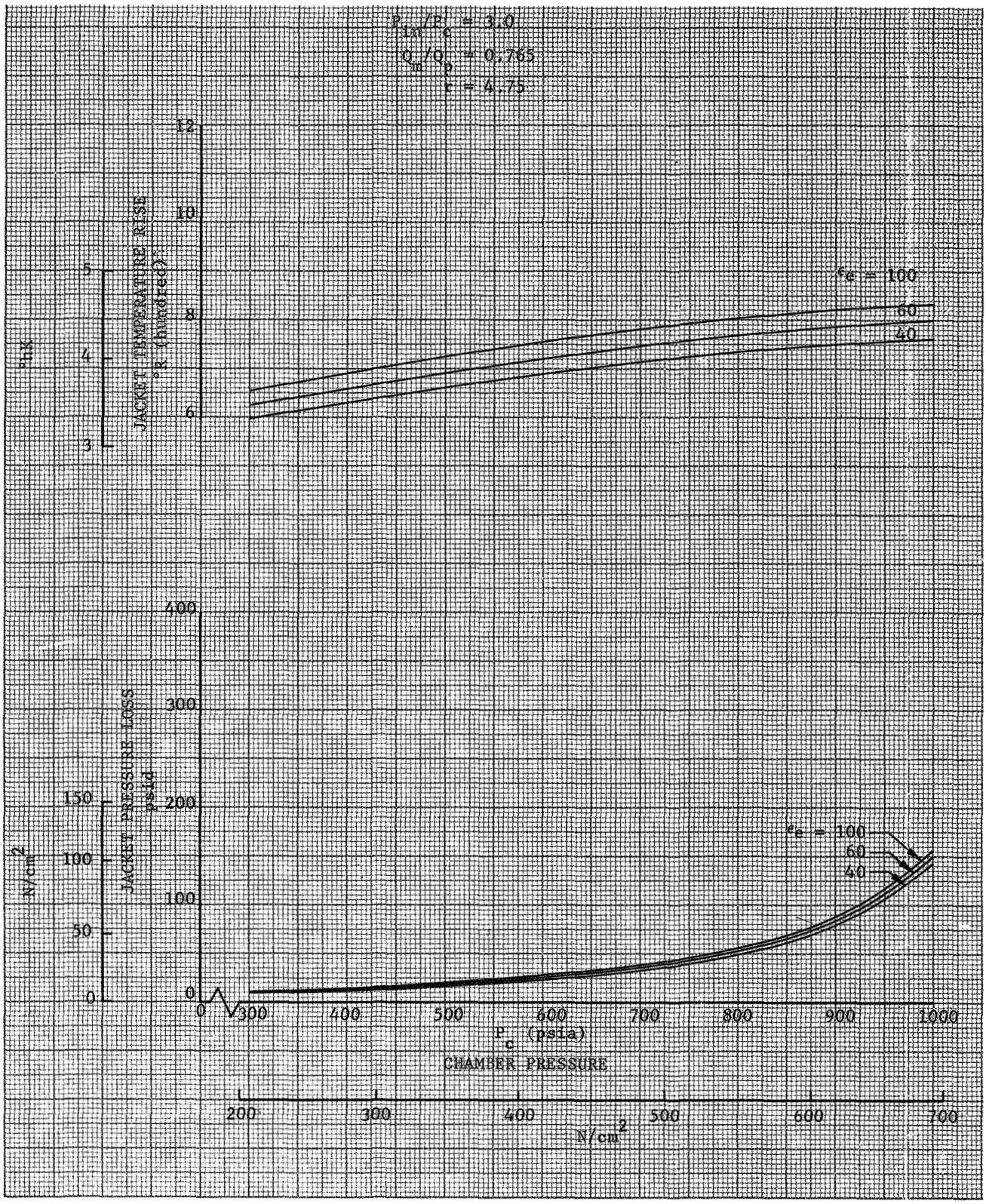


Figure A-19. Flox/Methane 5000-lb (22.24 kN) Coolant Temperature Rise and Pressure Loss - Case II DF 70819

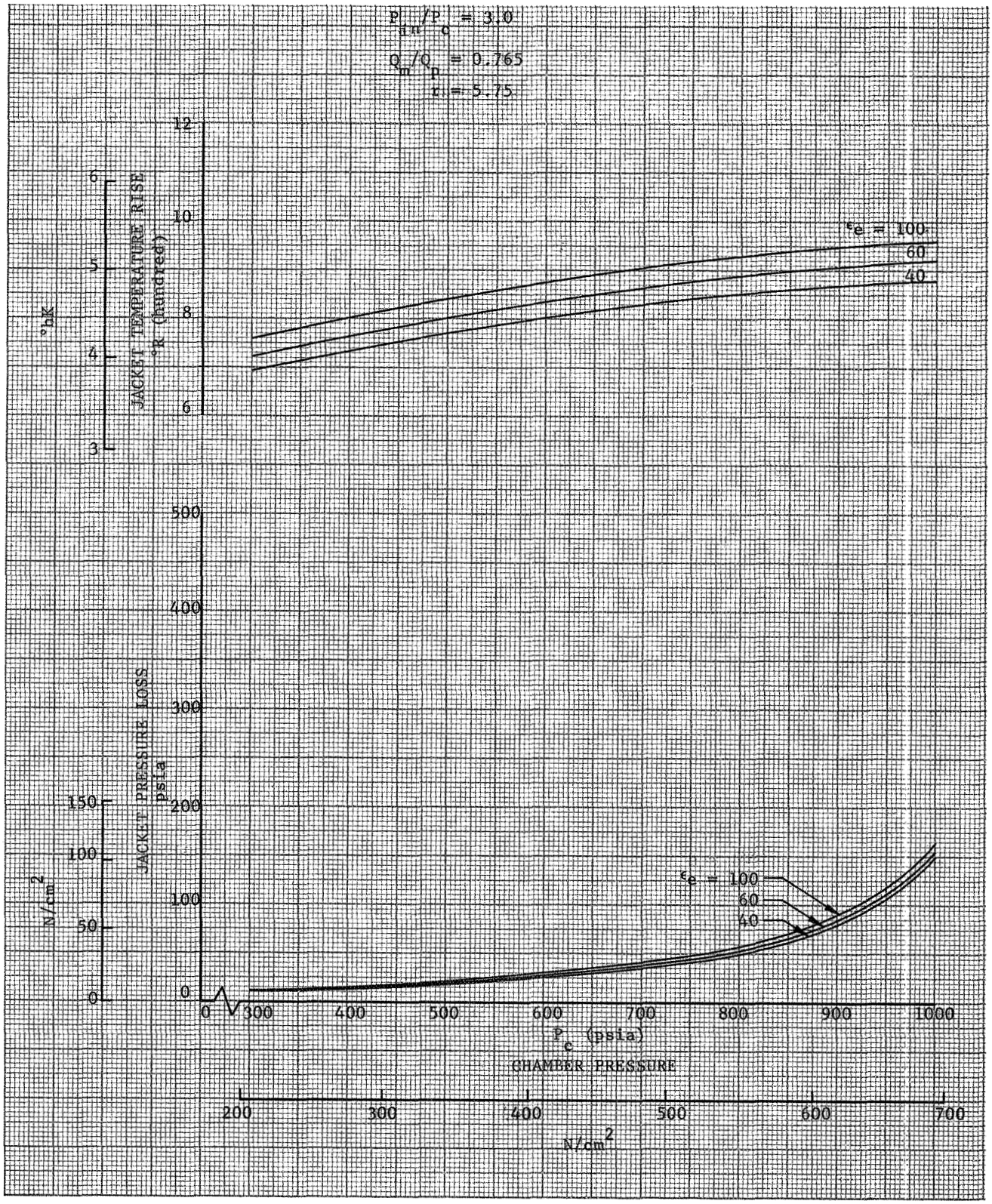


Figure A-20. Flox/Methane 5000-lb (22.24 kN) Coolant Temperature Rise and Pressure Loss - Case II

DF 70820

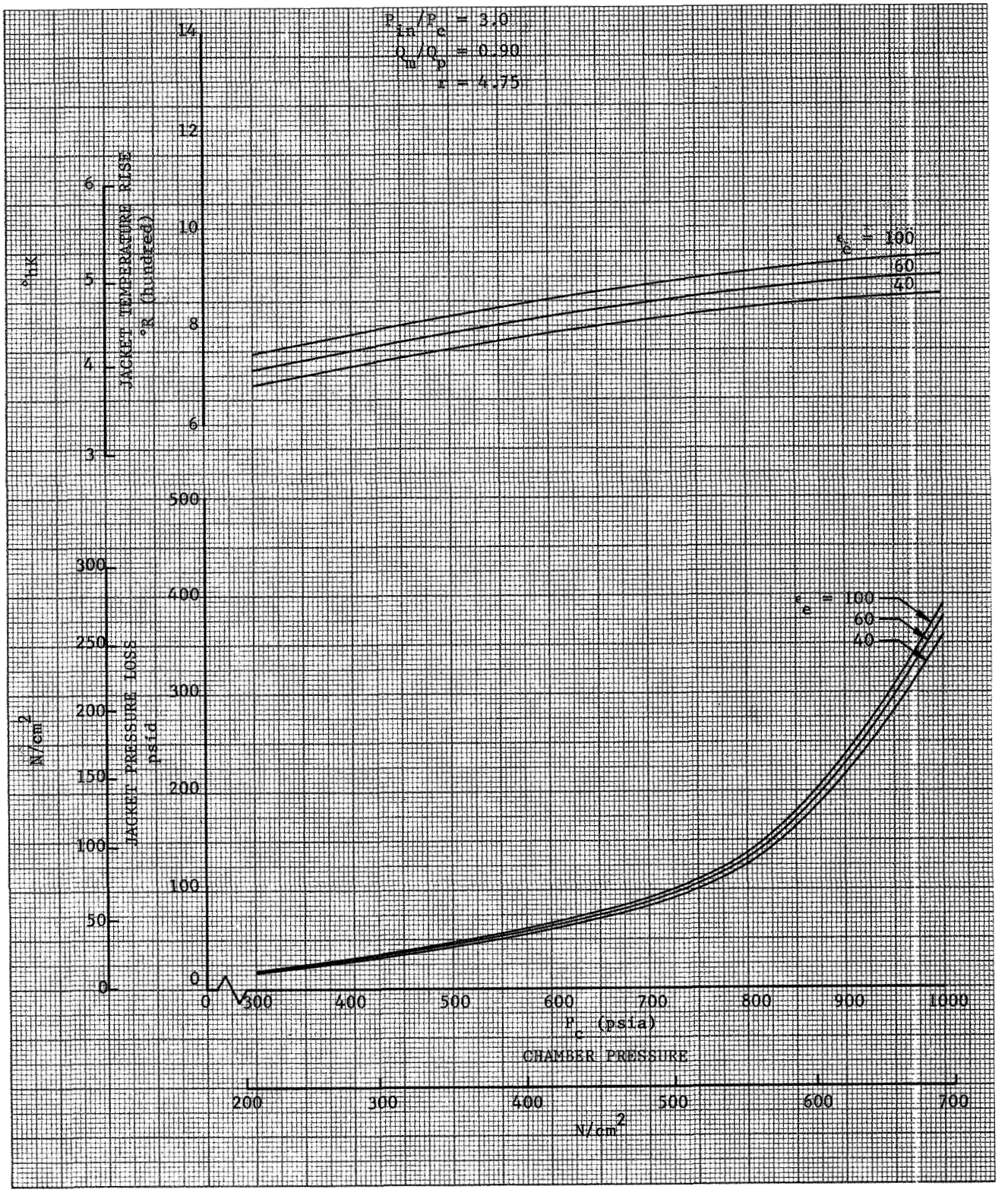


Figure A-21. Flox/Methane 5000-lb (22.24 kN) Coolant Temperature Rise and Pressure Loss - Case II DF 70821

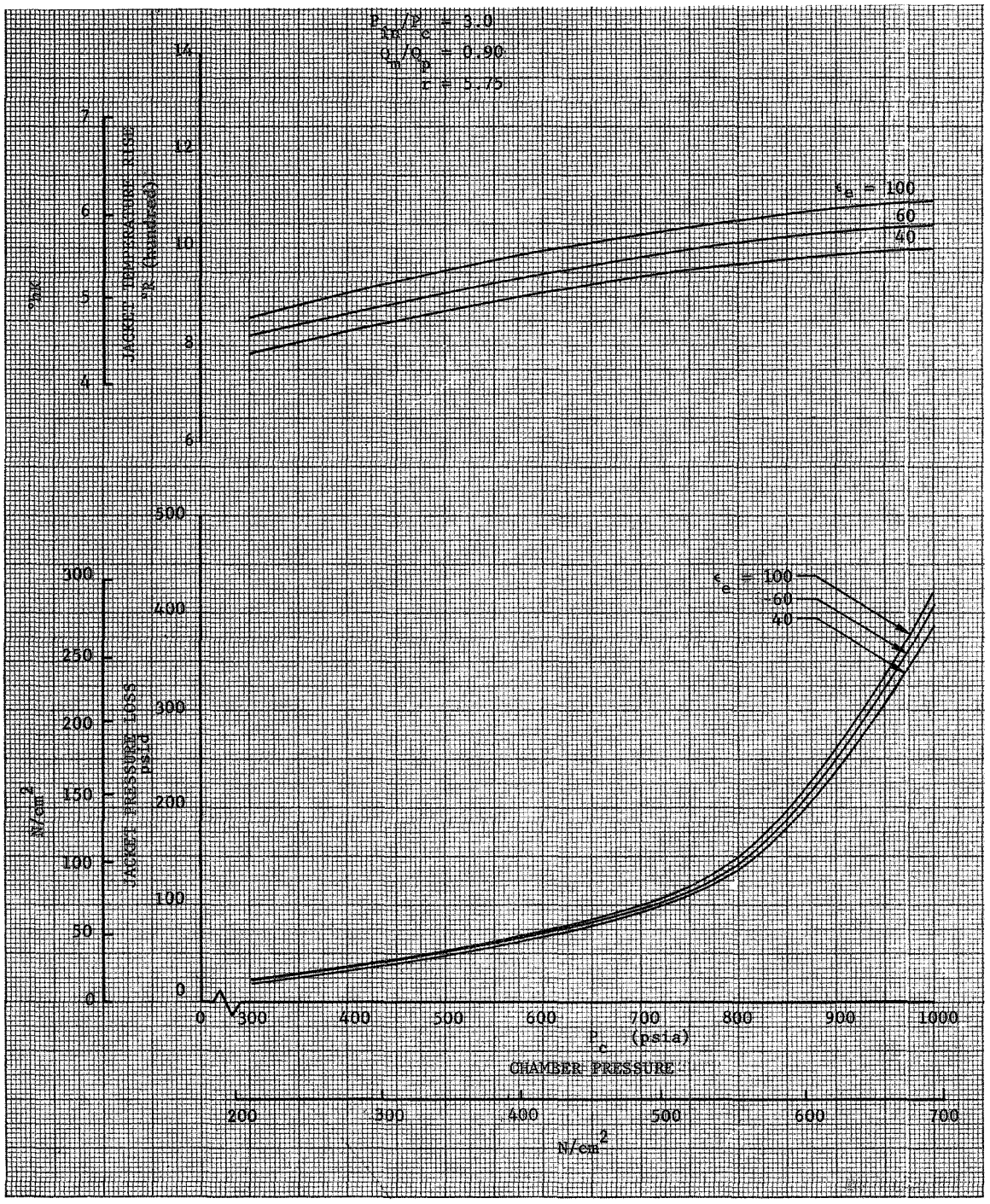


Figure A-22. Flox/Methane 5000-lb (22.24 kN) Coolant Temperature Rise and Pressure Loss - Case II DF 70822

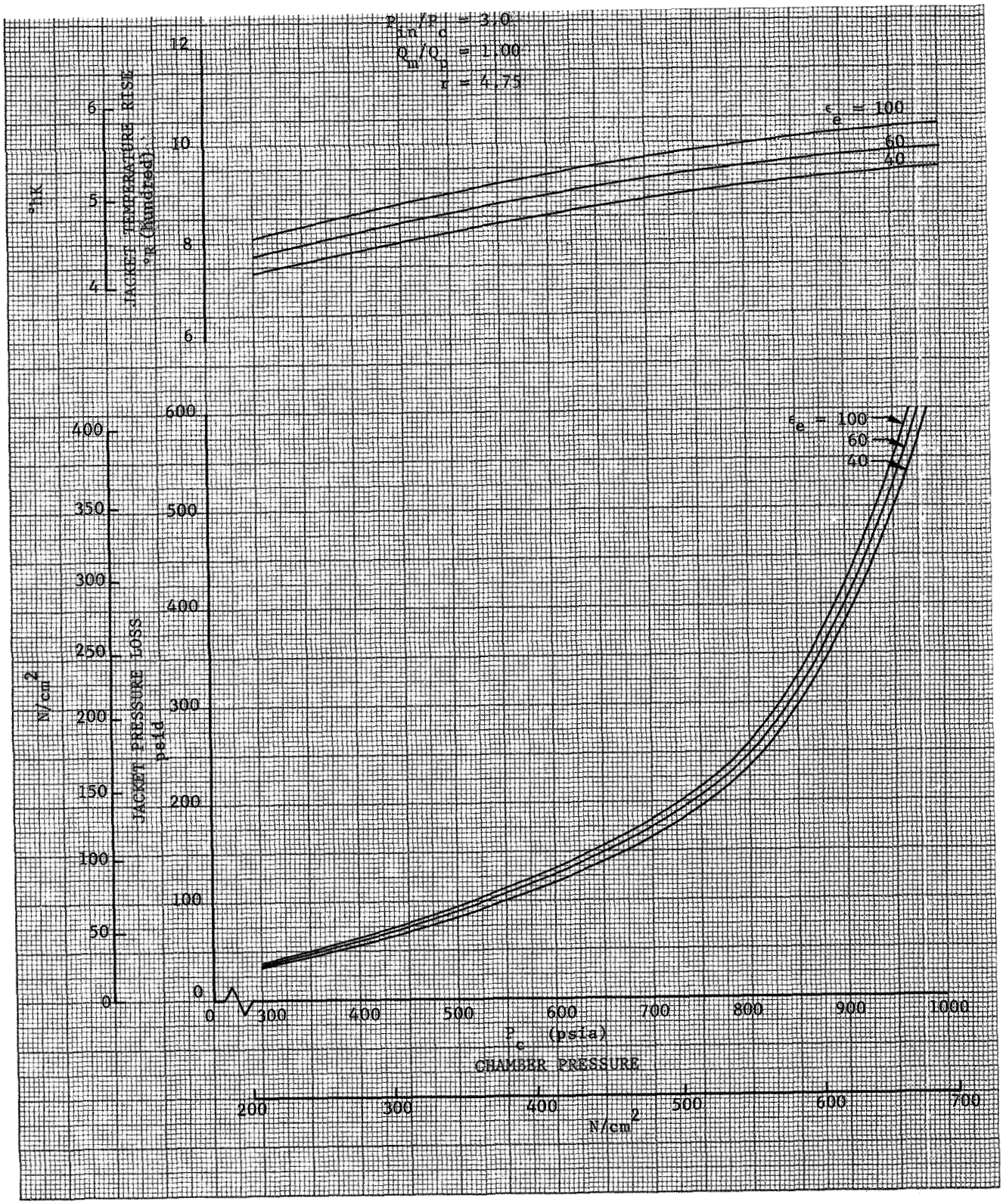


Figure A-23. Flox/Methane 5000-lb (22.24 kN) Coolant Temperature Rise and Pressure Loss - Case II

DF 70823

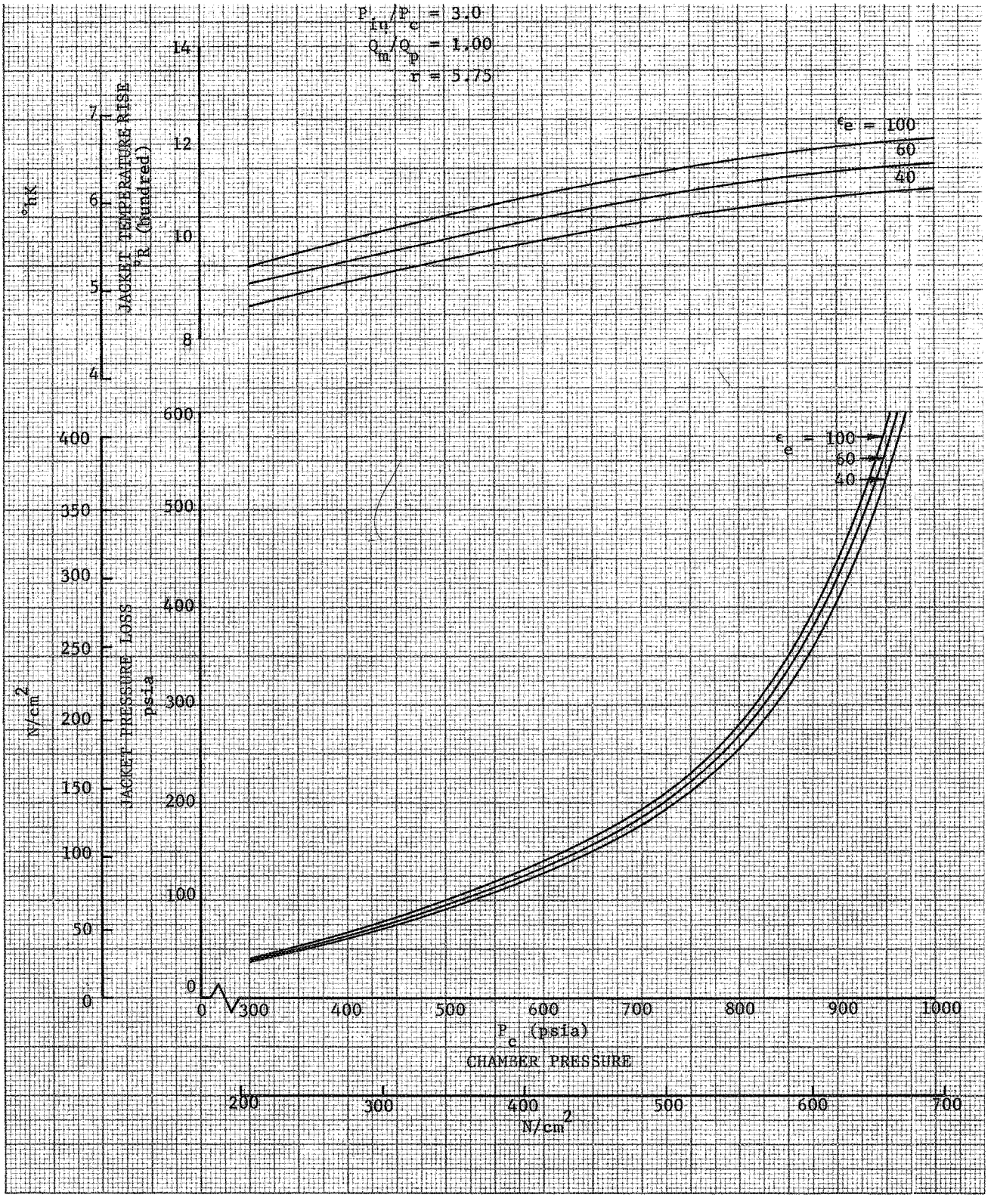


Figure A-24. Flox/Methane 5000-lb (22.24 kN) Coolant Temperature Rise and Pressure Loss - Case II DF 70824

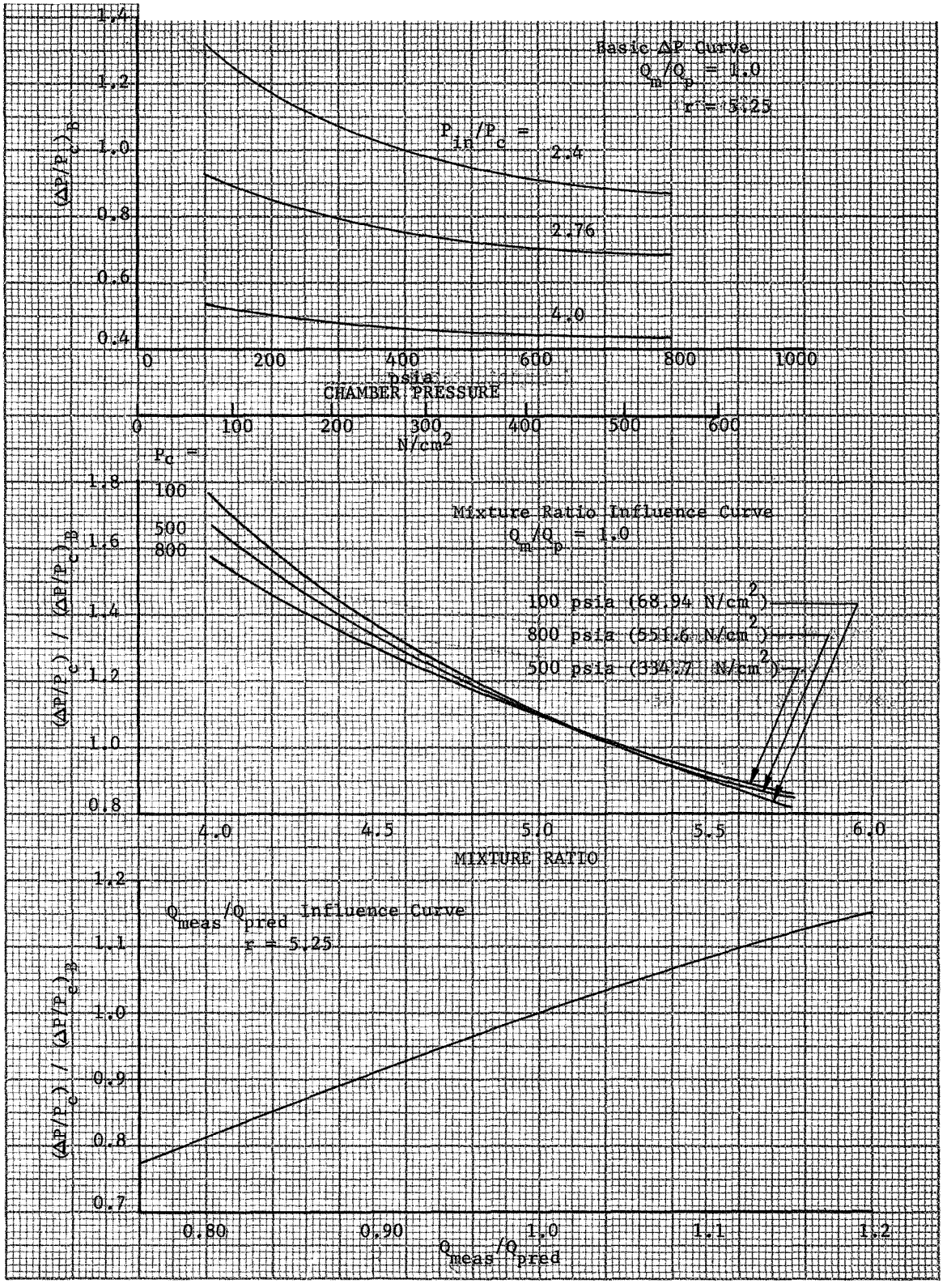


Figure A-25. Thrust Chamber Cooling Characteristics DF 70858
Design I - Expander Cycle Jacket Pressure Drop

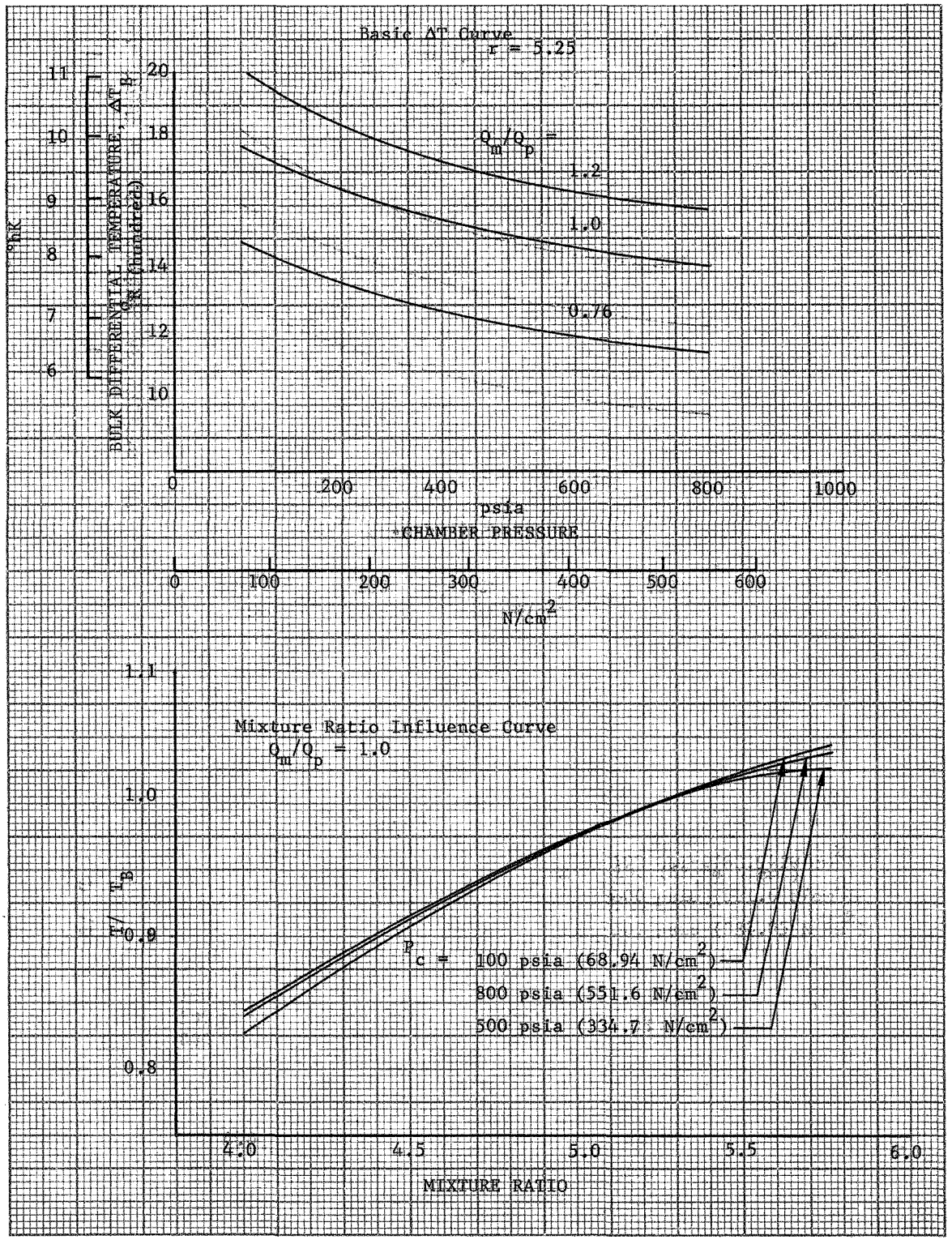


Figure A-26. Thrust Chamber Cooling Characteristics Design I - Expander Cycle Bulk Temperature Rise

DF 70859

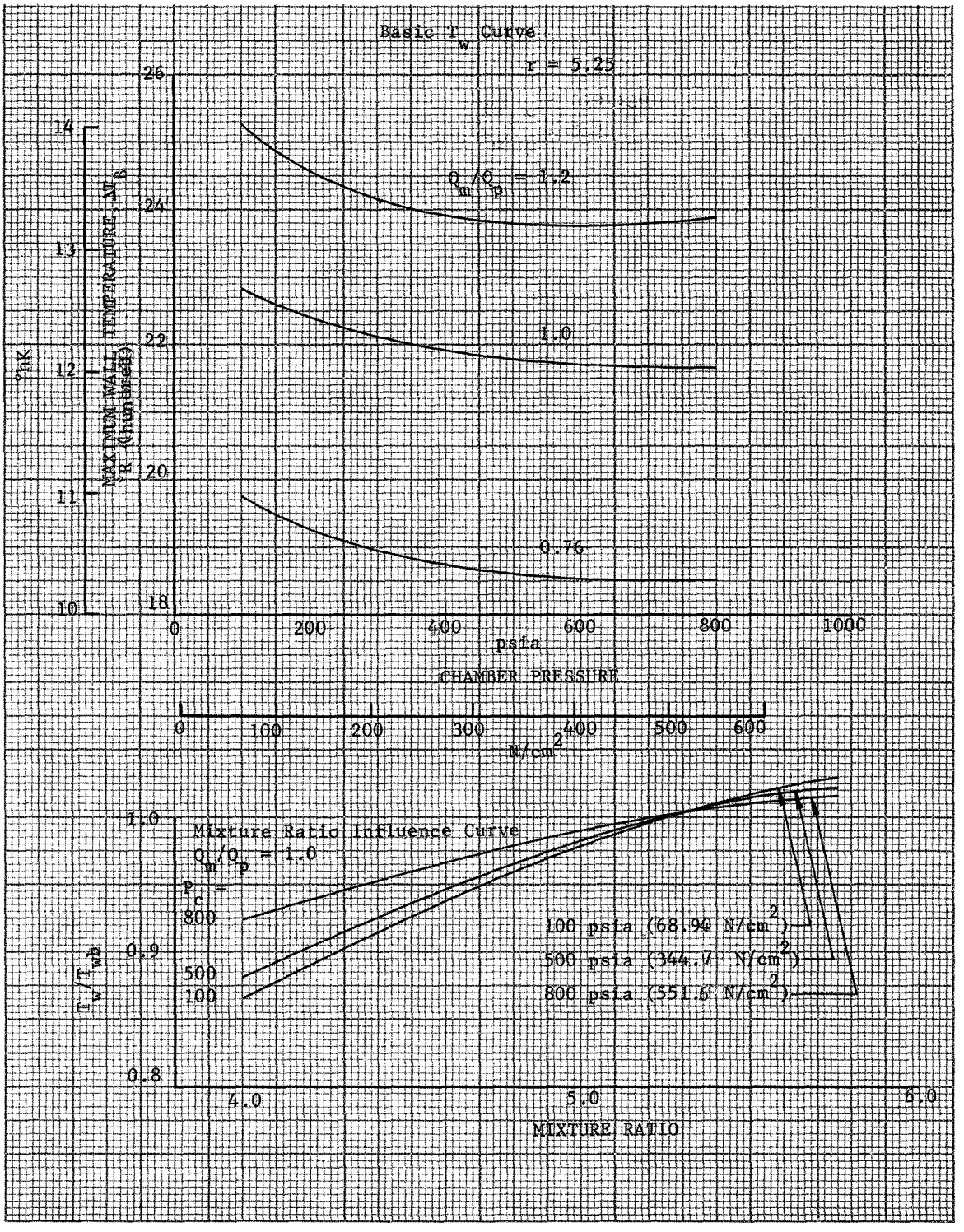


Figure A-27. Thrust Chamber Cooling Characteristics Design I - Expander Cycle Maximum Wall Temperature

DF 70860

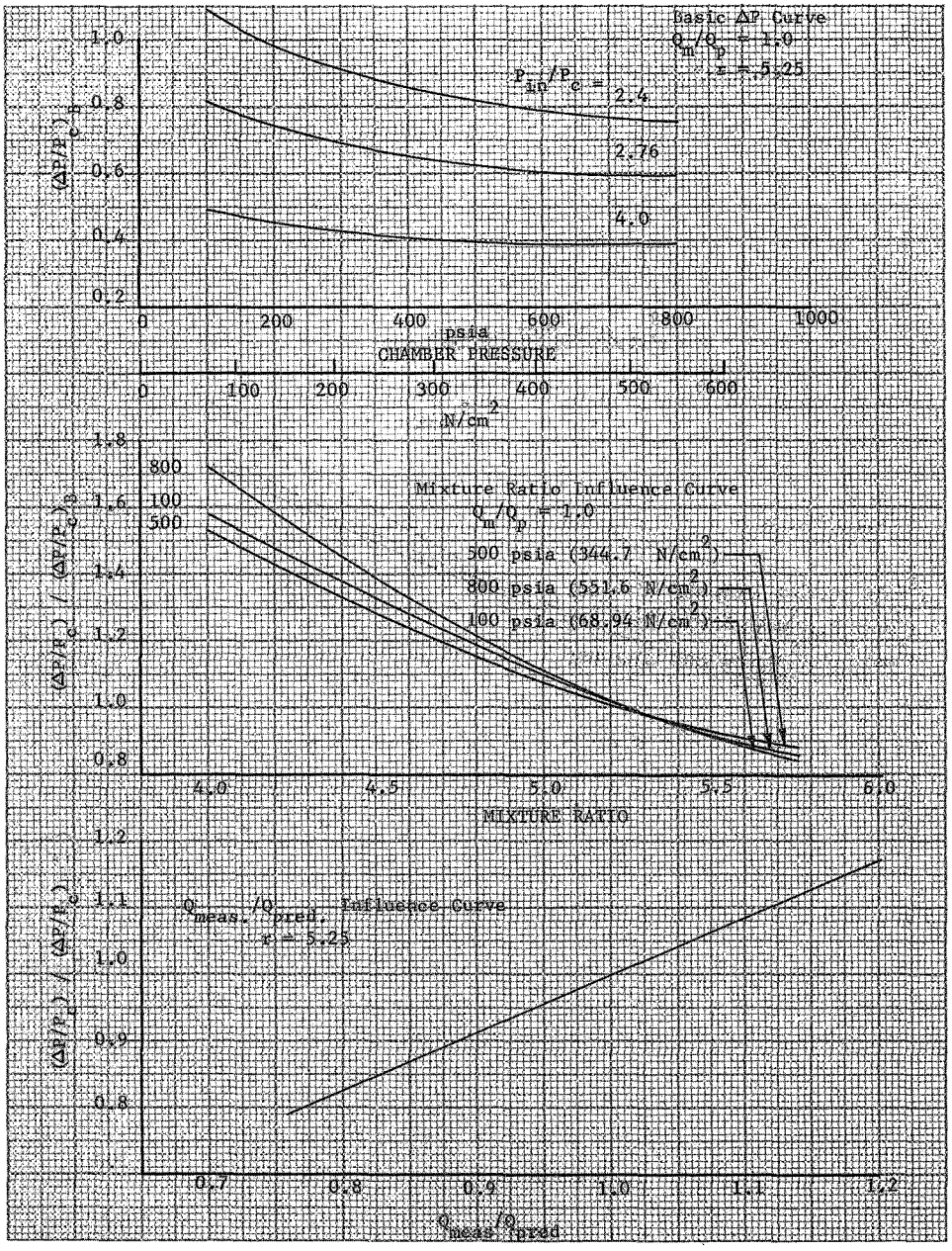


Figure A-28. Thrust Chamber Cooling Characteristics Design II - Expander Cycle Jacket Pressure Drop

DF 70861

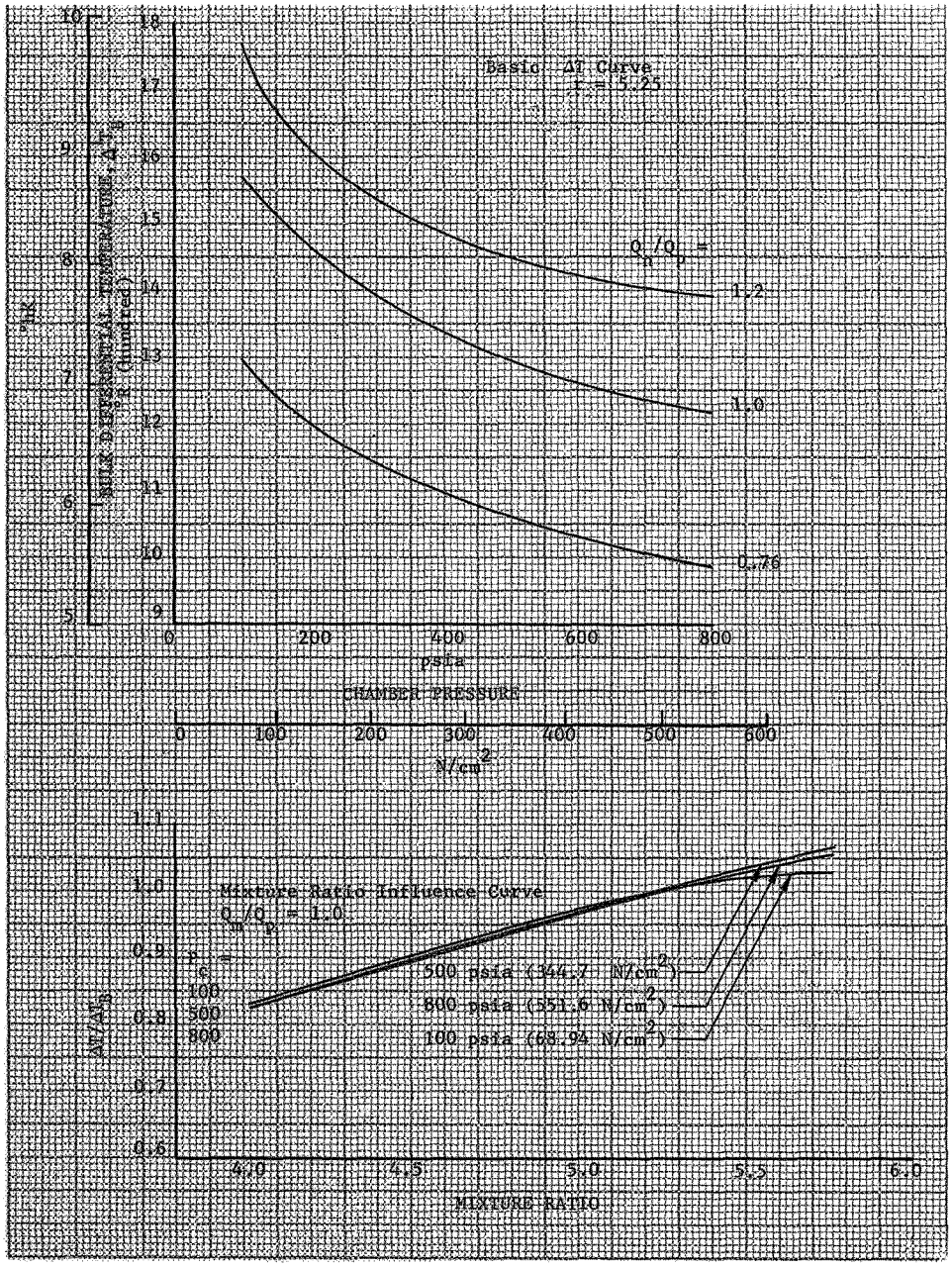


Figure A-29. Thrust Chamber Cooling Characteristics Design II - Expander Cycle Bulk Temperature Rise

DF 70862

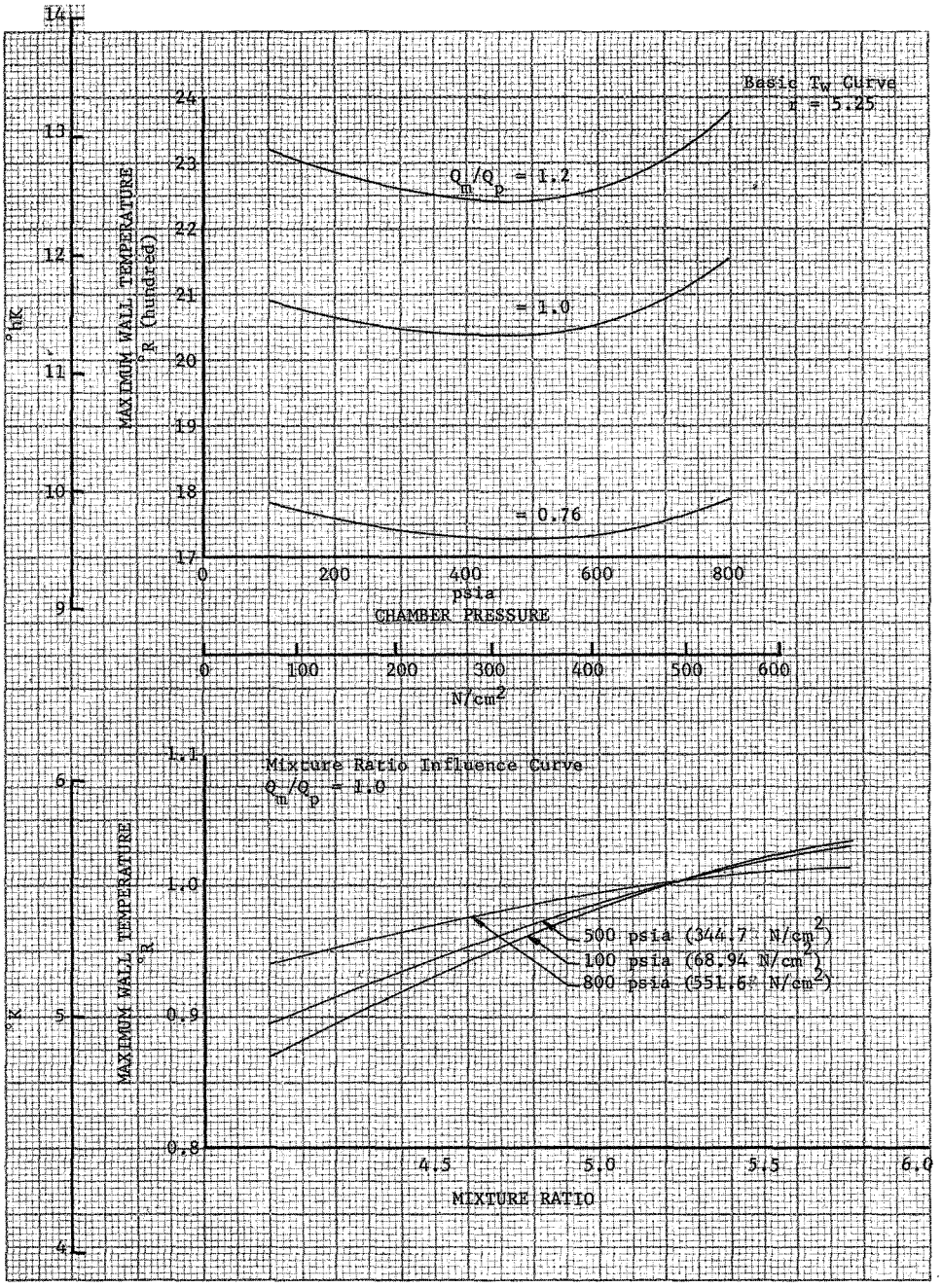


Figure A-30. Thrust Chamber Cooling Characteristics Design II - Expander Cycle Maximum Wall Temperature

DF 70863

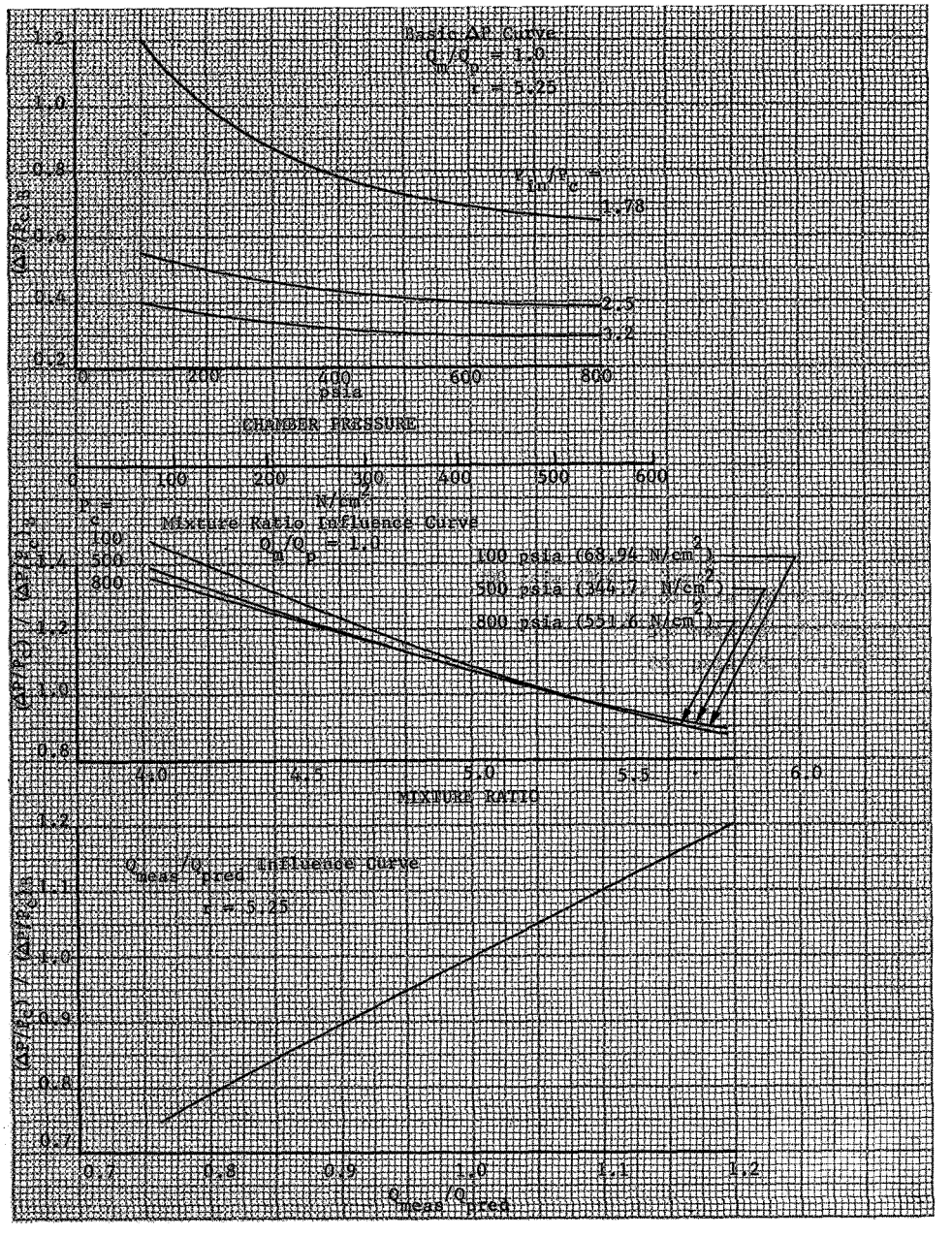


Figure A-31. Thrust Chamber Cooling Characteristics DF 70864
Design I - Auxiliary Heat Exchanger Cycle
Thrust Chamber Section

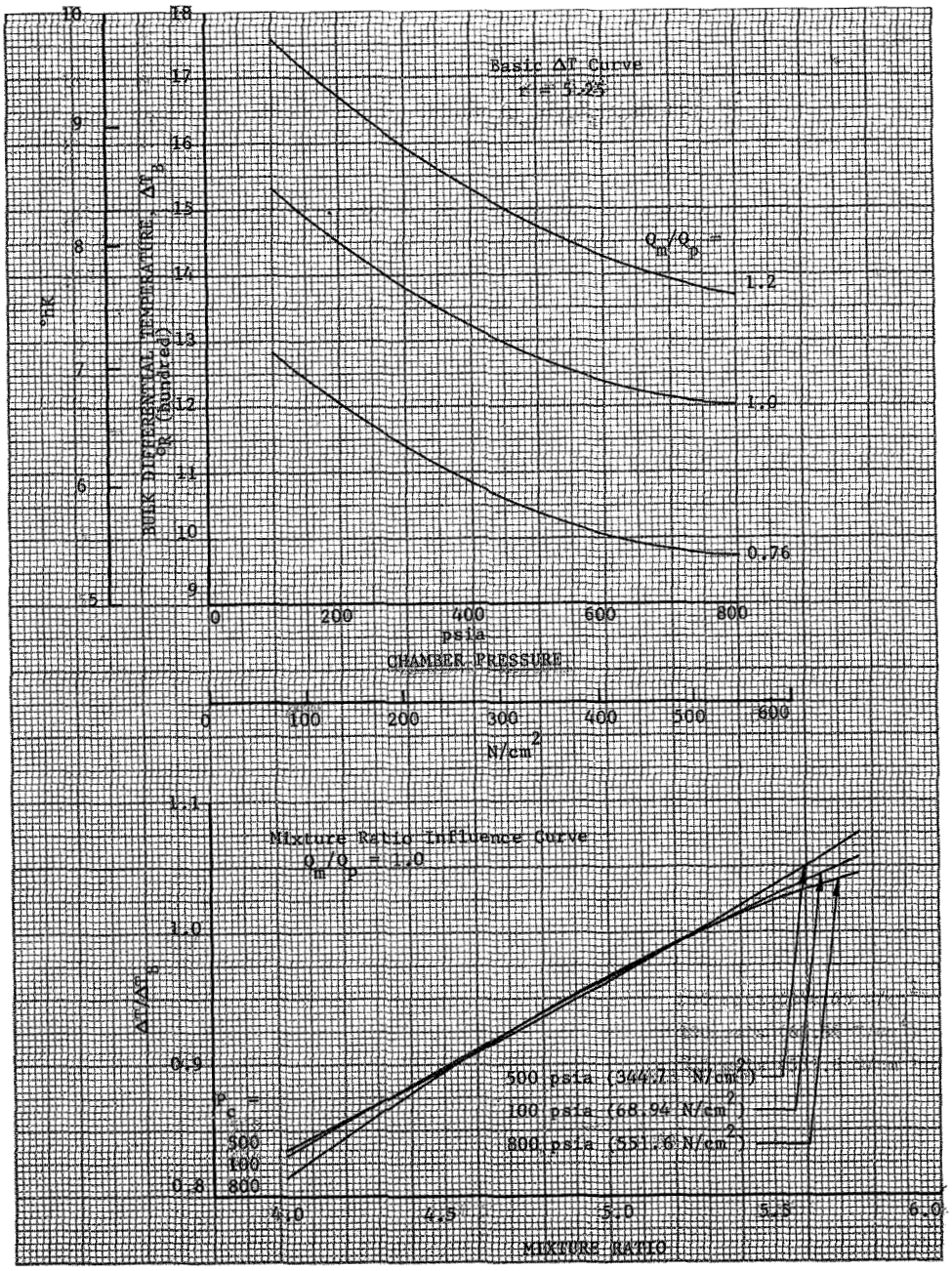


Figure A-32. Thrust Chamber Cooling Characteristics DF 70865
Design I - Auxiliary Heat Exchanger Cycle
Thrust Chamber Section

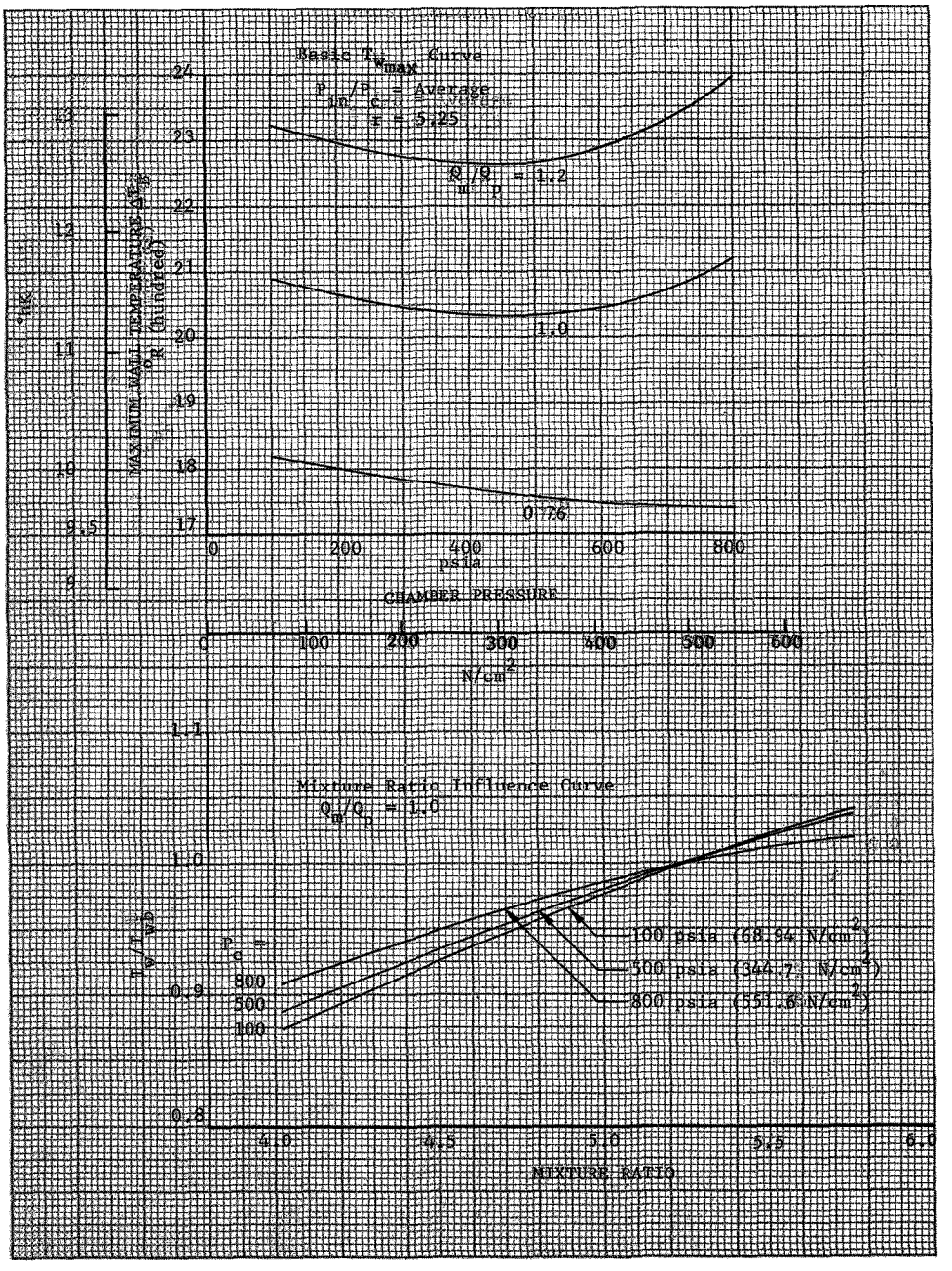


Figure A-33. Thrust Chamber Cooling Characteristics DF 70866
Design I - Auxiliary Heat Exchanger Cycle
Thrust Chamber Section

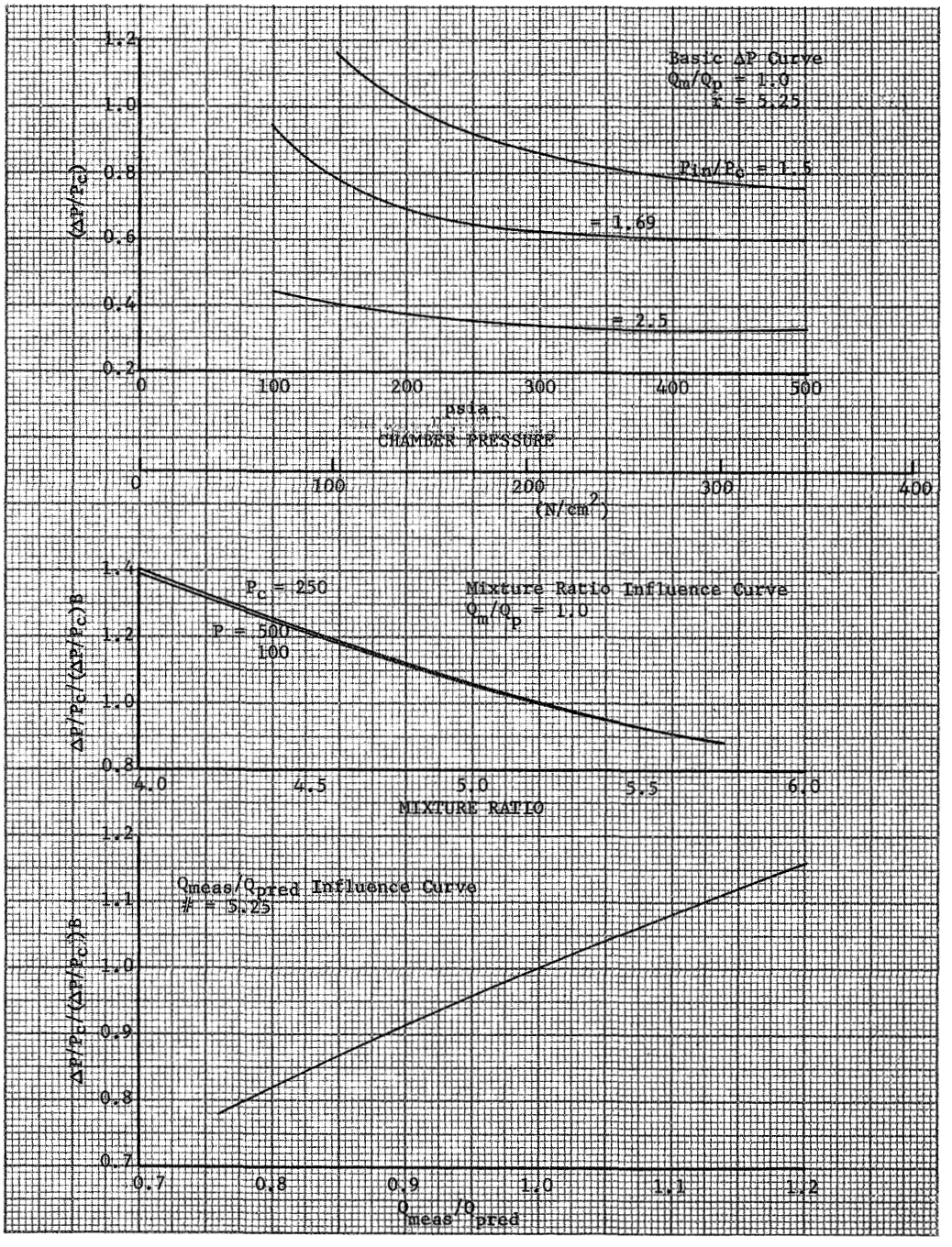


Figure A-34. Thrust Chamber Cooling Characteristics DF 69495
Design II - Auxiliary Heat Exchanger Cycle
Thrust Chamber Section

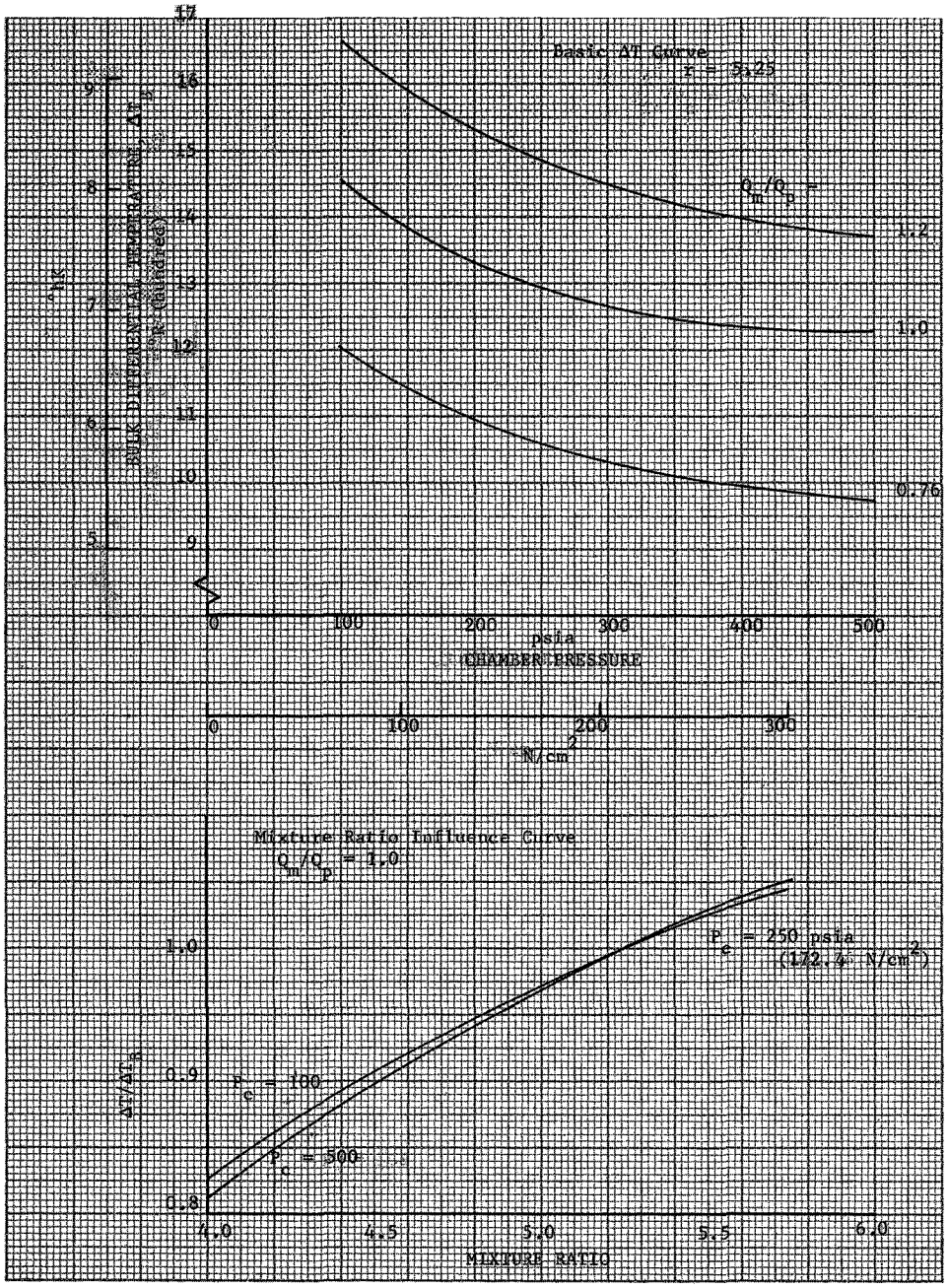


Figure A-35. Thrust Chamber Cooling Characteristics DF 70868
Design II - Auxiliary Heat Exchanger Cycle
Thrust Chamber Section

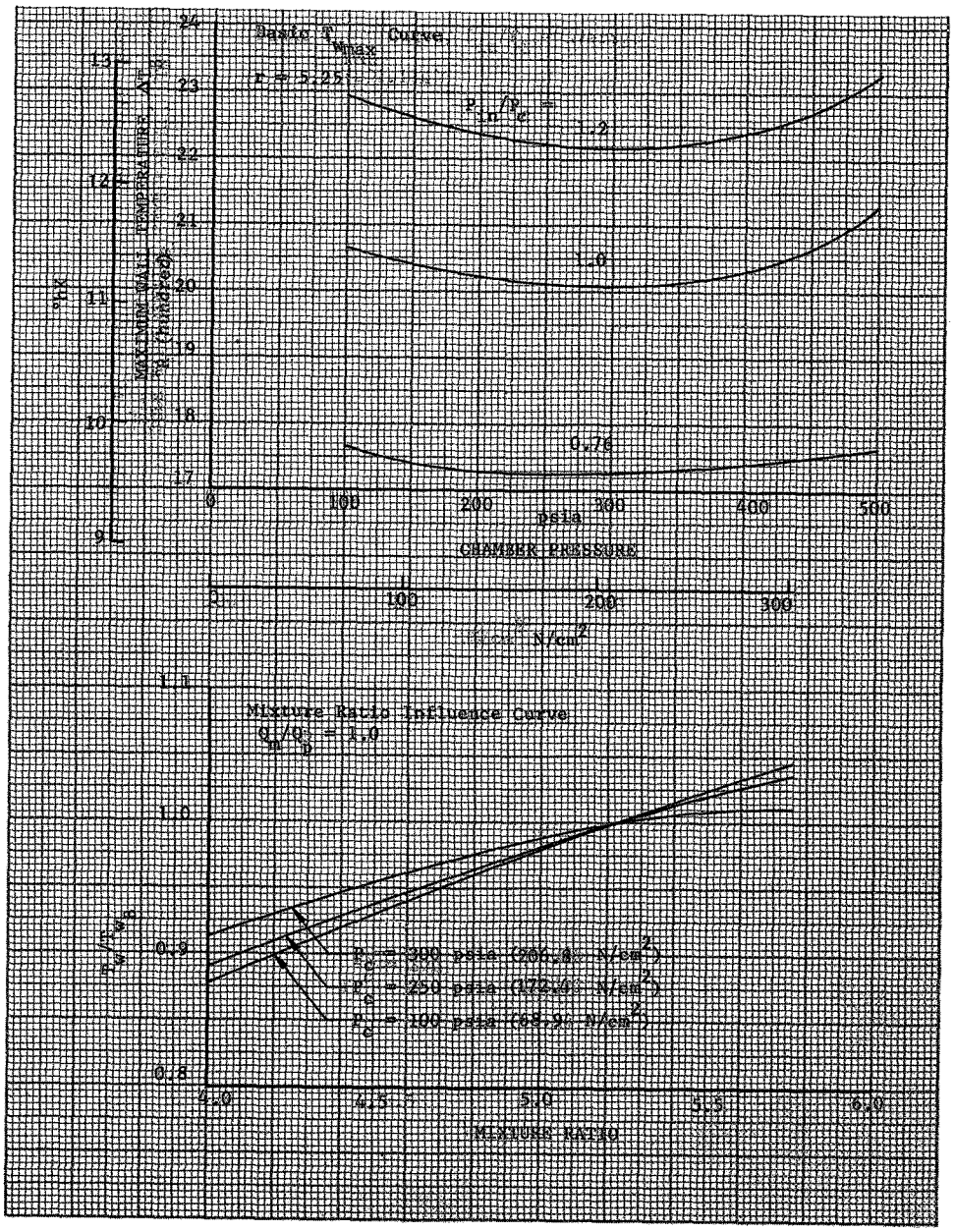


Figure A-36. Thrust Chamber Cooling Characteristics DF 70867
Design II - Auxiliary Heat Exchanger Cycle
Thrust Chamber Section Maximum Wall Temperature

## APPENDIX B
## NOMENCLATURE

| Symbol | Description | Unit |
|---|---|---|
| A | Area | $in.^2$ ($cm^2$) |
| ADM | Turbine admission area | |
| b | Coolant pressure drop influence coefficient | |
| b' | Coolant temperature rise influence coefficient | |
| c* | Characteristic velocity | ft/sec (m/sec) |
| $C_D$ | Discharge coefficient | |
| $C_F$ | Thrust coefficient | |
| $C_s$ | Theoretical stream thrust coefficient (predicted aerodynamic efficiency accounting for friction and divergence losses) | |
| d | Depth | in. (cm) |
| hp | Power | horsepower (W) |
| $I_{vac}$ | Vacuum specific impulse | $lb_f$-sec/$lb_m$ (N-sec/kg) |
| L* | Characteristic length | inches (cm) |
| N | Rotational speed | rpm (rad/s) |
| P | Pressure | psia ($N/cm^2$) |
| PR | Qualitative performance rating | |
| $Q_m$ | Estimated heat transfer rate based on experimental data | Btu/sec (joule/sec) |
| $Q_p$ | Theoretically predicted heat transfer rate based on Bartz boundary layer analysis | Btu/sec (joule/sec) |
| r | Oxidizer-to-fuel weight flow ratio | |
| s | Land width | |
| t | Temperature | $^oR$ ($^oK$) |
| w | Width | in. (cm) |

| Symbol | Description | Unit |
|---|---|---|
| w | Flowrate | $lb_m$/sec (kg/sec) |
| wt | Weight | $lb_m$ (kg) |
| $\beta$ | Blade tip angle | deg (rad) |
| $\epsilon$ | Area ratio | |
| $\eta$ | Efficiency | |
| $\delta$ | Wall thickness | in. (cm) |

Subscripts

| | |
|---|---|
| c | Thrust chamber |
| e | Nozzle exit plane |
| f | Fuel |
| ID | Point of incipient thermal decomposition |
| in | Coolant inlet conditions |
| o | Oxidizer |
| p | Oxidizer primary flow |
| s | Oxidizer secondary flow |
| T | Turbine inlet conditions |
| t | Nozzle throat conditions |
| v | Available turbine flow |
| vac | Vacuum conditions |
| w | Thrust chamber hot side wall conditions |

Superscripts

| | |
|---|---|
| | Theoretical value |

## REFERENCES


1. "Investigation of Light Hydrocarbon Fuels With Flox Mixtures as Liquid Rocket Propellants -- Final Report," PWA FR-1443, Contract NAS3-4195, NASA CR-54445, 1 September 1965.

2. "Investigation of Light Hydrocarbon Fuels with Fluorine-Oxygen Mixtures as Liquid Rocket Propellants -- Final Report," PWA FR-2227, Contract NAS3-6296, NASA CR-72147, 15 September 1967.

3. "Investigation of Light Hydrocarbon Fuels with Fluorine-Oxygen Mixtures as Liquid Rocket Propellants -- Final Report," PWA FR-2872, Contract NAS3-10294, NASA CR-72425, 15 November 1968.

4. "Flox/Methane Pump-Fed Engine Study -- Final Report," PWA FR-3040, Contract NAS3-7950, NASA CR-72485, 10 May 1969.

5. "Space Storable Regenerative Cooling Investigation -- Interim Report," PWA FR-2552, Contract NAS3-11190, NASA CR-72341, 26 July 1968.

6. "Space Storable Regenerative Cooling Investigation -- Final Report," Pratt & Whitney Aircraft, Contract NAS3-11190, To be Published.

7. Failkoff, S., Hammer, S. S., and Peschke, W., "Electroforming Liquid Propellant Rocket Motors," Space Aeronautics, October 1964.

8. "Research on a Hydrogen-Fluorine Propulsion System -- Final Report," PWA FR-1585, Contract NASW-754, NASA CR-72074, 21 October 1966 (Confidential).

9. Balje, O. E., "A Study on the Design Criteria and Matching of Turbomachines: Part A - Similarity Relations and Design Criteria of Turbines," ASME Paper No. 60-WA-230.

10. Brinkley, S. R., Jr., "Combustion Processes - Computational Methods in Combustion Calculations," High Speed Aerodynamics and Jet Propulsion, Volume II, Princeton University Press, Princeton 1956.

11. Zeleznik, E. S. and Gordon, S., "A General IBM 704 or 7090 Computer Program for Computation of Chemical Equilibrium Compositions, Rocket Performance and Chapmen-Jouguet Detonations," NASA TND-1454.

12. "Digital Computer Programs for Rocket Nozzle Design and Analysis, Bell Nozzle Design," Volume II, PWA FR-1021, prepared under NASA Contract NAS9-2487, 26 June 1964.

13. "Hydrogen/Fluorine Engine Evaluation - Quarterly Progress Report No. 7," PWA FR-2801, 15 April 1968.

14. Osborn, W. M., "Noncavitating and Cavitating Performance of a Liquid-Fluorine Pump Designed by Stream-Filiment Method," NASA Lewis Research Center TMX-722, July 1963.

15. "Final Report of High Energy Advance Throttling Concept Study," PWA FR-1573, Contract AF 04(611)-9965, AFRPL-TR-66-43, 7 March 1966 (Confidential).

16. "Final Report of Advanced Throttling Concept Study," Contract AF 04(611)-9575, AFRPL-TR-65-98, and PWA FR-1279, 19 March 1965 (Confidential).

17. "High Energy Advanced Throttling Concept - Final Report," Contract AF 04(611)-11611, PWA FR-2366 (Confidential).

18. Schmidt, H. W., "Handling and Use of Fluorine and Fluorine-Oxygen Mixtures in Liquid Rocket Systems," NASA SP, 1965.

19. "Final Report - Advanced Engine Design Study, Bell (AEB)," PWA FR-2372, 31 July 1967 (Confidential).

DISTRIBUTION LIST*

| Report Copies R | Report Copies D | Recipient | Designee |
|---|---|---|---|
| | | National Aeronautics & Space Administration<br>Lewis Research Center<br>21000 Brookpark Road<br>Cleveland, Ohio 44135 | |
| 1 | | Attn: Contracting Officer, MS 500-313 | |
| 5 | | Liquid Rocket Technology Branch, MS 500-209 | |
| 1 | | Technical Report Control Office, MS 5-5 | |
| 1 | | Technology Utilization Office, MS 3-16 | |
| 2 | | AFSC Liaison Office, MS 4-1 | |
| 2 | | Library | |
| 1 | | Office of Reliability & Quality Assurance, MS 500-111 | |
| 1 | | D. L. Nored, Chief, LRTB, MS 500-209 | |
| 3 | | J. W. Gregory, Project Manager, MS 500-209 | |
| 1 | | E. W. Conrad, MS 500-204 | |
| 1 | | R. H. Kemp, MS 49-1 | |
| 1 | | R. H. Knoll, MS 501-2 | |
| 1 | | Joseph Sivo | |
| 1 | | William Tomazic | |
| 2 | 1 | Chief, Liquid Experimental Engineering, RPX<br>Office of Advanced Research & Technology<br>NASA Headquarters<br>Washington, D. C. 20546 | Frank W. Stephenson, Jr. |
| 2 | | Chief, Liquid Propulsion Technology, RPL<br>Office of Advanced Research & Technology<br>NASA Headquarters<br>Washington, D. C. 20546 | |
| 1 | 1 | Director, Launch Vehicles & Propulsion, SV<br>Office of Space Science & Applications<br>NASA Headquarters<br>Washington, D. C. 20546 | Robert F. Schmidt |
| 1 | | Chief, Environmental Factors & Herodynamics<br>Code RV-1<br>Office of Advanced Research & Technology<br>NASA Headquarters<br>Washington, D. C. 20546 | |

*Final reports will be sent directly to the "recipient" and the "designee" per the quantities specified in the respective columns, R and D, with the following exceptions: (1) When copies specified in Column D are followed by an asterisk (*), a copy of the report will be sent to each designee whose name is preceded by an asterisk; and (2) when no copies are specified in Column D, only a copy of the letter will be sent to the person named as the "designee."

| Report Copies R | Report Copies D | Recipient | Designee |
|---|---|---|---|
| 1 | | Chief, Space Vehicles Structures<br>Office of Advanced Research & Technology<br>NASA Headquarters<br>Washington, D. C. 20546 | |
| 1 | | Director, Advanced Manned Missions, MT<br>Office of Manned Space Flight<br>NASA Headquarters<br>Washington, D. C. 20546 | |
| 6 | | NASA Scientific & Technical Information Facility<br>P. O. Box 33<br>College Park, Maryland 20740 | |
| 1 | | Director, Technology Utilization Division<br>Office of Technology Utilization<br>NASA Headquarters<br>Washington, D. C. 20546 | |
| 1 | | National Aeronautics & Space Administration<br>Ames Research Center<br>Moffett Field, California 94035<br>Attn: Library | E. R. Streed, SED<br>Hans M. Mark<br>Mission Analysis<br>Division |
| 1 | | National Aeronautics & Space Administration<br>Flight Research Center<br>P. O. Box 273<br>Edwards, California 93523<br>Attn: Library | |
| 1 | 1* | National Aeronautics & Space Administration<br>Goddard Space Flight Center<br>Greenbelt, Maryland 20771<br>Attn: Library | Merland L.<br>Moseson,<br>Code 620<br>*C. R. Gunn, Delta Pro<br>Office, Code 47 |
| 1 | | National Aeronautics & Space Administration<br>John F. Kennedy Space Center<br>Cocoa Beach, Florida 32931<br>Attn: Library | Dr. Kurt H.<br>Debus |
| 1 | | National Aeronautics & Space Administration<br>Langley Research Center<br>Langley Station<br>Hampton, Virginia 23365<br>Attn: Library | Ed Cartwright,<br>Director |

| Report Copies R | D | Recipient | Designee |
|---|---|---|---|
| 1 | 1* | National Aeronautics & Space Administration<br>Manned Spacecraft Center<br>Houston, Texas 77001<br>Attn: Library | J. G. Thiobodaux, Jr.<br>Chief, Propulsion & Power Division<br>*H. J. Brasseaux, PES Propulsion |
| 1 | 2* | National Aeronautics & Space Administration<br>George C. Marshall Space Flight Center<br>Huntsville, Alabama 35812<br>Attn: Library | *Keith Chandler, S&E-ASTN-PA<br>Hans G. Paul<br>Leon J. Hastings<br>James Thomas<br>E. H. Hyde<br>I. G. Yates<br>Clyde Nevins<br>Robert E. Shannon<br>J. Blumrich<br>*Lee W. Jones, S&E-ASTN-PAS |
| 1 | 2* | Jet Propulsion Laboratory<br>4800 Oak Grove Drive<br>Pasadena, California 91103<br>Attn: Library | Henry Burlage, Jr.<br>*Duane Dipprey<br>*W. B. Powell |
| 1 | | Defense Documentation Center<br>Cameron Station<br>Building 5<br>5010 Duke Street<br>Alexandria, Virginia 22314<br>Attn: TISIA | |
| 1 | | Office of the Director of Defense Research & Engineering<br>Washington, D. C. 20301<br>Attn: Office of Asst. Dir. (Chem. Technology) | |
| 1 | | RTD (RTNP)<br>Bolling Air Force Base<br>Washington, D. C. 20332 | |
| 1 | | Arnold Engineering Development Center<br>Air Force Systems Command<br>Tullahoma, Tennessee 37389<br>Attn: Library | Dr. H. K. Doetsch |
| 1 | | Advanced Research Projects Agency<br>Washington, D. C. 20525<br>Attn: Library | D. E. Mock |

| Report Copies R | D | Recipient | Designee |
|---|---|---|---|
| 1 | | Aeronautical Systems Division<br>Air Force Systems Command<br>Wright-Patterson Air Force Base,<br>Dayton, Ohio<br>Attn: Library | D. L. Schmidt<br>Code ARSCNC-2 |
| 1 | | Air Force Missile Test Center<br>Patrick Air Force Base, Florida<br>Attn: Library | L. J. Ullian |
| 1 | | Air Force Systems Command<br>Andrews Air Force Base<br>Washington, D. C. 20332<br>Attn: Library | Capt. S. W. Bowen<br>SCLT |
| 1 | | Air Force Rocket Propulsion Laboratory (RPR)<br>Edwards, California 93523<br>Attn: Library | |
| 1 | | Air Force Rocket Propulsion Laboratory (RPM)<br>Edwards, California 93523<br>Attn: Library | |
| 1 | | Air Force FTC (FTAT-2)<br>Edwards Air Force Base, California 93523<br>Attn: Library | Donald Ross |
| 1 | | Air Force Office of Scientific Research<br>Washington, D. C. 20333<br>Attn: Library | SREP, Dr. J. F. Masi |
| 1 | | Space & Missile Systems Organization<br>Air Force Unit Post Office<br>Los Angeles, California 90045<br>Attn: Technical Data Center | |
| 1 | | Office of Research Analyses (OAR)<br>Holloman Air Force Base, New Mexico 88330<br>Attn: Library | |
| 1 | | U. S. Air Force<br>Washington, D. C.<br>Attn: Library | Col. C. K.<br>Stambaugh,<br>Code AFRST |

| Report Copies R | D | Recipient | Designee |
|---|---|---|---|
| 1 | | Commanding Officer<br>U. S. Army Research Office (Durham)<br>Box CM, Duke Station<br>Durham, North Carolina 27706<br>Attn: Library | |
| 1 | | U. S. Army Missile Command<br>Redstone Scientific Information Center<br>Redstone Arsenal, Alabama 35808<br>Attn: Document Section | Dr. W. Wharton |
| 1 | | Bureau of Naval Weapons<br>Department of the Navy<br>Washington, D. C.<br>Attn: Library | J. Kay,<br>Code RTMS-41 |
| 1 | | Commander<br>U. S. Naval Missile Center<br>Point Mugu, California 93041<br>Attn: Technical Library | |
| 1 | | Commander<br>U. S. Naval Weapons Center<br>China Lake, California 93557<br>Attn: Library | W. F. Thorm<br>Code 4562 |
| 1 | | Commanding Officer<br>Naval Research Branch Office<br>1030 E. Green Street<br>Pasadena, California 91101<br>Attn: Library | |
| 1 | | Director (Code 6180)<br>U. S. Naval Research Laboratory<br>Washington, D. C. 20390<br>Attn: Library | H. W. Carhart<br>J. M. Krafft |
| 1 | | Picatinny Arsenal<br>Dover, New Jersey 07801<br>Attn: Library | I. Forsten |
| 1 | | Air Force Aero Propulsion Laboratory<br>Research & Technology Division<br>Air Force Systems Command<br>United States Air Force<br>Wright-Patterson AFB, Ohio 45433<br>Attn: APRP (Library) | R. Quigley<br>C. M. Donaldson |

| Report Copies R | D | Recipient | Designee |
|---|---|---|---|
| 1 | | Electronics Division<br>Aerojet-General Corporation<br>P. O. Box 296<br>Azusa, California 91703<br>Attn: Library | W. L. Rogers |
| 1 | | Space Division<br>Aerojet-General Corporation<br>9200 East Flair Drive<br>El Monte, California 91734<br>Attn: Library | S. Machlawski |
| 1 | | Ordanance Division<br>Aerojet-General Corporation<br>11711 South Woodruff Avenue<br>Downey, California 90241<br>Attn: Library | |
| 1 | | Propulsion Division<br>Aerojet-General Corporation<br>P. O. Box 15847<br>Sacramento, California 95803<br>Attn: Technical Library 2484-2015A | R. Stiff |
| 1 | | Aeronutronic Division of Philco Ford Corp.<br>Ford Road<br>Newport Beach, California 92663<br>Attn: Technical Information Department | Dr. L. H. Linder |
| 1 | | Aerospace Corporation<br>2400 E. El Segundo Blvd.<br>Los Angeles, California 90045<br>Attn: Library-Documents | J. G. Wilder |
| 1 | | Arthur D. Little, Inc.<br>20 Acorn Park<br>Cambridge, Massachusetts 02140<br>Attn: Library | A. C. Tobey |
| 1 | | Astropower Laboratory<br>McDonnell-Douglas Aircraft Company<br>2121 Campus Drive<br>Newport Beach, California 92660<br>Attn: Library | Dr.George Moe<br>Director Research |

| Report Copies R | D | Recipient | Designee |
|---|---|---|---|
| 1 | | Astrosystems, International<br>1275 Bloomfield Avenue<br>Fairfield, New Jersey 07007<br>Attn: Library | |
| 1 | | ARO, Incorporated<br>Arnold Engineering Development Center<br>Arnold AF Station, Tennessee 37389<br>Attn: Library | Dr. B. H. Goethert |
| 1 | | Susquehanna Corporation<br>Atlantic Research Division<br>Shirley Highway & Edsall Road<br>Alexandria, Virginia 22314<br>Attn: Library | Dr. Ray Friedman |
| 1 | | Battelle Memorial Institute<br>505 King Avenue<br>Columbus, Ohio 43201<br>Attn: Report Library, Room 6A | |
| 1 | | Beech Aircraft Corporation<br>Boulder Facility<br>Box 631<br>Boulder, Colorado<br>Attn: Library | Douglas Pope |
| 1 | | Bell Aerosystems, Inc.<br>Box 1<br>Buffalo, New York 14205<br>Attn: Library | T. Reinhardt<br>W. M. Smith |
| 1 | | Bendix Systems Division<br>Bendix Corporation<br>3300 Plymouth Street<br>Ann Arbor, Michigan<br>Attn: Library | John M. Brueger |
| 1 | | Bellcomm<br>955 L'Eufant Plaza, S.W.<br>Washington, D. C.<br>Attn: Library | H. S. London |

| Report Copies R | D | Recipeint | Designee |
|---|---|---|---|
| 1 | | Boeing Company<br>Space Division<br>P. O. Box 868<br>Seattle, Washington 98124<br>Attn: Library | J. D. Alexander<br>C. F. Tiffany |
| 1 | | Boeing Company<br>1625 K Street, N.W.<br>Washington, D. C. 20006 | |
| 1 | | Boeing Company<br>P. O. Box 1680<br>Huntsville, Alabama 35801 | Ted Snow |
| 1 | | Chemical Propulsion Information Agency<br>Applied Physics Labroatory<br>8621 Georgia Avenue<br>Silver Springs, Maryland 20910 | Tom Reedy |
| 1 | | Chrysler Corporation<br>Missile Division<br>P. O. Box 2628<br>Detroit, Michigan<br>Attn: Library | John Gates |
| 1 | | Chrysler Corporation<br>Space Division<br>New Orleans, Lousiana<br>Attn: Librarian | |
| 1 | | Curtiss-Wright Corporation<br>Wright Aeronautical Division<br>Wood-Ridge, New Jersey 07075<br>Attn: Library | G. Kelley |
| 1 | | University of Denver<br>Denver Research Institute<br>P. O. Box 10127<br>Denver, Colorado 80210<br>Attn: Security Office | |
| 1 | | Fairchild Stratos Corporation<br>Aircraft Missiles Division<br>Hagerstown, Maryland<br>Attn: Library | |
| 1 | | Research Center<br>Fairchild Hiller Corporation<br>Germantown, Maryland<br>Attn: Library | Ralph Hall |

| Report Copies R | D | Recipient | Designee |
|---|---|---|---|
| 1 | | Republic Aviation<br>Fairchild Hiller Corporation<br>Farmington, Long Island<br>New York | |
| 1 | | General Dynamics/Convair<br>P. O. Box 1128<br>San Deigo, California 92112<br>Attn: Library | Frank Dore<br>R. Roberts |
| 1 | | Missiles and Space Systems Center<br>General Electric Company<br>Valley Forge Space Technology Center<br>P. O. Box 855<br>Philadelphia, Pa. 190101<br>Attn: Library | A. Cohen<br>F. Schultz |
| 1 | | General Electric Company<br>Flight Propulsion Lab. Department<br>Cincinnati, Ohio<br>Attn: Library | D. Suichu<br>Leroy Smith |
| 1 | 1* | Grumman Aircraft Engineering Corporation<br>Bethpage, Long Island, New York<br>Attn: Library | Joseph Gavin<br>*Herb Siegel |
| 1 | | Hercules Powder Company<br>Allegheny Ballistics Laboratory<br>P. O. Box 210<br>Cumberland, Maryland 21501<br>Attn: Library | |
| 1 | | Honeywell Inc.<br>Aerospace Division<br>2600 Rdigeway Road<br>Minneapolis, Minnesota<br>Attn: Library | Gordon Harris |
| 1 | | IIT Research Institute<br>Technology Center<br>Chicago, Illinois 60616<br>Attn: Library | C. K. Hersh |
| 1 | | Kidde Aerospace Division<br>Walter Kidde & Company, Inc.<br>367 Main Street<br>Belleville 9, N.J. | R. J. Hanville |

| Report Copies R D | Recipient | Designee |
|---|---|---|
| 1 | Ling-Temco-Vought Corporation<br>P. O. Box 5907<br>Dallas, Texas 75222<br>Attn: Library | Warren G. Trent |
| 1 | Lockheed Missiles and Space Company<br>P. O. Box 504<br>Sunnyvale, California 94087<br>Attn: Library | J. Guill |
| 1 | Lockheed-California Company<br>10445 Glen Oaks Blvd.,<br>Pacoima, Claifornia<br>Attn: Library | |
| 1 | Lockheed Propulsion Company<br>P. O. Box 111<br>Redlands, California 92374<br>Attn: Library, Thackwell | H. L. Thackwell |
| 1 | Marquardt Corporation<br>16555 Saticoy Street<br>Box 2013 - South Annex<br>Van Nuys, California 91409 | Howard McFarland<br>L. R. Bell Jr. |
| 1 | Martin-Marietta Corporation (Baltimore Division)<br>Baltimore, Maryland 21203<br>Attn: Library | John Calathes |
| 1 | Denver Division<br>Martin-Marietta Corporation<br>P. O. Box 179<br>Denver, Colorado 80201<br>Attn: Library | Dr. Morganthaler<br>F. R. Schwartzberg<br>I. W. Murphy |
| 1 | Orlando Division<br>Martin-Marietta Corporation<br>Box 5827<br>Orlando, Florida<br>Attn: Library | J. Fern |
| 1 | Western Division<br>McDonnell Douglas Aircraft Company, Inc.<br>3000 Ocean Park Blvd.<br>Santa Monica, California 90406<br>Attn: Library | R. W. Hallet<br>G. W. Burke<br>Paul Klevatt |
| 1 | McDonnell Douglas Aircraft Corporation<br>P. O. Box 516<br>Lambert Field, Missouri 63166<br>Attn: Library | R. A. Herzmark |

| Report Copies R | D | Recipient | Designee |
|---|---|---|---|
| 1 | 2* | Rocketdyne Division<br>North American Rockwell, Inc.<br>6633 Canoga Avenue<br>Canoga Park, California 9134<br>Attn: Library, Department 596-306 | Dr. R. J. Thompson<br>*S. F. Iacobellis<br>*Spence Clapp |
| 1 | | Space & Information Systems Division<br>North American Rockwell<br>12214 Ladewood Blvd.<br>Downey, California<br>Attn: Library | |
| 1 | | Northrop Space Laboratories<br>3401 West Broadway<br>Hawthorne, California<br>Attn: Library | Dr. William Howard |
| 1 | | Purdue University<br>Layfette, Indiana 47907<br>Attn: Library (Technical) | Dr. Bruce A. Reese<br>Director, Jet Propulsion Center |
| 1 | | Radio Corporation of America<br>Astro-Electronics Products<br>Princeton, New Jersey<br>Attn: Library | |
| 1 | | Rocket Research Corporation<br>Willow Road at 116th Street<br>Redmond, Washington 98052<br>Attn: Library | F. McCullough, Jr. |
| 1 | | Stanford Research Institute<br>333 Ravenswood Avenue<br>Menlo Park, California 94025<br>Attn: Library | Dr. Gerald Marksman |
| 1 | | Thiokol Chemical Corporation<br>Redstone Division<br>Huntsville, Alabama<br>Attn: Library | John Goodloe |
| 1 | | TRW Systems Inc.<br>1 Space Park<br>Redondo Beach, California 90278<br>Attn: STL Tech. Lib. Doc. Acquisitions | D. H. Lee |
| 1 | | United Aircraft Corporation<br>Corporation Library<br>400 Main Street<br>East Hartford, Connecticut 06108<br>Attn: Library | Dr. David Rix<br>Erle Martin<br>Frank Owen<br>Wm. E. Taylor |

| Report Copies R | D | Recipient | Designee |
|---|---|---|---|
| 1 | | United Aircraft Corporation<br>United Technology Center<br>P. O. Box 358<br>Sunnyvale, California 94038<br>Attn: Library | Dr. David Altman |
| 1 | | Vickers Incorporated<br>Box 302<br>Troy, Michigan | |
| 1 | | Vought Astronautics<br>Box 5907<br>Dallas, Texas<br>Attn: Library | W. C. Trent |
| 1 | | Jim Markowsky<br>221 Upson Hall<br>Ithica, New York 14850 | |